# MOD-AIR QUALITY MODELING

**Third International Symposium**
**on**
**AIR QUALITY MANAGEMENT**
**at Urban, Regional and Global Scales**
**&**
**14 th IUAPPA Regional Conference**
**26-30 September 2005**
**Istanbul, Turkey**

## AIR QUALITY MODELING

*Proceedings of the Third International Symposium on Air Quality Management at Urban, Regional and Global Scales. 26-30 September 2005, Istanbul – Turkey*

# AIR POLLUTION MODELING IN THE MEDITERRANEAN REGION: FROM ANALYSIS OF EPISODES TO FORECASTING

**George Kallos, Marina Astitha and Petros Katsafados**

University of Athens, School of Physics, Division of Applied Physics,
Atmospheric Modeling and Weather Forecasting Group,
University Campus, Bldg. PHYS-V, Athens 15784, Greece
kallos@mg.uoa.gr

## ABSTRACT

Air pollution modeling in the Mediterranean Region is at its third decade now. The first step beyond the Gaussian-type plume dispersion was the combined use of mesoscale atmospheric models with 3-D dispersion ones. During the last decade computer power became very cheap and sophisticated configurations of atmospheric and photochemical models were applied in regional studies. Advanced modeling techniques have opened a new horizon in air pollution studies, providing the capability of forecasting air pollution episodes along with the traditional analysis of air quality measurements for specific cases of severe atmospheric pollution episodes.

**Key Words:** Air Pollution, Modeling, Particulate Matter, Photochemistry, Dust

## 1. INTRODUCTION

In the beginning of the 3D dispersion models the techniques used were either Eulerian or Lagrangian-type. Later, the first photochemical models were applied with Eulerian-type approach. The mesoscale models at the time were inititialized on a rather simplistic way by considering horizontally uniform initialization fields. The domain sizes were at the order of 100 km. Such type of modeling was appropriate for either conceptual type of analysis or for thermally-driven local circulations. This type of modeling was applied for urban regions. The problems were considerable and several of these simulations led to wrong conclusions. A typical example is Athens where the proposed conceptual models of the 80-ties were reproduced by the models. In these early simulations the recirculation of the air pollutants over an area of a few tens of kilometers was demonstrated and was widely adopted. During 90-ties the new generation of atmospheric models was in use where the initialization was performed on a non-uniform way and multi-scale type of approach was adopted (Kallos et al, 1995, 1997, 1999). In such simulations the role of various-scale flow interactions was demonstrated and conceptual model of recirculation of air pollutants within a few tens of kilometers showed its limitations.

During the last decade computer power became very cheap and sophisticated configurations of atmospheric and photochemical models were applied in regional studies (Kotroni et al, 1999). Such simulations demonstrated the role of Long-Range Transport on air quality degradation in various places around the Mediterranean. Phenomena like recirculation over realistic scales, multiple layering of different ages of air pollutants horizontal transport within or above the marine boundary layer together with the thermal circulations over the mountainous regions were the key issues. Despite this progress the problem related to emission inventory was still a real one.

With the experience gained during all these years the first attempts of operational air quality forecasts are evident. Such forecasting activities were organized recently from the Atmospheric Modeling and Weather Forecasting Group of University of Athens during the Athens Olympics. The forecasting activities were based on the SKIRON weather and Saharan dust forecasting system RAMS weather forecasting system, together with the CAMx photochemical model. These models run on nesting mode in order to cover the multi-scale flow and air pollution processes. The chemical processes include gaseous and particulate pollutants. The sources of air pollutants included in the system are both anthropogenic and natural origin (e.g. Saharan dust). In this presentation, the above issues are summarized and the experience gained from these operations is discussed.

## 2. MODEL DESCRIPTION

A short description of the modeling systems used for performing simulations is provided below.
*The SKIRON/ETA* is a modeling system developed at the University of Athens from the Atmospheric Modeling and Weather Forecasting Group (Kallos et al, 1997, Nickovic et al, 2001). It has enhanced capabilities with the unique one to simulate the dust cycle (uptake, transport, deposition).

*RAMS (Regional Atmospheric Modeling System)* is considered as one of the most advanced atmospheric models. Detailed information about RAMS model can be found in Cotton et al (2003).

*The Comprehensive Air Quality Model with Extensions (CAMx)* (Environ, 2003) is an Eulerian photochemical model that allows for integrated assessment of air-pollution over many scales ranging from urban to super-regional (http://www.camx.com). CAMx has also model structures for modeling aerosols, processes that are linked to the CB4 gas phase chemical mechanism, science modules for aqueous chemistry (RADM-AQ) inorganic aerosol thermodynamics/partitioning (ISORROPIA) and secondary organic aerosol formation/partitioning (SOAP).

## 3. AIR POLLUTION MODELING: ANALYSIS OF EPISODES

The paths and scales of transport and transformation of air pollutants in the Mediterranean Region have been identified in previous work carried out at the framework of various EU projects (Kallos et al, 1997, 1999). The results showed that

the synoptic/regional circulation during summer, favors long-range transport of air pollutants released from Southern and Eastern Europe and Central Mediterranean towards the Eastern Mediterranean, North Africa and Middle East (Figure 1).

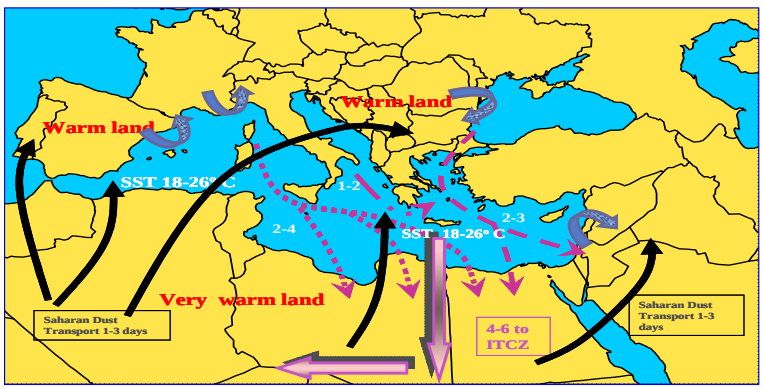


Figure 1. Characteristic paths and scales of transport of air masses in the Mediterranean Region.

Anthropogenic gases and particulate matter as well as natural aerosol like desert dust are the subject of modeling studies in conjunction with measurements of pollutants. Ozone is a well known secondary pollutant, which has been the primary target of several studies during the last 20 years. Ozone formation, destruction, transport and deposition patterns have been identified in various projects in the past. During the last years, a great number of studies focus on the important role of aerosols in the air quality of a specific area, due to the potential impact on human health and ecosystems (di Sarra et al, 2001, Rodriguez et al, 2001).Today the scientific interest focuses on the patterns that characterize aerosols in the atmosphere as well as the interaction between gases and particulate matter mainly of small sizes.

Concerning the anthropogenic aerosols, particulate sulfate production and transport is part of an on-going research using advanced modeling systems. In order to identify the paths and transformation of $SO_2$ to particulate sulfate, the sulfate ratio was calculated within the code of CAMx model. Sulfate ratio has been used in previous studies (Luria et al, 1996) to define the chemical age of air masses, based on measurements of sulfur dioxide and particulate sulfate. Sulfate ratio is characterized as the ratio of sulfate concentration to total sulfur concentration (meaning both $SO_2$ and particulate sulfate), leading to a dimensionless value from zero to unity. According to Luria (1996), the higher values for sulfate ratio (greater than 0.1) correspond to aged air masses, and the closer the ratio is to unity, the older the air mass and the longer its travel distance. CAMx model code was modified in order to calculate an average sulfate ratio for each hour of the simulation, using meteorological fields either from RAMS or from SKIRON/Eta model. Figure 2 shows one example of the analysis of episodes based on the comparison of modeling results with observations of particulate sulfate in Southern Greece (station located in Finokalia at northeastern Crete).

In addition to the anthropogenic produced aerosols, such as sulfates and/or nitrates, desert dust contributes significantly to the air quality degradation, due to the episodic

character of increased desert dust concentrations (Table 1). In general, air pollution episodes originated from anthropogenic activities occur together with desert dust transport episodes, because of the prevailing synoptic conditions favorable to dust transport (ahead of a trough or behind an anticyclone in the Mediterranean Region). Such synoptic conditions are most of the times associated with stable atmospheric conditions and stagnation (transport of warm air masses aloft that suppress vertical developments like updraft and convergence zones). The amount of Saharan dust deposited on the Mediterranean waters or over the European land exhibits significant seasonal and inter-annual variability (Papadopoulos et al, 2003), having a rather episodic character (Figure 3). The strength and the frequency of occurrence of the Saharan dust episodes define the annual deposition amounts and patterns of aerosols to a high degree, alternating the mean annual values. This leads to the fact that long-term modeling and measurement data are essential in understanding the synergetic effects of sulfates and desert dust in the atmosphere of the Mediterranean Region.

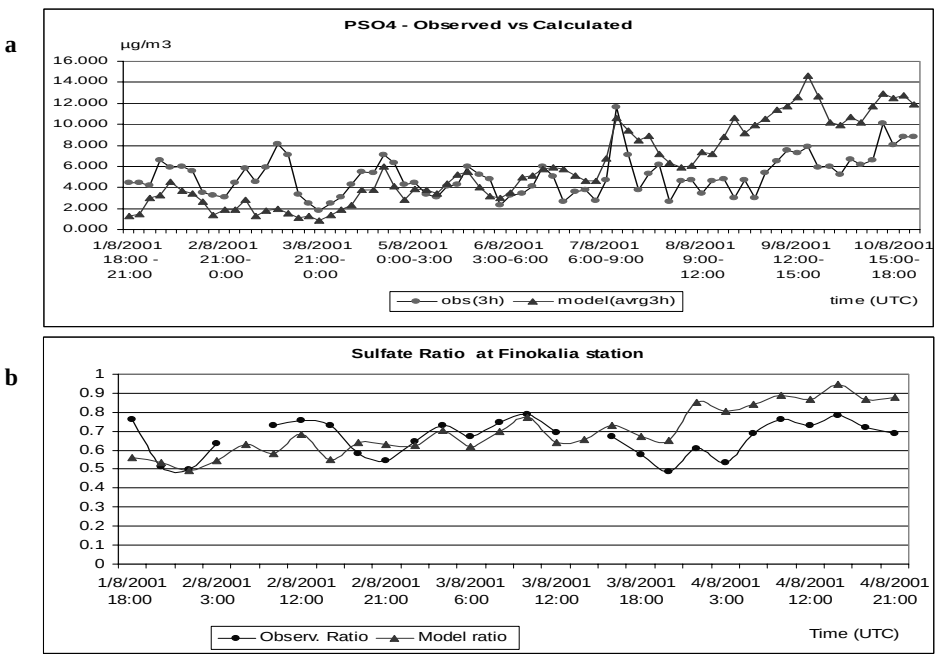


Figure 2. Intercomparison between measurements and model calculations of: a) particulate sulfate, and b) sulfate ratio, at Finokalia station, Crete, for August 2001.

Table 1. Desert dust episode for April, 2002, measured at Finokalia station, Crete.

| **Start date** | **End date** | **Saharan dust wet deposition (mg)** |
|---|---|---|
| 10/01/02 | 14/01/02 | 0 |
| 14/01/02 | 16/01/02 | 0 |
| 16/01/02 | 22/01/02 | 0 |
| 22/01/02 | 30/01/02 | 0.4 |
| 30/01/02 | 11/02/02 | 0.6 |
| 11/02/02 | 13/02/02 | 0 |
| 13/02/02 | 26/02/02 | 1.3 |
| 21/03/02 | 27/03/02 | 1.1 |
| 27/03/02 | 03/04/02 | 0 |
| 03/04/02 | 09/04/02 | 5.5 |
| ***09/04/02*** | ***16/04/02*** | ***179.6*** |
| 16/04/02 | 19/04/02 | 5.5 |
| | 26/05/02 | 0.4 |

## 4. AIR POLLUTION MODELING: OZONE AND DUST FORECASTING

The knowledge gained from years of modeling atmospheric and photochemistry processes, provided the ability for forecasting weather phenomena and air pollutant concentration in the Mediterranean Region. Since January 2000, the SKIRON/ETA model runs operationally covering the Mediterranean Region, providing 3-day forecasts of dust load and deposition (http://forecast.uoa.gr), among other meteorological parameters. The ozone forecasting system applied for the Mediterranean Region runs operationally since July 2004, for the Athens Olympic Games (http://forecast.uoa.gr). The system is based on CAMx photochemical model and utilizes meteorological fields from SKIRON and RAMS in order to produce long-range transport fields of ozone and particulate for Europe and the Mediterranean Region.

The operational use of atmospheric and air quality models provides the opportunity to study the photochemical activity, particle formation and transport in various scales, from mesoscale to regional, as shown in Figures 3-5. The effort for producing reliable air quality predictions is a well-based and on-going task. Continuous research and sufficient measurements of air pollutants should aid this effort into the future of accurate predictions.

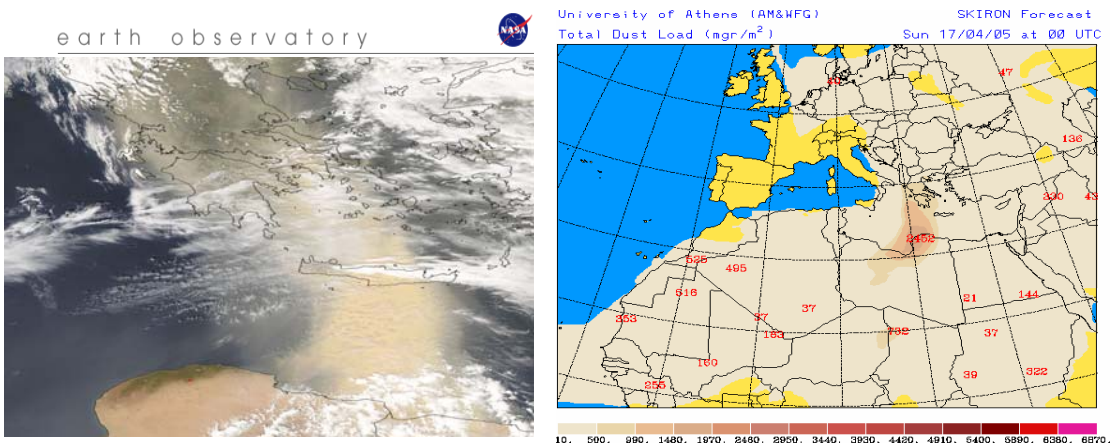


Figure 3. Saharan dust episode for April 17, 2005. *Left:* Dust over Greece, picture taken from NASA/GSFC satellite (2005/107 - 04/17 at 11:40 UTC). *Right:* Total dust load as simulated from SKIRON/Eta dust modeling system.

**a**

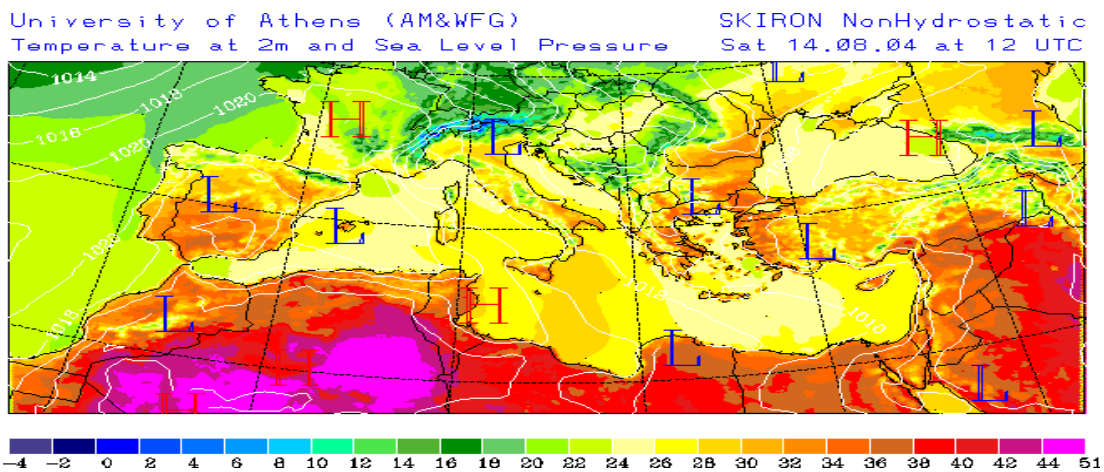


**b**

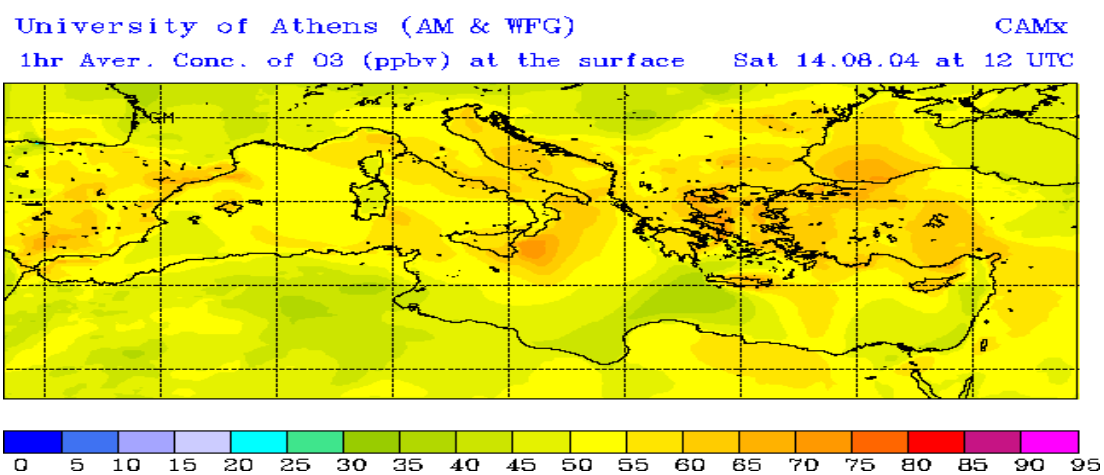


Figure 4. **a)** Regional weather forecasts from SKIRON/Eta and **b)** air quality forecasts from CAMx model (ozone) for the Mediterranean Region.

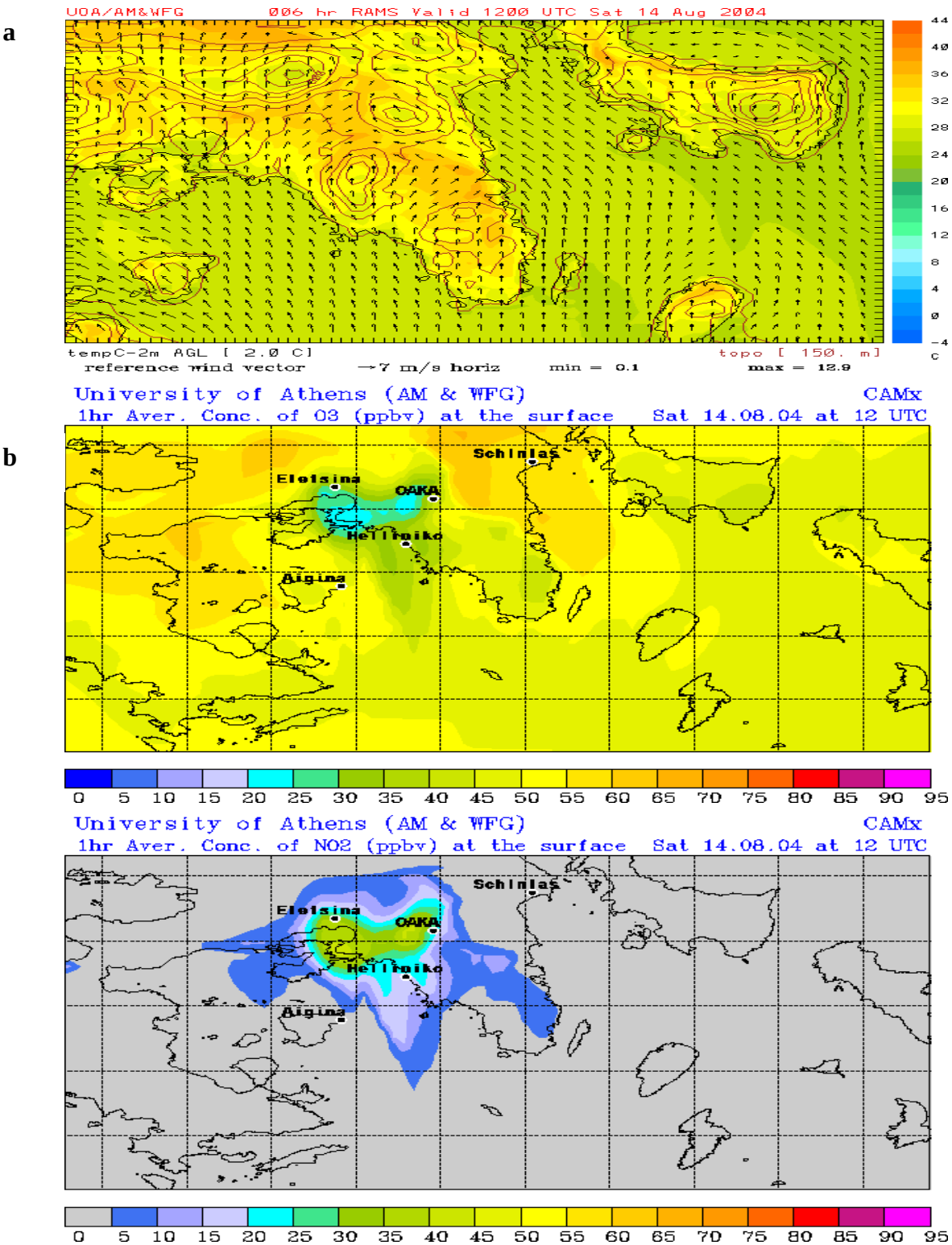


Figure 5. a) High resolution weather forecast from RAMS model and b) air quality forecasts ($O_3$, $NO_2$) from CAMx model for Athens Olympics (summer 2004).

## 5. CONCLUSIONS

The present study summarizes the multi-year research modeling studies for identification of the characteristic spatial and temporal scales of photochemical activity along the previously defined main transport routes over the Mediterranean Region. Air quality degradation in the area is influenced by photochemical pollutants like ozone as well as aerosols such as particulate sulfate and desert dust. The photochemical activity, particle formation and transport are examined with the implication of model simulation in conjunction with measurements in several locations in the area. The remarks concluded from this work are summarized as follows:

The sulfate ratio sensitivity tests performed in this work showed results similar to those of Luria (1996), confirming the long range transport paths of sulfur towards the Middle East coast, during summer. Usually, high concentrations of sulfate, nitrate and other particles of anthropogenic origin, are associated with transport of desert dust due to the formation of stable atmospheric conditions. There are indications that the multi-scale transport and transformation processes might have significant climatic impacts. More specifically, there can be effects on rain and therefore the water balance in a region where the water budget is critical. This is possible through the increase of the number of Cloud Condensation Nuclei (CCN) and through the direct warming of the lower tropospheric layers (up to about 3 km) without an increase in the specific humidity. Of course, these processes are further more complicated because of the appearance of desert dust particles in the atmosphere which, in a wet environment, may be coated by sulfates and on that way they become very effective CCN.

The above conclusions are a result of the on-going research based on using modeling techniques for assessing the air quality over specific areas. Modeling tools are subject to continuous development in order to eliminate as many errors as possible. Thus, the on-going development has showed the way to producing real time forecasts of air pollution episodes in different scales: from urban to regional. The operational use of advanced atmospheric and air quality models has provided reliable predictions of several air quality episodes in the Mediterranean Region. Nevertheless continuous research and sufficient measurements of air pollutants should aid this effort into the future of accurate predictions.

## 6. ACKNOWLEDGMENTS

This work was supported by the following projects: ADIOS, EU/DG-XII: EVK3-CT-2000-00035, MERCYMS, EU/DG EVK3-2002-00070. Measurements of air pollutants from Finokalia station, Crete were provided by professor N. Mihalopoulos (Environmental Chemical Process Laboratory, Department of Chemistry, University of Crete, Greece).

## REFERENCES


Cotton, W.R.; Pielke Sr., R.A.; Walko, R.L.; Liston, G.E.; Tremback, C.J.; Jiang, H.; McAnelly, R.L.; Harrington, J.Y.; Nicholls, M.E.; Carrio, G.G.; McFadden, J.P., 2003, “RAMS 2001: Current Status and Future Directions, Meteorology and Atmospheric Physics” (Volume 82 Issue 1-4).

di Sarra, A., T. Di Iorio, M. Cacciani, G. Fiocco, and D. Fuà, 2001. Saharan dust profiles measured by lidar from Lampedusa. J. Geophys. Res., 106, 10,335-10,347.

Environ 2003: User’s Guide to the Comprehensive Air Quality Model with Extensions (CAMx). Version 4.00. Prepared by ENVIRON International Corporation, Novato, CA.

Kallos G., V. Kotroni, K. Lagouvardos, M. Varinou, A. Papadopoulos, 1995: "Possible mechanisms for long range transport in the eastern Mediterranean". 21st NATO/CCMS ITM on Air Poll. Model. and Its Applic., 6-10 Nov., Baltimore, USA. Plenum Press, N.York, Vol 21, pp.99-107.

Kallos, G., V., Kotroni, K., Lagouvardos, M., Varinou, M., Uliasz, A., Papadopoulos 1997: Transport and Transformation of air pollutants from Europe to East Mediterranean Region (T-TRAPEM). Final Report. Athens, Greece, pp.298

Kallos, G., 1997. The regional weather forecasting system SKIRON: an overview. Proceedings of the symposium on regional weather prediction on parallel computer environments, University of Athens, Greece, pp. 109-122.

Kallos, G., V. Kotroni, K. Lagouvardos, and A. Papadopoulos, 1999: On the transport of air pollutants from Europe to North Africa. Geophysical Research Letters. 25, No 5, 619-622.

Kotroni, V., G. Kallos, K. Lagouvardos, M. Varinou, and R. Walko, 1999: Numerical simulations of the meteorological and dispersion conditions during an air pollution episode over Athens, Greece. J. Appl. Meteorol., **38**, pp.432-447.

Luria M., M. Peleg, G. Sharf, D. Siman Tov-Alper, N. Schpitz, Y. Ben Ami, Z. Gawi, B. Lifschitz, A. Yitzchaki, and I. Seter,1996:Atmospheric Sulphur over the East Mediterranean region. JGR, 101, (25917).

Nickovic, S., G.Kallos, A. Papadopoulos and O. Kakaliagou, 2001: A model for prediction of desert dust cycle in the atmosphere. J. Geophysical Res., Vol. 106, D16, 18113-18129.

Papadopoulos A., P. Katsafados, G. Kallos and S. Nickovic, S. Rodriguez, X. Querol, 2003. Contribution of Desert Dust Transport to Air Quality Degradation of Urban Environments, Recent Model Developments. 26th NATO/CCMS ITM on Air Pollution Modeling and its Application, Istanbul, Turkey. Proceedings.

Rodriguez S., Querol X., Alastuey A., Kallos G. and Kakaliagou O., 2001. Saharan dust inputs to suspended particles time series (PM10 and TSP) in Southern and Eastern Spain. Atm. Env. 35/14, 2433-2447.

*Proceedings of the Third International Symposium on Air Quality Management at Urban, Regional and Global Scales. 26-30 September 2005, Istanbul – Turkey*

# MODELLING THE ATMOSPHERIC CHEMISTRY, TRANSPORT, AND DEPOSITION OF SEMI-VOLATILE TOXIC POLLUTANTS

**P.Gbor, F.Meng, D.Wen, F.Yang, B.Zhang and J.J.Sloan***

Waterloo Centre for Atmospheric Sciences, University of Waterloo, 200 University Avenue West, Waterloo, Ontario, N2L 3G1 Canada, *sloanj@uwaterloo.ca

## ABSTRACT

We have investigated the atmospheric chemical and physical transformation and long range transport of toxic materials using the Models-3/*CMAQ* regional chemical transport modelling system. In this report, we focus on the behaviour of mercury and PCBs. For this work, we have added gas phase OH reactions and gas-particle partitioning of these substances to the existing model platform. The results show that long range transport on both particles and in the gas phase occurs to a significant extent for both materials. In the case of mercury, natural emission sources are sometimes larger than anthropogenic ones and in any case must be considered in order to understand the local concentrations.

**Key Words:** Atmospheric Transport, Deposition, Persistent Organic Pollutant, Mercury, Regional Atmospheric Model

## 1. INTRODUCTION

The atmospheric transport and deposition of semi-volatile toxic materials continues to be a significant problem in many parts of the world. (Tsapakis et al., 2003) Long range transport of these compounds is a particular threat to environmentally sensitive areas such as the Arctic. These substances include mercury, pesticides and a wide variety of industrially-related toxins such as PCBs and dioxins. Due to their toxicity and persistence in the environment, many of these, such as PCBs and certain pesticides have been banned for industrial and commercial applications in North America. Despite this, they continue to enter the atmosphere in significant quantities, both from a small number of direct emission sources and from the soil and water residues that remain from previous use. Extensive studies of the movement of these compounds have shown that they are transported for very long distances from the point of emission. The mechanism for this transport is thought to be largely in the gas phase, but it is known that many of these materials partition to aerosols as well (Cousins and Mackay, 2001) and this provides an additional means for their transport.

WCAS has undertaken a program to investigate the atmospheric chemistry, transport and deposition of a series of toxic pollutants. For this presentation, we will focus on Mercury and PCBs. The objectives of the mercury studies are the assessment of the relative importances of anthropogenic and natural mercury emissions and the elucidation of the mechanisms and patterns of its long range transport. To ensure

proper treatment of the global background, we also explored the sensitivity of the model to the mercury boundary conditions. The objectives of the PCBs studies are to compare the roles and contributions of gas and particle phase transport mechanisms and to assess the effects of atmospheric chemistry and physical deposition in their removal.

## 2. METHODOLOGY

### 2.1. Models

The modelling tools used in these studies are based on the U.S. EPA's Models-3/*CMAQ* regional modelling system, driven by the *MM5* meteorology model. For the purposes of these studies, we use special versions of *CMAQ* chemical transport model (CTM) that were modified to handle mercury and PCBs. Details about the *CMAQ-Hg* model can be found in (Bullock and Brehme, 2000).

The *CMAQ* model has been expanded to simulate the transport, transformation and deposition of PCBs. The new *CMAQ* components describe gas/particle partitioning of PCBs and their chemical reactions with OH radicals. In this work, 22 PCB congeners, or specifically PCB-5,PCB-8,,PCB-18,PCB-28,PCB-31,PCB-52,PCB-70,PCB-90,PCB-101,PCB-105,PCB-110,PCB-118,PCB-123,PCB-132,PCB-138,PCB-149,PCB-153,PCB-158,PCB-160,PCB-180,PCB-194,PCB-199, are studied.

PCBs are semi-volatile and partition between the gas and particle phases. In the current model, the major chemical transformations occur in the gas phase (OH reactions) and the major removal occurs in the particle phase (Atkinson R., 1996). Thus the partitioning process is a key factor that controls the behavior and fate of PCBs in atmosphere. In this work, the Junge-Pankow adsorption model is used to describe the gas/particle partitioning(Pankow J.F., 1987). According to this model, the fraction of a semi-volatile organic compound adsorbed to particles, $\phi$, depends on the vapor pressure of the substance at ambient temperature, $P_L$, and the specific surface area of the particles, $\theta$ ($cm^2/cm^3$):

$$\phi = c\theta / (P_L + c\theta) \tag{1}$$

where c is a parameter depending on the chemical being adsorbed and on the nature of the particle.

$$\log P_L = m_L / T + b_L \tag{2}$$

Falconer *et al*.(Falconer R.L., 1994), derived parameters for calculating the temperature dependence of $P_L$ for 32 PCB congeners from available data and used this information to estimate the temperature dependence of 148 PCBs as a function of homolog and number of ortho-chlorines.

The Junge-Pankow model needs the aerosol surface area, which is somewhat uncertain in most regional atmospheric models. In our work, the aerosol surface area is taken to be the sum of the Aitken mode and the accumulation mode calculated by

the *CMAQ* aerosol model. There are also uncertainties in the parameter c and in the low-temperature vapour pressure, but these are less important than those in the surface area.

The possible chemical transformations of PCBs include photolysis and reaction with the hydroxyl (OH) radical, reaction with nitrate(NO3) radical and reaction with ozone(O3). At the present time, we have only implemented the reaction with OH. The rate constants used for the gas-phase reactions of OH with some PCB congeners are taken from the work of Atkinson (Atkinson R., 1996). In the future we will examine the importance of other reactions, including the photolysis of gas-phase PCDD/Fs and the reaction of gas-phase PCDDs with the $NO_3$ radical.

### 2.2. Emissions

Anthropogenic emissions of criteria species and the toxic pollutants were obtained from the US EPA, the US NEI emission inventory and the Canadian NPRI database. The data include waste incineration, power/energy generation, metallurgical processes, chemical manufacturing/processing and other high temperature sources.

The PCB emission inventory is not well developed; there are uncertainties in both emission factors and in the data based on human activities, such as open burning, traffic, manufacturing, etc. In this work, we use the global emission data by (Breivik, 2002;Breivik et al., 2002) which have been developed using a mass-balance approach. The 22 PCB congeners are speciated from total PCB emissions and allocated to grid cells using the population surrogate using the SMOKE emission preprocessing model. The result is shown in Figure 1.

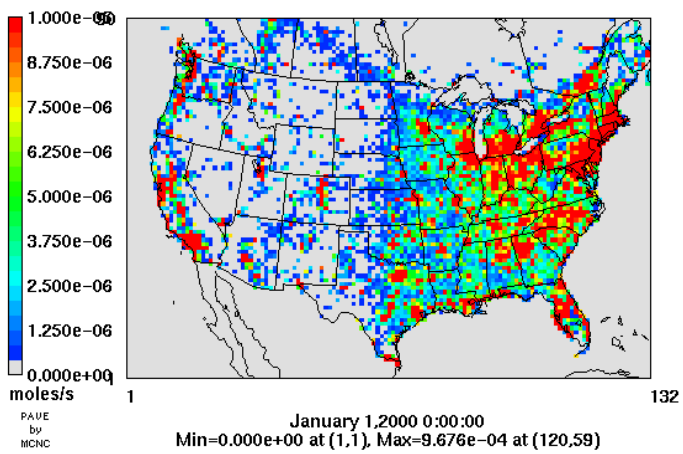


Figure 1. Emission of PCBs at 0:00:00 January 1, 2000

Significant amounts of mercury are known to arise from natural sources. To obtain mercury emissions from natural sources, we created a model to describe the emission of mercury from vegetation, soil and water, using published measurements and laboratory data. Equation 3 is used to estimate Hg transpiration from vegetation (Xu et al., 1999).

$$F = E_c C_s \quad (3)$$

where, $F$ is the $Hg^o$ flux, $E_c$ is the canopy transpiration and $C_s$ is the concentration of $Hg^o$ in the surface soil solution. For emission from bare soil and soil under vegetation canopy, we used Equations 4 and 5 respectively,

$$\ln F = -\frac{\beta}{T_S} + n \ln[Hg]_S + \gamma \tag{4}$$

$$\ln F = aR_{Gc} + b \ln[Hg]_S + c \tag{5}$$

where, $[Hg]_s$ is Hg soil concentration, $T_s$ is the soil temperature, $R_{Gc}$ is the solar radiation reaching the soil under the canopy and $\beta$, $\gamma$, $n$, $a$, $b$, $c$ are constants. Emission from water was estimated using

$$F_W = K_W C_W \tag{6}$$

where, $K_w$ is the mass transfer coefficient and $C_w$ is the concentration of dissolved gaseous mercury in the water. Details of the natural mercury emission model can be found in (Gbor et al., 2004).

## 3. SIMULATION

The mercury simulations were carried out on a domain covering eastern North America, with 75 x 70 grid squares, 36 km grid size and 21 vertical sigma layers, for the period from May 1 to September 30, 2000. The PCB simulations were carried out on a domain covering North America, with 132 x 90 grid squares, 36 km grid size and 15 vertical sigma layers, for the period from January 1 to July 28, 2000. Version 3.6 of the PSU/NCAR *MM5* meteorology model and the Pleim-Xiu Land Surface Model (LSM) (Xiu and Pleim, 2001) were used to generate the meteorology data, which were then processed using *MCIP*. The natural mercury emission model was incorporated into *MCIP*. The mercury and PCB emissions were merged with anthropogenic mercury and criteria emissions using *SMOKE*. The gridded emissions output from *SMOKE* were fed to the modified *CMAQ* model to simulate the behaviour of the toxic substances in the atmosphere. The models were run for several scenarios to examine the effects of reducing or eliminating various combinations of the anthropogenic and natural mercury emissions.

## 4. RESULTS AND DISCUSSIONS

### 4.1. Mercury

The comparison between natural and anthropogenic mercury emissions is shown in Figure 2. High anthropogenic mercury emissions occur in the north eastern part of the U.S., while natural emissions dominate in the northern and western part of the domain. Emissions from the lakes and ocean were obtained using the natural mercury emission model. The anthropogenic emission averaged over the whole domain for the modelling period was 1.4 $ngm^{-2}h^{-1}$ while the natural emission was 2.9 $ngm^{-2}h^{-1}$. This is consistent with the estimate that natural emissions are about twice the anthropogenic emissions on a global scale (Seigneur et al., 2004).

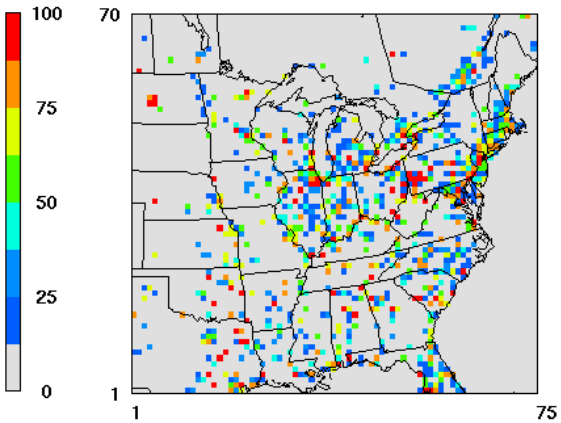


Figure 2. Percent of mercury emissions contributed by anthropogenic emissions for each grid cell from May to September, 2000

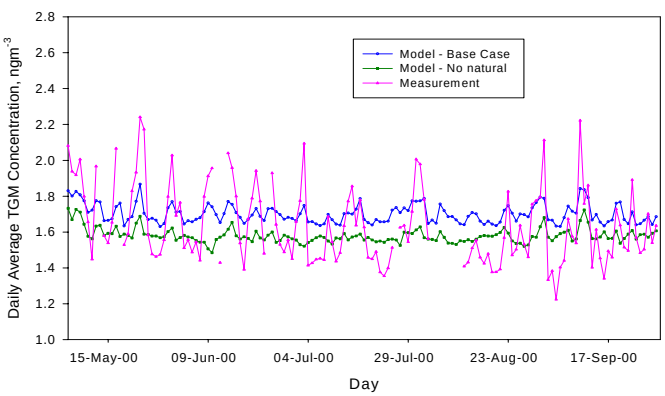


Figure 3. Modeled and measured daily average TGM for Egbert, Ontario, from May to September, 2000.

Figure 3 shows a comparison between model and measurements of Total Gaseous Mercury (TGM) for the Egbert, Ontario site, which is a rural area north of Toronto. The model reproduced the concentration trends quite well (R = 0.8162). Neglecting natural emission reduced the correlation (R = 0.5115). Similar results were obtained for all three monitoring sites within the domain. The effect of global background on mercury concentration is illustrated in Figure 4. The background contributes over 80% of the average TGM concentration in the domain. This illustrates the global nature of mercury pollution. Elemental mercury has atmospheric residence time of about 1 to 2 years and as such can be transported through long distances. Though the global background contributes significantly to total gaseous mercury in the atmosphere, local anthropogenic emissions may have a greater importance for

mercury deposition near the sources. Figure 5 shows the effects of local emissions on deposition of mercury. It shows dry deposition of elemental, divalent and particulate mercury attributed to anthropogenic emissions in Canada. The spread of elemental mercury deposition (Figure 5a) is wider than that of divalent mercury (Figure 5b), illustrating the larger transport distance of elemental mercury, compared to divalent and particulate mercury. It also indicates that anthropogenic emissions have a more direct effect on locations closer to the emission sources. Anthropogenic emissions in Canada are about 10 times less than those in the U.S., but mercury is transported in both directions across the U.S./Canada border, depending on the synoptic weather. These results show that regional as well as global cooperation is required if the problem of mercury pollution is to be resolved.

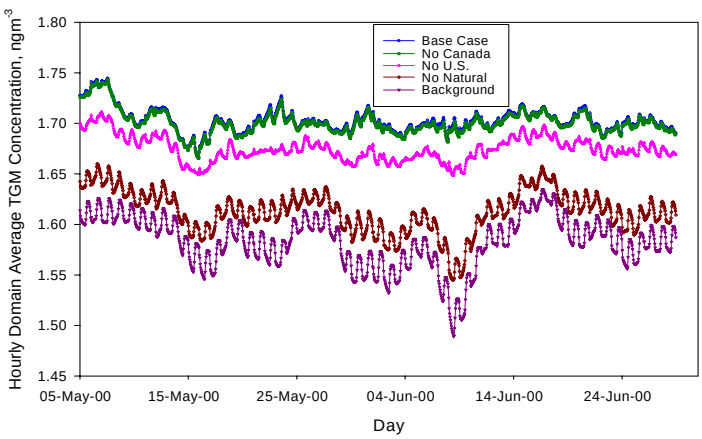


Figure 4. Average TGM concentration in domain for different scenarios.

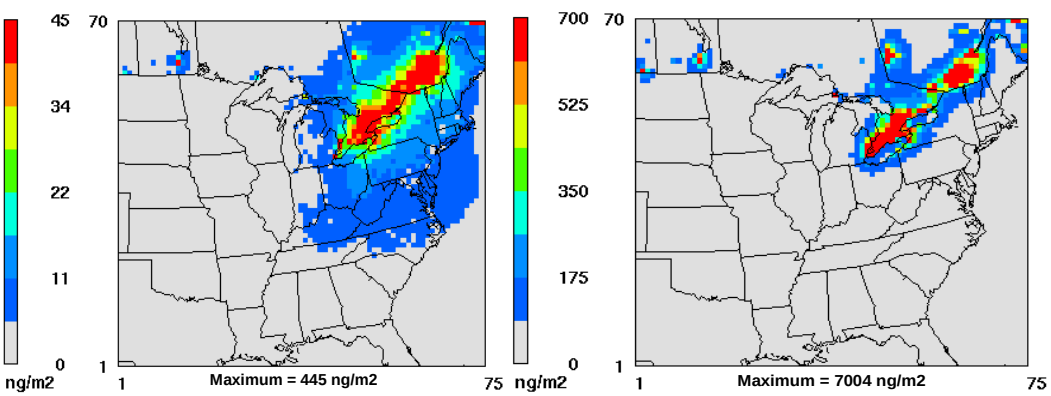


Figure 5. Total deposition of (a) elemental and (b) sum of divalent and particulate mercury in domain due to anthropogenic emissions in Canada. Note: Maximum colour scale is 10% of the maximum grid value.

### 4.2. PCBs

The modelled concentration distributions of all PCB congeners are similar since their emissions are speciated proportionally from total emission data. Figure 6 shows the gas- and particle-phase concentration and deposition of the PCB-8 congener. Compared with the distribution of emissions shown in Figure 6, these concentration data show that considerable regional transport of these materials occurs. For example, a plume of high concentration extends from the northeastern US into the Atlantic ocean and from the southwestern US into the Gulf of Mexico. High concentrations occur in the eastern continental US and Canada including the densely populated Great Lakes area. California also has high concentrations. (Although they are probably significant, emissions from Mexico were ignored in this work due to lack of quantitative emission data.) most of the concentration of PCB-8 is in the gas phase due to its relatively high vapour pressure. As the number of chlorine atoms in the PCB molecule increases, the amount partitioning to particles also increases.

The most important removal process is wet deposition, even for congeners like PCB-8 which has only two chlorine atoms and is mostly found in the gas phase. The maximum wet deposition of particle-phase PCB-8 in the domain is 2.393E-08 kg/hectare while maximum wet deposition of gas-phase PCB-8 is 3.852E-10 kg/hectare and the dry deposition of gas-phase PCB-8 is only 6.791E-12 kg/hectare.

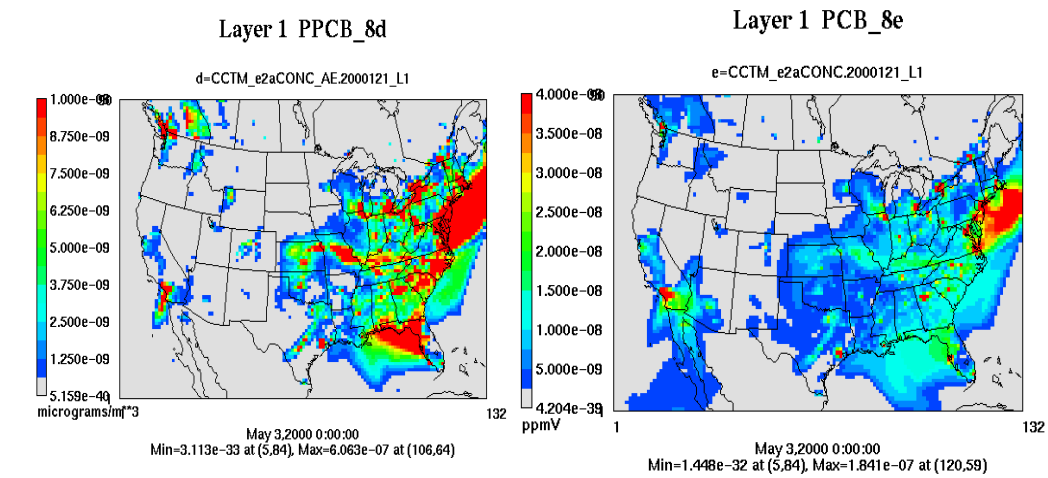


**(a)** **(b)**

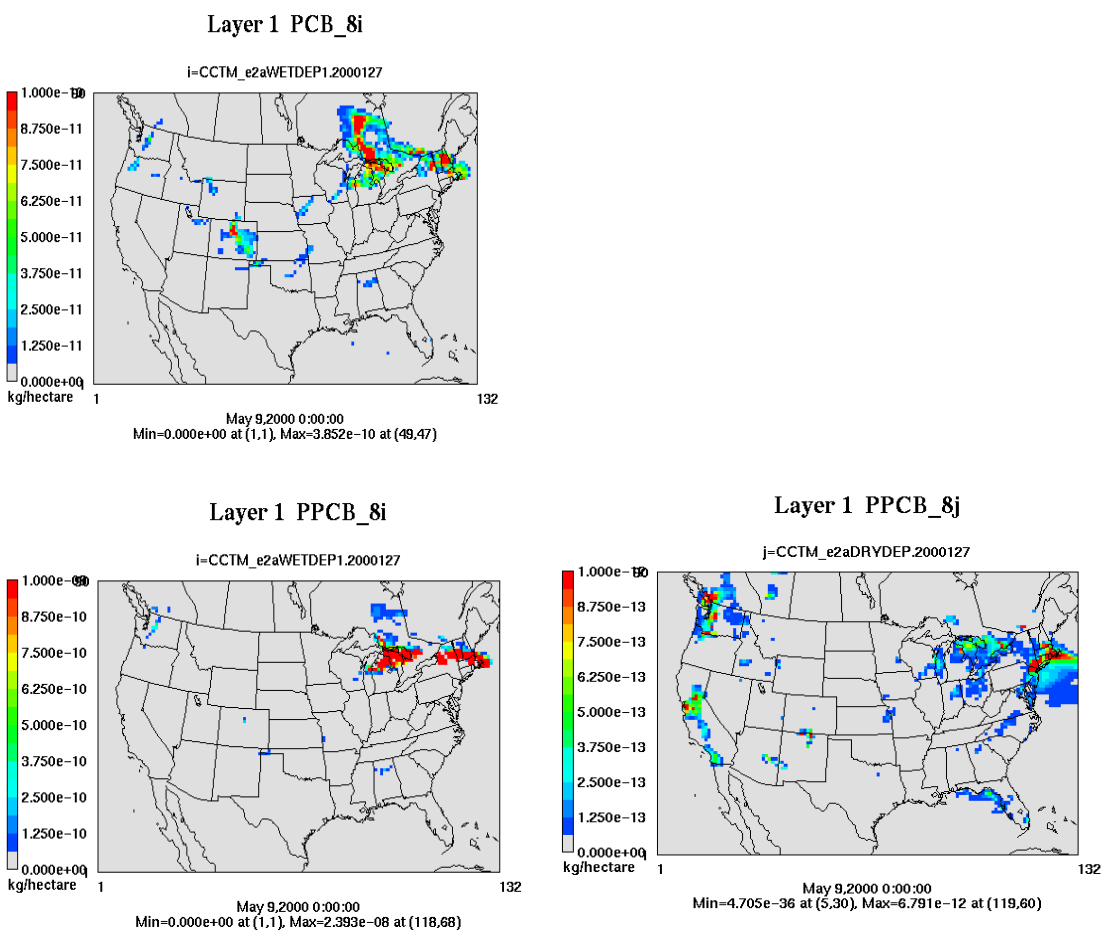


(c) (d)

Figure 6. Concentration and deposition of gas and particle phase PCB-8 at 0:00GMT May 9, 2000. (a) concentration of gas-phase PCB-8; (b) concentration of particle-phase PCB-8; (c) wet deposition of gas-phase PCB-8; (d) wet deposition of particle-phase PCB-8; (e) dry deposition of particle-phase PCB-8

Figure 7 shows the comparison of modeling results with measured gas-phase PCB data from the Integrated Atmospheric Deposition Network(IADN). The model results show fair agreement with the measurements. For most stations, the model results are over estimated except for one remote station (EGH).

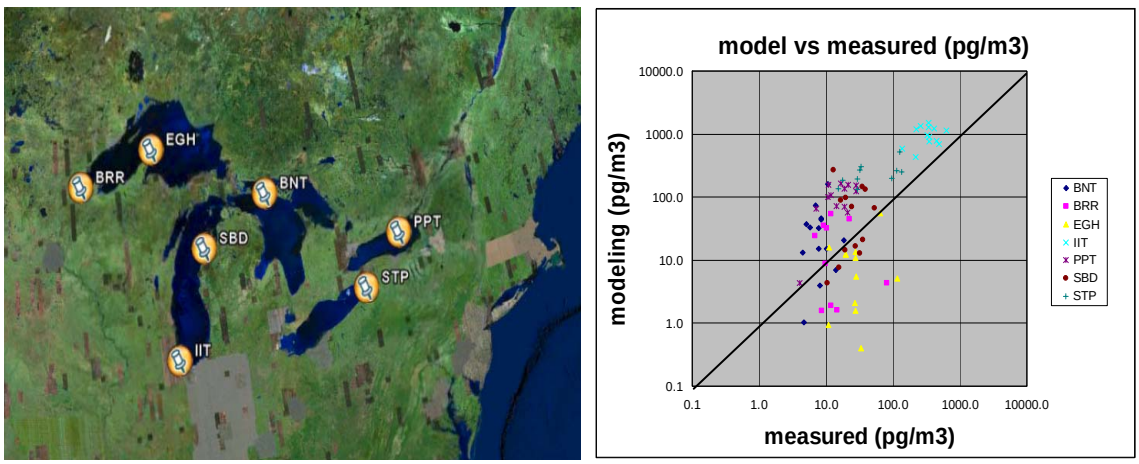


Figure 7. Comparison of modelling results with measured gas-phase PCBs data from the Integrated Atmospheric Deposition Network(IADN) for the period of January – August, 2000

## 5. CONCLUSIONS

The atmospheric transport and deposition of mercury and PCBs, which are representative of several varieties of semi-volatile toxic materials, were studied using modified versions of EPA's *CMAQ* model.

Mercury emissions from natural sources were found to be very important, contributing

about two-thirds of the total emission in the domain. Anthropogenic emissions were concentrated mainly in urban centers and areas with large combustion facilities. Good correlation was found between model simulations of total gaseous mercury and measurements, especially if natural emissions are considered. The results also show that long range transport of anthropogenic mercury is very important throughout North America, but transport distances differ for the common mercury species (elemental, divalent and particulate). Furthermore, the global background was found to contribute significantly to the amount of mercury in the domain. Therefore global efforts are required if the impact of mercury pollution on our ecosystem is to be minimized.

The *CMAQ* model has been expanded to include OH chemistry and gas-particle partitioning of PCBs. The Junge-Pankow model was used to describe the adsorption partitioning. Emissions data have been spatially allocated to the model grid by population. For most monitoring stations of the IADN, the simulations show generally acceptable agreement with measurement, but more detailed information about the location of the emission sources would lead to better model performance.

The results show that there exists significant regional scale transport. Deposition of the particle phase material is the most important removal process of PCBs in the atmosphere.

The aerosol surface area is important in the Junge-Pankow gas/particle partitioning model, which is unfortunate, because there are still uncertainties in the aerosol component of the *CMAQ* model. In particular, the description of the primary emission may not be complete and accurate. There is also some uncertainty in the secondary organic aerosol formation. Preliminary comparison with measured results shows that the model underestimates the total aerosol surface area concentration. Although it is still unclear, this might be due to averaging over a relatively coarse grid, which would reduce peak concentrations. As a consequence of this, the removal of particle phase of PCBs may be underestimated. Further comparison with measured deposition data is in progress.

## REFERENCES


Atkinson R., 1996, Atmospheric Chemistry of PCBs, PCDDs and PCDFs: Issues in Envrionmental Sciences and Technology, v. 6, p. 53-72.

Breivik,K, 2002, Towards a global historical emission inventory for selected PCB congeners - a mass balance approach 1. Globla production and consumptioin: the Science of the Total Environment, p. 181-198.

Breivik,K, A Sweetman, J M Pacyna, K C Jones, 2002, Towards a global historical emission inventory for selected PCB congeners - a mass balance approach 2. Emission: the Science of the Total Environment, v. 290, p. 199-224.

Bullock,OR, K A Brehme, 2000, Atmospheric Environment, v. 36, p. 2135-2146.

Cousins,IT, D Mackay, 2001, Gas - Particle partitioning of organic compounds and its interpretation using relative solubilities: Environmental Science & Technology, v. 35, p. 643-647.

Falconer R.L., 1994, Vapor pressures and predicted particle/gas distributions of polyrinated biphenyl congeners as functions of temperature and ortho-chlorine substitution: Atmospheric Envrionment, v. 28.

Gbor,PK, D Wen, F Meng, F Yang, J J Sloan, 2004, Modeling of Mercury Emission Transport and Deposition in North-Eastern North America: Abstract of Papers, 2004 Models-3 Conference, Chapel Hill, NC, United States, October 18 - 20, 2004.

Pankow J.F., 1987, Review and comparative analysis of the theories on partitioning between the gas and aerosol particulate phases in the atmosphere: Atmospheric Envrionment, v. 21, p. 2275-2283.

Seigneur,C, K Vijayaraghavan, K Lohman, P Karamchandani, C Scott, 2004, Global Source Attribution for Mercury Deposition in the United States: Environmental Science and Technology, v. 38, p. 555-569.

Tsapakis,M, E G Stephanou, L Karakassis, 2003, Evaluation of atmospheric transport as a nonpoint source of polycyclic aromatic hydrocarbons in marine sediments of the Eastern Mediterranean: Marine Chemistry, v. 80, p. 283-298.

Xiu,AJ, J E Pleim, 2001, Development of a land surface model. Part I: Application in a mesoscale meteorological model: Journal of Applied Meteorology, v. 40, p. 192-209.

Xu,XH, X S Yang, D R Miller, J J Helble, R J Carley, 1999, Formulation of bi-directional atmosphere-surface exchanges of elemental mercury: Atmospheric Environment, v. 33, p. 4345-4355.

*Proceedings of the Third International Symposium on Air Quality Management at Urban, Regional and Global Scales. 26-30 September 2005, Istanbul – Turkey*

# THE EVALUATION OF THE AIR QUALITY IMPACT OF AN INCINERATOR BY USING MM5-CMAQ-EMIMO MODELLING SYSTEM: NORTH OF SPAIN CASE STUDY

**R. San José[1], J. L. Pérez[1] and R. M. González[2]**

[1]Environmental Software and Modelling Group, Computer Science School, Technical University of Madrid, Campus de Montegancedo, Boadilla del Monte 28660 Madrid (Spain) roberto@fi.upm.es
[2]Department of Meteorology and Geophysics, Complutense University of Madrid, 28040 Madrid (Spain)

## ABSTRACT

The use of sophisticated air pollution modeling systems to evaluate the impact of different industrial plant emissions is currently done in extensive way. MM5-CMAQ (PSU/NCAR and EPA, USA) is one of the most applicable air quality modeling systems to evaluate those impacts. In this contribution we present the methodology and results obtained when applying the MM5-CMAQ air quality modeling system for evaluating the potential impact of an incinerator in San Sebastian (Basque Country, Spain). We have used the EMIMO (UPM, Spain) emission model to simulate the emissions from biogenic and anthropogenic sources including traffic and tertiary sector sources. The application also includes the study of the relative impact of a section of an important highway in the surrounding areas of the expected location of the incinerator. The system has been prepared to simulate also Cadmium, Arsenic, Nickel, Lead and Benzo(a)pyrene air quality impacts. The PCDD/F air concentrations have been determined for the 16 toxic dioxins and furans as determined in the bibliography. The criteria pollutants such as CO, NOx, SO2, PM10 and O3 have also been determined according to the different EU Directives which limit the values of such a pollutants for different periods of time.

**Key Words:** Air Quality, Ozone Concentration, Suspended Particulate Matter, Dioxins and Furans, Incinerator

## 1. INTRODUCTION

The use of complex numerical air quality modelling systems has increased in the last years for evaluating the impact of different industrial plants and also for air quality simulations over city and regional areas. The main reason to use these sophisticated air quality modelling systems is the increase on computer power availability. Due to the high accuracy of the so-called third generation of air quality modelling systems – which includes complex chemical carbon mechanism, aqueous and aerosol chemistry – the use of these systems is highly recommended particularly for secondary pollutants such as O3 and PAN and for chemically active primary pollutants such as NO and NO2. The complexities involved in the particulate matters transformations recommend the use of these complex numerical models. In this contribution we show

the implementation of a modified version of MM5-CMAQ-EMIMO for carrying on an air quality impact analysis for installing an incinerator in the San Sebastián – Donostia (Basque Country (Spain). The study includes also the relative impact of six large industrial plants located in the surrounding area and already existing and finally the relative impact of an important highway located also in the surrounding area.

The modified CMAQ model (EPA USA, 2004) includes Poly-Chlorinated Dibenzo-p-Dioxins and Dibenzo-Furans (dioxins and furans). The model represents their cogeners as divided between gaseous and aerosol forms that exchange mass based on theoretical coefficients for gas to particle portioning. Modelled metals are included in CMAQ as part of the non-reactive aerosol component. Metals modelled are: As, Cd, Ni and Pb. In additional Benzo(a)pyrene (PAH) is also modelled. The model is implemented in a cluster platform in order to be used as a real-time air quality forecasting system by using the ON-OFF approach. The emissions of the projected incinerator in the ON run are incorporated by using the height of the chimney, the prescribed exit gas velocity, diameter of chimney and the limit emission values (worst scenario) prescribed in the Directive/2000/76/CE. The OFF run is done by using EMEP POP and PAH emission inventory. The system is mounted over one mother domain of 400 x 400 km with 9 km spatial resolution and two nesting levels: 100 km model domain with 3 km spatial resolution and 24 km with 1 km spatial resolution. All model domains with 23 vertical layers up to 100 mb and centered over the UTM coordinates prescribed for the projected incinerator. EPER EU industrial emissions (May, 2004) of the surrounding large point industrial sources are used. Results are compared with the target values included in the proposal for a Directive of the European Parlament and of the Council (ENV 194 CODEC 439).

Different other meteorological and dispersion modeling systems exist such as EMEP, RSM, CAMx, etc. (Cleverly et al., 1997; Collins et al., 1997; Derwent, R. and Jenkin M., 1991; Lagner et al., 1998; Roemer et al., 1996; Whitby K.T., 1978; Walcek C., 2000; Schmidt et al. 2001; San José et al. 1994,1996 and 1997) which have similar performance than the one used in this application.

## 2. THE MM5-CMAQ-EMIMO MODELLING SYSTEM

The MM5 model is a non-hydrostatic mesoscale meteorological model (Pennsylvania State University / National Center for Atmospheric Research) (Dudhia, 1993; Grell et al. 1994) which is widely used around the world for meteorological research and also for operational meteorological use. The MM5 meteorological model is capable to produce 3D wind, temperature, humidity and other important meteorological parameters and variables during simulations of several hours and days. MM5 is a nested-grid primitive-equation model, which uses a terrain following sigma (non-dimensionalized) vertical coordinates. CMAQ model (Community Multiscale Air Quality Modelling System) (Byun et al., 1998) is a Comprehensive Air Quality Model which simulates the chemical transformations and the dispersion of the pollutants in a 3D domain. The input meteorological data is taken from the MM5 meteorological model. CMAQ model is structured in a full modular way. The different configurations should be consistent with those prepared for the meteorological model simulations. Both models, MM5 and CMAQ, are feed with

emission data sets which in our case are produced by the EMIMO modeling system (San José et al., 2002). EMIMO is using different global and European data sets which are produced as official data, to estimate the emissions at very high spatial and temporal resolutions (1 km, and 1 hour). EMIMO is currently using EMEP, GEIA and EDGAR global and European datasets (European Topic Center on Air and Climate Change; Gardner et al., 1997; Pacyna et al., 1999; San José et al., 1998, 2004).

The MM5 model has been implemented over three nesting domains (one mother level and two nesting levels). Figure 1 shows the three nesting domains centered in the location where the incinerator is planned in San Sebastian (North of Spain).

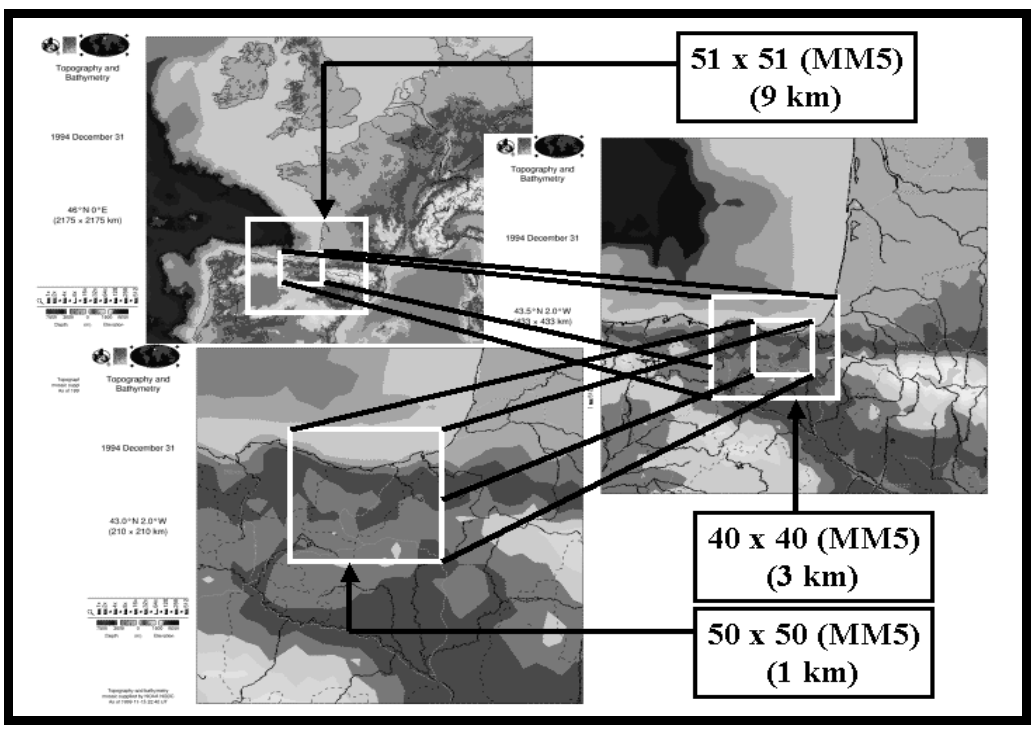


Figure 1. MM5 architecture design over the location in San Sebastián where the incinerator is planned.

The MM5 model is using GSM model (Global Spectral Model) output for initial and boundary conditions. In case of CMAQ, default profiles are used according to CMAQ configuration file. The MM5-CMAQ-EMIMO modeling system has been run for 12 periods of 120 hours each one for the three different model domains along the Nov., 2003 – Oct.,2004 year. Each 120 hour period has been selected for each month. The selection procedure is based on the mobile average over 120 hours for each month by using monitoring data from different air quality monitoring stations. So that, the selected periods corresponds with average pollution periods for the different criteria pollutants. The MM5 model has been run by using the assimilation meteorological data from the Basque Country meteorological network for the selected period of time. The CMAQ model has been implemented exactly into the MM5 model domains. In both models, 23 vertical layers have been used.

CMAQ – EMIMO modeling system has been run simultaneously over the 1440 hours (covering the period Nov., 2003 – Oct., 2004) with two different scenarios: ON and OFF. The OFF scenarios is a full emission scenario including biogenic and antropogenic sources provided by EMIMO. These includes all EPER emission data sets and information provided by different industrial emission sources which are not included in EPER but provided directly by the different companies. The ON scenarios is exactly the same than OFF scenario but including the characteristics and emissions of the projected incinerator. This information includes: a) height of the chimney; b) Diameter of the internal output area in the chimney; c) Temperature at exit of emitted gases; d) Exit velocity of gases; e) Flux of gases emitted for each pollutant. So that, the differences in time and space between both simulations are the expected pollution impact of the projected incinerator over the different model domains for each pollutant. In addition to this, several additional impact studies were performed in order to know the relative importance of such a impact compared with the emissions in the 45 km of the highway surrounding the location of the projected incinerator. Additionally, 6 different large industrial plants located in the 1 km model domain (45 x 45 km) were studied by using the same procedure.

In order to establish the relative impact of the A8 Highway in the surrounding areas, a detailed traffic emission inventory was performed based on the accounting detailed data sets provided by the Basque Country Government.

The chemical mechanism used in CMAQ model was the CBM-IV with aqueous and aerosol chemistry (Gery et al. 1989; Stockwell et al. 1977). We have added the different metals (non-reactive species) to the chemical FORTRAN code and also we have implemented the dioxins and furans mechanism provided by Hutzell W.T. (2002). The PCDD/F chemical mechanism incorporates 10 different furans and 6 dioxins as shown in Table 1.

Table 1. Toxic Dioxins and Furans analyzed in the present experiment and the correspondent Toxic Equivalent Factor.

| | Name | Toxic Equivalent Factor |
|---|---|---|
| 2,3,7,8 | TCDD | 1 |
| 1,2,3,7,8 | PeCDD | 0,5 |
| 1,2,3,4,7,8 | HxCDD | 0,1 |
| 1,2,3,6,7,7 | HxCCD | 0,1 |
| 1,2,3,7,8,9 | HxCDD | 0,1 |
| 1,2,3,4,6,7,8 | HpCDD | 0,01 |
| 2,3,7,8 | TCDF | 0,1 |
| 2,3,4,7,8 | PeCDF | 0,5 |
| 1,2,3,7,8 | PeCDF | 0,05 |
| 1,2,3,4,7,8 | HxCDF | 0,1 |
| 1,2,3,6,7,8 | HxCDF | 0,1 |
| 1,2,3,7,8,9 | HxCDF | 0,1 |
| 2,3,4,6,7,8 | HxCDF | 0,1 |
| 1,2,3,4,6,7,8 | HpCDF | 0,01 |
| 1,2,3,4,7,8,9 | HpCDF | 0,01 |
| | OTCD | 0,001 |

The MM5-CMAQ-EMIMO modeling system has been calibrated by comparing the model results with the observations taken in the different monitoring stations (18) located at the Basque Country and provided by the Basque Government. Figure 2 and 3 show the comparison between observations at Mondragón and Azpeitia monitoring stations for O3 and PM10 with the simulated data obtained by the MM5-CMAQ-EMIMO modeling system.

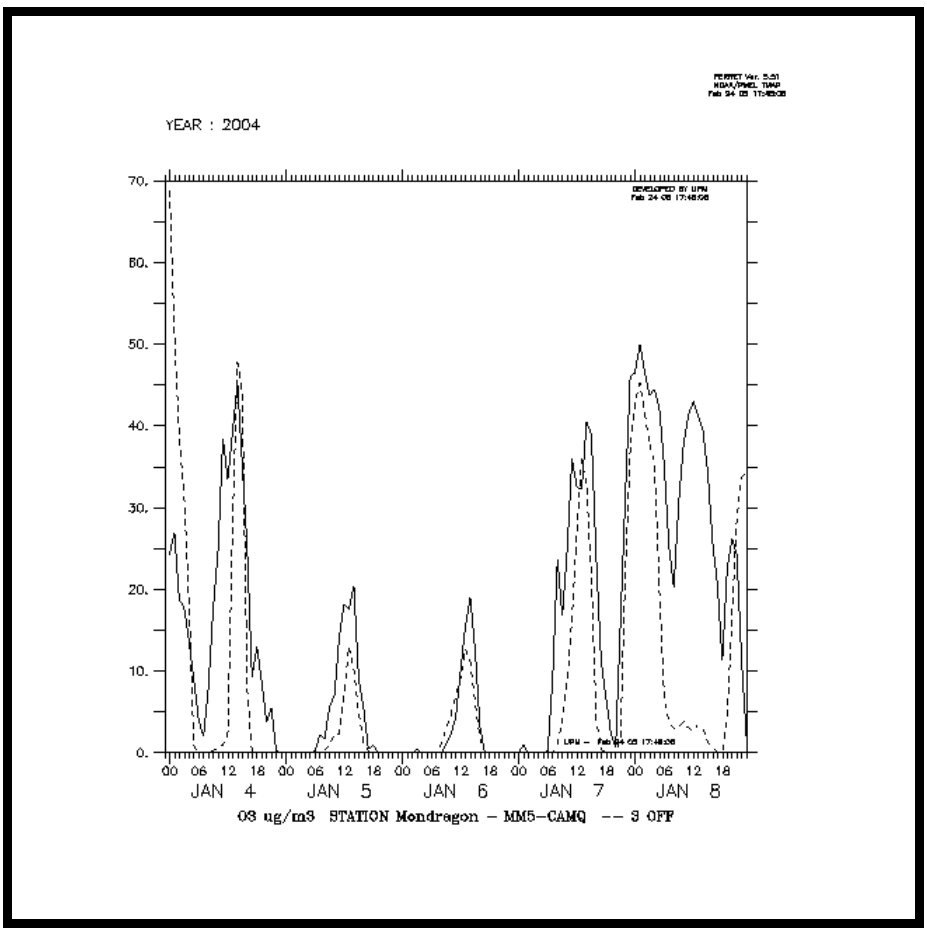


Figure 2. Comparison between O3 observations and simulated data as produced by MM5-CMAQ-EMIMO modelling system for Jan, 4-8, 2004 at Mondragón monitoring station in the 3 km spatial resolution model domain

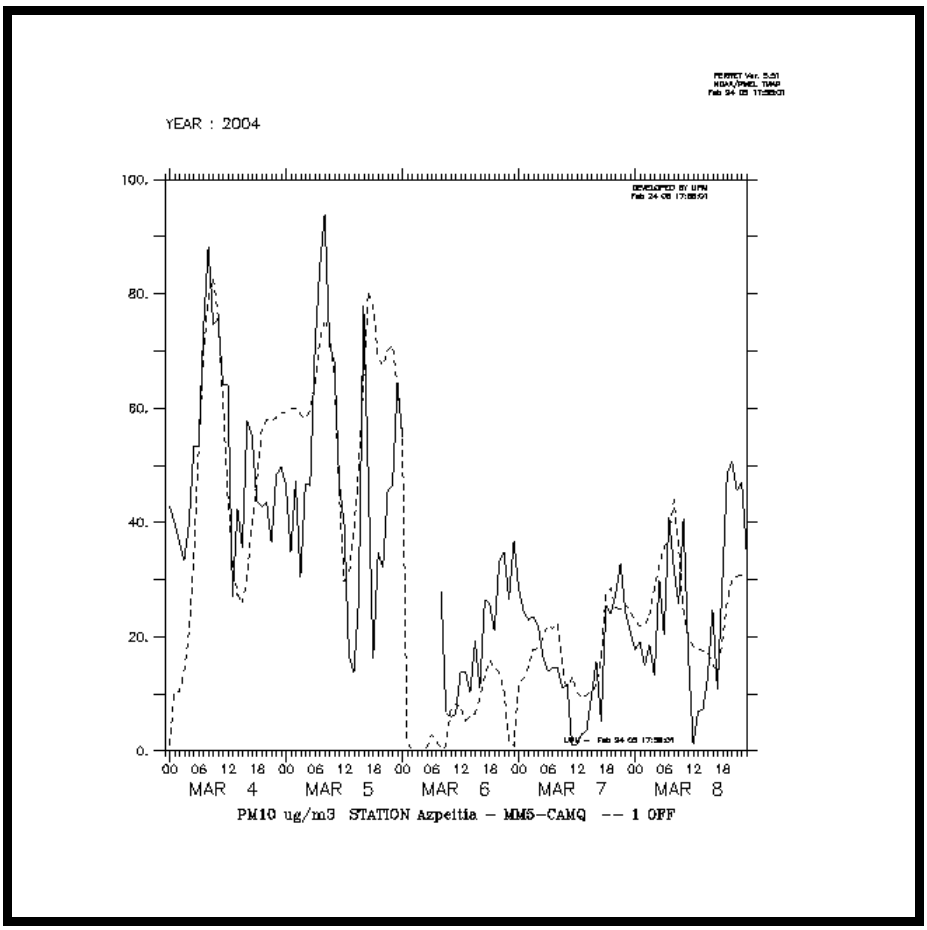


Figure 3. Comparison between PM10 observations and simulated data as produced by MM5-CMAQ-EMIMO modelling system for March, 4-8, 2004 at Azpeitia monitoring station in the 1 km spatial resolution model domain.

## 3. RESULTS

The results are a huge database of approximately 100 Gbytes of information which should be scanned according to the rules expressed in the different EU Directives to establish the possible exceedances and determine those due to the projected incinerator emissions. The results show that the PCDD/F impact is reduced although in some areas and times the percentage increase can be up to 70 %. The PCDD/F values are not limited in the actual EU Directives but WHO rules indicate that the concentrations should be as low as possible. The levels found are in the order of magnitude of fentogramme ($10^{-15}$). Figure 4 shows the averaged values between ON and OFF scenarios for the total PCDD/F species (16). Figure 5 shows the percentile 99,8 of the absolute differences between both scenarios for NO2 over the 1 km spatial resolution model domain. Maximum vales are not higher than 65 $\mu g m^{-3}$.

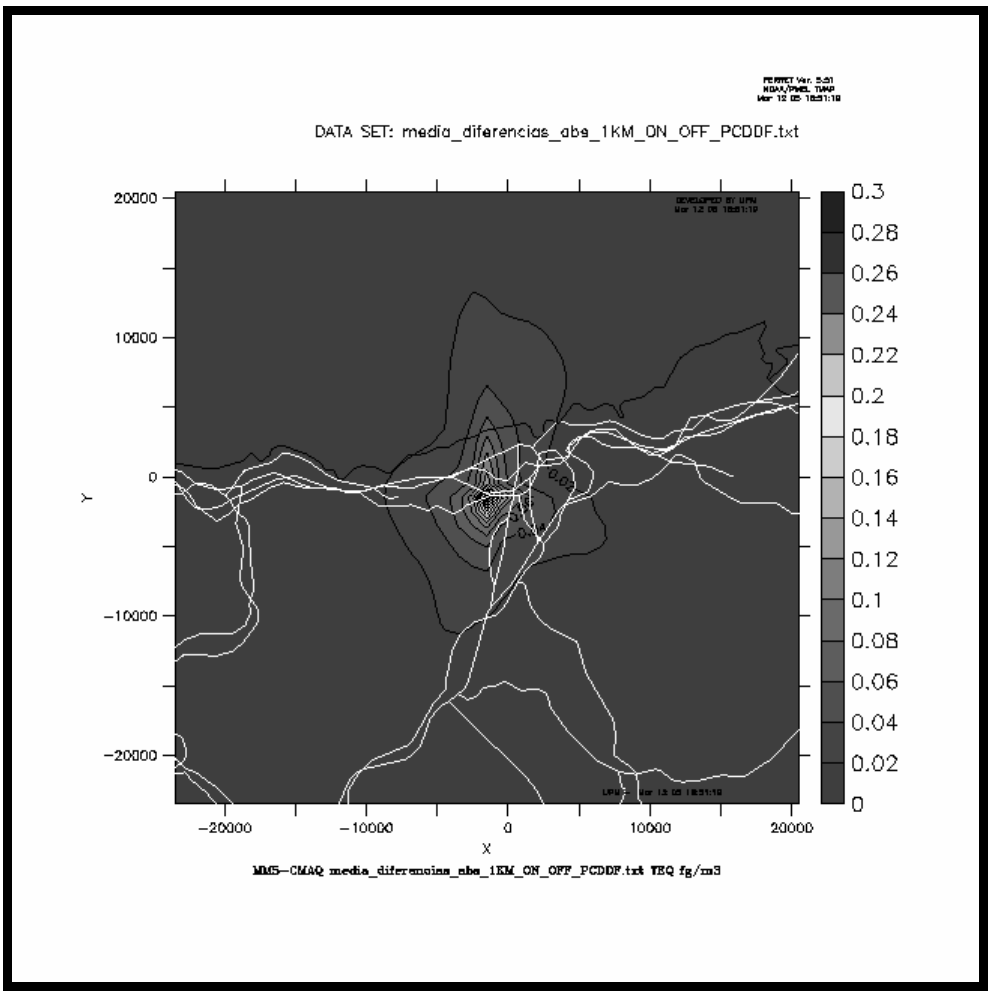


Figure 4. Average (60 days) of the differences between scenarios ON and OFF for the dioxins and furans for the 1 km spatial resolution model domain. Maximum differences are up to 0,5 $10^{-15}$ TEQ g/m3.

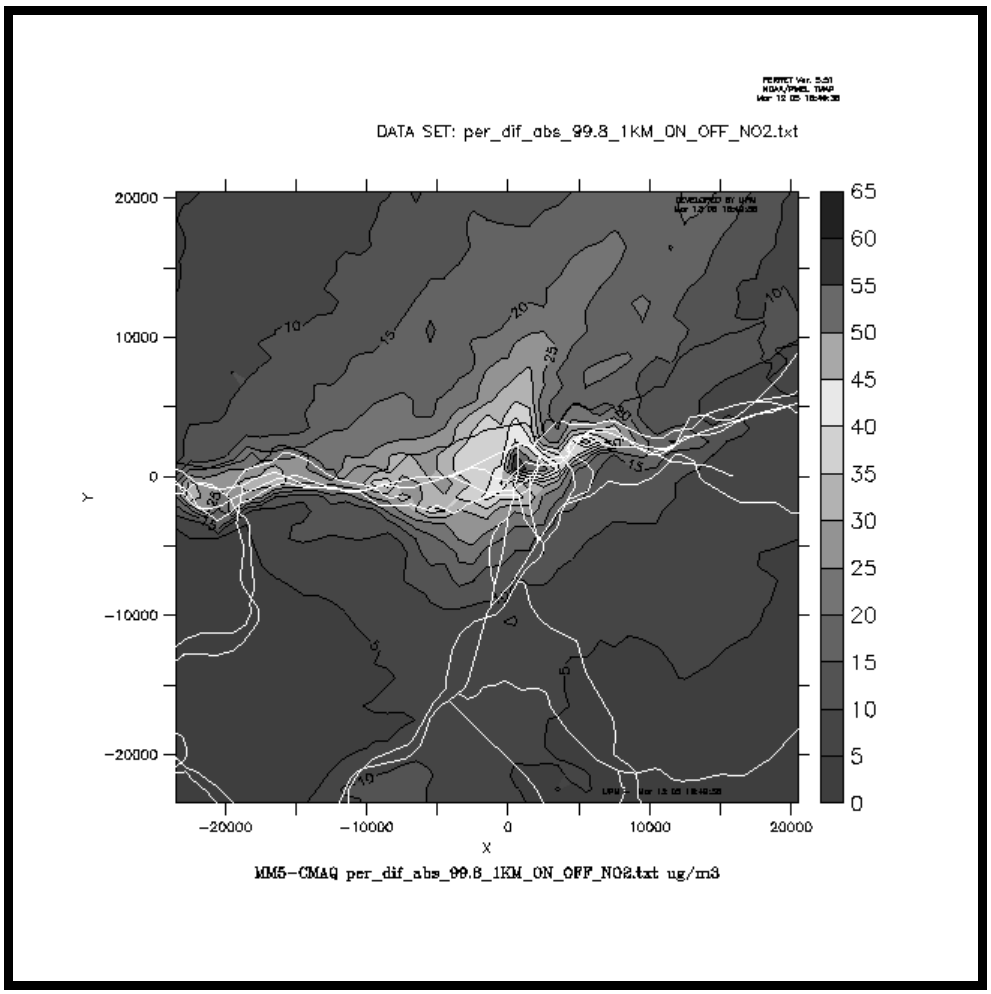


Figure 5. Percentile 99,8 of the absolute differences between scenarios ON and OFF for NO2 in the 1 km spatial resolution model domain. Maximum differences are about 65 $\mu gm^{-3}$

## 3. CONCLUSION

We have implemented the MM5-CMAQ-EMIMO model domain to study the impact of a projected incinerator in the suburban areas of San Sebastián (Basque Country, Spain). The system has been proved to be an excellent tool for such a type of studies since it is capable to analyze with high accuracy differences in the order of magnitude of fentogrammes (dioxins and furans). The system has also been used to compare the results with those obtained with actual large industrial plants located in the area and compare the impacts with those expected to be obtained by the projected incinerator. The study has cover the criteria pollutants (CO, NOx, SO2, PM10 and O3), EU Directive metals and PAH (Nickel, Cadmium, Arsenic and B[a]P) and 16 dioxins and furans (10 dioxins and 6 furans) following the chemical mechanism proposed by Hutzell W.T. (2002) (EPA, USA).

## 4. ACKNOWLEDGEMENTS

We would like to thank W.T. Hutzell for the PCDD/F mechanism implemented into the CMAQ modeling system. PSU/NCAR and EPA (US) for the MM5-CMAQ modeling system. Basque Country Government for the air quality monitoring, meteorological and industrial datasets.

## REFERENCES

Byun, D.W., J. Young, G. Gipson, J. Godowitch, F. Binkowski, S. Roselle, B. Benjey, J. Pleim, J.K.S. Ching, J. Novak, C. Coats, T. Odman, A. Hanna, K. Alapaty, R. Mathur, J. McHenry, U. Shankar, S. Fine, A. Xiu and C. Jang (1998). Description of the Model-3 Community Multiscale Air Quality (CMAQ) model. Proceedings of the American Meteorological Society 78th Annual Meeting, Phoenix, AZ, Jan 11-16, 1998: 264-268.

Cleverly, D. H., Schaum, J., Schweer, G., Becker, J., and Winters, D. (1997). "The Congener Profiles of Anthropogenic Sources of Chlorinated Dibenzo-p-Dioxins and Chlorinated Dibenzofurans in the United States," Organohalogen Compounds, 32: 430-435.

Collins W.J., Stevenson D.S., Johnson C.E. and Derwent R.G. (1997). Tropospheric ozone in a global scale3D Lagrangian model and its response to NOx emission controls. J. Atmos. Chem., 86, 223-274.

Derwent, R. and Jenkin M. (1991). Hydrocarbons and the long-range transport of ozone and PAN across Europe. Atmospheric Environment 8, 1661-1678.

European Topic Center on Air and Climate Change (http://air-climate.eionet.eu.int/databases/MDS/index_html).

Gardner R.K., Adams K., Cook T., Deidewig F., Ernedal S., Falk R., Fleuti E., Herms E., Johnson C., Lecht M., Lee D., Leech M., Lister D., Masse B., Metcalfe M., Newton P., Schmidt A., Vandenberg C. and van Drimmelen R. (1997). The ANCAT/EC global inventory of NOx emissions from aircraft. Atmospheric Environment 31, 1751-1766.

Gery M.W., Whitten G.Z., Killus J.P. and Dodge M.C (1989), A photochemical kinetics mechanism for urban and regional scale computer modelling, Journal of Geophysical Research, 94, D10, pp. 12925-12956.

Grell G.A., Dudhia J. And Stauffer D.R. (1994). A description of the Fifth-Generation Penn State/NCAR Mesoscale Model (MM5). NCAR/TN- 398+ STR. NCAR Technical Note.

Hutzell, W.T. A regional model for PCDD/F's based on a photochemical model for air quality and particulate matter. Presented at: Special Session on Air Toxics American Geophysical Union, San Francisco, CA, December 6-10, 2002.

Langner J., Bergstrom R. and Pleijel K. (1998). European scale modeling of sulfur, oxidized nitrogen and photochemical oxidants. Model development and evaluation for the 1994 growing season. SMHI report RMK No. 82. Swedish Met. And Hydrol. Inst., SE-601 76 Norrkoping, Sweden.

Pacyna J.M., Breivik K. and Wania F.. [1999] Final report for Project POPCYCLING-Baltic. EU DGXII, Environment and Climate Program ENV4-CT96-0214. Available on CD-rom including technical report, the emission and

environmental databases as well as the POPCYCLING-Baltic model. NILU, P.O. Box 100, N-2027 Kjeller, Norway.
Roemer M., Boersen G., Builtjes P. and Esser P. (1996). The budget of ozone and precursors over Europe calculated with the LOTOS model. TNO publication P96/004, Apeldoorn, The Netherlands.
San José R., Rodriguez L., Moreno J., Palacios M., Sanz M.A. and Delgado M. (1994) Eulerian and photochemical modelling over Madrid area in a mesoscale context, Air Pollution II, Vol. 1Computer Simulation, Computational Mechanics Publications, Ed. Baldasano, Brebbia, Power and Zannetti., pp. 209-217.
San José R., Cortés J., Moreno J., Prieto J.F. and González R.M. (1996) Ozone modelling over a large city by using a mesoscale Eulerian model: Madrid case study, Development and Application of Computer Techniques to Environmental Studies, Computational Mechanics Publications, Ed. Zannetti and Brebbia, pp. 309-319.
San José R., Prieto J.F., Castellanos N. and Arranz J.M. (1997) Sensititivity study of dry deposition fluxes in ANA air quality model over Madrid mesoscale area, Measurements and Modelling in Environmental Pollution, Ed. San José and Brebbia, pp. 119-130.
San José R., Cortés J., Prieto J.F and González R.M. (1998) Accurate ozone prognostic patterns for Madrid area by using a high spatial and temporal Eulerian photochemical model. Environmental Monitoring and Assessment, Vol. 52, pp. 203-212 (1998) Ed: Kluwer Academic Publishers. (ISSN: 0167-6369; ISBN: 0-7923-5127-4).
San José R., Pérez J.L. and González R.M. (2004) A mesoscale study of the impact of industrial emissions by using the MM5-CMAQ modelling system, International Journal of Environment and Pollution 2004 - Vol. 22, No.1/2 pp. 144 – 162.
Schmidt H., Derognat C., Vautard R. and Beekmann M. (2001). A comparison of simulated and observed ozone mixing ratios for the summer 1998 in Western Europe. Atmospheric Environment, 35, 6277-6297.
Stockwell W., Kirchner F., Kuhn M. and Seefeld S. (1977). A new mechanism for regional atmospheric chemistry modeling. J. Geophys. Res., 102, 25847-25879.
Walcek C. (2000) Minor flux adjustment near mixing ration extremes for simplified yet highly accurate monotonic calculation of tracer advection. J. Geophys. Res., 105, 9335-9348.
Whitby, K.T. (1978) “The physical characterization of sulfur aerosols”, Atmos. Environ., 12, 135-159.

*Proceedings of the Third International Symposium on Air Quality Management at Urban, Regional and Global Scales. 26-30 September 2005, Istanbul – Turkey*

# DETERMINATION OF THE SPATIAL AIR POLLUTANTS DISTRIBUSTION ON THE ISLAND OF CYPRUS USING DIFFUSIVE SAMPLING AND STATISTICAL MODELLING

**Guenter Baumbach, Heiko Pfeiffer, Leire Sarachaga-Ruiz, Savvas Kleanthous[*] and Ersever Beyaz[**]**

Dept. of Air Quality Control in Institute of Process Engineering and Power Plant Technology, Universitaet Stuttgart, Baumbach@ivd.uni-stuttgart.de
* Greek Cypriot Community, Nicosia, **Turkish Cypriot Community, Nicosia

## ABSTRACT

The objective of this work was to determine and to depict the spatial distribution of air pollutants over the whole area of Cyprus in air pollutants distribution maps. During the UNOPS project "Preliminary Assessment of Ambient Air Quality in Cyprus" $NO_2$ diffusive samplers were exposed at 250 sites, $SO_2$ and hydrocarbon samplers at 80 sites during several campaigns over one year. At first the spatial distribution was determined by interpolation. Better results were obtained by a new developed Neural Network simulation tool with the input parameters emissions inventory and population density and trained by the results of diffusive sampling. The resulting pollution map reflects very well the real conditions.

**Key Words:** Air pollutants distribution, $NO_2$, $SO_2$, benzene, Interpolation, Neural Network,Cyprus

## 1. INTRODUCTION

### 1.1 Methods of Diffusive Sampling

The Diffusive Sampling is an ideal measurement technique for large scale air pollution surveys with a large number of sampling points, which allow high spatial resolution. It is one of the approaches used in this project (Baumbach and Pfeiffer 2004) to perform a Preliminary Air Quality Assessment, as recommended in the Guidance report on preliminary assessment under EC air quality directives (Hout, 2000).The analytical methods used for the diffusive sampling analyses of $NO_2$, $SO_2$, and $O_3$ are listed in Table 1 (Hangartner, 2001).

Table 1. Components and applied methods of Diffusive Sampling

| Component | Principle | Analytical method |
|---|---|---|
| Nitrogen dioxide $NO_2$ | Absorption on triethanolamine | Photometry |
| Sulphur dioxide $SO_2$ | Absorption on potassium carbonate and glycole | Ion Chromatography |
| Volatile Organic Compounds VOC | Adsorption on activated charcoal | Gas Chromatography |

A quality assurance has been carried out by comparison of diffusive sampling results with according continuous monitoring averages. The results were very sufficient and will be presented in the paper. For the component ozone continuous monitoring had been preferred and background sites.

### 1.2 Sites and Periods

The distribution of sampling sites in Cyprus is shown in Figure 1. For the component $NO_2$ 250 sites had been chosen, for $SO_2$ and VOC 80 sites. The density of the sampling sites was based on the spatial variability of the pollution levels, which vary with the type of pollutant, source distribution, local orography and meteorology. In the cities the sampling site density was concentrated. The required sampling period shall cover 14 % of the reference period of the one year limit value for $NO_2$, $SO_2$ and VOC, according to Council Directives 1999/30/EC (1999) and 2000/69/EC (2000). In this Preliminary Assessment $NO_2$ and $SO_2$ were sampled every second month over one year period. The exposure time per campaign was one month, therefore the time coverage is approximately 50% within the year's period. The sampling period for VOCs was 15 months, having each campaign a duration of 1 month, thus, the time coverage was 100%.

## 2. POLLUTANT CONCENTRATIONS AT THE SITES

### 2.1 Nitrogen dioxid - $NO_2$

The results of diffusive sampling are evaluated for each site and each component as average over the whole sampling period (annual averages) as colored points. ).In Figure 1 these points are depicted exemplarily for the component nitrogen dioxide ($NO_2$).

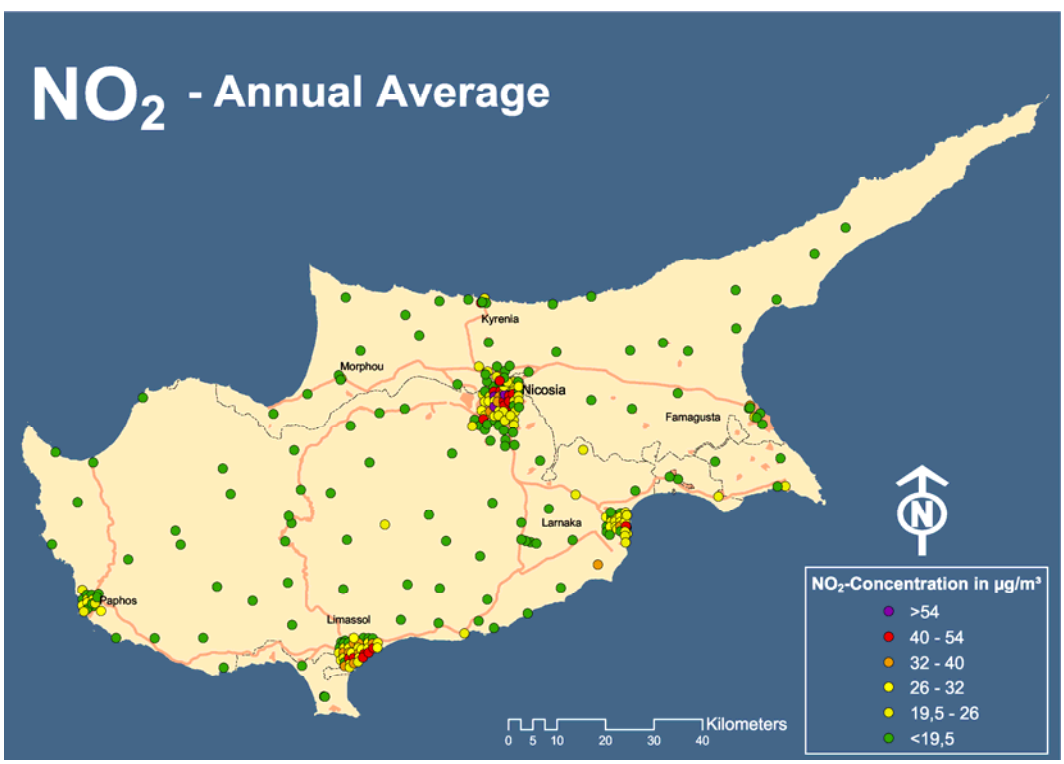


Figure 1. $NO_2$ concentrations in Cyprus – annual average values 2002/2003

For a preliminary assessment of air quality under EU directive 96/62/EC (1996) the overall goal is to obtain an overview of the temporal and spatial distribution of air pollutants. This allows to locate zones of exceedances or near-exceedances of relevant EU limit values. Due to the fact that ambient air quality measurements deliver only point values of pollutant concentrations, additional efforts have to be carried out to obtain a spatial distribution. The European Commission recommends for this purpose the diffusive sampling technique in combination with modeling - which modeling method is not specified, only a summary of available methods is given in the Guidance on Assessment under the EU Air Quality Directives (2002). The most commonly used method is the application of interpolation algorithms. Therefore, interpolation maps have been produced from the average results of point measurements (Figure 1) to get an overview of the pollutants distribution and to provide a widely applied method. These interpolated maps are showing a realistic picture of the air quality situation in Cyprus, since the diffusive sampling measurement campaign was carried out with an unusual high density of sampling sites. In the following, a selection of results of interpolation calculations are presented as pollutant maps of annual and seasonal averages in µg/m³. In the project report the maps are available for the whole island and all major cities of Cyprus and contain all pollutants measured by diffusive sampling ($NO_2$, Benzene, $SO_2$ and Ozone). The interpolated concentration values are depicted in a 1x1 km grid over Cyprus, which is aligned to the geographic coordinate system UTM, WGS 1984. For the cities this grid is too coarse, therefore filled contours have been chosen. In the Cyprus maps as well as in the city maps each colour shows the average pollutant level of the observed location. The chosen concentration scales are adapted to present and EU limit values. Transition colours have been avoided, since this would pretend a non-existent spatial resolution and precision regarding the predictions – therefore concentration ranges are shown. To find ones way in the maps, the major roads and the green line are depicted. For the cities, topographic maps are lying beneath the transparent interpolation results.

### 2.2 Sulfur dioxid – $SO_2$

In Figure 2 the mean summer season $SO_2$ distribution over Cyprus is depicted. Large, continuous parts of Cyprus are not affected by $SO_2$ especially the mountain areas in the west part Troodos and Akamas and the finger in north east (Karpasia). They are marked dark green, indicating $SO_2$ concentrations below 5 µg/m³. Yellow (8-12 µg/m³) and orange (12-20 µg/m³) colours occur mainly at the south coast in a coherent area from Larnaca and Limassol and also in the city of Nicosia (in the middle). The most important $SO_2$ sources are the power plants of Kyrenia at the north coast (yellow) and Vassilikos, Moni and Dhekelia at the south coast. All of them cause average concentration values in their close vicinity of 8 to 12 µg/m³ (yellow), respectively up to 20 µg/m³ (orange) in the case of the power plants of Moni and Vassilikos. Shorter Peak values are much higher, of course. Especially in summer with a general high power consumption due to the extensive use of air conditioning units they emerge quite clearly, in winter they are superposed by other emission sources and also there are more windy situations, thus the plumes from the power plants are spread over wider areas and the concentrations are lower.

## 2.3 Benzene distribution in urban areas

The Benzene distribution (as most important VOC component) in urban areas is depicted in Figure 3 as example for the city of Nicosia. It shows concentrations up to 8 µg/m³ and higher. The highest concentrations occur in the city centers with the highest traffic loads.

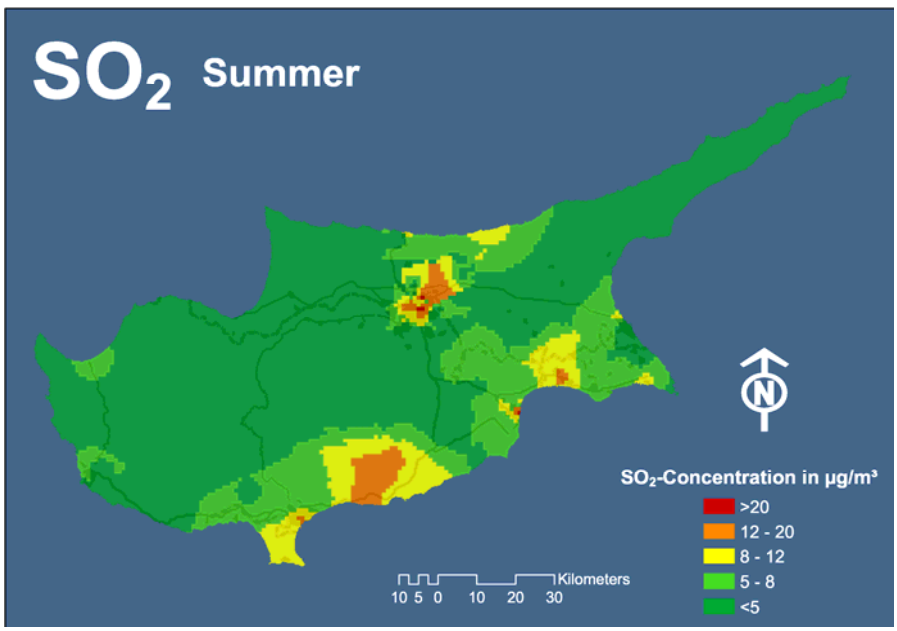


Figure 2. Mean interpolated $SO_2$ distribution over Cyprus for summer season

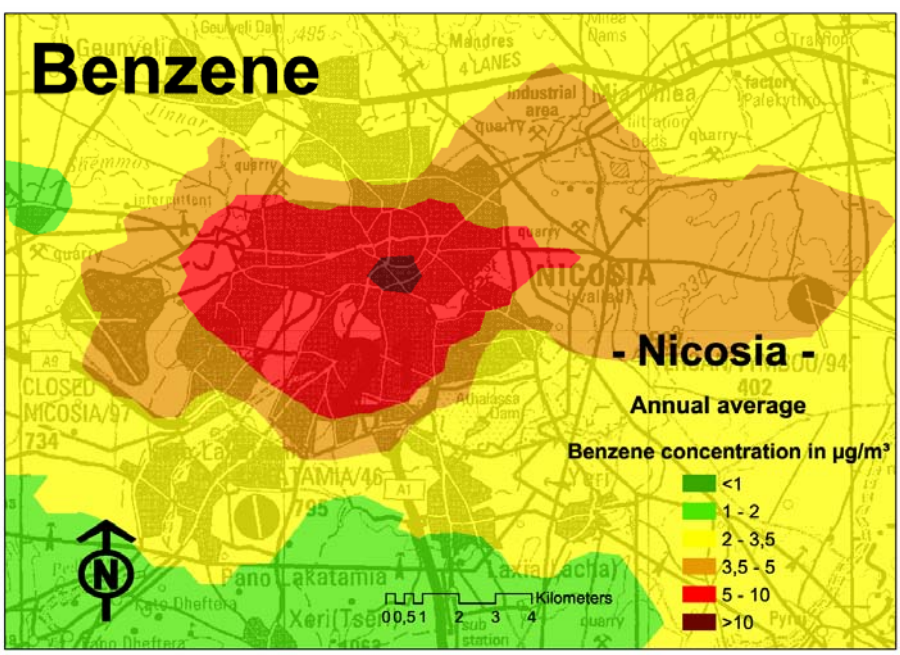


Figure 3. Mean annual interpolated Benzene distribution in Nicosia

# 3. NEURAL NETWORK MODELLING

## 3.1 General aspects

Neural Networks are a powerful flexible tool for finding systematics and dependencies in very complex processes and which considers all the concentrations measured by diffusive sampling and other important parameters: The idea behind this is to rebuild the human neural network in a computer software environment. Just like in nature, such a software can learn from the data that have been fed into it and find dependencies between different parameters. The distribution of air pollutants mainly depends on (Baumbach 1996):

- Meteorological conditions, especially wind speed and wind direction. Both parameters generate a wind field that influences strongly the dispersion of gaseous pollutants.
- Emission sources are the cause for air pollution. They are mapped in an emissions inventory. The population density indicates further emission sources, not captured in the emissions inventory.
- The topography directs the wind field and therefore influences the dispersion of air pollutants. The spatial distance of a certain site to an emission source correlates with the measured pollutant concentration, depending on the dispersion conditions and is therefore an important input variable for modeling a concentration field. In addition, the elevation correlates with the formation of certain pollutants, especially Ozone.

A realistic modeling approach should, if possible, include the parameters described above and regard the local conditions of the investigated area. At present there exists no stand alone method, that considers all these parameters: Different tools are incorporated into modelling systems.

## 3.2 Input Parameters for neural networks

For air pollution modelling, the neural network is trained with measured data of pollutant concentrations, meteorological data, topographical data and data from the emissions inventory.

A so called “controlled” training algorithm has been applied within this project (Pfeiffer 2005): The operator provides the network, the real results of actually measured values of all input parameters and also the desired output of the network - the pollutant concentration as measured by diffusive sampling.

A randomly selected part of the training data is set aside for later model validation.

All links between the different network layers and neurons are now set, their functions and weightings are determined. In the recall mode, the trained network is fed with the input data. These input variables have been prepared in a one by one km grid, that covers the whole island of Cyprus. The network now applies the learned correlations of the training sites to this grid and calculates the pollutant concentrations at the sites where no pollutant measurements exist, but the training input data.

The neural network was trained with the following variables:

- NOx emissions:
  The most important emissions in Cyprus have been distributed around their source according to wind statistics.
  - In the case of the point sources which are the power plants and the cement factories, a Gaussian dispersion model was run for each of these sources.
  - In the case of the highways a decay curve from the diffusive sampling measurements was applied (Figure 4).
  - Also for the cities a decay curve was calculated and weighted with wind statistics, so that a plume for each major city in Cyprus could be calculated.
- Population density:

  For the population density a new digital map was created, since the original data were only provided as points or as polygons of the district. For this purpose every village in Cyprus was digitised according to it's actual shape. The base for this was the 1:250.000 map of Cyprus.

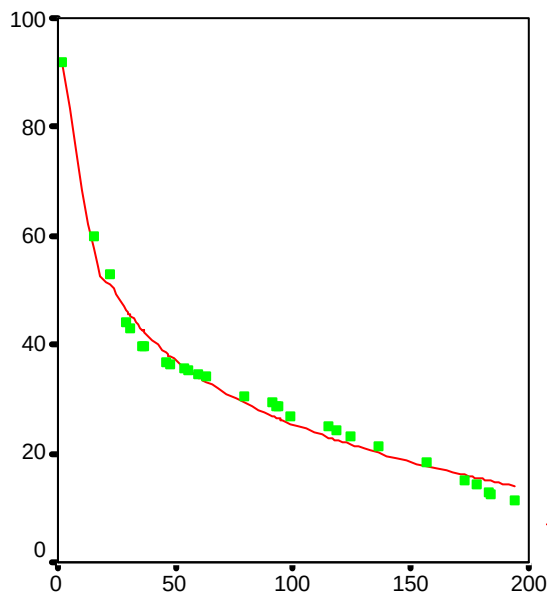


Figure 4. Decay of $NO_2$ with increasing distance to highway

### 3.3 Results of Neural Network modelling

The pollutant distribution map calculated by the neural network is depicted in Figure 5.

The features that don't appear in the interpolated maps like the highways and major roads are captured in this map since more variables are considered rather than the spatial distance between the diffusive sampling sites. Whether important emissions sources can be seen in the interpolation maps depends very much on the location of the diffusive sampling sites. This doesn't happen with the neural network model, since one part of its input is the emissions inventory.

The training data set for $NO_2$ was very good since it was measured at 250 places over Cyprus. The more input the neural network gets, the better it can learn the dependencies and correlations between the different parameters.

To assess the quality of the modelled map, the results of a test set from 50 diffusive sampling sites which has not been used for the training of the Neural Network model were compared with the modelled results for these sites. This comparison is shown in Figure 5. Some higher $NO_2$ values are underestimated by the model, because they are situated close to sources. The correlation coefficient could be determined as 0.62 – a very good result for a comparison of modelling and real measurements.

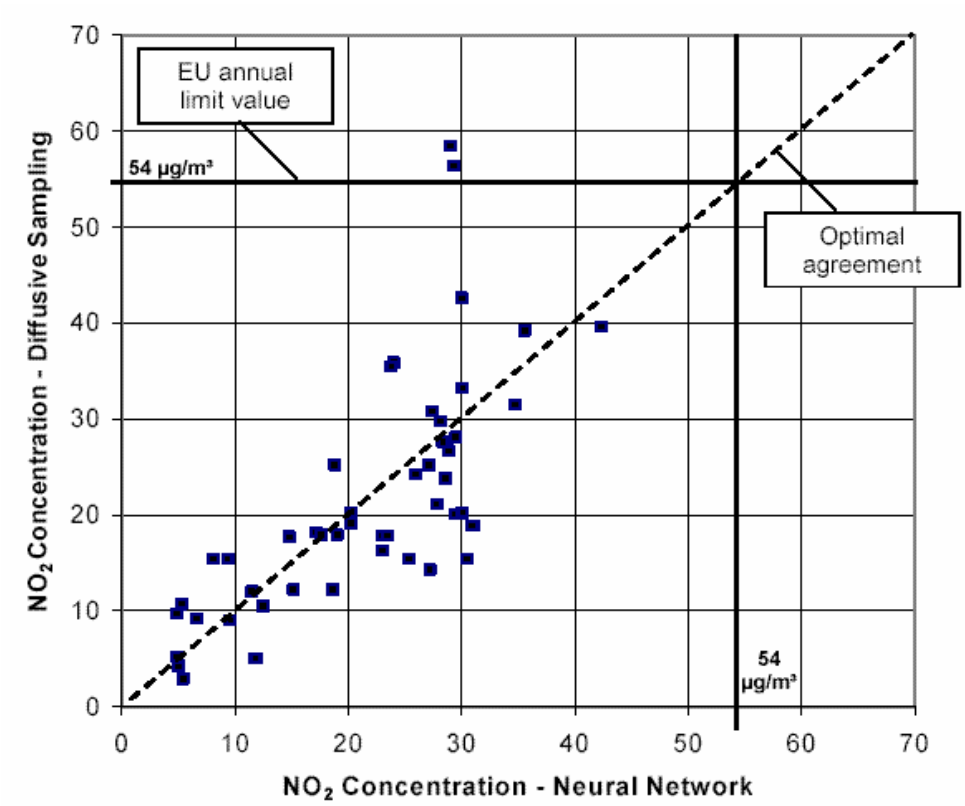


Figure 5. Quality assurance of the final model – comparison of NO2 diffusive sampling results from the test data set and modelled NO2 values with n= 50

## 4. INTERPRETATION AND CONCULUSIONS

The highest pollutant loads are located in the major cities of Cyprus, especially Nicosia, Limassol and Larnaca. Here, the highest concentration values are measured by diffusive sampling and the emission sources are densely concentrated. Some special features deserve more attention: The highway between Nicosia and Larnaca up to Limassol emerges very clearly as the major line source in Cyprus since these are the largest cities and furthermore the major airport of Cyprus is in Larnaca. Other important $NO_2$ sources are the power plants and a cement factory. They are very well reflected in the $NO_2$ distribution map (see Figure 6). Large parts of Cyprus have a low $NO_2$ level (green colour), since there are no major sources – especially the Troodos mountains (west part of Cyprus) and the area in the north, where agricultural usage dominates, partly even without machines.

Finally it can be stated that the Neural Network is a good method for modelling if a great number of measurement results is available and if these results shall be used

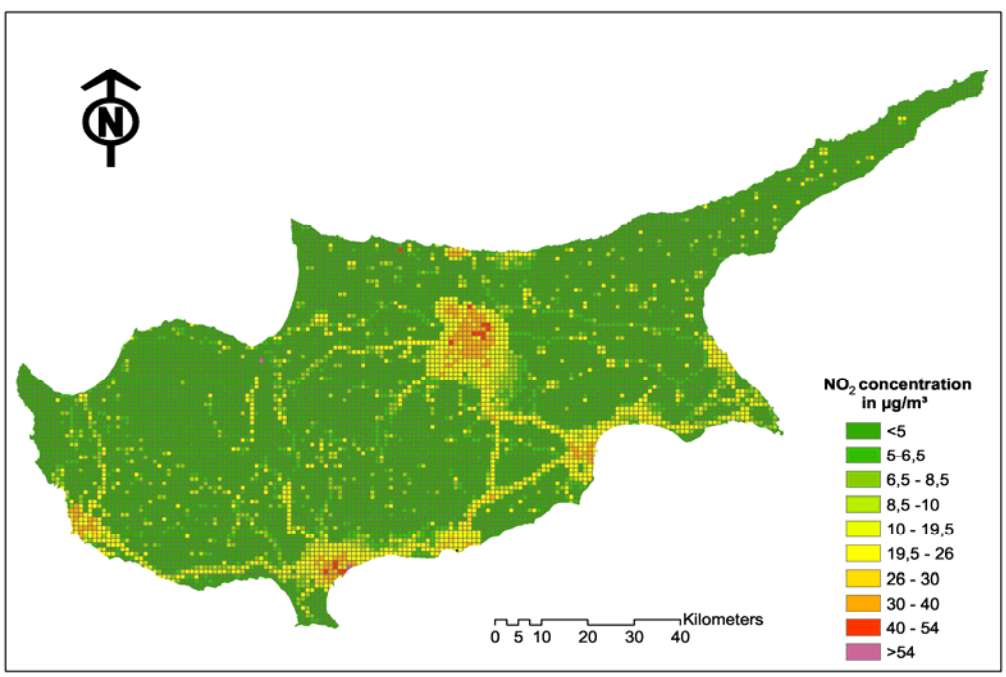


Figure 6. Annual average $NO_2$ distribution calculated with neural network

directly as input data for training the model. The neural network is more flexible than the usual statistic methods since it finds out the best correlation by training with real values.

## 5. ACKNOWLEDGEMENTS

This work was carried out within the project “Preliminary Assessment of Ambient Air Quality in Cyprus”. The project was funded by the US Agency of International Development (USAID), the United Nations Development Programme (UNDP) and the United Nations Office for Project Services (UNOPS). It has been executed by the Department of Air Quality Control of the Institute of Process Engineering and Power

Plant Technology of the Universitaet Stuttgart in cooperation with the Greek Cypriot and Turkish Cypriot Communities and with medisell Ltd, Nicosia.

We like to thank the following persons who were especially involved in this part of the project: Amelia de Coster, Olga Poulida, George Othodoxou, Lefteris Demetriou, Ioannis Diakos, Aytekin Bagcier, Tolga Baki, Martin Winter, Patrick Moenckert, Ulrich Vogt, Dieter Straub, Aynul Bari , Andrea Krusch, Heike Gruener, Bernd Janisch and others.

## REFERENCES

Baumbach, G., 1996. Air Quality Control. Textbook. Springer Berlin, Heidelberg, London, New York, Tokyo

Baumbach, G. and Pfeiffer, H., 2004. Preliminary Assessment of Ambient Air Quality in Cyprus. Final Report. Department of Air Quality Control, Institute of Process Engineering and Power Plant Technology, Universitaet Stuttgart

Hangartner, M., 2001. Influence of meteorological factors on the performance of diffusive samplers. Intern. Conference measuring air pollutants by diffusive sampling. Proceedings, Montpellier.

Hout, D. et al., 2000. Guidance on Assessment under the EU Air Quality Directives, European Environment Agency. Copenhagen 2002.

Pfeiffer, H., 2005. Neural Modelling of the Spatial Distribution of Air Pollutants. Doctoral Thesis. Universitaet Stuttgart, Germany

The council of the European Union, 1996. Council Directive 96/62/EC of 27 September 1996 on ambient air quality assessment and management. Official Journal of the European Union L 296, 1996.

The council of the European Union, 1999. Council Directive 1999/30/EC of 22 April 1999 relating to limit values for sulphur dioxide, nitrogen dioxide and nitrogen oxides, particulate matter and lead in ambient air. Official Journal of the European Union L 163/41.

The council of the European Union, 2000. Council Directive 2000/69/EC of 16 November 2000 relating to limit values for benzene and carbon monoxide in ambient air. Official Journal of the European Union L 313/12.

*Proceedings of the Third International Symposium on Air Quality Management at Urban, Regional and Global Scales. 26-30 September 2005, Istanbul – Turkey*

# RECEPTOR MODELLING OF TOXIC AIR POLLUTANTS IN ANKARA ATMOSPHERE

**Öznur Oğuz Kuntasal[1*], Deniz Karman[2] and Gürdal Tuncel[1]**

[*1]Middle East Technical University, Department of Environmental Engineering 06531 Ankara, Turkey oznuro@metu.edu.tr, tuncel@metu.edu.tr
[2]Carleton University, Department of Civil and Environmental Engineering, 1125 Colonel By Drive, Ottawa, Ontario, K1S 5B6 Canada, Deniz_Karman@carleton.ca

## ABSTRACT

Positive matrix factorization (PMF) receptor model is applied to volatile organic compound (VOC) data collected at a residential site in Ankara, Turkey during summer of 2003. Data set includes 98 compounds containing, isoprene, halogenated compounds, aromatics, paraffins and olefins. The PMF model explained at least 96% of variation in the data. The sources and computed average source contribution estimates (SCE) are; gasoline vehicle exhaust 42%, diesel vehicle exhaust 30%, architectural coating 11%, biogenic emissions 9% and solvent use 8%. Motor vehicle emissions are the major source of VOCs measured at residential station in Ankara during summer.

**Key Words:** Positive Matrix Factorization, Receptor Modeling, Volatile Organic Compounds, Source Contribution Estimate.

## 1. INTRODUCTION

Receptor models are mathematical procedures for identifying and quantifying the sources of air pollution at a site (i.e., receptor), primarily on the basis of concentration measurements at the receptor site and generally, without need of emission inventories and meteorological data (Watson et al., 2001). Receptor modeling is a critical tool in developing air quality management plans. In this research, Positive Matrix Factorization (PMF) is applied to volatile organic compound (VOC) data collected at a residential site in Ankara, Turkey during summer of 2003.

Positive Matrix Factorization is a new variant of receptor models. Unlike more conventional methods of factor analysis such as principal component analysis (PCA), PMF produces non-negative factors, aiding factor interpretation, and utilizes error estimates of the data matrix. PMF assumes that $X$ is the matrix of observed data and $\sigma$ is the known matrix of standard deviations of elements of $X$. Both $X$ and $\sigma$ have dimensions of $nxm$. The model solves bilinear matrix problem $X=GF+E$ where $G$ is the unknown factor scores matrix of dimensions $nxp$, $F$ is the unknown factor loadings matrix of dimensions $pxm$, and $E$ is the matrix of residuals. The problem is solved in the weighted least square sense. Furthermore the solution is constrained so that all the elements of $G$ and $F$ are required to be non-negative (Paatero and Tapper, 1994). Over the past few years PMF has been successfully applied in many

atmospheric studies (Hopke, 2003; Paterson et al., 1999; Polissar et al., 1998; Zhao et al., 2004).

The aim of this research is to perform source apportionment of VOCs in Ankara. Source apportionment is an important step in the development of air pollution control strategies. This is the first receptor modeling study conducted to apportion sources of speciated VOCs measured in an urban atmosphere in Turkey.

## 2. MATERIALS AND METHODS

Ambient air measurements were conducted as part of this research to generate VOC data set. The sampling was conducted at consecutive 4-hour intervals over a 24-hour period for two months in summer and two months in winter seasons at a nose-level sampler located on a residential site in Ankara. Samples were also collected at a tunnel and underground garage to generate motor vehicle related source profiles. Samples were collected onto cartridges packed with Tenax TA and Carbopack B resins. Analysis was performed by thermal desorption followed by gas chromatography coupled to a mass selective detector (GC/MSD). Time resolved data provide information on ambient levels of 98 VOCs ranging from C5 to C12, including, isoprene, halogenated compounds, aromatics, paraffins and olefins. This is the first speciated VOC data set generated in Ankara. Detailed information on sampling and analytical methodology is provided by Kuntasal et al. (2004).

Two-dimensional Positive Matrix Factorization (PMF2) receptor model is applied to Ankara VOC data. There are two types of input to the model, namely; i) data matrix and ii) error estimates of the data matrix. A pretreatment of data is required prior to utilize in the model. Although PMF2 can handle incomplete data, very high amount of below detection limit (BDL) or missing values might result in erroneous results. In this study, a method suggested by Paatero and Hopke (2003) for discarding or down weighting of high-noise variables was utilized. In the suggested method, a variable is called “weak” variable if it contains signal (S) and noise (N) in comparable amounts. Similarly, variables containing much more noise than the signal are termed “bad” variables. The element with the S/N larger than 2 and between 0.2 and 2 can be considered as a normal and a weak element, respectively. However, the element with the $S/N<0.2$ can be considered as “bad” variable. The bad element should be excluded from analysis, unless it is an important marker for one of the sources.

The model is computed under different initial conditions in order to obtain optimum solution. A critical step in PMF analysis is determination of the number of factors (i.e., sources). The rules suggested by Zhao et al. (2004) are used in this research. Model performance parameters including sum of squares errors (Q) and distribution of scaled residuals helped ascertain the optimum solution. PMF2 runs with 5 factors yield optimum solution.

In general, bilinear factor analysis has rotational ambiguity (Paatero et al., 2002). In the PMF2, FPEAK option is used to control rotation problem. Effect of this parameter is investigated. PMF2 is computed with 5 factors and FPEAK values

ranging from -1.0 to 1.0 for the summer data set. Model runs with FPEAK values of -1.0, -0.5, -0.1, 0.0, 0.1, 0.5, 0.7 and 1.0 yield calculated Q values of 3415, 3173, 3112, 3113, 3109, 3176, 3230, and 3289, respectively. The calculated Q value increases by an increase in absolute value of FPEAK. FPEAK value of -0.5 results in a slight change in source profiles. FPEAK value of zero where the change in Q is slight is accepted as the optimum value.

## 3. RESULTS AND DISCUSSIONS

Utilization of PMF2 with robust mode, FPEAK value of 0.0 and five factors yielded the optimum solution that explains variation in the VOC data generated at residential site in Ankara during summer campaign. Factors identified by PMF2 are interpreted qualitatively by evaluating source profiles (i.e., factor loadings), time variations in source contributions (i.e., factor scores) and explained variations (EV) that are generated by the model. The source profiles are used as the final criteria for source identification. The EV profiles are provided for reference only. Source profiles generated by the model for summer data set are shown in Figure 1.

Source profile computed for Factor 1 (F1 in Figure 1) shows that isoprene and n-pentane are the most abundant species in this factor. This factor explains greater than 80% of the variance in isoprene concentration. Isoprene is a very well known marker for biogenic emissions (Watson et al., 2001). Source contribution for this factor is the highest during daytime and the lowest during nighttime sessions. This pattern indicates the relationship between sunlight and emission from Factor 1, which agrees with the sunlight dependence of emissions from plants. Factor 1 is identified as biogenic emission source.

Source profile computed for Factor 2 (F2 in Figure 1) indicates that toluene is the most abundant compound in this factor. Greater than 30% of variances in chloroform, toluene and cyclohexane concentrations are explained by Factor 2. Source contribution for Factor 2 is the highest during morning session and negligible during night session. Source profile for Factor 2 is compared with the profiles available in the literature to identify the source accurately. Among various profiles used in comparison, Factor 2 shows the best fit ($R^2$>0.90) with architectural coating profiles (i.e., Na et al., 2004; Scheff et al., 1989). Contributions of toluene, m&p-xylene and o-xylene are 62%, 6% and 2% in Factor 2, respectively. High abundance of aromatic compounds in Factor 2 indicates that Factor 2 is solvent-based architectural coating source rather than water-based coating.

Source profile for F3 depicted in Figure 1 shows that toluene, m&p-xylene, benzene and 2-methylpentane are among the most abundant compounds in Factor 3. This factor explains variation in most of the light hydrocarbons. Abundance of BTEX compounds and the source profile pattern indicate that this profile could be associated with motor vehicle emissions.

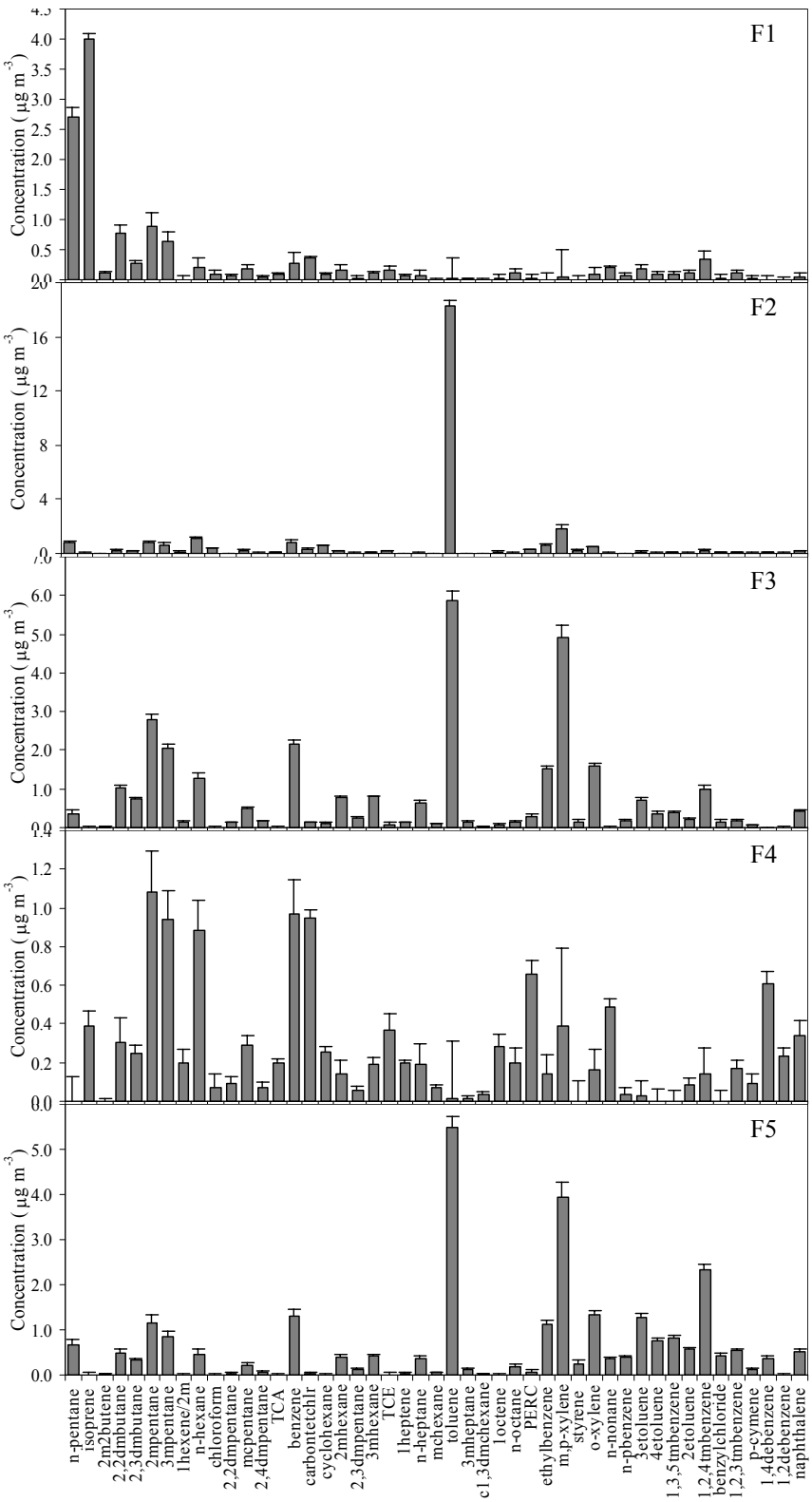


Figure 1. Source profiles computed by PMF2 for summer data set.

Source contribution averaged over sampling sessions for Factor 3 show a well-defined diurnal variation, which is typical for traffic emissions with high contributions during morning and evening rush hours and low contribution during noon session. The source profile is compared with the running vehicle exhaust and fuel profiles generated as part of this research and presented by Kuntasal et al. (2005). Good correlation ($R^2$>0.90) is observed with exhaust profiles. Correlation with gasoline fuel profile is better than diesel fuel profile. Thus, Factor 3 is identified as motor vehicle exhaust associated mostly with gasoline-derived vehicles.

Factor 4 source profile (F4 in Figure 1) shows that carbon tetrachloride, benzene, perchloroethylene (PERC) are among the most abundant compounds. PERC is a very well known marker for dry cleaning (Scheff *et al.*, 1989; Watson *et al.*, 2001). Factor 4 explains most of the variation in carbon tetrachloride, 1,1,1-trichloroethane (TCA) and trichloroethylene (TCE) that are commonly used in industrial processes and household cleaners and polishes (Nazaroff and Weschler, 2004). The source contribution does not present a significant diurnal pattern for this factor. Factor 4 is identified as a solvent-use source from various applications.

Toluene, m&p-xylene, 1,2,4-trimethylbenzene and benzene are the most abundant compounds in the source profile for Factor 5 (F5 in Figure 1). This factor explains variation in most of the heavy hydrocarbons. Source contribution indicate a diurnal variation that is very similar to that observed for Factor 3 that is higher source contributions during morning and evening rush hours than noon hours are observed. Factor 5 is compared with the running vehicle exhaust and fuel profiles generated as part of this research. Good correlations ($R^2$>0.90) are observed with exhaust profiles. As this profile explains most of the variation in heavy hydrocarbons, Factor 5 is identified as running vehicle exhaust strongly influenced by diesel emissions.

The source contribution estimates (SCE) are calculated for each identified factor using linear regression method that is suggested by Andersen et al. (2001). The results are provided in Table 1. Gasoline vehicle exhaust (42%) and diesel vehicle exhaust (30%) sources contribute most of the VOC emissions observed at the residential station during summer campaign. Architectural coating is the third most abundant source with 12% contribution. Biogenic emissions and solvent use account for 9% and 8% of the total VOC concentration, respectively.

Table 1. Summary of VOC sources and computed SCEs at residential station.

| **VOC Source** | **SCE (%)** |
|---|---|
| Gasoline vehicle exhaust | 41.77 |
| Diesel vehicle exhaust | 29.71 |
| Architectural coating (solvent based) | 12.11 |
| Biogenic emissions | 8.75 |
| Solvent use | 7.66 |

Model performance is also evaluated. Linear regression between the modeled (i.e., predicted) and measured (i.e., observed) VOC data is performed. The model results reveal a very good fit with the measured VOC data (see Figure 2) with $R^2$ value of 0.99 and intercept of 1.05. Ratio of the modeled to measured total VOC concentration is 0.95.

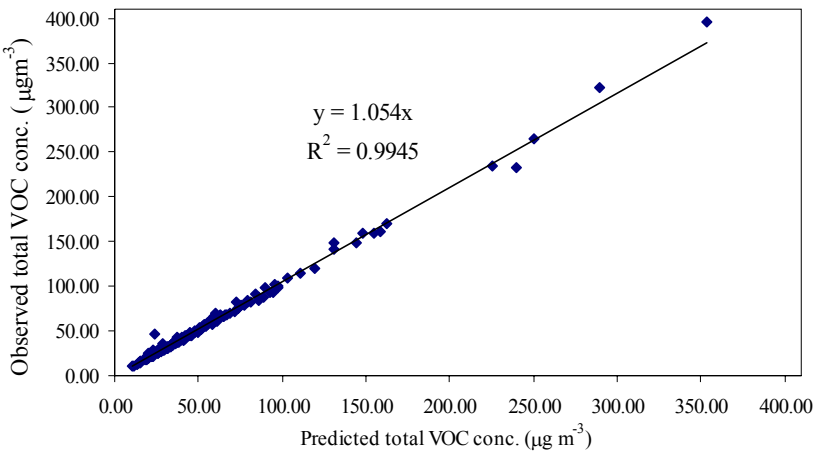


Figure 2. Observed vs. Predicted VOC concentration

Scaled residual errors are also inspected to investigate performance of the model. Most of the scaled residuals are between -2.0 and 2.0 with a random distribution of positive and negative values. The frequency distributions of scaled residual errors for isoprene, TCA, n-octane and 2-ethyltoluene are shown in Figure 3 as example.

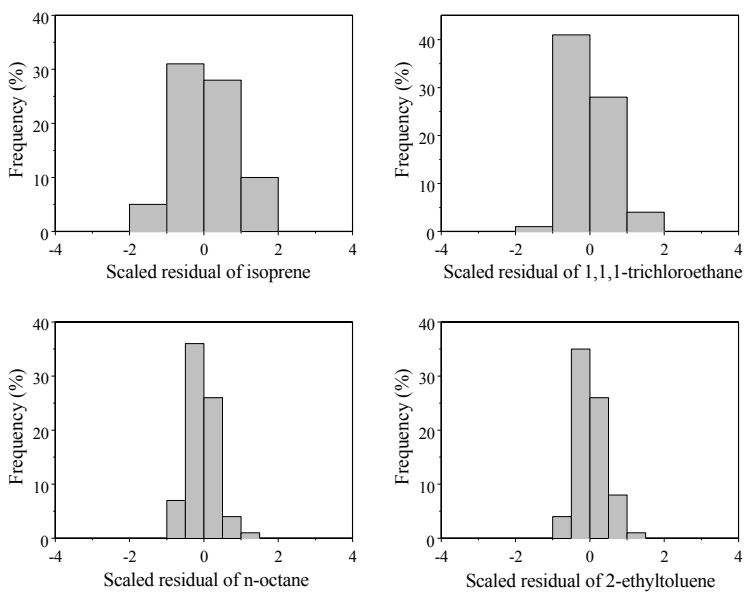


Figure 3. Frequency distribution plot for scaled residual errors.

## 4. CONCLUSIONS

Receptor modeling technique is applied for the first time in Turkey to VOC data collected in an urban atmosphere. Positive Matrix Factorization model is used to apportion sources of VOCs at a residential site in Ankara during summer season. On the average, motor vehicle related sources contribute to 72% of the total VOC concentration. The solvent related sources including solvent use and the architectural coating result in about 20% contribution. Motor vehicles are the major source of VOCs measured at the residential station in Ankara during summer campaign. PMF runs also successfully resolved biogenic emission source that is effective during summer campaign.

## 5. ACKNOWLEDGEMENTS

Authors thank to Dr. Daniel Wang from Environment Canada and Prof. Stuart Batterman from University of Michigan for their helps during development of analytical methodology via personal communications; and Gürkan Kuntasal, Ozan Aktan and Kutay Erbayat for their enormous help during fieldwork.

## REFERENCES

Anderson, M.J., Miller, S.L. and Milford, J.B., 2001. "Source apportionment of exposure to toxic volatile organic compounds using positive matrix factorization", Journal of Exposure Analysis and Environmental Epidomiology, Vol. 11, pp. 295-307.

Hopke, P.K., 2003. "Recent developments in receptor modeling", Journal of Chemometrics, Vol. 17, pp. 255-265.

Kuntasal, Ö.O, Karman, D., Tuncel, S.G. and Tuncel, G., 2004. "Determination of Volatile Organic Compounds in Ambient Air by Multibed Adsorption/Short Path Thermal Desorption-GC/MS", Proceedings of the 4th Aegean Analytical Chemistry Days, September 29 - October 3, Kuşadası, Turkey, pp. 339-341

Kuntasal, Ö.O., Tuncel, G. and Karman, D., 2005. "Motorlu Taşıtlardan Kaynaklanan Toksik Hava Kirleticilerinin Emisyon Profillerinin Tayini", Proceedings of the IX. Otomotiv ve Yan Sanayi Sempozyumu, organized by Turkish Chamber of Mechanical Engineers, May 27-28, Bursa, Turkey, pp. 111-114. (in Turkish)

Na, K., Kim, Y.P., Moon, I. and Moon, K.C., 2004. "Chemical composition of major VOC emission sources in the Seoul atmosphere", Chemosphere, Vol. 55, pp. 585-594.

Nazaroff, W.W. and Weschler, C.J., 2004. "Cleaning products and air fresheners: exposure to primary and secondary air pollutants", Atmospheric Environment, Vol. 38, pp. 2841-2865.

Paatero, P. and Tapper, U., 1994. "Positive matrix factorization: A non-negative factor model with optimal utilization of error estimates of data values", Environmetrics, Vol. 5, pp. 111-126.

Paatero, P., Hopke, P.K., Song, X.H. and Ramadan, Z., 2002. “Understanding and controlling rotations in factor analytic models”, Chemom. And Intelligent Laboratory Systems, Vol. 60, pp. 253- 264.

Paterson, K.G., Sagady, J.L., Hooper, D.L., Bertman, S.B., Carroll, M.A. and Shepson, P.B., 1999. “Analysis of air quality data using positive matrix factorization”, Environmental Science and Technology, Vol. 33, pp. 635-641.

Polissar, A.V., Hopke, P.K., Malm, W.C. and Sisler, J.F., 1998. “Atmospheric aerosol over Alaska: 2. Elemental composition and sources”, J. of Geophysical Research, Vol. 103, pp. 19045-19057.

Scheff, P.A., Wadden, R.S., Bates, B.A. and Aronian, P.F., 1989. “Source fingerprints for receptor modeling of volatile organics”, JAPCA, Vol. 39, pp. 469-478.

Watson, J.G., Chow, J.C. and Fujita, E.M., 2001. “Review of volatile organic compounds source apportionment by chemical mass balance”, Atmospheric Environment, Vol. 35, pp. 1567–1584.

Zhao, W., Hopke, P.K. and Karl, T., 2004. “Source identification of volatile organic compounds in Houston, Texas”, Environmental Science and Technology, Vol. 38, Iss. 5, pp. 1338-1347.

*Proceedings of the Third International Symposium on Air Quality Management at Urban, Regional and Global Scales. 26-30 September 2005, Istanbul – Turkey*

# A PREDICTIVE MODEL TO ASSESS THE IMPACT OF EMISSIONS ON URBAN SCALE AIR QUALITY IN COASTAL REGIONS

Erez Weinroth[1], William Stockwell[1], Darko Koracin[1], Julide Kahyaoğlu-Koračin[1], Menachem Luria[2], Travis McCord[1], Domagoj Podnar[1] and Alan Gertler[1,*]

[1] Desert Research Institute, Reno, Nevada, U.S.
[2] The Hebrew University, Jerusalem, Israel
[*]Alan.Gertler@dri.edu

## ABSTRACT

Many areas suffering from elevated pollutant levels are located in regions where there is significant uncertainty in predicting pollutant transport and dispersion (e.g., coastal zones). Traditional approaches to assess the impact of emissions in complex environments have included the application of statistical, Gaussian dispersion, single chemical box, Lagrangian, and Eulerian models. Each of these models has distinct advantages and disadvantages. This paper describes the development of a meteorological air quality model with in-line chemistry that combines the advantages of the Eulerian and Lagrangian models. As part of the model validation, simulation results for a case study in the San Diego area of southwestern California are also discussed.

**Key Words:** Air quality modeling, coastal meteorology, atmospheric chemistry, emissions modeling, model validation

## 1. INTRODUCTION

Elevated levels of ozone ($O_3$) remain a serious issue throughout the U.S. The American Lung Association has identified 25 metropolitan areas as having the worst $O_3$ air pollution in the country. Nine of these areas are located in California, with seven of them in the top ten (Carlton 2004). All the major urban areas in California are classified as non-attainment for 1-hr $O_3$ standard (Alexis et al., 2000).

In order to control elevated $O_3$ levels, there is a need to develop forecasting models that incorporate the processes leading to secondary pollutant formation. These processes include emissions, meteorology (transport and dispersion), and transformation chemistry (Brasseur and Pszenny 1998).

Currently there are three approaches to model transport, dispersion, and transformation of pollutants. These include Eulerian, Lagrangian, and mixed approaches. Briefly, the Eulerian method divides the atmosphere into fixed grid cells for which the continuity equation is solved. Current Eulerian models include CAMx (Comprehensive Air Quality Model with extensions), CMAQ (Community Multiscale Air Quality modeling system), and MM5-chem (Meteorological Model 5

with chemistry), among others. This approach is used to represent the primary processes affecting chemical transformations; however, while the chemistry is well represented, dispersion and transport is limited by the size of the grid cells employed. This can lead to appreciable numerical errors.

The Lagrangian approach is generally used for non-reactive species and avoids the computational complexities associated with the simulation of the chemical reactions. This leads to improved performance in assessing transport and dispersion (Stohl, 1998; Peters et al., 1995). Lagrangian models describe a hypothetical air parcel that is carried along the air parcel trajectory. Only first-order chemical reactions can be incorporated under this approach (Song et al., 2003; Stein et al., 2000).

The hybrid approach combines the strengths of both the Eulerian and Lagrangian methods and may provide a unique approach for the next generation of chemical transport simulations. Hybrid models such as HYSPLIT4-chem (Stein et al., 2000) employ detailed non-linear Eulerian chemistry (CheM) together with the HYSPLIT (Hybrid Single Particle Lagrangian Integrated Trajectory) model. This model has been used to analyze spatial and temporal $O_3$ concentrations in Pennsylvania (Stein et al., 2000). Another example of a hybrid model is the 3-D Lagrangian particle dispersion model with photochemical reactions developed by Song et al. (2003). In both cases the chemistry and transport-dispersion are lumped together making it difficult to modify the modules.

In this paper we describe the development and validation of a new approach for a hybrid model that does not incorporate the chemistry module within the dispersion-advection module but rather implements the chemistry module in a post-processing mode. The advantage of this approach is a modular system that can readily employ alternative chemical and transport-dispersion modules. The model was validated in a region of complex terrain (land-sea interface) using extensive aircraft data obtained during a period of elevated $O_3$ over the San Diego area of south western California (Luria et al., 2005).

## 2. MODEL COMPONENTS

In this section we briefly describe the various components used in the hybrid modeling system. These include the MM5 for the meteorological fields, a Lagrangian particle model (LAP) for advection and dispersion, and a Eulerian chemical model within the Linkage module for the transformations. The Linkage module couples the Lagrangian and Eulerian parts of the model. Another key component is the emissions inventory for the region (Kahyaoğlu-Koračin et al., 2005).

### 2.1 Meteorological Module

For the meteorological module we used MM5, the Fifth-Generation Pennsylvania State University (PSU)/NCAR prognostic meso-meteorological model (Dudia 1993; 2001; Dudia and Bresch 2002; Dudia et al., 2003, Grell et al., 1994). MM5 is non-

hydrostatic, fully compressible, and uses terrain-influenced, vertical sigma-coordinates on a nested horizontal, rectangular staggered-grid. For this study the outer domain was 1125 x 1125 km with a cell size of 15 x 15 km and an inner domain of 275x 305 km with a cell size of 5 x 5 km located over the San Diego area.

### 2.2 Transport and Dispersion Module

For the transport and dispersion module we used the LAP developed based on the approach described by Pielke (1984). Details of the model structure and applications are described by Koracin et al. (1998; 1999; 2000). Meteorological input to the LAP includes 3-D wind fields, as well as the potential temperature.

Advection and dispersion calculations are made in a Lagrangian framework. The model uses a volume size (mass/volume) that can be changed to calculate concentrations. Meteorological data were based on MM5. LAP uses the same map projection as MM5. The model includes a parameterization of drift velocity, which prevents non physical accumulation of Lagrangian particles during weak-wind conditions. Emission sources of various geometries including elevated and moving sources with arbitrary time-variable or time limited emission rates can be modeled.

### 2.3 Chemistry Module

For the chemical transformation module we used the Regional Atmospheric Chemistry Mechanism (RACM, Stockwell et al., 1997). The RACM mechanism is a revised version of the RADM2 mechanism (Stockwell et al., 1990), which is widely used in modeling studies. There are a total of 237 reactions in the RACM mechanism. We calculated photolysis rate coefficients for the specific location and time of year according to Madronich (1987).

Simulations were performed using a box model (SBOX, Seefeld, 1997). The chemical compiler reads an input file in which the mechanism's chemical reactions and their rate coefficients are written in a format that is very similar to standard chemical notation.

### 2.4 Lagrangian-Eulerian Linkage

The linkage between the Eulerian and Lagrangian components is based on the concept of a concentration grid cell (Stein et al., 2000). An enhancement was needed for the LAP model to produce a particle specific “name” (ID) for each particle. This enables us to link each particle to a specific set of attributes (i.e., location, meteorological fields, and chemical composition).

The size of the Eulerian cells can be varied. While very small cells result in homogenous mixing and better spatial resolution of the chemical species, in this study larger cells were used due to computational constraints. We assumed the LAP particles had different compositions based on their original source. A unique feature

of this approach is it enabled us to trace any particle at any given time back to its origin and to observe its transformation over time and space.

For each time step and grid cell the particles were disaggregated and the different chemical species were then lumped together accordingly. At this point the chemical model was applied. At the end of each time step (1-hr, the same time step as the output from the LAP model), new concentrations within each grid cell were predicted. Apportionment of the chemical concentrations to the individual original particles was made by weighted average. Distribution of newly produced chemical species was based on the diffusion time scale, mixing height, and turbulence intensity.

This is shown schematically in figures 1A-C. As shown in the figure, each particle has individual identity denoted by different symbols. This identity contains source and composition information. The two layers (each 1 km in height) from the box model are shown in 1A. Most particles are located in the lowest level, which represents the mixed layer. In 1B the map of the study area can be seen in low resolution, with the grid surrounding the San Diego metropolitan area. Gray dots represent clusters of particles. When we zoom out (1C), we can see the box model cells (15 x 15 km), along with the MM5 inner grid cells (5 x 5 km). In the example 11 particles are shown but the model can handle up to 20,000 particles per grid cell. After each time step the species are redistributed and new particle positions are calculated by the LAP.

### 2.5 Emission inventory

In this study we used the emission inventory developed by Kahyaoğlu-Koračin et al. (2005). This was based on the Southern California Oxidant study (SCOS) 1997 day-specific emissions inventory and the California Air Resources Board (CARB) annual inventory. The inventory domain contained 110 x 74 grid cells of 5 x 5 km. Species included $NO_x$, $SO_x$, CO, PM, and TOG for all sources, including on-road and off-road mobile sources, industrial sources, commercial and U.S. Navy marine vessels, and commercial, civil, and military aircrafts. The biogenic component of the inventory was recalculated for the validation period using observed temperatures and day-specific solar radiation values.

## 3. MODEL VALIDATION

In order to validate the modeling system, we used data from and an airborne sampling study conducted in the San Diego area during July 2003. The dates of this study (July 7, 9, and 17, 2003) were characterized by high levels of $O_3$ throughout the region.

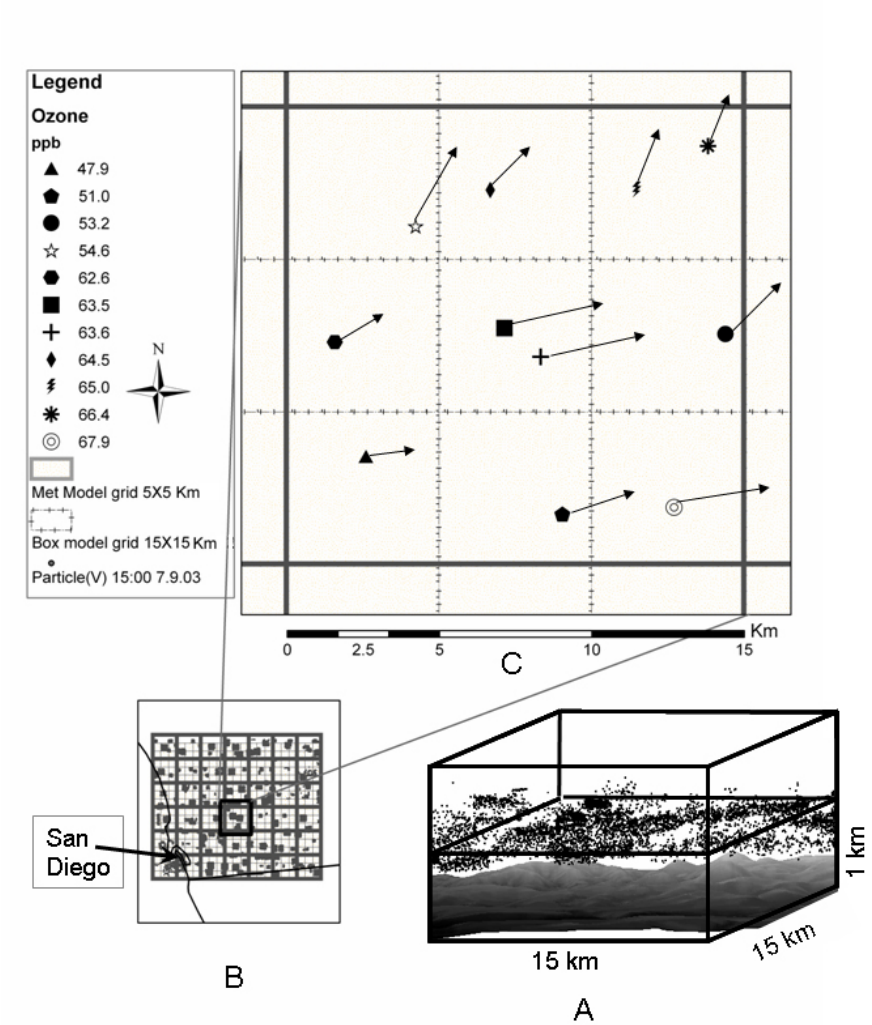


Figure 1. Schematic showing the main features of the Lagrangian – Eulerian linkage. (A) results from 2 levels of the LAP. (B) Bird's-eye view of the Eulerian grid above the study area. (C) Enlargement of Eulerian cell superimposed on the meteorological model inner grid. Particles shown in (C) have different composition as denoted by the different symbols. Arrows are grid specific vectors of wind speed and direction.

### 3.1 Airborne Measurements

A total of 10 research flights were carried out during the period of July 7 to 25, 2003. The flights began at shortly before noon and lasted approximately 5 hours. The flights covered an area of approximately 100 x 100 km with the San Diego harbor being the southwest corner of the domain. Measurements included NO, $NO_2$, $NO_x$, $NO_y$, $SO_2$, CO, $O_3$, light scattering, speciated hydrocarbons and aldehydes, pressure, temperature, humidity, and wind speed and direction. A complete description of the measurements is contained in Luria et al. (2005).

### 3.2 Comparison between Observations and Predictions

Examples of model results versus airborne measurements can be seen in Figures 2 – 4. The flight path is shown as the colored dots, which also represent the observed $O_3$ concentration. Modeled $O_3$ concentrations were calculated for each particle during each hour of the flight period. A kriging interpolation was performed for the predicted $O_3$ concentrations for each hourly period. To compare the model results with the observations, the mapped kriging results were cut into hourly sections corresponding to the flight time and location. A mosaic from the hourly sections was assembled to match the flight information. In this manner, a direct comparison between the measured and predicted results can be made and readily observed (Figures 2 – 4).

For July 7 (Figure 2), four kriging interpolation segments were combined to cover the time period from 12:00 to 16:00. Good agreement between the model results and the fight observations is seen. For the 12:00 to 13:00 segment, the model predicts low $O_3$ levels (40 - 60 ppb) similar to that seen in the airborne observations. The small regional $O_3$ peak at observed in the center of the figure is also well predicted. $O_3$ is underpredicted towards the south east section (lower right corner) but is well reproduced later along the flight track.

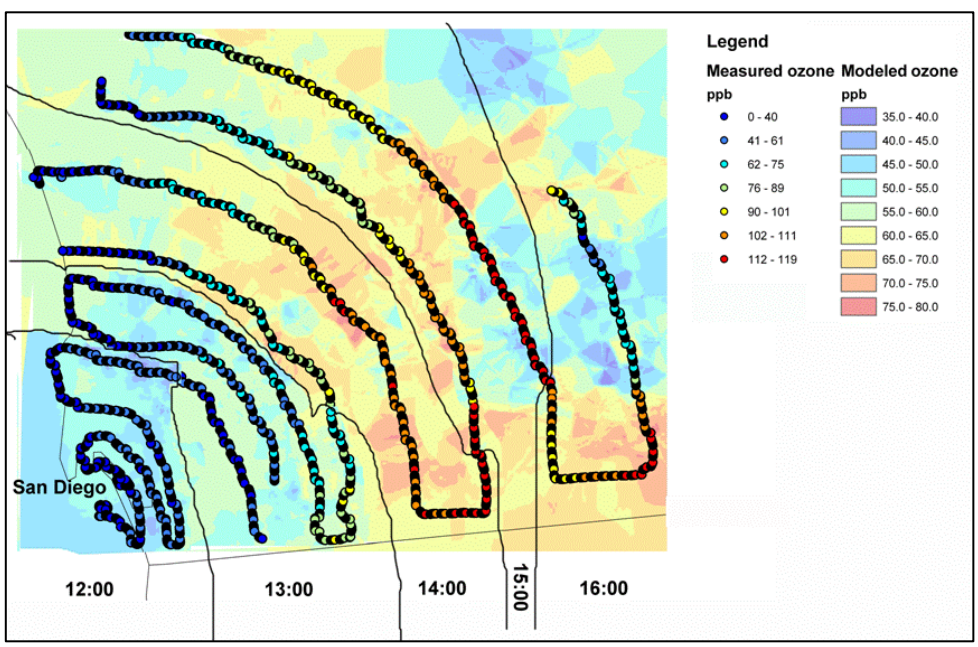


Figure 2. Comparison of observed vs. predicted $O_3$ concentrations for July 7, 2003 12:00-16:00.

On July 9 (Figure 3) reasonable agreement is recorded between the model and measured $O_3$ concentrations. During the beginning part of the flight path two high levels are seen in the harbor and slightly inland. The model does not capture these hotspots, likely due to the coarse resolution of the inventory. For the 13:00 period,

lower levels are seen slightly inland from the downtown area, consistent with the predictions. Over the next two hours (14:00 – 15:00) the model predicts elevated levels inland toward the mountains, as seen in the aircraft observations; although, an overprediction is seen in the northwest corner of the region (near Camp Pendleton).

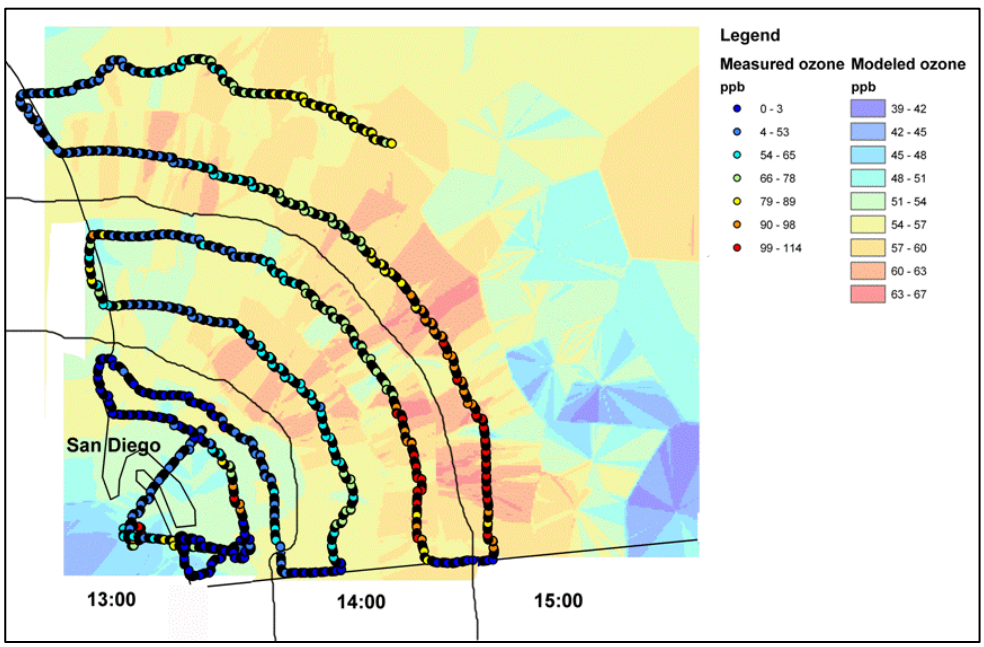


Figure 3. Comparison of observed vs. predicted $O_3$ concentrations for July 9, 2003 13:00-15:00.

In the last example (July 17, Figure 4), aside from localized hotspots, the predictions and observations have good spatial and temporal correlation. During the early period the model and measurements agree on the location of the $O_3$ trough over the San Diego metropolitan area. Later in the day, generally uniform levels of ozone reside over the most of the study area (except for the border with Mexico) as seen in the measurements.

In general, the model successfully predicted high $O_3$ levels for July 7 and July 9 and lower levels on July 17. These predictions are consistent with the flight observations and the synoptic situation that indicated a shallower low pressure system over San Diego on July 17. The model consistently predicted low $O_3$ concentrations to the east of the Laguna Mountains, an area that due to its topography is not influenced by sources to the west. Further, for all three cases, the model correctly predicted low $O_3$ over the harbor and downtown areas during the beginning part of the flight period (corresponding to the earliest part of the measurement day). Later in the day, with the flights progressing inland and the air mass aging, $O_3$ levels were predicted to gradually build up, again consistent with the observations. The buildup terminates as the air masses meet the inland mountain area.

While the spatial and temporal patterns are consistent, the model tended to under predict the observed absolute values. Measurements ranged between of background

of approximately 40 ppb up to a maximum of nearly 120 ppb. Model predictions did not exceed 80 ppb. This is typical problem observed in other studies and is generally corrected by adjusting the inventory to "calibrate" the model. Another possible explanation is the duration of the simulation at each grid cell needs to be extended. Presently the duration of the chemical simulation inside the box model is equal to the residence time of the particle in the box and there is no spin-up period for the chemical reactions. An extension of the time period for the box reactions may address this issue; however, with our current computational resources this is not yet practical.

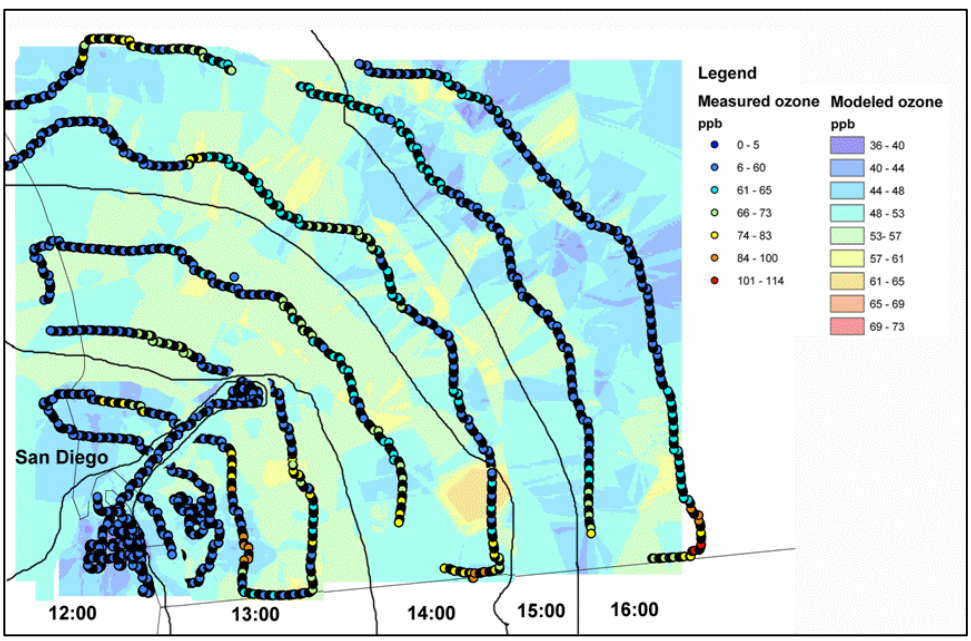


Figure 4. Comparison of observed vs. predicted $O_3$ concentrations for July 17, 2003 12:00-16:00.

## 4. CONCLUSION

Many areas that suffer from high levels of air pollution are located in coastal regions where the meteorology is complex. While current air pollutant modeling systems can accurately predict chemical transformations under these conditions, they have difficulty predicting pollutant transport and dispersion. In order to reduce this uncertainty, there is a need to develop more effective predictive tools if we are to implement effective strategies to improve air quality. To address this issue, this we developed a hybrid model that does not incorporate the chemistry module within the dispersion-advection module but rather implements the chemistry module in a post-processing mode. Thus we were able to take advantage of the strengths of the various approaches and use a Lagrangian model to predict transport and dispersion and a Eulerian approach to predict the chemical transformations. A further advantage of this approach is it is a modular system that can readily employ alternative chemical and transport-dispersion modules. .

Model testing and validation was performed using extensive aircraft data obtained during a period of elevated $O_3$ over the San Diego area of south western California. To directly compare the observations with predictions, a kriging interpolation was performed for the predicted $O_3$ concentrations for each hourly period and the mapped results were cut into hourly sections corresponding to the flight time and location. A mosaic from the hourly sections was then assembled to match the flight information. While the spatial and temporal patterns are consistent, the model tended to underpredict the observed peak values. This is likely due to inventory uncertainty and/or the need to extend the time period for the chemical simulations.

## 5. ACKNOWLEDGEMENTS

The authors wish to acknowledge Dr. Roger Tanner, R.J. Valente, S.T. Bairai, Vince Van Pelt and David Branscomb of TVA for their assistance with the airborne measurements. This study was sponsored by the Strategic Environmental Research and Development Program (SERDP), under contract CP-1253, Dr. Robert Holst program manager.

## REFERENCES

Alexis, A., Gaffney, P., Garcia, C., Nystrom, M., Rood, R., 2000. The 1999 California Almanac of Emissions and Air Quality. California Air Resources Board, Sacramento, California.

Carlton, J., 2004. Wall Street Journal (Eastern Edition). New York, N.Y., Nov 17, 2004, p.D.1

Brasseur, G., Pszenny, A., 1998. Draft prospectus for the IGAC integration & synthesis (I&S), http://medias.obs-mip.fr:8000/igac/.

Dudhia, J., 1993. A Nonhydrostatic Version of the Penn State–NCAR Mesoscale Model: Validation tests and simulation of an Atlantic cyclone and cold front. Monthly Weather Review 121, 1493–1513.

Dudhia, J., 2001. Mesoscale model nesting and boundary conditions. National Center for Atmospheric Research, Boulder, Colorado, http://meteo.usc.es/ documents/jm.pdf.

Dudhia, J., Bresch, J.F., 2002. A global version of the PSU-NCAR mesoscale model. Monthly Weather Review 130, 2898-3007.

Dudhia, J., Gill, D., Manning, K., Wang, W., Bruyene, C., 2003. PSU/NCAR Mesos-cale Modeling System Tutorial Class Notes (MM5 modeling system version 3), http://www.mmm.ucar.edu/mm5/ documents/tutorial-v3-notes.html.

Grell, G., Dudhia, J., Stauffer, D., 1994. A description of the Fifth-Generation Penn State/NCAR Mesoscale Model (MM5). NCAR/TN-398+STR, 117 pp, http://www.mmm.ucar.edu/mm5/doc1.html.

Kahyaoğlu-Koračin, J., Bassett, S., Mouat, D., Gertler, A.W., 2005. A scenario-based modeling system to predict the air quality impact from future growth. Presented at AQM2005, Istanbul, Turkey, 25-30 September 2005.

Koračin, D., Isakov V., Frye, J., 1998. A Lagrangian particle dispersion model (LAP) applied to transport and dispersion of chemical tracers in complex terrain.

Presented at the Tenth Joint Conference on the Applications of Air Pollution Meteorology, Phoenix, AZ, 11-16 January 1998.
Koračin, D., Frye, J., Isakov, V., 2000. A method of evaluating atmospheric models using tracer measurements. Journal of Applied Meteorology 39, 201-221.
Koračin, D., Isakov, V., Podnar, D., Frye, J., 1999. Application of a Lagrangian random particle dispersion model to the short-term impact of mobile emissions. Proceedings of the Transport and Air Pollution conference, Graz, Austria, 31 May - 2 June 1999.
Luria, M., Tanner, R.L., Valente, R.J., Bairai, S.T., Koracin, D., Gertler, A.W., 2005. Local and transported pollution over San Diego California. Atmospheric Environment, in press.
Madronich, S., 1987. Photodissociation in the atmosphere; 1. actinic flux and the effects on ground reflections and clouds. Journal of Geophysical Research 92, 9740-9752.
Peters, L.K., Berkowitz, C.M., Carmichael, G.R., Easter, R,C., Fairweather, G., Ghan, S.J., Hales, J.M., Leung, L.R., Pennell, W.R., Porta, F.A., Saylor, R.D., Tsang, T.T., 1995. The current state and future direction of Eulerian models in simulating the tropospheric chemistry and transport of trace species – a review. Atmospheric Environment 29, 189-222.
Pielke, R. A., 1984. Mesoscale Meteorological Modeling. Academic Press. 612pp.
Seefeld, S., 1997. Laboratory kinetic and atmospheric modelling studies of the role of peroxyacyl nitrates in tropospheric photo-oxidant formation. Ph.D. Thesis, Swiss Federal Institute of Technology Zurich (ETH).
Song, C.K., Kim, C.H., Lee, S.H., Park, S.U., 2003. A 3-D Lagrangian particle dispersion model with photochemical reactions. Atmospheric Environment 37, 4607-4623.
Stein, A.F., Lamb D., Draxler, R.R., 2000. Incorporation of detailed chemistry into a three-dimensional Lagrangian-Eulerian hybrid model: Application to regional tropospheric ozone. Atmospheric Environment 34, 4361-4372.
Stockwell, W.R., Kirchner, F., Kuhn, M., Seefeld, S., 1997. A new mechanism for regional atmospheric chemistry modeling. Journal of Geophysical Research 102, 25847-25879.
Stockwell, W.R., Middleton, P., Tang, X., Chang, J.S., 1990. The second generation regional acid deposition model chemical mechanism for regional air quality modeling. Journal of Geophysical Research 95, 16343-16367.
Stohl, A., 1998. Computation, accuracy and applications of trajectory- a review and bibliography. Atmospheric Environment 32, 947-966.

*Proceedings of the Third International Symposium on Air Quality Management at Urban, Regional and Global Scales. 26-30 September 2005, Istanbul – Turkey*

# EMISSION SOURCES AND THEIR EFFECT ON MAXIMUM OZONE CONCENTRATIONS OVER GREECE

**Poupkou Anastasia[1,a], Symeonidis Panagiotis[1,b], Lisaridis Iraklis[1,c], Ziomas Ioannis[2], Melas Dimitrios[1,d], Yay Ozan Devrim[1,e] and Balis Dimitrios[1,f]**

1. Aristotle University of Thessaloniki, Laboratory of Atmospheric Physics, Greece, [a]poupkou@auth.gr, [b]symeonidis@draxis.gr, [c]hralys@auth.gr, [d]melas@auth.gr, [e]odyay@anadolu.edu.tr, [f]balis@auth.gr
2. National Technical University of Athens, Department of Chemical Engineering, Greece, ziomas@orfeas.chemeng.ntua.gr

## ABSTRACT

The purpose of this study is to investigate the impact of the anthropogenic emissions from maritime transport and from Greece's neighboring countries on the maximum ground-level $O_3$ concentrations over Greece during the summer period when enhanced photochemical $O_3$ production is favored. The photochemical model Urban Airshed Model (UAM-V) coupled with the meteorological model MM5 was used to address this issue.

**Key Words :** Anthropogenic Emissions, Ozone, Photochemical Modeling

## 1. INTRODUCTION

Ozone is of concern because of its adverse effects both on human health and on ecosystems. As a secondary pollutant, it is not emitted directly, but is generated in the atmosphere through complex series of chemical reactions initiated by absorption of solar energy [Seinfeld and Pandis, 1998]. Its generation is typically favored in high-pressure, stagnant atmospheric systems at locations with substantial concentrations of oxides of nitrogen (NOx) and volatile organic compounds (VOCs). Both NOx and VOCs originate either from anthropogenic source sectors, e.g. the industrial and the transport sector, or from biogenic sources. Both anthropogenic and biogenic sources play roles in $O_3$ formation and accumulation. While the impact of biogenic emissions on surface $O_3$ has been more thoroughly examined by many studies (Roselle et al., 1991; Pierce et al., 1998; Varinou et al., 1999; Tao et al., 2003), the role of anthropogenic emission sources in the production of ground-level $O_3$ has not been extensively investigated.

Greece is situated at the Eastern Mediterranean which is an area characterized by enhanced regional levels of $O_3$, especially during the summer months, as a result of both the long-range transport in the area of significant $O_3$ and $O_3$ precursors' amounts from continental Europe and the high levels of solar radiation in combination with the local anthropogenic and biogenic $O_3$ precursors' emissions (Zerefos et al., 2002; Kouvarakis et al., 2002). Increased $O_3$ concentrations over Greece have been measured both on urban and regional scale (Kourtidis et al., 2002; Ziomas et al., 1998). The greater part of Greece is surrounded by maritime areas. Sea transport

activities are an important emission source of the area. In addition Greece is neighboring with other Balkan countries significantly heterogeneous not only in environmental but also in economic and social aspects.

The principle purpose of this work is to assess the effect of the emissions from sea transport and from Greece's neighboring countries on the ground-level $O_3$ concentrations over Greece using the air quality model Urban Airshed Model (UAM-V) coupled with the meteorological model MM5. The study domain covers Greece, Albania, FYROM, western Turkey, southern Serbia and Montenegro and the greater part of Bulgaria. We base the modeling on a 2000 summer period, and select the absolute maximum hourly $O_3$ concentrations for in depth analysis.

## 2. MODELS AND DATA USED

The UAM-V model is a 3-D regional photochemical grid model designed to calculate the concentrations of both inert and chemically reactive pollutants by simulating the physical and chemical processes in the atmosphere that affect pollutant concentrations (SAI, 1999). The basis for the model is the atmospheric diffusion or species continuity equation. The major processes that the model simulates which also affect $O_3$ levels are: 1) the spatial and temporal distribution and the composition of emissions of NOx and VOCs, 2) the spatial and temporal variations in the wind fields, the temperature and the solar insolation, 3) the dynamics of the boundary layer, 4) the loss of $O_3$ and $O_3$ precursors by dry and wet deposition, 5) the ambient background of VOCs, NOx, and other species and 6) the chemical reactions involving VOC, NOx, and other important species. The UAM-V program employs an extension of version IV of the Carbon Bond Mechanism (CB-IV) for solving chemical kinetics which is called CB-IV-TOX.

The meteorological model MM5 was used to produce the hourly meteorological fields necessary for the implementation of the UAM-V model. The Mesoscale Model MM5 is a limited-area, nonhydrostatic, terrain-following sigma-coordinate model designed to simulate or predict mesoscale and regional-scale atmospheric circulation (Grell et al., 1994). Using the capability of MM5 for multiple nesting, the model run with the option of two way nesting for two domains (figure 1). The large domain, covering the South-Eastern Mediterranean, was consisted of 55 x 55 grid points having 30km x 30km spatial resolution. The finer domain, covering the study area, was consisted of 115 x 115 grid points having 10km x 10km spatial resolution. Simulations starting at 18:00 UTC and ending after 78 hours were performed in order to produce meteorological data for a time period extending from 11 June 2000 to 31 July 2000. MM5 simulations were initialised and developed lateral boundary conditions using NCEP Global Analyses. Both of the domains had the same vertical structure consisted of 33 $\sigma$ levels.

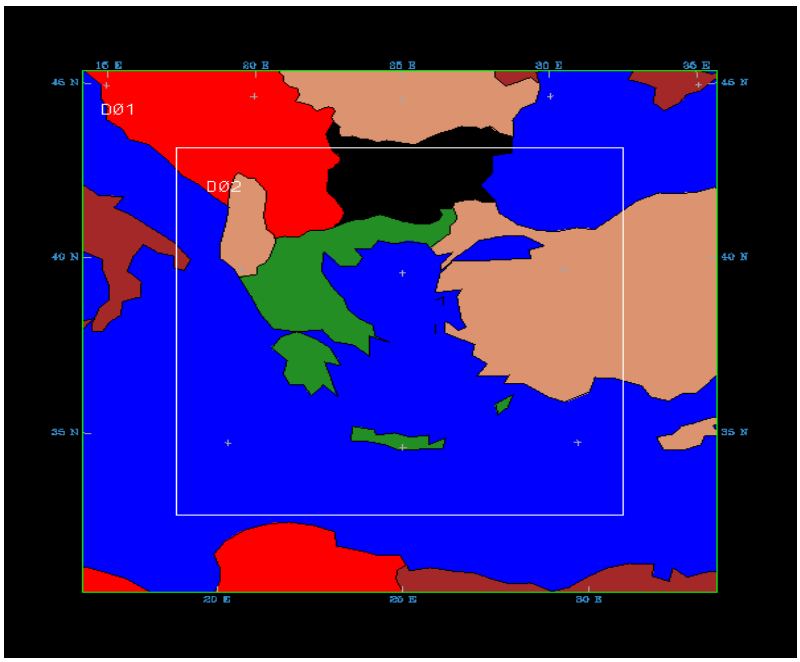


Figure 1. MM5 modeling domains.

The gridded, hourly, and speciated biogenic and anthropogenic emissions data used as input data to the photochemical model were based on an emission inventory compiled for the Balkan Region having high spatial and temporal resolution (Symeonidis et al., 2004; Poupkou et al., 2004). Following the methodology of the EMEP/CORINAIR emission inventory guidebook (EMEP/CORINAIR Guidebook, 2002), typical diurnal biogenic emission variations of isoprene and monoterpenes, emitted from different land use types (forests, shrub species and agricultural crops) extracted from satellite data, were calculated for every month of the year with spatial resolution of 10km x 10km. Using the top-down methodology on reported emission data of the years 1994-2000 (Ritter, 1997; EMEP/MSC-W, 2002), annual emission fields of NOx, NMVOCs and CO for different anthropogenic emission source sectors such as the transport sector, the industrial sector and the central heating sector were estimated with spatial resolution of 10km x 10km. More detailed was the transport sector emission inventory for Greece calculated using methodologies of the EMEP/CORINAIR emission inventory guidebook (EMEP/CORINAIR Guidebook, 2002). The anthropogenic annual emission data were temporally disaggregated in order to get seasonal and diurnal emission variations.

Figure 2 presents, for each of the 3 anthropogenic pollutants, percentage emission contributions by geographical area of the study domain. The different geographical areas that are separately being examined are the continental parts of the countries included in the study domain and the maritime area considered as a whole. NOx emissions from maritime transport activities represent about 34% of the annual total anthropogenic NOx emissions and are comparable to NOx emissions of continental Greece which have a percentage contribution of almost 29%. NOx emissions of continental western Turkey have an 18% share in overall NOx emissions. Summing

NOx emissions of all other geographical areas we calculate a 19% contribution to NOx emissions total. NMVOCs emitted from continental Greece and western Turkey respectively account for 47% and 35% of the annual total anthropogenic NMVOCs emissions while less important is the contribution of the rest of the geographical areas to NMVOCs emissions. Most significant are the CO amounts emitted from continental Greece and western Turkey each one representing 36% of the total CO emissions. CO emissions of the continental part of Bulgaria included in the area of study have a 17% share in the overall CO emissions.

It can be pointed out that sea transport activities at the maritime area of the study domain are an important NOx emission source. Pollutants' emissions from the rest geographical areas other than Greece seem to be less significant compared to emissions of continental Greece. The only exception is western Turkey representing pollutants' emissions which, despite the fact that in some cases are less than those of Greece, they can be however considered comparable. It is worth noticing that the contribution of the other countries than Greece to the total pollutants' emissions might be underestimated since these emissions are poorly reported.

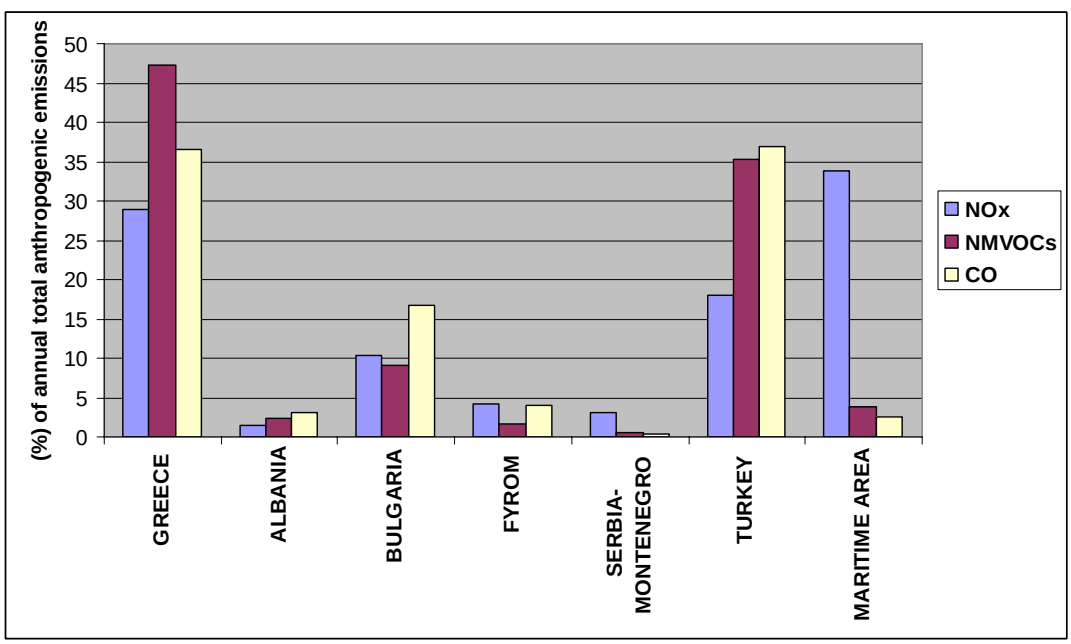


Figure 2. Percentage emission contributions by geographical area of the study domain.

UAM-V was used to simulate ambient $O_3$ concentrations across the domain and to quantify the effect of the anthropogenic emissions from sea transport and from Greece's neighboring countries on the ground-level $O_3$ concentrations over Greece. The domain was divided into 110 rows by 110 columns with a horizontal grid resolution of 10 km. There were 5 vertical layers extending from surface to approximately 2.5 km above the ground. The vertical layers were unevenly distributed with higher resolution at the near-surface layers. The first layer height was 50 m. The analysis of the model results concerns the first layer of the model. To

run UAM-V, proper initial and boundary conditions must be prescribed. The boundary conditions used represent background atmospheric conditions. The boundary concentrations for $O_3$ were set to 40 ppb. In this study the initial conditions were set using the preconditioning technique which began with an initial guess of the species concentrations and was followed by a 3-day ‘‘spin-up’’ simulation. The final hour concentration of each species from the preconditioning run was then set as the initial conditions for the full period simulation. Successive 3-day model simulations were performed in order to calculate hourly $O_3$ concentrations for the time period of interest extending from 14 June 2000 to 31 July 2000.

The UAM-V model was implemented considering 3 different emission scenarios. According to them $O_3$ concentrations were calculated with the use of:

1. Base emission scenario: Biogenic and all anthropogenic emissions.
2. 2nd emission scenario: Biogenic and anthropogenic emissions excluding maritime transport sector emissions.
3. 3rd emission scenario: Biogenic and anthropogenic emissions excluding the anthropogenic emissions of all continental geographical areas of the study domain other than Greece.

Our study focuses in the study of spatial distribution of the differences (df) defined as:

$$df = [O_3]_{i\ emission\ scenario} - [O_3]_{base\ emission\ scenario} \qquad (i = 2nd, 3rd) \qquad (1)$$

where $[O_3]$: absolute maximum hourly $O_3$ concentration (figures 3, 4).

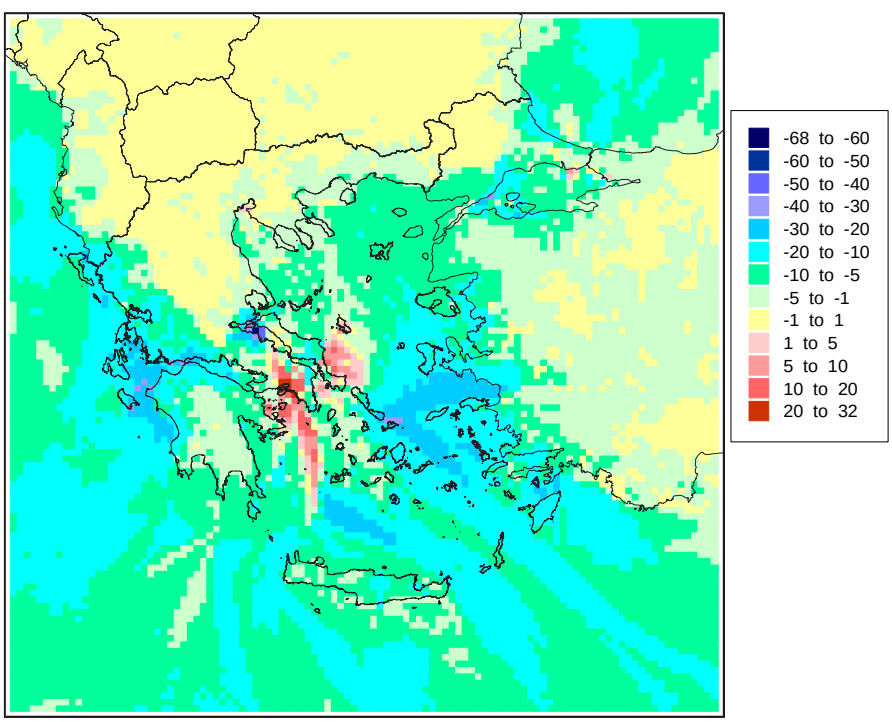


Figure 3. The impact of the maritime transport emissions on the absolute maximum hourly $O_3$ concentrations (ppb) as calculated with equation (1).

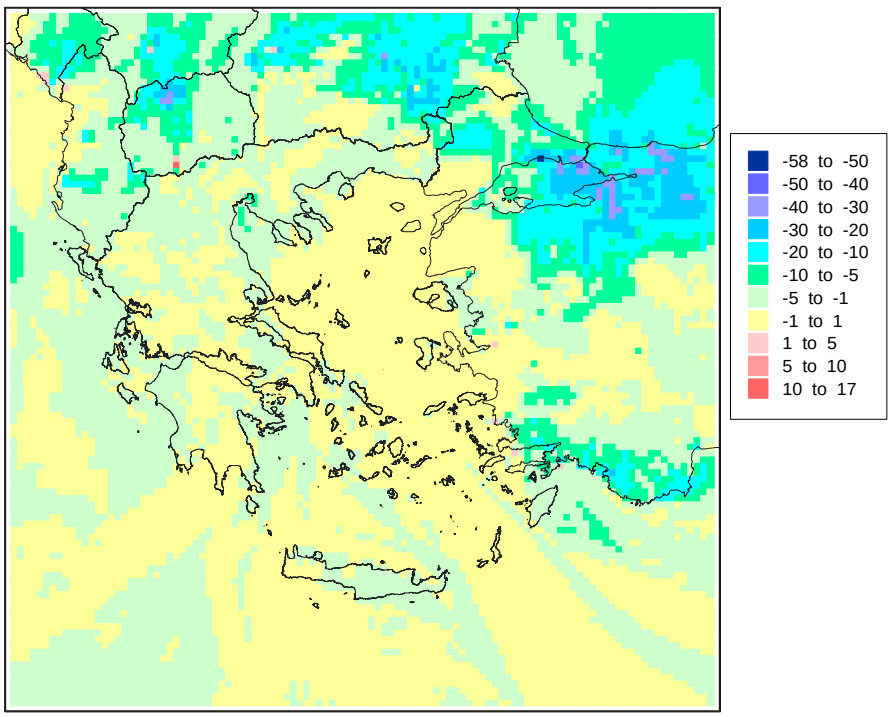


Figure 4. The impact of the anthropogenic emissions of all continental geographical areas of the study domain other than Greece on the absolute maximum hourly $O_3$ concentrations (ppb) as calculated with equation (1).

## 3. DISCUSSION - CONCLUSIONS

The influence of maritime transport emissions on the maximum $O_3$ concentrations over Greece is significant. When these emissions are not taken into account for the calculation of $O_3$ concentrations there is a general reduction of absolute maximum hourly $O_3$ levels over Greece. Over the continental part of the country $O_3$ reduction can be on the order of 20 ppb. Over maritime areas the decrease is more pronounced reaching 68 ppb. However, over the greater Athens area and the maritime region southern of the city, maximum $O_3$ levels increases are observed ranging from 10 ppb to 32 ppb. Such areas are influenced by high NOx amounts that are emitted from the sea transport activities. The elimination of these emissions prohibits $O_3$ destruction which is photochemically produced by $O_3$ precursors released in significant amounts by the emission sources of the large urban agglomeration of Athens.

Small decrease of maximum $O_3$ levels on the order of 5 ppb is estimated over Greece when continental anthropogenic emissions of all countries other than Greece are considered equal to zero. The greater area of Thessaloniki, which is a large city situated at northern Greece, is more affected since there the reduction of maximum $O_3$ levels ranges from 5 ppb to 10 ppb. Ozone concentrations are reduced over the greater part of the rest modeling domain. The reductions are larger (maximum values up to 58 ppb) over areas where large urban centers or important emission sources are

located, for example over the northern part of western Turkey, over the central Bulgaria and northern FYROM.

In conclusion, the emissions from maritime transport are estimated to have greater impact on maximum ozone levels over Greece compared to the emissions of countries neighboring with Greece. However, as emissions of Balkan countries are generally poorly reported their contribution might be underestimated. Improved emission estimations for the whole area of study are undoubtedly suggested.

## 4. ACKNOWLEDGEMENTS

This research was financially supported by the Greek Ministry of Education (research program PYTHAGORAS).

## REFERENCES

EMEP/CORINAIR Emission Inventory Guidebook - 3rd edition, 2002. European Environment Agency.

EMEP/MSC-W, 2002. Emission data reported to UNECE/EMEP: Quality assurance and trend analysis & Presentation of WebDab. MSC-W Status Report 2002, EMEP/MSC-W NOTE 1/2002.

Grell, G. A., Dudhia, J. and Stauffer, D. R., 1994. A description of the fifth-generation Penn State/NCAR mesoscale model (MM5). NCAR Technical Note, NCAR/TN-398+STR.

Kourtidis, K., Zerefos, C., Rapsomanikis, S., Simeonov, V., Balis, D., Perros, P. E., Thompson, A. M., Witte, J., Calpini, B., Sharobiem, W. M., Papayannis, A., Mihalopoulos, N. and Drakou, R., 2002. Regional levels of ozone in the troposphere over eastern Mediterranean. Journal of Geophysical Research, 107, NO. D18, 8140, doi:10.1029/2000JD000140.

Kouvarakis, G., Vrekoussis, M., Mihalopoulos, N., Kourtidis, K., Rappengluck, B., Gerasopoulos, E., Zerefos, C., 2002. Spatial and temporal variability of tropospheric ozone ($O_3$) in the boundary layer above the Aegean Sea. Journal of Geophysical Research 107 (D18): art. no. 8137.

Pierce, T., Geron, C., Bender, L., Dennis, R., Tonnesen, G., Guenther, A., 1998. Influence of increased isoprene emissions on regional ozone modeling. Journal of Geophysical Research 103, 25,611–25,629.

Poupkou, A., Symeonidis, P., Lisaridis, I., Pouspourika, E., Yay, O.D., Melas, D., Ziomas, I., Balis, D. and Zerefos, C., 2004. Compilation of an emission inventory for the purpose of studying the regional photochemical pollution in the Balkan Region. In: Proceedings of Quadrennial Ozone Symposium 2004, pp. 902-903.

Ritter, M., 1997. CORINAIR 94 Summary Report, Final Version. European Topic Centre on Air Emissions, European Environmental Agency.

Roselle, S.J., Pierce, T.E., Schere, K.L., 1991. The sensitivity of regional ozone modeling to biogenic hydrocarbons. Journal of Geophysical Research 96, 7371–7394.

SAI, 1999. User's Guide to the Variable-Grid Urban Airshed Model (UAM-V). Systems Applications International Inc., SYSAPP 99-95/27r3.

Seinfeld, J. H. and P. J. Pandis, 1998. Atmospheric Chemistry and Physics: From Air Pollution to Climate Change, John Wiley, New York.
Symeonidis, P., Ziomas, I. and Proyou, A., 2004. Development of an emission inventory system from transport in Greece. Environmental Modelling & Software, Vol. 19, Num 4, 413-421.
Tao, Z., Larson, S.M., Wuebbles, D.J., Williams, A., Caughey, M., 2003. A summer simulation of biogenic contributions to ground-level ozone over the continental United States. Journal of Geophysical Research 108 (D14), 4404.
Varinou, M., Kallos, G., Tsiligiridis, G. and Sistla, G., 1999. The role of anthropogenic and biogenic emissions on tropospheric ozone formation over Greece. Phys. Chem. Earth (C), 24, pp. 507–513.
Zerefos C., K. Kourtidis, D. Melas, D.S. Balis, P. Zanis, H. T. Mantis, C. Repapis, I. Isaksen, J. Sundet, J. Herman, P.K. Bhartia and B. Calpini, 2002. Photochemical Activity and Solar Ultraviolet Radiation Modulation Factors (PAUR): An overview of the project. Journal of Geophysical Research 107, D18, 10.1029/2000JD000134.
Ziomas, I., Tzoumaka, P., Balis, D., Melas, D., Zerefos, C. and Klemm, O., 1998. Ozone episodes in Athens, Greece. A modelling approach using data from the MEDCAPHOT-TRACE. Atmospheric Environment, 32, pp. 2313-2321.

*Proceedings of the Third International Symposium on Air Quality Management at Urban, Regional and Global Scales. 26-30 September 2005, Istanbul – Turkey*

# ON THE PARAMETERIZATION OF MAXIMAL AND CRITICAL CHARACTERISTICS FROM CONTINUOUS POINT SOURCE AT DIFFERENT METEOROLOGICAL CONDITIONS

**E. Syrakov and M. Tsankov**

University of Sofia, Faculty of Physics, Department of Meteorology and Geophysics, J. Baucher str. 5, Sofia 1164, Bulgaria, esyrakov@phys.uni-sofia.bg

## ABSTRACT

On the basis of generalization of Ragland's (1976) method, it is determined the maximal and critical (worst-case) pollutant parameters from Gaussian dispersion plume model. It is used Brigg's formula for effective height and dispersions $\sigma_z, \sigma_y$, which are approximated with power laws.

It is considered the effects of gravity deposition, inversion and the dependence of the wind speed on the height. At these conditions general analytical expressions are derived for urban and rural regions for the critical concentration and its location, critical wind speed at ten meters height, the "minimal" stack height for newly planned industrial sources, etc. The meteorological conditions are parameterized in terms of the Pasquill-Turner stability classes A-F.

It is considered and some of these problems with application to non-Gaussian diffusion model.

The result can be used to estimate and standardize the worst-case ambient air concentrations from continuous sources and for determination of the meteorological conditions at which they occur.

**Key Words:** Critical Parameters, Stability Classes, Deposition, Inversion, Gaussian and non-Gaussian Model.

## 1. INTRODUCTION

The maximal concentration obtained from the stack of a given industrial region depends mainly on the stack parameters and the meteorological conditions. To find the critical (maximal of the maximal) concentration, the distance, wind speed and the stratification conditions under which it occurs is more important task. The critical parameters allow to estimate the worst-case ambient pollution conditions, to determinate the stack height of newly planned industrial sources, and also for evaluation of the environmental impact of already existing sources.

Basic method for determination of the critical parameters at power laws for the dispersions and constant with the height speed gives Raglang (1976). Here we will extend the application of this approach considering some more complex diffusion and meteorogical conditions and actualized data for the dispersions and the effective height of the source. On the basis of power law approximation of the well known dispersion curves of Briggs for $\sigma_z(x)$ and $\sigma_y(x)$, it appeared to be possible to obtain analytical expressions for the critical parameters for a relatively wide range of diffusion and meteorological conditions.

## 2. FORMULATION OF THE PROBLEM

Let's use the Gaussian pollution distribution formula, from source situated in the point $x = y = 0$. The ground level ( $z = 0$ ), concentration $C$ along the plume centerline ( $y = 0$ ) is given by:

$$C = \frac{Q}{\pi U_H \sigma_y \sigma_z} \exp\left[-H^2 / 2\sigma_z\right]$$

(1)

where $Q$ is emission rate, $U_H$ is the wind speed at the effective stack height $H$. The quantity $H$ is calculated according Briggs formula (see Hanna, 1982).

$$H = h_s + \Delta h \,, \Delta h = F U_s^{-l} \,,$$

(2)

where $h_s$ is the geometric stack height, $\Delta h$ is the plume rise, $U_s = U(z = h_s)$, $F$ is characteristic technological parameter, $l$ is parameter with value 1or1/3 (see table.1). Wind profile $U(z)$ is given as:

$$U(z) = U_{10}(z/10)^m$$

(3)

where $U_{10}$ is the wind speed at standard level 10m and the parameter $m$ depends on the Pasquill stability classes (Hanna, 1982), see table.1.

Taking into account (3) we receive the following expressions for $U_H$ and $U_s$:

$$U_H \equiv U(z = H) = U_s \left(\frac{H}{h_s}\right)^m \,, U_s \equiv U(z = h_s) = U_{10}\left(\frac{h_s}{10}\right)^m$$

(4)

For dispersion parameters $\sigma_z(x)$, $\sigma_y(x)$, it is used the well known formulas of Briggs. In the present work they are approximated with enough precision with the convenient for work power laws:

$$\sigma_z(x) = ax^b \,, \sigma_y(x) = cx^d \,,$$

(5)

where the approximation coefficients $a, b, c, d$ are given in table 1.

Table1. Values of the used parameters for calculation for rural and urban regions.

| | $Z_0$=0.03m - Rural | | | | | | $Z_0$=1m - Urban | | | | | |
|---|---|---|---|---|---|---|---|---|---|---|---|---|
| *Kl.* | m | a | b | c | d | l | m | a | b | c | d | l |
| A | 0,17 | 0,20 | 1,00 | 0,36 | 0,92 | 1 | 0,06 | 0,08 | 1,15 | 1,42 | 0,76 | 1 |
| B | 0,175 | 0,12 | 1,00 | 0,34 | O,89 | 1 | 0,07 | | | | | |
| C | 0,2 | 0,30 | 0,79 | 0,25 | 0,87 | 1 | 0,075 | 0,20 | 1,00 | 1,32 | 0,72 | 1 |
| D | 0,27 | 0,76 | 0,57 | 0,20 | 0,86 | 1 | 0,13 | 0,91 | 0,72 | 1,14 | 0,70 | 1 |
| E | 0,39 | 1,04 | 0,47 | 0,26 | 0,80 | 1/3 | 0,33 | 0,93 | 0,69 | 0,87 | 0,69 | 1/3 |
| F | 0,61 | 1,15 | 0,39 | 0,34 | 0,73 | 1/3 | 0,54 | | | | | |

### 2.1 Maximal parameters and normalization procedure

Differentiating (1) by $x$, taking into account (5), and nullifying the obtained expression, leads to the following relation for distance $x_m$ at which the surface concentration has maximum(Ragland, 1976):

$$x_m = k_1 H^{1/b}, k_1 = \left[\frac{b}{a^2(b+d)}\right]^{1/2b} \quad (6)$$

The dependence of $x_m$ on $H$ ( taking into account the parameters of table.1.) is demonstrated in Fig.1. Inserting (6) in (1), taking into account (4) and (5), we define the maximal surface concentration $C_m$:

$$C_m = \frac{Q}{\pi U_{10}} \frac{k_2 10^m}{k_1^{b+d}} H^{-\left(m+\frac{b+d}{b}\right)}, \qquad k_2 = \frac{\exp((b+d)/2b)}{ac} \quad (7)$$

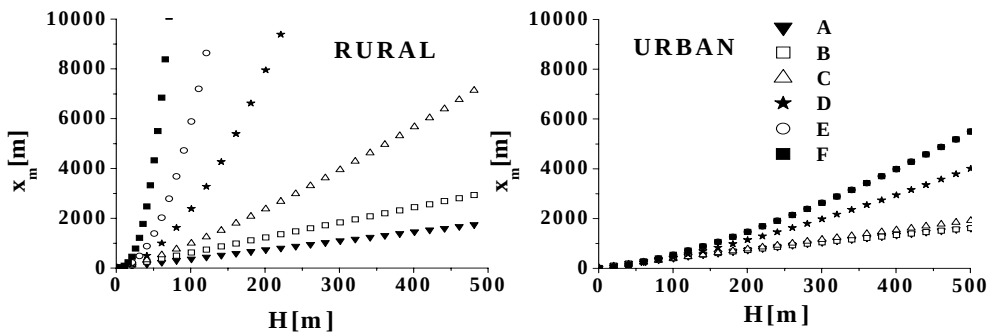


Figure 1. The dependence of $x_m$ on $H$ at different stability classes for rural and urban region.

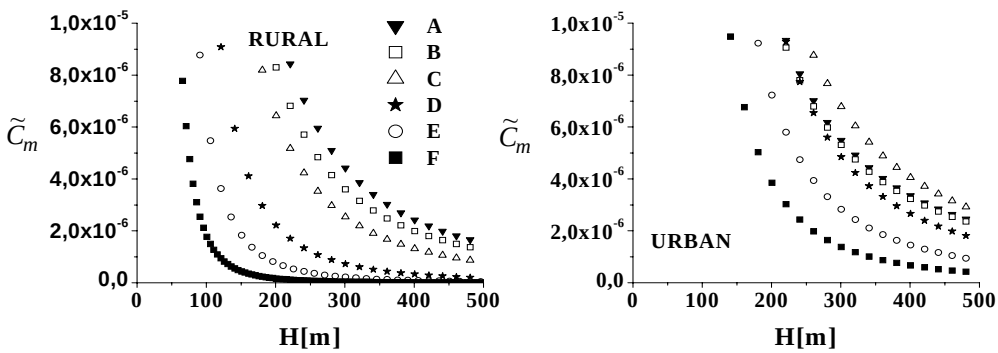


Figure 2. Same as in Fig. 1, but for $\widetilde{C}_m$.

On Fig.2 is demonstrated the dependence of $\widetilde{C}_m = C_m/(Q/\pi U_{10})$ on $H$ for rural and urban region.. It can be seen that $\widetilde{C}_m$ is greater for urban region because of the more intensive mixing turbulent processes over it. Using the so determined maximal parameters $x_m$ and $C_m$ and considering (5), the surface concentration (1) can be normalized:

$$C_s = \frac{\exp(2r)}{\widetilde{x}^{4r}} \exp\left[-\frac{2r}{\widetilde{x}^2}\right],$$

where $C_s = C/C_m$, $\widetilde{x} = (x/x_m)^b$, $r = (1/2)(1 + d/b)$. The dependence of $C_s$ on $\widetilde{x}$ for different stability classes is presented on Fig.3

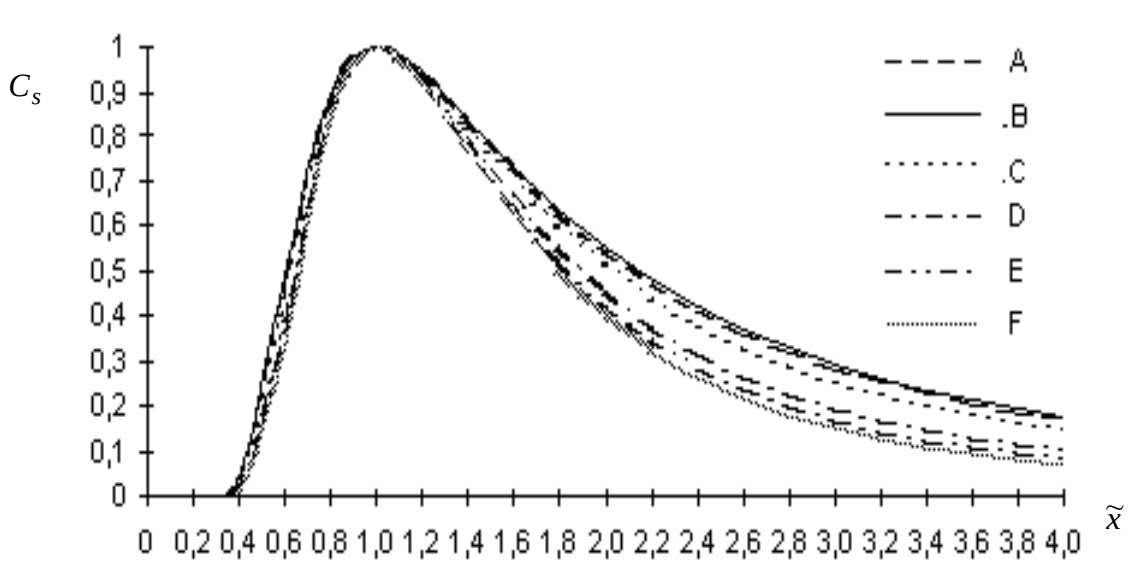


Figure 3. Dependence of the normalized surface concentration $C_s = C/C_m$ on dimensionless distance $\widetilde{x} = (x/x_m)^b$ at different stability classes

### 2.2 Critical parameters

A great practical interest is the finding of a critical value $U_{10cr}$, at which for all meteorological conditions, the concentration $C_m$ is maximized. Taking into account (2), (4) and differentiating $C_m$ from (7) by $U_{10}$ and setting the obtained expression equal of zero (condition for extremum), the following expression of critical wind velocity value $U_{10cr}$ can be obtained:

$$U_{10cr} = F^{1/l} 10^m k_3^{1/l} h_s^{-\frac{1+ml}{l}},$$

(8)

where $k_3 = l(m+k)-1, k = 1+\frac{d}{b}$.

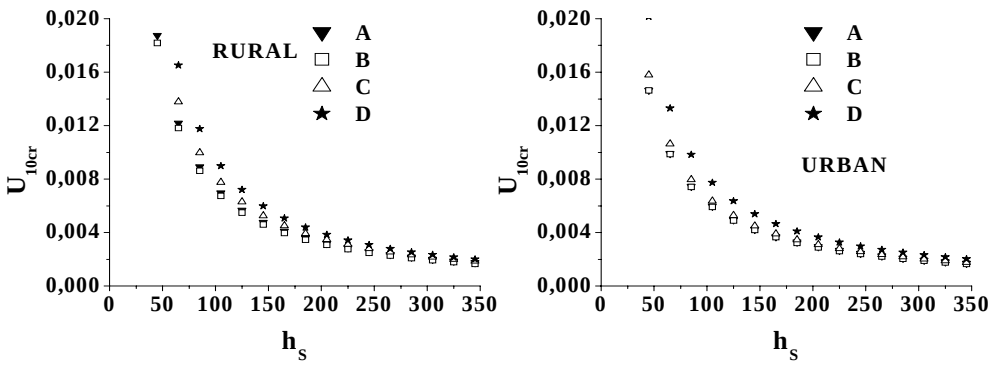


Figure 4. The dependence of the critical speed $U_{10cr}$ on $h_s$ at different stability classes for rural and urban region.

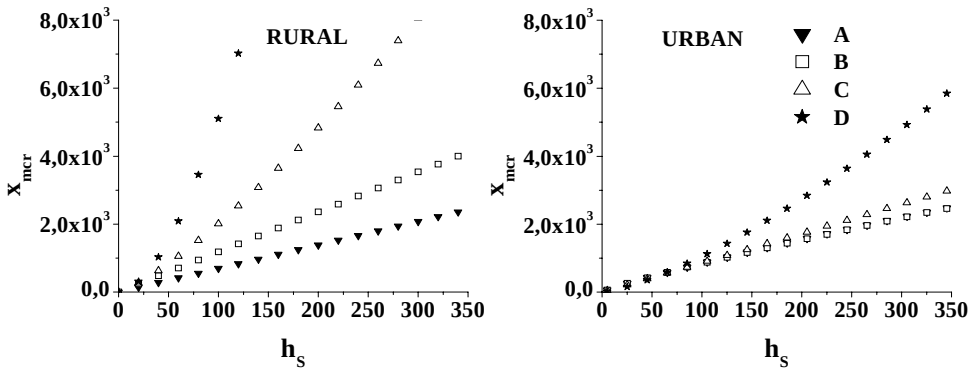


Figure 5. Same as Fig.4, but for $x_{mcr}$.

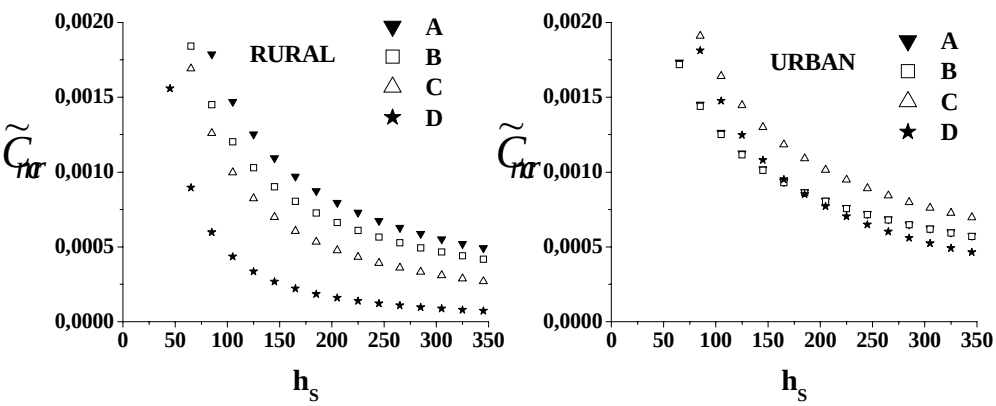


Figure 6. Same as Fig.4, but for $\tilde{C}_{mcr}$.

Now substituting (8) in (6), taking into account (4), we obtain the critical distance $x_{mcr}$ at which $C_{mcr}$ is realized:

$$x_{mcr} = k_1\left(1+\frac{1}{k_3}\right)^{1/b} h_s^{1/b}.$$

(9)

Considering (8), (9), (2), (4) from (7), we determine the critical (maximal of the maximal) surface concentration $C_{mcr}$ :

$$C_{mcr} = \frac{Q}{\pi}\frac{k_2}{k_1^{b+d}}\left(\frac{h_s}{F}\right)^{1/l} h_s^{-\frac{b+d}{b}}\left(1+\frac{1}{k_3}\right)^{-m-\frac{b+d}{b}} k_3^{-1/l}$$

(10)

On Fig.4-6 are presented the dependence of critical parameters $U_{10cr}$, $x_{mcr}$ and $\widetilde{C}_{mcr}$ on $h_s$ at selected stability classes A, B, C, D at which it is more likely to form critical condition for high stack sources.

Let's now determine the so called stack height of a planned new source $h_{sp}$ so, that at any meteorological conditions the surface pollution concentration does not exceed the Limit Admissible Concentration (LAC)- $C_{LAC}$ ( for given pollutant.) i.e. $C_{mcr} = C_{LAC}$ :

$$h_{sp} = \left[C_{LAC}\frac{\pi}{Q}F^{1/l}\frac{k_1^{b+d}}{k_2}\left(1+\frac{1}{k_3}\right)^{m+\frac{b+d}{b}}\right]^{\frac{bl}{b-bl-bd}}$$

(11)

Here we will give only qualitative analyze of some calculated critical parameters ( because of the limit space) for high ($h_s \in 120-320m$), strong overheated ($\Delta T_s \in 100-160K^o$), with diameter ($D \in 5-12m$), emission speed. $(V_s \in 6-20\,m/s)$ and emission of $SO_2$ ($0.1-10\,kg/s$) sources. The respective critical parameter are in the range $U_{10cr} \in 4-9\,m/s$, corresponding for classes $C-D$, $C_{mcr} \in (1.3-4.5)C_{LAC}$ and $x_{mcr} \in 4-40km$.

### 2.3 Effect of gravity deposition

In the case with gravity deposition velocity $w_0$, formula (1) turns to the form (see Wark and Warner 1976):

$$C = \frac{Q}{\pi U_H \sigma_y \sigma_z}\exp\left[-\left(H-\widetilde{w}_0 x\right)^2/2\sigma_z\right]$$

(12)

where $\widetilde{w}_0 = w_0/\overline{U}$, $\overline{U} = (1/H)\int_0^H U(z)dz = \frac{U_{10}}{1+m}\left(\frac{H}{10}\right)^m$

Applying similar procedure as at the determination of (6) (at $w_0 = 0$), but taking into account (12), now we obtain the following algebraic equations for determination of $x_{mw}$ in the case of considering gravity deposition:

$$a^2(b+d)x_{mw}^{2b} + \widetilde{w}_0(2b-1)Hx_{mw} + \widetilde{w}_0^2(1-b)x_{mw}^2 - bH^2 = 0 .$$

(13)

Equation (13) can be easily numerically integrated. Here we will limit to the cases $b = 1$ and $b = 1/2$, at which (13) becomes a quadratic equation which have analytical solution. We will note that most of the values of $b$ are in the range 0.5-1. At $b = 1/2$ (around that value approximately is related the stability classes D, E, F at rural region) the solution of (13) is:

$$x_{1mw} = x_{1m}\varphi_1, \varphi_1 = \frac{2}{1+\sqrt{1+4\widetilde{w}_0 p x_m}}, \qquad p = 4a^2/(1+2d)$$

(14)

where $x1_m$ is given with (6) at $b = 1/2$. Obviously at $w_0 = 0$ (14) coincide with (6).

At $b = 1$ (the classes A, B, C approximately unites around this value), the respective solution of (13) is:.

$$x_{2mw} = x_{2m}\varphi_2, \qquad \varphi_2 = \frac{1}{\widetilde{w}_0 \Big/ 2a(1+d)^{1/2} + \sqrt{\left(\widetilde{w}_0 \Big/ 2a(1+d)^{1/2}\right)^2 + 1}},$$

(15)

where $x_{2m}$ is given with (6) at $b = 1$.

Taking into account (14), (15) identically to the determination of (7) at $w_0 = 0$, we find now:

$$C_{1mw} = C_{1m} f_1, \qquad f_1 = \frac{1}{\varphi_1^{L_1}} e^{-L_1(R_1-\varphi_1)/\varphi_1}, \qquad R_1 = \left[1 - \frac{\widetilde{w}_0 H \varphi_1}{a^2(1+2d)}\right]^2, \qquad L_1 = \frac{1+2d}{2}$$

(16)

$$C_{2mw} = C_{2m} f_2, \qquad f_2 = \frac{1}{\varphi_2^{1+d}} e^{-L_2\left(R_2-\varphi_2^2\right)/\varphi_2^2}, R_2 = \left[1 - \frac{\widetilde{w}_0 \varphi_2}{a(1+d)^{1/2}}\right]^2, L_2 = \frac{1+d}{2},$$

(17)

where $C_{1m}$ and $C_{2m}$ are given by (7) at $b = 1/2$ and $b = 1$ respectively.

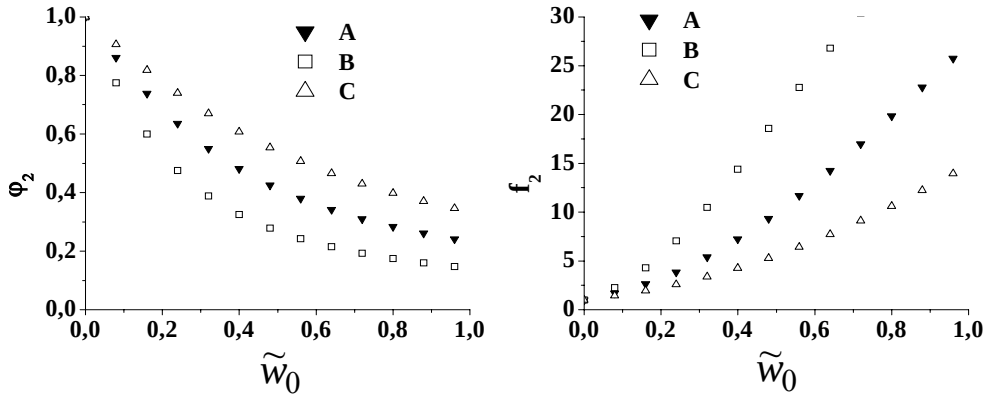


Figure 7. Dependence of correction deposition functions $\varphi_2 = x_{2mw}/x_{2m}$ and $f_2 = C_{2mw}/C_{2m}$ on $\widetilde{w}_0$ at different stability classes A, B, C for rural region.

As it can be seen from (14)-(17) the maximal characteristics $x_{mw}$ and $C_{mw}$ are expressed with the respective values for the case $\widetilde{w}_0 = 0$ and corrections functions considering the gravity deposition. So for example the dependence of the deposition correction functions $\varphi_2$ and $f_2$ on the parameter $\widetilde{w}_0$ and the stability classes is shown on Fig 7. From this figure it can be seen the different degree of decreasing of $x_{2mw}$ and respective increasing of $C_{2mw}$ depending on the gravity deposition parameter $\widetilde{w}_0$ at stability classes A, B, C.

### 2.4 Inversion effect

In the inversion case with gravity deposition, the ground level concentration along the plume center line is given by:

$$C = \frac{Q}{\pi\sigma_y\sigma_z U_H}\sum_{n=-\infty}^{\infty}\exp\left[-\frac{\left(\widetilde{H}-2nh_I\right)^2}{2\sigma_z^2}\right],$$

(18)

where $\widetilde{H} = H - \widetilde{w}_0 x$, $h_I$ is the inversion height. The worst case will occur when the plume rise is just up to the inversion layer ($H \equiv h_I$). If we take only the first two main terms of the series we receive for the critical concentration the expression:

$$C_{cr} = \frac{Q}{\pi\sigma_y\sigma_z U_H}\left\{\exp\left[-\left(H-\widetilde{w}_0 x\right)^2/2\sigma_z^2\right]+\exp\left[-\left(H+\widetilde{w}_0 x\right)^2/2\sigma_z^2\right]\right\}$$

(19)

In the private case $w_0 = 0$, from (19) follows the received by Ragland (1976) formula. The consideration of the gravity deposition makes more complex the

problem for determination of $x_{mcr}$ and $C_{mcr}$. In this case for the determination of $x_{mcr}$ we have an equation of type like (13), which can be solve numerically.

### 2.5 On the non-Gaussian model application

If we represent the solution of the steady-state diffusion equation for continuous point source in PBL:

$$U(z)\frac{\partial C}{\partial x}+V(z)\frac{\partial C}{\partial y}=\frac{\partial}{\partial z}\left(k_z(z)\frac{\partial C}{\partial z}\right)+\frac{\partial}{\partial y}\left(k_y\frac{\partial C}{\partial y}\right)$$

(20)

in the form $C=C_1(x,z)C_2(x,y)$, taking into account Taylor's frozen turbulence hypothesis: $k_y=(1/2)U(z)\left(d\sigma_y^2/dx\right)$, we obtain (Syrakov, Stefanova 2001):

$$C=C_1(x,z)C_2(x,y), \qquad C_2=\frac{1}{\sqrt{2\pi}\sigma_y}\exp\left[-\frac{(y-Rx)^2}{\sigma_z^2}\right],$$

(21)

where $C_1$ describes the vertical ( from linear source at the axis Oy), and $C_2$ - the horizontal diffusion. The parameter $R$, determined according to the condition imposed by the splitting of the problem (20): $V(z)/U(z)$~const, is:

$$R=\frac{\overline{V}}{\overline{U}}=\frac{\sin\alpha+C_d^2\cos\alpha}{\cos\alpha-C_d^2\sin\alpha}, \qquad (22)$$

where $\overline{U}$, $\overline{V}$ are the averaged with the height in PBL components of the wind velocity, received by considering the equations of motion, $C_d=U_*/G_0$ is the geostrophic resistance coefficient, $\alpha$ - angle of full turning of the wind in PBL (between the surface and geostrophic wind). At $R=0\left(\overline{V}=0\right)$ follows the well known Gaussian distribution for $C_2$ perpendicular to the wind velocity. At $R\neq 0$ the integral average turning of the wind ($\overline{\alpha}=arctgR$) in the whole PBL is considered in $C_2$. On Fig.8 is presented the parameterized, by the Pasquill stability classes, integral turning parameter $R$ (Syrakov, Stefanova 2001). It can be seen that with increasing of atmospheric stability the integral effect of turning of the wind in PBL also increases.

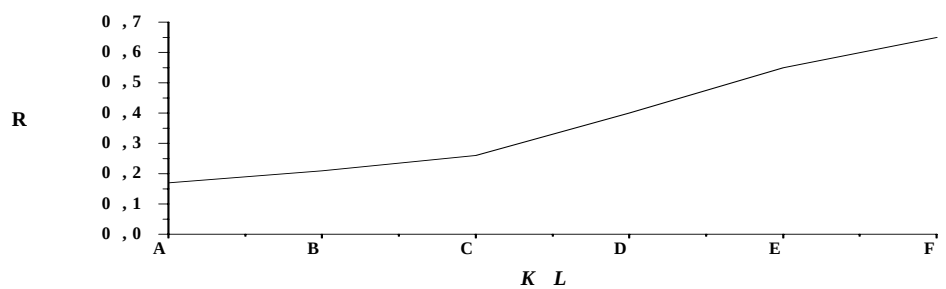


Figure 8. Values of integral wind turning parameter $R$ on stability classes.

Let's now see the vertical diffusion $C_1$. At power laws for $U(z)$ and $k_z(z)$:

$$U(z) = a_u z^m, k_z = b_k z^n,$$

(23)

Huang (1979) received the following analytical solution:

$$C_1 = Q \exp\left[ -\frac{a_u\left(z^\alpha + H^\alpha\right)}{b_k \alpha^2 x} \right] \frac{(zH)(1-n)/2}{b_k \alpha x} I_{-\nu}\left[ \frac{2a_u (zH)^{\alpha/2}}{b_k \alpha^2 x} \right],$$

(24)

where $\alpha = 2 + m - n$, $\nu = (1-n)/\alpha$, $I_{-\nu}$ is a modified Bessel function of first kind of order $(-\nu)$, $Q$ is the source strength, $H$ is effective height given by (2). This solution is detailly explored and used for determination of the statistical moments in (Brown et al,. 1997). From the non-Gaussian solution (21), (24), at $z = 0$, $y = 0$ and $R = 0$ we obtain respective expression for the surface, along the plume axis, concentration. Considering that $a_u = U_{10} 10^{-m}$ ( from the comparison of (23) and (3)) follows that this concentration depends on $U_{10}$. From the condition for extremum about $U_{10}$ and using a procedure identical to that in paragraph ( 2.2), now we can receive analytical expression for all critical parameters (8)-(11). For example for $U_{10cr}$ and $X_{mcr}$, we have:

$$U_{10cr} = B^{1/l} 10^m M^{1/l} h_s^{-(ml+1)/l},$$

(25)

$$x_{mcr} = \frac{1}{b_k \alpha^2 (1 - \nu + d)} B^{1/l} \left(1 + \frac{1}{M}\right)^\alpha h_s^{\frac{(2-n)l-1}{l}},$$

(26)

where $M = l[m + k_2/k_1] - 1$, $k_1 = -(1+d)$, $k_2 = d(n-2) - 1$. These parameters are modification of (8) and (9) for the case when it is used the non-Gaussian plum model. The difference is that instead of $\sigma_z(x)$ in the non-Gaussian model it's used $k_z$-closure. Besides that and at the non-Gaussian model, we can determine the respective dispersion $\sigma_z(x)$, using the definition formula $\int_0^\infty (z - \bar{z})^2 \overline{C}(x,z) dz \Big/ \int_0^\infty \overline{C}(x,z) dz$, where $\overline{C}(x,z)$ is the integrated by $y$ concentration $C$. For surface source ( $H = 0$ ) and $R = 0$ for $\sigma_z$ we have:

$$\sigma_z(x, H = 0) = \frac{\Gamma(3/2)}{\Gamma(1/2)} \left( \frac{b_k \alpha^{2x}}{a_u} \right)^{2/\alpha} - \bar{z}^2(x, H = 0),$$

(27)

where $\Gamma$ is the Gamma function, $\bar{z}(x) \sim x^{2/\alpha}$ is centroid of concentration distribution. Considering the asymptotic results for $U(z)$ and $k_z(z)$ (given by (23)) following by

Monin-Obukhov similarity theory: free convection $(m=-1/3, n=4/3)$, neutral stratification $(m \approx 1/7, n=1)$ and strong ("z-less") stability $(m=1, n=0)$, we have:

$$\sigma_z(x) \sim \begin{cases} x^{3/2} & \text{at free convection} \\ x^{7/8} & \text{at neutral stratification} \\ x^{1/3} & \text{at strong stability.} \end{cases} \quad (28)$$

In a identical way it can be determine the quantity skewness, which appear to be different from zero in correspondence with the non-Gaussian model (21), (24).

## 3. CONCLUSI0N

On the basis of power law approximation of the well known dispersion curves of Briggs in the frames of Gaussian and non-Gaussian Pollution model, it had been determined a series of main maximal and critical diffusion parameters and meteorological conditions at which they occur characterized by the Pasquill stability classes.

The majority of the results are given as exact analytical solutions which make them easy to use for estimation of the worst-case ambient conditions.

In result of taking into account the integral effect of wind turning in the non-Gaussian model it is easy to see that the maximal and critical diffusion parameters decrease compared to this determined with the Gaussian model in the other paragraphs.

A detail joint study of these effects together with the gravity deposition inversion effect is in interest of a future analysis.

## REFERENCE


Brown M., Arya S., Snyder W., 1997. Plume descriptors derived from a non-Gaussian concentration model. Atmospheric Environment 31, №2, 183-189.

Hanna S., 1982. Review of atmospheric diffusion models for regulatory application. Technical Note № 177, WMO 581, 42p.

Huang C., 1979. A theory of dispersion in turbulent shear flow. Atmospheric Environment 13, 453-463.

Ragland K., 1975. Worst case ambient air concentrations from point sources using the Gaussian plume model. Atmospheric Environment 10, 371-374.

Syrakov E., Stefanova M., 2001. On the moments of concentration and critical parameters on air pollution from continuous point source. Ann.de L'Uni. de Sofia, Faculty of Physics, vol. 94, 15-44.

Wark K., Warner C., 1976. Air pollution. It's origin and control. Harper & Row, publishers.

*Proceedings of the Third International Symposium on Air Quality Management at Urban, Regional and Global Scales. 26-30 September 2005, Istanbul – Turkey*

# ESTIMATION OF OZONE POLLUTION LEVELS IN SOUTHEAST EUROPE USING US EPA MODELS-3 SYSTEM

**Maria Prodanova**[1], **Dimiter Syrakov**[1], **Zahari Zlatev**[2], **Kiril Slavov**[1]
**Kostadin Ganev**[3], **Nikolaj Miloshev**[3] **and Evelina Nikolova**[4]

[1] National Institute of Meteorology and Hydrology (NIMH), Sofia 1784, Bulgaria
maria.prodanova@meteo.bg, dimiter.syrakov@meteo.bg, kiril.slavov@meteo.bg
[2] National Environmental Research Institute, Roskilde, Denmark, zz@bmu.dk
[3]Geophysical Institute, Bulgarian Academy of Sciences, Sofia 1111, Bulgaria
kganev@geophys.bas.bg, miloshev@geophys.bas.bg
[4]Executive Environment agency, Sofia, Bulgaria, serafimov@nfp-bg.eionet.eu.int

## ABSTRACT

Air quality modeling becomes an important tool for investigation of air pollution levels in different scales. In the paper, experiments are made as to determine the degree of reaction of the US EPA Models-3 system on change in emissions. Tree domains are set over Europe with resolution 90-30-10 km, the last one embracing entirely Romania, Bulgaria and Greece. MM5 is run over these domains for June 2000 with NCEP 1x1 degree Global Analysis data. CMAQ is run on the two inner domains only. EMEP inventory grid data with 50 km resolution is used to prepare the emission input for the 30-km domain and its 16.67 km desagregation - for the finer one. Proper time profiles, monthly, weekly and daily, are imposed upon yearly values. The CMAQ "default profiles" are used as initial and boundary conditions on the 30-km grid. A set of runs are performed with aqueous CB-IV chemical mechanism on. It includes a full emission base case run and three control emission scenarios of reduced NOx(50%), VOC(50%) and combination NOx(50%)-VOC(25%) as to check the influence of different geographical regions on ozone formation. Comparison between different runs and between the basic case calculations and measurements are shown and commented.

**Key Words:** Air Pollution Modelling, CMAQ Model, Ozone Pollution

## 1. INTRODUCTION

During the last two-three decades, the international collaboration decreased the threat of acid rains in almost all Europe. In place of acid rains new threats for the population, nature and historical heritage emerge. The increase of $NO_x$ emissions and the photochemical processes in the atmosphere led to formation of high ozone levels at the ground surface. This is a relatively new problem, more severe in Western European countries, but promising to arise to threat in the East as well. The European ozone directives (EC, 1998, 1999, EP, 2002) are aimed to put limits to high level ozone exposure and to set common control strategy by assessing current and future air quality regulations designed to protect human health and welfare.

Air quality models provide powerful and reliable tools for performing such assessment. A big number of models and model systems with different level of complexity were developed, lately. Many of them can be found in the EEA Model Documentation System (http://air-climate.eionet.eu.int/databases/MDS/index_html) or in the respective site of US EPA (http://www.epa.gov/scram001/tt22.htm#rec).
Many scientists, especially those from Central and Eastern European countries, face a number of problems in dealing with air pollution matter – from environmental impact assessment to forecast of photochemical smog and formation of high ozone levels, when working to meet the requirements of respective EU Directives.
The forthcoming accession of Bulgaria to EU sets a number of problems related to the necessity of operating a contemporary air pollution modeling system. The choice, studying and implementation of such a tool to different regional and local problems were the aim of the 5$^{th}$FP funded project BULAIR (http://www.meteo.bg/bulair). The first task of the team was to make an extensive review of the existing models and to choose suitable one/ones. It occurs that the Model-3 system of US EPA is one of the best modeling tools. It continues to be developed intensively by the efforts of a big community of scientists both in the US and Europe.
The system consists of three parts: the 5$^{th}$ generation PSU/NCAR Meso-meteorological Model MM5 (Dudhia, 1993, Grell et al., 1994) used as meteorological pre-processor; the Sparse Matrix Operator Kernel Emissions (SMOKE) Modeling System (CEP, 2003) and the Community Multiscale Air Quality System CMAQ (Byun et al., 1998, Byun and Ching, 1999). Important advantages of this software are that it is free downloadable and can be run on contemporary PCs. In the same time, this is a modeling tool of large flexibility, with a range of options and possibilities to be used for different applications/purposes. Many research groups in Europe already use the Model-3 system or some of its elements and this number is increasing rapidly. In the light of the above, the main goal of this paper is to show the first results of implementing the MM5-CMAQ system for estimation of pollution levels in southeast Europe.
In Bulgarian National Institute of Meteorology and Hydrology, the PSU/NCAR mesoscale model **MM5**, non-hydrostatic version 3-6-1, and the EPA Models-3 CMAQ model, version 4.3, are installed on PC Dell dual CPU Xeon 2.8 GHz computer under RedHat Linux 7.3 operational system using Portland Group 4.02 FORTRAN compiler. In-depth descriptions of MM5 can be found in Dudhia (1993) and Grell et al. (1994), and at http://box.mmm.ucar.edu/mm5/. On the sight http://www.epa.gov/asmdnerl/CMAQ/CMAQscienceDoc.html all documentation of CMAQ is available. Free download of all Models-3 elements is available at http://www.cmascenter.org/.

## 2. MODELING DOMAIN

The MM5 preprocessing program TERRAIN is used to define three domains with 90, 30 and 10 km horizontal resolution (51×45, 79×61 and 160×103 grid points, respectively). These three nested domains are chosen in such a way that the finer resolution domain contains Bulgaria and two neighboring Balkan countries - Romania and Greece. Lambert conformal conic projection, with true latitudes at 30°N and 60°N, and the central point with coordinates 41.5°N and 24°E are chosen.

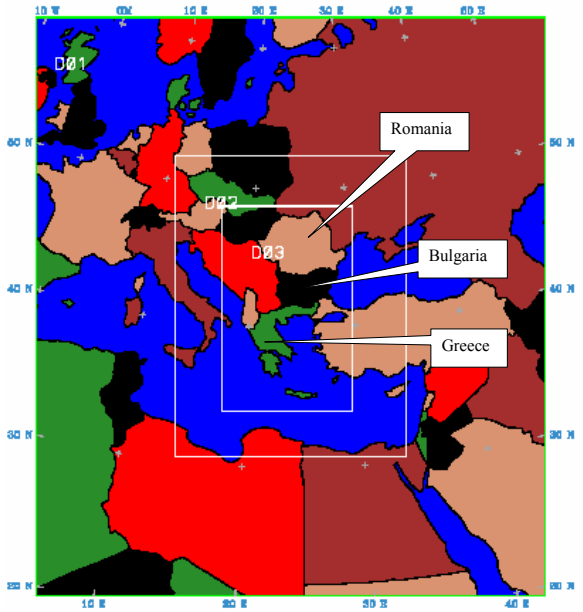


**Fig. 1.** The three computational domains

Together with grids definition TERRAIN specifies the raw topographic, vegetative, and soil type data to all grid points. The Land-Surface Model is included, so besides of elevation height and land-use data some additional fields such as enhanced soil types, vegetation fraction, and annual deep soil temperature are also generated.
The model domains are shown in Fig. 1. The other pictures refer the inner grid only.

## 3. Meteorology

Meteorological database suitable for air quality modeling with CMAQ is generated by exploiting the US NCEP Global Analyses data for the year 2000 (http://dss.ucar.edu/datasets/ds083.2/). The data has 1×1 degree grid resolution covering the entire globe, the time resolution is 6 hours. NCEP derives these data from the FNL (final weather forecast run) which assimilates observations collected through at least six hours after the synoptic term. This FNL dataset has surface level, tropospheric levels, tropopause, and lower stratospheric levels analyses.

## 4. MM5 SIMULATION

CMAQ modeling guidance suggests that each grid on which the air quality model is to be run should be provided with MM5 meteorological fields that are developed independently in “one way” nesting mode. Here, CMAQ is run on the two finer grids only. So, MM5 is run on both outer grids (90 and 30 km) simultaneously with “two-way” nesting mode on, first. Then, after extracting the initial and boundary conditions from the resulting fields for the 10 km simulation, MM5 is run on the finer 10 km grid as a completely separate simulation with “one-way” nesting mode on. In this approach, information from the 30 km grid is transferred to the 10-km domain through boundary conditions during the simulation, but there is no feedback from the 10-km fields up-scale to the 30 km domain. All simulations are made with 23 σ-levels going up to 100 hPa height. Proper physical options are set in MM5.
The model may be set to relax toward observed temperature, wind and humidity through four dimensional data assimilation, known as FDDA (Stauffer and Seaman, 1990). FDDA amounts to adding an additional term to the prognostic equations that serves to “nudge” the model solution toward the individual observations. This significantly reduces the drift in the solution for simulations of several days or more. The NCEP data set does not include observations, but analyzed data every 6 hours in all its grid points. MM5 is configured with FDDA option on as to nudge the model toward analyzed data on the 90 km grid only.

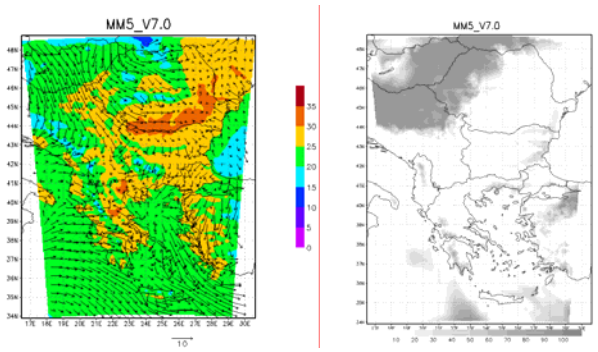


**Fig. 2.** Temperature (colored), wind and low cloud coverage on June 7, 2000, 14:00.

The 2000 annual simulation with MM5 is made on portions of 4 days. Every portion has additional 12 hours that are an initial spin-up period that overlaps the last 12 hours of the preceding run. Further on, the MM5 output for June is used to run CMAQ. In Fig.2, a temperature and wind combined map and a low level cloud cover map are shown.

## 5. EMISSION INPUT TO CMAQ

CMAQ demands its emission input in specific format reflecting the time evolution of all polluters accounted for in the used chemical mechanism. The emission inventory usually is made on annual basis and many pollutants are estimated as groups ($NO_x$, $SO_x$, VOC - Volatile Organic Compounds). In preparing CMAQ emission file a number of specific estimates must be done. First, organic gases emissions estimates, and to a lesser extent $SO_x$ and $NO_x$ estimates, must be split, or "speciated", into more defined compounds in order to be properly modeled for chemical transformations and deposition. Secondly, time variation profiles must be over-posed on these annual values to account for seasonal, weekly and daily variations. Finally, all this information must be gridded. The different types of sources (area, elevated point, mobile and biogenic) are treated in specific way. Obviously, emission models are necessary as reliable emission input to the chemical transport models to be produced. Such a component in EPA Models-3 system is SMOKE. Unfortunately, it is highly adapted to the US conditions - emission inventory, administrative division, motor fleet etc. Many European scientific groups are working now for adapting SMOKE to European conditions (see Borge et al., 2004).

Here, the CMAQ emission input is prepared exploiting the EMEP 50×50 km gridded inventory (Vestreng, 2001) for the entire EMEP area and its desagregation described in Ambelas Skjøth et al. (2002). The values over the grid points of the 30-km domain of this study are obtained by bi-linear interpolation over the 50 km EMEP gridded emissions and for the inner 10-km grid – over the desagregated 16.67-km inventory. Additional corrections are included for congruence between both inventories.

As to prepare the CMAQ emission input file the computer code **E_CMAQ** is created. The gridded (30 and 10 km) annual emission rates of 5 generalized pollutants – $SO_x$, $NO_x$, VOC, $NH_3$ and CO – are introduced in E_CMAQ and are speciated following the way recommended Smylie et al. (1991). The final speciation to 13 compounds, required by CB-IV chemical mechanism of CMAQ, is presented in Table 1:

**Table 1.** Speciation of "lumped" species as required by CB-IV.

| No. | POLLUTANT | Split factor | Molecular Weight |
|---|---|---|---|
| | SOx (as SO2): | | |
| 1 | SO2 | 0.85 | 64.065 |
| 2 | SULF | 0.15 | 96. |
| 3 | NH3 | | 17.031 |
| 4 | CO | | 28.01 |
| | NOx (as NO2): | | |
| 5 | NO2 | 0.15 | 46.006 |
| 6 | NO | 0.85 | 30 |
| | VOC: | | |
| 7 | OLE | 0.087306 | 27.74 |
| 8 | PAR | 0.56023 | 13.87 |
| 9 | TOL | 0.139938 | 97.09 |
| 10 | XYL | 0.09172 | 110.96 |
| 11 | FORM | 0.01242 | 13.87 |
| 12 | ALD2 | 0.018304 | 27.74 |
| 13 | ETH | 0.105674 | 27.74 |

The molecular weight of every compound is necessary for transforming individual emission rates from 1000tone/year to [mole/s] as required by CMAQ. The next modification of the so prepared data is the over-posing of proper time variation profiles (monthly, weekly and hourly). The methodology developed in USA EPA Technology Transfer Network (http://www.epa.gov/ttn/chief/emch/temporal/index.html) is adopted. As far as in the used gridded inventory the type of sources is not specified, some common enough area sources are chosen from the EPA SCC (Source Category Code) classification and their profiles are averaged. The resulting profiles are implemented. Finally, all the data, day by day, is written in the specific format required by CMAQ.

It must be stressed here that the biogenic emissions of VOC are not included in this study and this fact have to be taken into consideration when interpreting model results.

## 6. CMAQ SIMULATION

The CMAQ model requires inputs of three-dimensional gridded wind, temperature, humidity, cloud/precipitation, and boundary layer parameters. A meteorological database suitable for air quality modeling with CMAQ was generated by performing a year-long run with MM5 as described above. From this MM5 output CMAQ meteorological input was created exploiting the newest version of the CMAQ meteorology-chemistry interface - MCIP, v2.3. In the same time, the computational domains decrease by 6.5 points (boundary points) from every side and the dot- and the cross points exchange their place (that is why the half point appear).

CMAQ has been run from 00:00 UTC of 01 June to 00:00 UTC of 09 June, 2000, day by day on both domains at 6 vertical layers. The period is chosen without any specific consideration. The Chemical Transport Model has been run on both processors using an open-source, portable implementation of the Message-Passing Interface Standard (MPICH), version 1.2.5. The CB-4 chemical mechanism with Aqueous-Phase Chemistry and MEBI solver has been exploited.

The CMAQ pre-defined (default) concentration profiles are used for initial conditions over both domains at the beginning of the simulation. The concentration fields obtained at the end of a day's run are used as initial condition for the next day. Default profiles are used as boundary conditions of the 30-km domain during all period. The boundary conditions for the inner domain are determined through the nesting capabilities of CMAQ. Further on, results for the last 4 days of this period (5-8 June 2000) will be presented as to avoid the influence of the artificial initial conditions. This is the reason to interpret only the results on the inner 10-km domain.

## 7. SENSITIVITY OF CMAQ PHOTO-CHEMICAL CALCULATIONS

The elaboration of effective control strategy for decreasing ozone levels requires a knowledge of the response of ozone concentrations to the variation of its main precursors –$NO_x$ and VOC. This response depends nonlinearly on spatially and temporarily variable factors. A big number of researches with different level of complexity are devoted to this problem for particular areas and weather conditions leading to classification of ozone formation into categories of chemical regime (Sillman, 1995). The detailed classification of ozone production regime helps to determine which of the two precursors must be targeted in ozone reduction strategy. Examples of such diagnose and of high-order sensitivity analysis are shown in Cohan, Hu and Russell (2004) and Cohan and Russell (2004).

The aim of this study is much more modest. It is to demonstrate the ozone formation sensitivity of CMAQ CB-4 chemical mechanism to variations in the main ozone precursors for a randomly selected period of time over specific geographical area. For the purpose, four emission scenarios are run with CMAQ. The basic scenario exploits the emissions described above (scenario **a**). The other three are: $NO_x$ emissions reduced to 50% (scenario **b**), VOC emissions reduced to 50% (scenario **c**) and both $NO_x$ and VOC emissions reduced twice simultaneously (scenario **d**).

The meteorological situation over the Balkan Peninsula for this period can shortly be described as follows: (a) the dominant wind was from North and North-East in Bulgaria and Romania and mainly from West for the remaining part of the domain; (b) the temperature was between 20 and 30 degrees Celsius, but the wind speed was high (especially at the end of the period) and (c) it was cloudy most of the time.

This shows that one should not expect very high ozone concentrations. This is confirmed by the results of calculations. Moreover, in the Western part of the region (where the wind was from the West) the ozone concentrations are higher.

As already said, the model was run for a period of 8 days (1-8 June, 2000) but only the last four days are commented, here. The graphical presentation of the results for only one of these days (7 June, 2000) is given in Fig. 3. The same trends are also observed for the other days in the period.

The $NO_2$ concentrations during all the time are below 3 ppb in the whole space domain excepting small regions around Athens and Istanbul, as well as (but in a smaller degree) in Bucharest. Some special behaviour of the results obtained with the $NO_x$ scenarios could be expected in these regions. The results obtained by the scenario **b** 50% reduction of the $NO_x$ emissions) confirm this. In the upper-right-graph in Fig. 3, the ratios of the ozone concentrations obtained by the scenario **b** and by the Basic scenario (scenario **a**) are given (in %). It is seen that the reduction of the $NO_x$ emissions leads to a considerable reduction of the ozone concentrations in nearly the whole space domain. However, the ozone concentrations in the regions around Athens and Istanbul are increased. This effect is not pronounced for the region around Bucharest, where the $NO_2$ concentrations are not much higher.

The VOC scenario (scenario **c**) does not lead to great changes of the ozone concentrations. In the lower-left plot of Fig. 3, the ratios of the scenario **c** produced ozone concentrations and those obtained by the Basic scenarios are given. It is seen that the ozone concentrations in a large part of the domain are slightly increased when the VOC scenario is used.

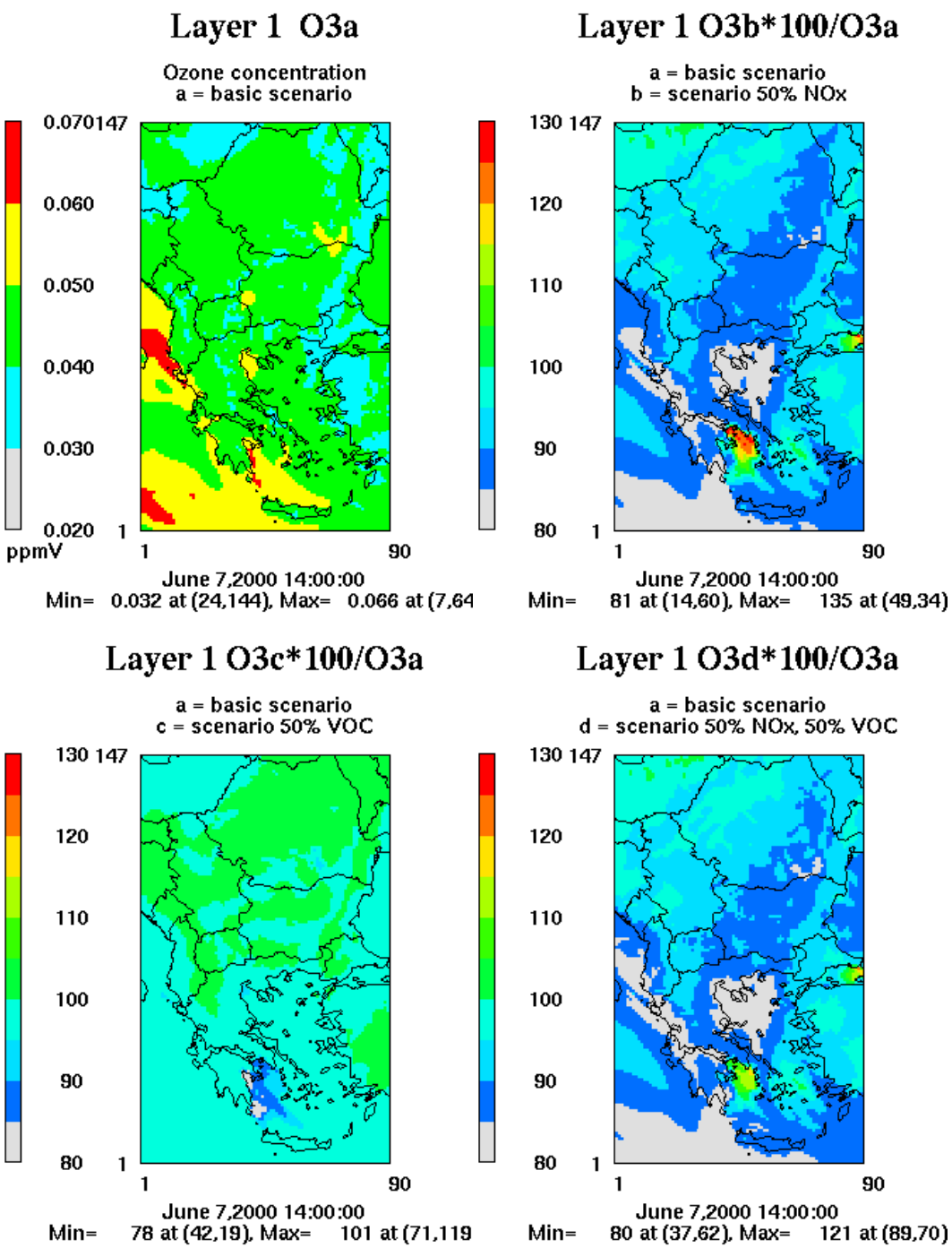


**Fig. 3.** CMAQ produced ozone fields for 7 June, 2000, 14:00 UTC: up-left: ozone concentrations (Scenario **a.**); up-right: Scenario **b**/Scenario **a** in %; down-left: Scenario **c**/Scenario **a** in %; down-right: Scenario **d**/Scenario **a** in %).

The results obtained by scenario **d** are compared with the results obtained by the Basic scenario on the lower-right plot of Fig. 3. It is seen that the results are quite similar to the results obtained when only the $NO_x$ emissions are reduced. Two effects should be noted: (a) the areas where the reduction of only the $NO_2$ emissions leads to

an increase of the ozone concentrations are now reduced considerably and, moreover, the increased values are lower than the corresponding values in the in the upper-right plot and (b) the sizes of the areas where the reduction of the ozone concentrations is considerable (more than 10%) are slightly increased.

## 8. VERIFICATION AGAINST MEASUREMENT DATA

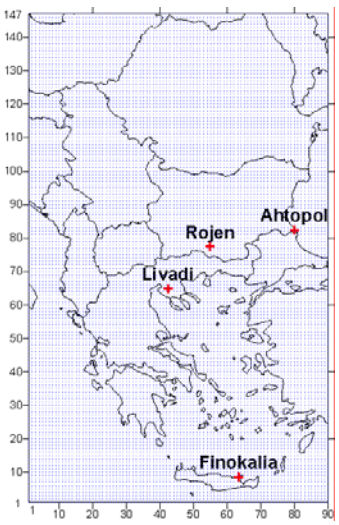


The number of background stations monitoring the ozone concentration is quite limited in the region. One can obtain only two such stations belonging to EMEP monitoring network that used to operate all the year 2000. These are the Greek stations GR02-Finokalia (35N30, 26E10, altitude 0 m) and GR03-Livadi (40N32, 23E15, altitude 850 m). It is worth to say that the coordinates of Finokalia in EMEP station list are wrong. The right values are (35N20, 25E40). Source of the data: http://www.nilu.no/projects/ccc/emepdata.html.

It occurs that during all the year 2000 two more stations were monitoring the ozone concentrations in Bulgaria in the frame of a research project (Donev et al., 1999, 2000). These stations are BG02-Rojen (41N40, 24E48, altitude 1700 m) and BG03-Ahtopol (41N58, 27E57, altitude 0 m). From these 4 stations two are at the see shore, one is in-land (Halkidiki peninsula) and one - in the Rhodope mountain, peak Rozhen. Their location is shown in the picture on the left.

Comparison of CMAQ calculated and DEM interpolated hourly ozone values with the measurements performed in these four stations for the period 5-8 June, 2000 can be seen in Fig. 4.

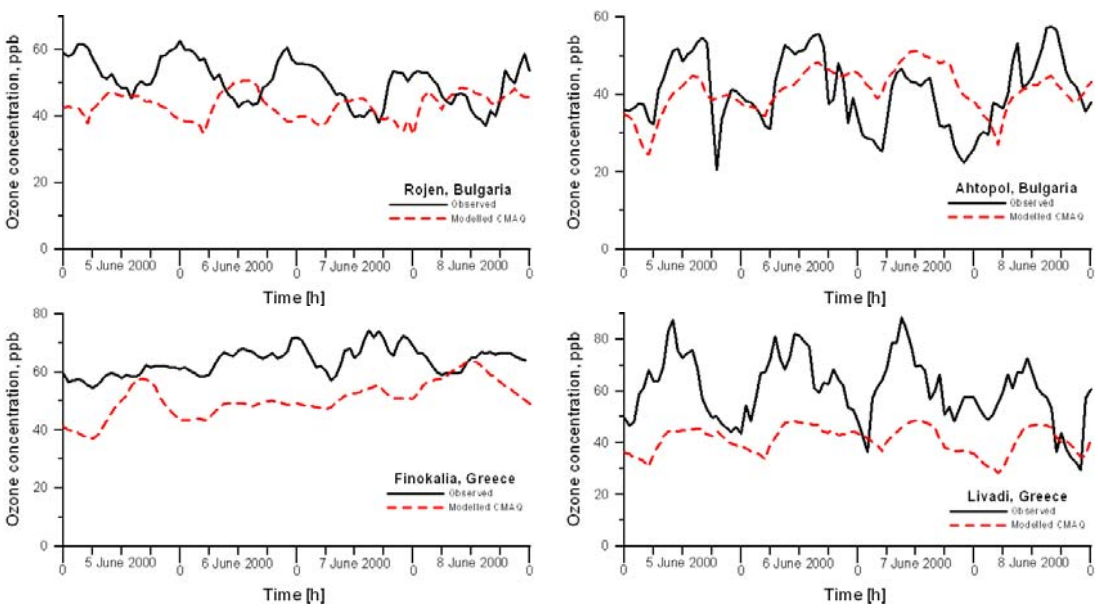


**Fig.4.** Comparison of CMAQ calculations with observations

The main features in Fig. 4 can be commented as follow:

- **Finokalia**: There are practically no diurnal variations of the measured ozone concentrations and of the CMAQ results.
- **Livadi and Ahtopol**: Both the model results and the measurements show the typical for the ozone concentrations diurnal cycles. The maxima and the minima of the model results are slightly shifted forward in relation to the corresponding minima and maxima of the measurements.
- **Rojen:** The measurement results at Rozhen show somewhat strange behaviour. They demonstrate opposite to the normal ozone diurnal cycle which, obviously, means that the ozone measured there is not produced in place but transported from some other regions. This possibly is the reason that stations with altitude over 1200 m are not usually used for comparisons with model data (Berge et al., 1994). The model produces maximal concentrations during the day and minimal concentrations during the night.

The main conclusion from Fig. 4 is that CMAQ-produced ozone concentrations underestimate the observed values all the time and in all stations. In the same time, the diurnal amplitudes are less than the observed ones. The basic reason for this is possibly the fact that the biogenic VOC emissions are not accounted for in the E_CMAQ calculations. These emissions would play considerable role in the ozone formation in this relatively worm region because of the intensive production of isoprene and other VOC with well expressed diurnal variations. One of the most important tasks in future investigations will be the attempt to include a reliable biogenic emission mechanism in CMAQ pre-processing software.

## 9. CONCLUSIONS

It can be concluded from these preliminary results that Models-3 air quality system describes quite reasonably the ozone formation in southeast Europe and it can be used for further complicated investigations of photo-oxidation regime on the base of specialized indexes determining the damages caused by high ozone levels in the region (as done in Zlatev and Syrakov, 2004b). For the purpose a lot of additional investigations and tests must be done in order to obtain realistic results to be used in emission trade negotiation process, as well as in decision making for elaboration of proper abatement strategies.

## 10. ACKNOWLEDGEMENTS

This study is made under the financial support of European Commission – 5$^{th}$FP project BULAIR (Contract Nr. EVK2-CT-2002-80024) and the 6$^{th}$FP Network of Excellence ACCENT (Contract Nr. GOCE-CT-2002-500337), as well as of the Bulgarian National Science Council (Contract No. ES-1002/00). The contacts within the framework of the NATO Collaborative Linkage Grant EST.CLG 979794 were extremely simulating as well.

Deep gratitude is due to all organizations providing free of charge data and software used in this study, namely US EPA, US NCEP and European EMEP Programme. Without their support this study would not be possible. Finally, gratitude is due to Prof. E.Donev from Sofia University for providing Bulgarian ozone measurements.

## REFERENCE


Ambelas Skjøth, C., Hertel, O., Ellermann, T., (2002) Use of the ACDEP trajectory model in the Danish nation-wide Background Monitoring Programme. Physics and Chemistry of the Earth, **27**, Pergamon Press, 1469-1477.

Berge, E., Schaug, J., Sandnes, H. and Kvalvågnes, I. (1994) A comparison of results from the EMEP/MSC-W Acid Deposition Model and EMEP monitoring sites during the four seasons of 1989, EMEP/MSC-W/CCC Note 1/94, Norwegian Meteorological Institute, N-0313 Oslo 3, Norway.

Borge, R., Lumbreras, J., Rodríguez, M.E., (2004) Preparation of emission data for modeling with CMAQ from Spanish emission inventories and emission projections, Proceedings of the 28th NATO/CCMS International Technical Meeting on Air Pollution Modelling and Its Application, 24-29 October 2004, Banff, Alberta, Canada.

Byun, D., Ching, J. (1999) Science Algorithms of the EPA Models-3 Community Multiscale Air Quality (CMAQ) Modeling System. EPA Report 600/R-99/030, Washington DC. http://www.epa.gov/asmdnerl/models3/doc/science/science.html.

Byun, D., J. Young, G. Gipson, J. Godowitch, F.S. Binkowski, S. Roselle, B. Benjey, J. Pleim, J. Ching, J. Novak, C. Coats, T. Odman, A. Hanna, K. Alapaty, R. Mathur, J. McHenry, U. Shankar, S. Fine, A. Xiu, and C. Jang, (1998) Description of the Models-3 Community Multiscale Air Quality (CMAQ) Modeling System, 10th Joint Conference on the Applications of Air Pollution Meteorology with the A&WMA, 11-16 January 1998, Phoenix, Arizona, 264-268.

CEP (2003) Sparse Matrix Operator Kernel Emission (SMOKE) Modeling System, University of Carolina, Carolina Environmental Programs, Research Triangle Park, North Carolina.

Cohan, D., Russell, A. (2004) Cost-Optimized Air Pollution Control Using High-Order Sensitivity Analysis, Proceedings of the 27th International Technical Meetings on Air Pollution Modelling and Its Application, 24-29 October 2004, Banff, Alberta, Canada, 73-80.

Cohan, D., Hu, Y., Russell, A. (2004) Alternative Approaches to Diagnosing Ozone Production Regime, Proceedings of the 27th International Technical Meetings on Air Pollution Modelling and Its Application, 24-29 October 2004, Banff, Alberta, Canada, 65-72.

Derwent R.G., Jenkin, M.E., Saunders, S.M., and Pilling, M.J. (1998), Photochemical Ozone Creation Potentials for Organic Compounds in North West Europe Calculated with a Master Chemical Mechanism. Atmospheric Environment, **32**, 2419-2441.

Donev E., Ivanova D., Avramov A., Zeller K. (1999) Rank correlation approach to assessing influence of mountain valey winds on ozone concentration. Journal of Balkan Ecology, **2**, 79-85.

Donev, E., Zeller, K. and Avramov, A. (2002) Preliminary background ozone concentrations in the mountain and coastal areas of Bulgaria. Environmental Pollution, **17**, 281-286.

Dudhia, J. (1993) A non-hydrostatic version of the Penn State/NCAR Mesoscale Model: validation tests and simulation of an Atlantic cyclone and cold front. Mon. Wea. Rev. **121**, pp.1493-1513.

EMEP (1998) Transboundary acidifying air pollution in Europe, EMEP/MCS-W Report 1/1998, Norwegian Meteorological Institute, Oslo, Norway.

EC (1998) Amended draft of the daughter directive for ozone, Directorate XI – Environment, Nuclear Safety and Civil Protection, European Commission, Brussels.

EC (1999) Ozone position paper, Directorate XI – Environment, Nuclear Safety and Civil Protection, European Commission, Brussels.

EP (2002) Directive 2002/3/EC of the European Parliament and the Council of 12 February 2002 relating to ozone in ambient air. Official Journal of the European Communities, **L67**, 9.3.2002, pp. 14-30.

Grell, G.A., J. Dudhia, and D.R. Stauffer, 1994: A description of the Fifth Generation Penn State/NCAR Mesoscale Model (MM5). NCAR Technical Note, NCAR TN-398-STR, 138

Jenkin, M.E. and Hayman, G.D. (1999) Photochemical ozone creation potentials for oxygenated organic compounds: sensitivity to variations in kinetic and mechanistic parameters. Atmospheric Environment, **33**, 1275-1293.

Sillman, S. (1999) The relation between ozone, $NO_x$ and hydrocarbons in urban and polluted rural environment, Atmospheric Environment, **33**,1821-1845.

Smylie M., Fieber J.L., Myers T.C., Burton S. (1991) A preliminary examination of the impact on emissions and ozone air quality in Athens-Greece from various hypothetical motor vehicle control strategies. European conference on New Fuels and Clean Air. Antwerp, Belgium.

Stauffer, D.R. and N.L. Seaman (1990) Use of four-dimensional data assimilation in a limited area mesoscale model. Part I: experiments with synoptic data. Mon. Wea. Rev. **118,** pp.1250-1277.

Vestreng, V. (2001) Emission data reported to UNECE/EMEP: Evaluation of the spatial distribution of emissions. Meteorological Synthesizing Centre - West, The Norwegian Meteorological Institute, Oslo, Norway, Research Note 56, EMEP/MSC-W Note 1/2001.

Zlatev, Z. and Syrakov, D. (2004) A fine-resolution modelling study of pollution levels in Bulgaria. Part 2: high ozone levels. International Journal of Environment and Pollution, **22**, No.1/2, 203-222.

*Proceedings of the Third International Symposium on Air Quality Management at Urban, Regional and Global Scales. 26-30 September 2005, Istanbul – Turkey*

# THREAT TO TURKEY FROM POTENTIAL ACCIDENTS AT THE SOVIET-DESIGNED METSAMOR NUCLEAR POWER PLANT, ARMENIA: TRACER AND TRAJECTORY ANALYSES AND EPISODE STUDIES

**Tayfun Kindap[a] , S.H. Chen[b], Umit Anteplioglu[c], Ufuk U. Turuncoglu[d] , Ozan M. Göktürk[a] and Mehmet Karaca[a,e]**

[a] Eurasia Institute of Earth Sciences, Istanbul Technical University, 34469, Istanbul, TURKEY, kindap@itu.edu.tr
[b] Dept. of Atmospheric Science, University of California Davis, USA, shachen@ucdavis.edu
[c] Kandilli Observatory and Earthquake Research Institute, Bosphorus University, Istanbul, TURKEY, anteplio@boun.edu.tr
[d] Institute of Informatics, Istanbul Technical University, Istanbul, TURKEY, ufuk.turuncoglu@itu.edu.tr
[e] Faculty of Mining, Istanbul Technical University, 34469, Istanbul, TURKEY, karaca@itu.edu.tr

## ABSTRACT

After the Chernobyl accident, several European countries were affected by large and highly radioactive particles. In the Chernobyl accident most of the particulate material was deposited within 20 km of the plant, but about one-third was transported even thousands of kilometers. There is no doubt that at a relative remote distance from the accident site, the Turkish territory was affected by depositions and high concentrations of radioactive pollutants released to the atmosphere during the accident. In contrast, Turkish authorities have not been concerned sufficiently about the different aspects of safety at nuclear installations in the former Soviet Union.

The Metsamor nuclear power plant in Eastern Armenia is the closest (16 km) Russian-designed nuclear power plant to Turkey. One of the main concerns regarding nuclear power plants is the possibility of accidents. In addition to old technologies and unsatisfactory safety measures, the location of the power plant exposed to severe seismic waves gives a high possibility of accidents. The estimation of the probability that air in the Metsamor region would be transported to Turkey following a hypothetical accident has been used in the MM5 tracer and trajectory model.

**Key Words:** Trajectory Analysis, Criteria for Worst Case, Nuclear Accidents, Travel Time Statistics

## 1. INTRODUCTION

The Chernobyl Nuclear Plant Accident, which occurred in 1986, has unfortunately not been the center of concern in Turkey. Recently, because of the increasing number of cancer diseases in Northern Turkey which was the most affected area of Turkey

from the accident, his has become a current issue. Actually, even today, scientists in many countries are still interested in the problem concerning the consequences of the accident in affected areas, primarily related to the state of the health of today's and future generations. The results of Fesenko et al. (2005) study showed that in the early period after the Chernobyl accident for many biota species (primarily for terrestrial flora and fauna) in the most affected areas, an excess of irradiation over the critical levels has been observed. On the other hand, after the Chernobyl accident, several European countries were affected by large and highly radioactive particles (Pöllanen et al., 1997). In the Chernobyl accident most of the particulate material was deposited within 20 km of the plant, but about one-third was transported even thousands of kilometers (Powers et al., 1987).

During the Chernobyl accident, a large quantity of radionuclide was released into the troposphere, transported partially over long distances and it contaminated a wide geographical area (Tschiersch and Georgi, 1987; IAEA, 1991). Even though the Turkish territory was thought to be at a safe distance from the site of the accident, it was affected by large depositions and high concentrations of radioactive pollutants released to the atmosphere during the accident (e.g. Pöllanen et al., 1997; Langner et al., 1998). A similar hazard could be faced in the near future and this time could pose a more dangerous threat for Turkey. The Metsamor nuclear power plant in Eastern Armenia is the closest (16 km) Russian-designed nuclear power plant to Turkey (Figure1). One of the main concerns regarding nuclear power plants is the possibility of accidents. In addition to old technologies and unsatisfactory safety measures, the location of the power plant exposed to severe seismic waves gives a high possibility of accidents.


**Figure 1**. The location of Metsamor Nuclear Power Plant and some big cities of Turkey near Metsamor.

The European Union will allocate 100 million Euros to Armenia for bringing the Metsamor Nuclear Power Plant to a halt and searching for new energy sources. However, the grant was frozen and will not be allotted unless the Armenian government announces the precise term to close down the plant. The Armenian government declares that some 800 million Euro is necessary to close the Metsamor and for other relevant arrangements, as well as for developing alternative energy systems (ArmeniaNow.com, 2004).

Our aim here is to show the scale of the approaching hazard and to fix Turkish territories which could be possibly affected.

## 2. METHODOLOGY

The estimation of the probability that air in the Metsamor region would be transported to Turkey following a hypothetical accident has been used in the MM5 tracer model. This on-line approach avoids temporal interpolation errors that can inherently limit the accuracy of more commonly used off-line calculations of pollutant transport and diffusion.

Fifth-Generation NCAR / Penn State Mesoscale Model (MM5; Grell et al. 1994) V3.6, on-line tracer model (MM5T) was used here. A single domain with grid-spacing of 9 km is configured, and it covers the entire Turkey and the Caspian Sea. There are 200 x 300 x 23 grids in the east-west, north-south, and vertical directions, respectively. Tracers in MM5T are carried in a 4D array and the transport of tracers due to advection, MRF boundary layer mixing (Hong and Pan 1996), and Kain-Fritsch cumulus convection (Kain 2004) is taken into account. Other chosen physics options are the RRTM (Rapid Radiative Transfer Model) radiation scheme (Mlawer et al. 1997) and simple ice microphysics scheme (Dudhia 1989).

On the other hand, a hypothetical accident has been studied with the trajectory approach in the MM5. Based on the same configuration with the tracer study, forward trajectories also indicated similar source/receptor relationships between the Metsamor and Turkey.

## 3. DISCUSSION

An example of the worst-case synoptic conditions for Eastern Turkey is seen in the combined sea level pressure and wind chart of March 14th, 2004 (Figure2).

Counter-clockwise circulation around the low pressure center located on Iraq, and the clockwise flow induced by the strong high pressure center on Eastern Europe, both make conditions favorable for N-NE winds over Eastern Turkey. This pattern, especially the extended dominance of ridges over cold Eastern European land mass is very common in winter months.

## Tracer

After 48 h of integration in the model, a synoptic-scale circulation pattern that favors pollutant transport into Turkey is quite evident (Fig. 2). Simulated tracer transport from the Metsamor can be seen in Fig. 3. For the simulation period (00 UTC 5 July to 00 UTC 7 July), the tracer distribution at 12, 24, 36 and 48 hours are demonstrated in a, b, c, and d panels respectively.

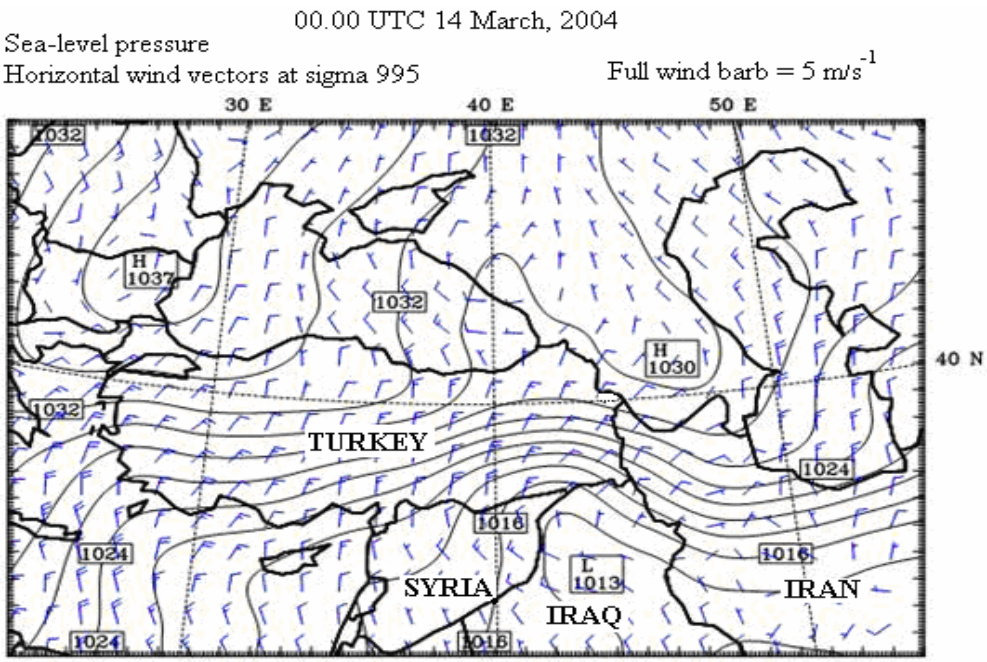


**Figure 2**. 24 h forecast from the model, showing sea level pressure (solid line; hPa), and wind vectors (at sigma 955) at 00 UTC14 March, 2004.

While the tracer had almost equivalent impact for each direction after 12 hours later (Fig3-a), it widened to the west which covered Eastern Turkey by the end of 24 hours (Fig3-b).

The South East of Turkey is relatively far away from the Metsamor, yet tracers reached this area after about 36 hours of transport (by 12 UTC 6 July). On the other hand, the tracer began losing its intensity when it moved to the inside of Turkey (Fig3-c). Finally, 48 hours later, the tracer lost most of its intensity and it crossed the Turkish south-eastern border (Fig3-d).

**a)**

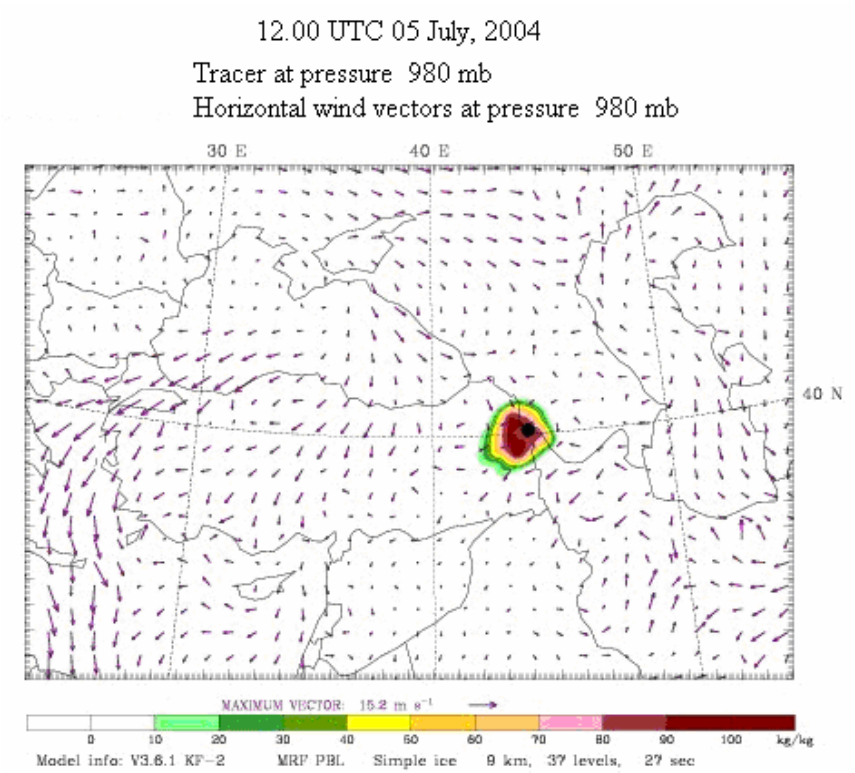
12.00 UTC 05 July, 2004
Tracer at pressure 980 mb
Horizontal wind vectors at pressure 980 mb
30 E
40 E
50 E
40 N
MAXIMUM VECTOR: 15.2 m s-1
0 10 20 30 40 50 60 70 80 90 100 kg/kg
Model info: V3.6.1 KF-2 MRF PBL Simple ice 9 km, 37 levels, 27 sec

**b)**

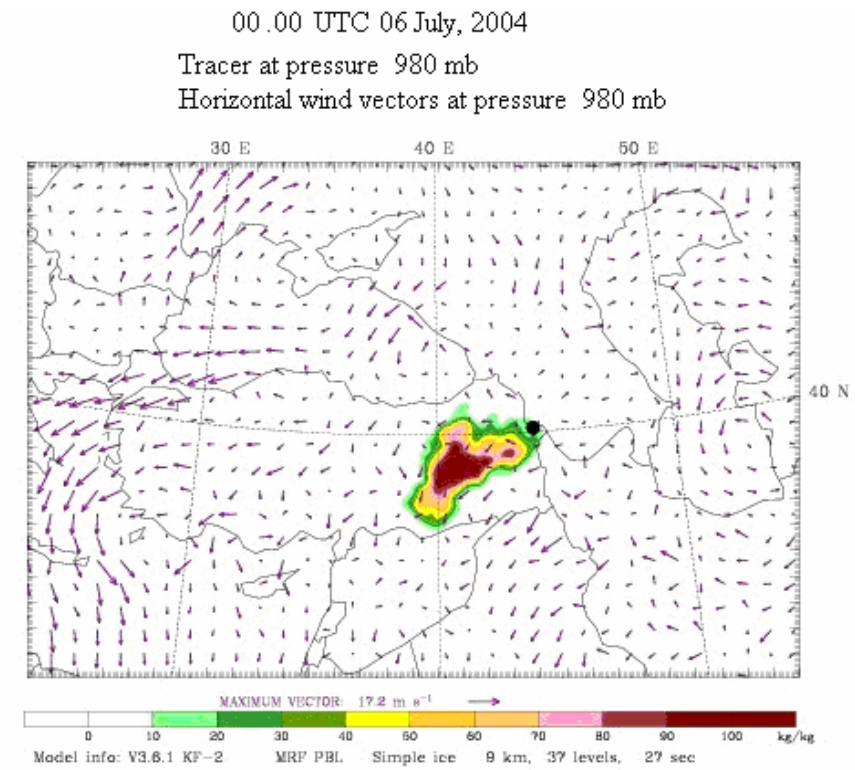
00.00 UTC 06 July, 2004
Tracer at pressure 980 mb
Horizontal wind vectors at pressure 980 mb
30 E
40 E
50 E
40 N
MAXIMUM VECTOR: 17.2 m s-1
0 10 20 30 40 50 60 70 80 90 100 kg/kg
Model info: V3.6.1 KF-2 MRF PBL Simple ice 9 km, 37 levels, 27 sec

**c)**

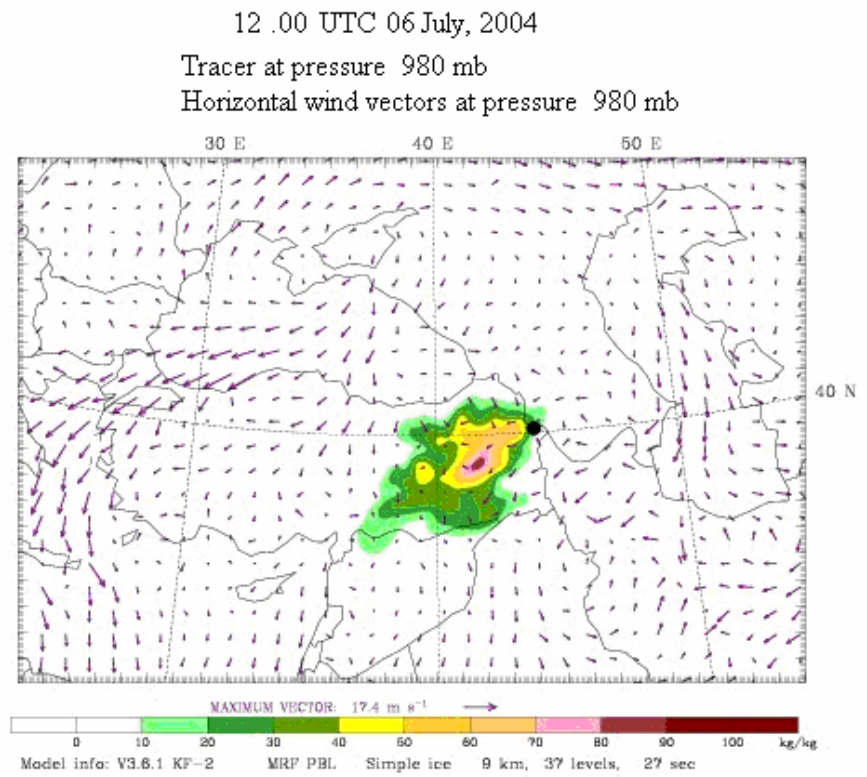


**d)**

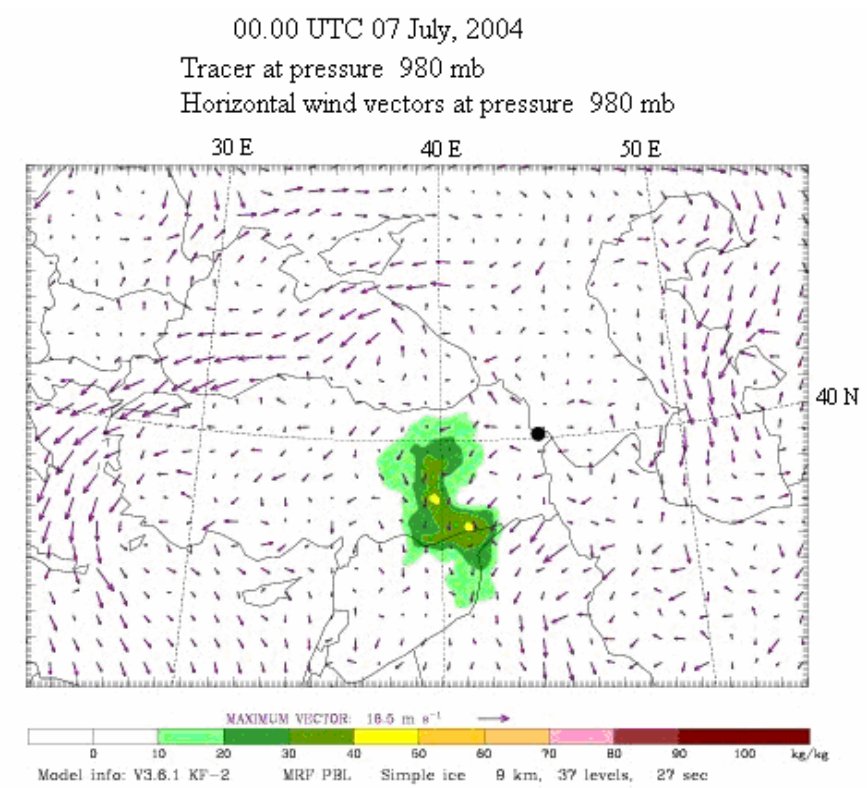


**Figure 3.** Simulated tracers and wind vectors at the 980 mb height at (a) 12-h simulation (b) 24-h simulation (c) 36-h simulation and (d) 48-h simulation.

**Forward Trajectories**

The forward trajectory method was used in the MM5 to determine the transport path of dangerous material to Turkey following a hypothetical accident in the Metsamor. Figure 4 shows 48-h forward trajectories for a summer episode. Starting at the Metsamor on 00:00 UTC July 5 from near the ground level (0.1 km) in the vicinity of the plant, forward trajectories had almost a 5-km height at the end of the simulation. These trajectories indicate the possibility of long-range transport from the Metsamor to Turkey. This result supports our hypothesis that transport from the Metsamor might play an important role in the high radioactive pollution episodes experienced in eastern Turkey during the summer episode in addition to the winter episode.

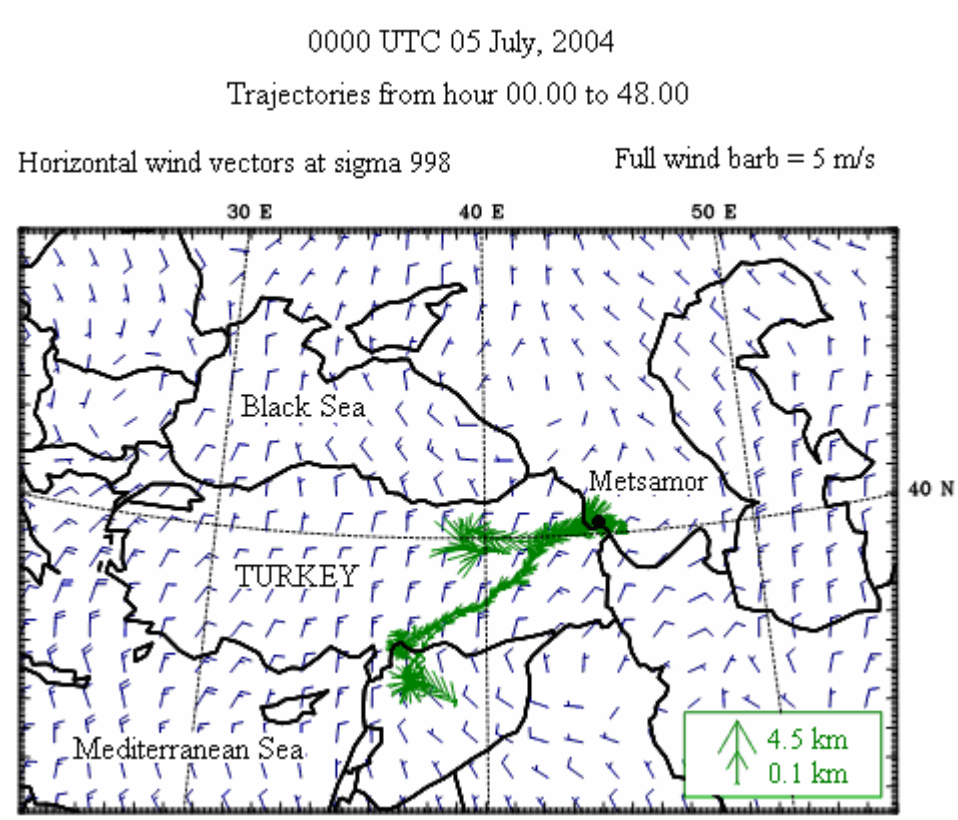


**Figure 4**. The model-generated forward trajectories calculated over 48-hour periods. The box which is on the bottom right hand corner of the figure indicates the initial and final heights of the trajectories.

## 4. CONCLUSION

Turkish authorities have not paid sufficient attention to the different aspects of safety at nuclear installations in the former Soviet Union, even though we faced a terrible experiment about nuclear accidents and their consequences connected to the Chernobyl Accident in 1986. Unsatisfactory safety at the Metsamor Nuclear Power Plant has not been the focus of attention in any official reports. As a result, an emergency response system has not been constituted up to now.

This study focuses on the threat from accidents at the Metsamor Nuclear Power Plant and the subsequent atmospheric transport of radioactive material. A tracer and trajectory analysis was chosen as a method to evaluate the problem. In the beginning, the analysis was carried out as case studies. While the tracer method was performed for the winter episode, the trajectory approach was used for the summer episode (Figure 3). The simulated tracer evolution provided qualitative proof that transport of probable radioactive emissions from the Metsamor could have an impact over Turkey with the worst-case synoptic conditions for Eastern Turkey (Figure 2). In addition, similar results have been obtained by the forward trajectory with prevailing eastern and north -eastern winds for the area (Figure 4).

Actually, the analysis of the tracer and the trajectory should be used to cover a reasonably long period of time. These studies will provide us with an impact map for the zone under study. In addition, they will enable us to see the statistical distribution of the travel time. The Metsamor project with transport simulations will give a risk map in terms of both location and time to the Turkish people from such a worst-case situation.

The above mentioned MM5T on-line model brings with itself some advantages that avoid temporal interpolation errors. The accuracy of the model is likely to enable to Turkish authorities to put forward the right precautions. All in all, it could be used as an “emergency tool” to serve Turkish alertness against nuclear accidents.

## 5. ACKNOWLEDGEMENTS

The authors (Kindap T. and Karaca M) would like to thank ITU Scientific Research Fund and TUBITAK for their support.

## REFERENCES

ArmeniaNow.com, 2004, armenianow.com Jun 4, 2004.

Dudhia, J., 1989: Numerical study of convection observed during the winter monsoon experiment using a mesoscale two-dimensional model. J. Atmos. Sci., 46, 3077-3107.

Fesenko, S. V., Alexakhin, R. M., Geras’kin, S. A., Sanzharova, N. I., Spirin, Ye. V., Spiridonov, S. I., Gontarenko, I. A., Strand, P., 2005, Comparative radiation impact on biota and man in the area affected by the accident at the Chernobyl nuclear power plant, Atmospheric Environment, 80, 1-25.

Grell, G. A., J. Dudhia, and D. R. Stauffer, 1994: A description of the fifth-generation Penn State/NCAR mesoscale model (MM5). NCAR/TN-398+STR, National Center for Atmospheric Research, Boulder, CO, 122 pp.

Hong, S.-Y., and H.-L. Pan, 1996: Nonlocal boundary layer vertical diffusion in a medium-range forecast model. Mon. Wea. Rev., 124, 2322-2339.

IAEA, 1991, The International Chernobyl Project: An Overview.

Kain, J. S., 2004: The Kain-Fritsch convective parameterization: An update. J. Appl. Meteor., 43, 170-181.

Langner, J., Robertson, L., Persson, C., and Ullerstig, A., 1998, Validation of the Operational Emergency Response Model at the Swedish Meteorological and Hydrological Institute Using Data from Etex and the Chernobyl Accident, Atmospheric Environment, 32 (24), 4325-4333.
Mlawer, E. J., S. J. Taubman, P. D. Brown, M. J. Iacono, and S. A. Clough, 1997: Radiative transfer for inhomogeneous atmosphere: RRTM, a validated correlated-k model for the long-wave. J. Geophys. Res., 102 (D14), 16663-16682.
Pöllanen, R., Valkama, I., and Toivonen, H., 1997, Transport of Radioactive Particles from the Chernobyl Accident, Atmospheric Environment, 31(21) 3575-3590.
Powers, D. A., Kress, T. S. and Jankowski, M. W., 1987, The Chernobyl source term, Nuclear Safety, 28, 10-28.
Tschiersch J, Georgi B., 1987, Chernobyl Fallout Size Distribution in Urban Areas, J. Aerosol Sci., 18, 689-692.

*Proceedings of the Third International Symposium on Air Quality Management at Urban, Regional and Global Scales. 26-30 September 2005, Istanbul – Turkey*

# 3-DIMENSIONAL MODELING OF GASEOUS AND PARTICULATE POLLUTANTS IN SWITZERLAND

**Sebnem Andreani Aksoyoglu, Johannes Keller and Andre S.H. Prevot**

Paul Scherrer Institute, Villigen PSI, 5232, Switzerland
sebnem.andreani@psi.ch

## ABSTRACT

An exceptionally hot and dry period in August 2003 was simulated using the 3-dimensional CAMx air quality model. The formation and transport of ozone and secondary aerosols were evaluated. Simulations suggest that the speed reduction of vehicles from 120 km $h^{-1}$ to 80 km $h^{-1}$ on the highways in Switzerland would have a small effect (1 %) on peak ozone concentrations. However, it should be noted that the $NO_x$ and primary particle concentrations would decrease leading to an additional improvement of the air quality. The secondary aerosols such as particulate nitrate, sulfate, ammonium and secondary organic aerosols (SOA) smaller than 2.5 μm were calculated for the same period. The modelled secondary aerosol mass concentrations in Switzerland, averaged over the entire period vary between 5 - 8 μg $m^{-3}$ depending on location. In southern Switzerland higher concentrations were predicted. The contribution of biogenic sources to SOA is quite high (around 70%) in the north whereas it is relatively lower in southern Switzerland (40%). These results agree well with findings from measurements. Importance of initial and boundary conditions were also discussed. Model results suggest that enough ammonia exists to neutralize sulphate and then to produce ammonium nitrate in the northern part of the domain. Sensitivity test using reduced $NH_3$ and $NO_x$ emissions suggest that secondary aerosol formation is unlikely to be limited by $NH_3$ in northern Switzerland but rather by $HNO_3$. On the other hand, aerosol formation in the region of Milan was predicted to be limited by $NH_3$.

**Key Words** : Air Quality Modeling, Aerosols, Ozone, SOA, CAMx, MM5

## 1. INTRODUCTION

The exceptionally hot and dry summer in 2003 led to ozone levels exceeding the ambient air quality standards in many parts of Europe (Buwal, 2003). The long heat wave during the first half of August caused severe health problems especially in western Europe. As an emergency action to reduce ozone levels in southern Switzerland, the speed limit on some highways in Canton Ticino and in Canton Graubünden was reduced from 120 km $h^{-1}$ to 80 km $h^{-1}$ during one week. However, it was not possible to assess the effectiveness of the speed limit reduction due to the cold front arrived in the south towards the end of that period. In the first part of this modeling study, we investigated the effectiveness of speed reduction to reduce ozone levels.

In the second part of the study, we modelled secondary aerosols. Although formation of gaseous pollutants such as ozone is well known, there is still a lack of knowledge about aerosol formation, especially about the formation of secondary organic aerosols (SOA). But also little is known about the concentrations of inorganic aerosols in Switzerland. Gehrig and Buchmann (2003) evaluated the long-term PM2.5 and PM10 (particles smaller than 2.5 and 10 μm in diameter, respectively) measurements at various sites in Switzerland. The chemical composition of atmospheric PM on the other hand, was investigated by Hueglin et al. (2005). The legal threshold for yearly average is 20 μg $m^{-3}$ for PM10 in Switzerland. As a short-term threshold, the concentration averaged over 24 hours may exceed 50 μg $m^{-3}$ only once a year. PM10 concentrations in Switzerland frequently exceed the limit values especially in the south of the Alps. Although the health relevant particles are probably those with smaller sizes (< 1 μm or < 2.5 μm), at present there is no ambient air quality standard for PM1 or PM2.5 in Switzerland. Understanding the partitioning behavior of semi-volatile species between the gas and aerosol phases can help us predict how changes in anthropogenic and biogenic activity will influence formation of aerosols in the atmosphere. With this understanding, appropriate control strategies could be developed. However, applications of aerosol models are partly limited due to lack of speciated aerosol measurements with high time and space resolution. Most of the aerosol model applications have been performed in the United States and Canada (Held et al. 2004; Yin et al. 2004). There are very few applications in Europe (Bessagnet et al. 2004; Cousin et al. 2005). Aerosols have been introduced as air quality indicators through PM10 and in the near future PM2.5 will be introduced. In view of the forthcoming European legislation on particles, air quality simulations including aerosol processes are urgently needed. Although some 3-dimensional modeling studies were conducted for ozone in Switzerland (Andreani-Aksoyoglu et al. 2001; Kuebler et al. 2002) there is hardly any model study on PM yet (Andreani-Aksoyoglu et al. 2003). In this study, the secondary aerosols such as particulate nitrate, sulfate, ammonium and secondary organic aerosols (SOA) were calculated for the particle size smaller than 2.5 μm, for the same period as described in the first part.

## 2. MODELLING METHOD

A period between 4 and 7 August 2003 was simulated using the 3-dimensional CAMx (Version 4.11s) air quality model with 2 nested domains (Environ, 2004). The size of the coarse domain was 35 grid cells in the east-west direction and 29 grid cells in the north-south direction with a resolution of 27 km x 27 km. The fine domain contained 68 and 50 grid cells in the east-west and north-south direction, respectively, with a resolution of 9 km x 9 km. There were 10 σ-layers in a terrain-following Lambert Conic Conformal coordinate system, the first being about 30 m above ground. The fine domain covered Switzerland and some part of the surrounding countries including the greater Milan area. Meteorological data such as 3-dimensional wind fields, temperature, pressure, water vapour, vertical diffusivity, and clouds/rainfall were calculated by the MM5 meteorological model (PSU/NCAR, 2004). MM5 was initialized by data of the Alpine Model (aLMo) of MeteoSwiss. The four dimensional data assimilation was conducted using surface measurements,

balloon soundings and aLMo upper level data. The emission inventory was prepared by compiling European and Swiss anthropogenic emissions from various data sources. Using land use and meteorological data, biogenic emissions were calculated by means of temperature and irradiance dependent algorithms. Initial and boundary conditions were obtained from the European model REM-3/CALGRID output. Calculations of aerosols smaller than 2.5 μm were performed with the fine/coarse option of the aerosol module. Primary particle emissions were not considered due to the lack of a particle emission inventory. The sensitivity of aerosol formation to ammonia and nitric acid was studied by performing two simulations where $NH_3$ and $NO_x$ emissions were reduced by 50 %, respectively.

## 3. RESULTS AND DISCUSSION

### 3.1 Ozone

The highest ozone mixing ratios in the lowest layer were predicted generally in the afternoon around 15:00 UTC. As seen in Figure 1, highest levels were predicted around Lugano, in southern Switzerland under the influence of southerly winds with polluted Po Basin air (see Figure 2 for the wind fields). The comparison of the model predictions and measurements is given in detail elsewhere (Keller et al. 2004).

One of the short-term measures to reduce ozone levels discussed during that hot period in 2003 was to decrease the speed limit on the highways. We investigated the effect of such emission reductions on ozone in a scenario case. In this scenario, the maximum speed limit on the Swiss highways was reduced from 120 to 80 km $h^{-1}$ and corresponding emission rates were used in the model simulations. The decrease in $NO_x$ emissions due to this kind of speed reduction is about 4% of the total Swiss $NO_x$ emissions. On the other hand, VOC emissions are not significantly affected. The effect of speed reduction on ozone is small, less than 1% in the afternoon (Figure 3). The main reason for this low number is the fact that the homemade fraction of ozone due to Swiss emissions is around 25%. It should be noted that the $NO_x$ concentrations and the primary particle concentrations would also decrease in such a scenario. This leads to a relief in addition to the small ozone reduction during these summer smog conditions. The effect on primary aerosols cannot be evaluated in this study due to the lack of primary particle emissions. We conclude that the local and short-term emission reductions are not large enough to reduce ozone levels effectively. Long-term emission developments in Switzerland as well as in the surrounding countries are more important.

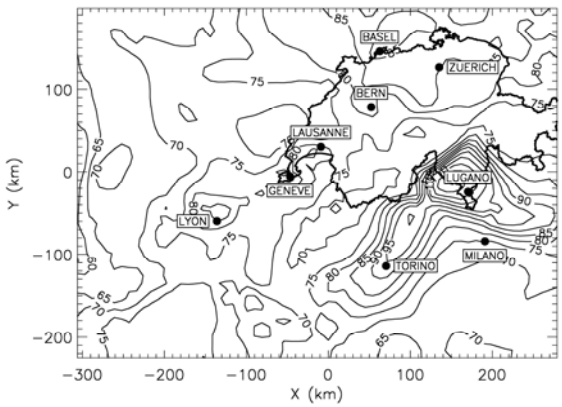


Figure 1. Modelled $O_3$ mixing ratios (ppb) in the fine domain on 5 August 2003, at 14:00-15:00 UTC.

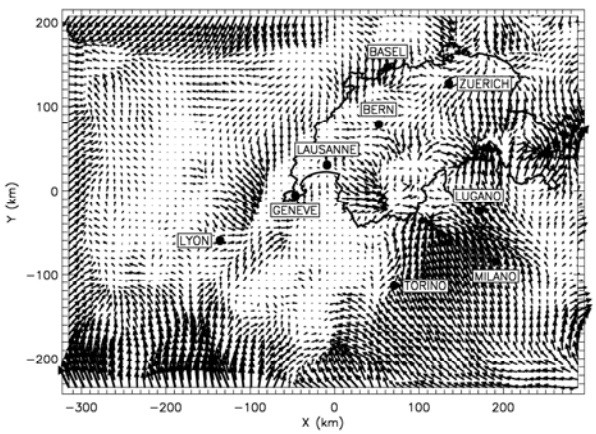


Figure 2. Modelled wind fields in the fine domain on 5 August 2003, at 14:00-15:00 UTC.

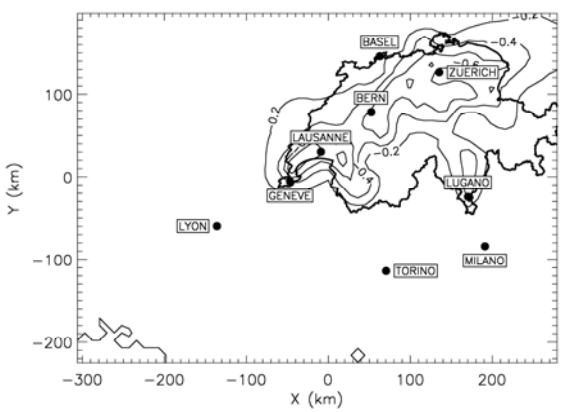


Figure 3. Predicted change in $O_3$ mixing ratios (%) due to speed limit reduction in the fine domain on 7 August 2003, at 13:00-14:00 UTC.

### 3.2. Secondary Aerosols

As seen in Figure 4, the highest afternoon secondary aerosol mass concentrations were predicted in the south. The modelled secondary PM2.5 concentrations averaged over the entire period vary between 5-8 μg $m^{-3}$ in Switzerland. The diurnal variations of predicted individual particulate species show a good correlation between ammonium (blue) and nitrate (red) concentrations at locations in the north such as Zurich and Taenikon (east of Zurich), whereas sulfate (green) levels remain almost constant, around 2-3 μg $m^{-3}$ (Figure 5). These results suggest that in northern Switzerland, enough ammonia exists to neutralize sulfate and then to produce ammonium nitrate. On the other hand, at the southern site Lugano, nitrate levels are very low and the correlation between sulfate (green) and ammonium (blue) indicate the deficiency of ammonia to produce ammonium nitrate in the south. Around Milan, aerosol concentrations are higher than in Switzerland. The average secondary PM2.5 during the period studied is about 15 μg $m^{-3}$. Especially sulfate concentrations are higher than those in the north.

Calculations suggest that the contribution of biogenic SOA to total SOA is quite high, about 70% in the north on average over the entire period (see Figures 6 and 7). These results are in a good agreement with measurements including particulate $^{14}C$ analysis in Zurich (Szidat et al. 2004). The high biogenic contribution is due to the high monoterpene emissions from Norway Spruce trees. On the other hand, biogenic contribution to SOA is relatively lower in the south, for example 40% in Lugano and about 23 % around the polluted area of Milan. Unfortunately there is no speciated aerosol measurements during the period we studied. We compared therefore our results with ambient aerosols measured in summer 2002 in Zurich (Szidat et al. 2004). Measurements cover 4 periods between 16 August and 8 September 2002 (Table 1). Model predictions in general, are in the same range as the measurements. The high biogenic contribution is also in a good agreement with measurements.

Initial and boundary conditions (IC and BC, respectively) used in the model simulations may have significant effects on the results. In order to check for these effects, three more simulations using different IC and BC values were carried out in addition to the base case. As seen in Table 2, in the first case, very low values ($1.10^{-9}$ μg $m^{-3}$) were used for particles in IC and BC files and they were constant in time and space. In the second case, annual means of long-term measurements given by Hueglin et al. (2005) were used. In the third case REM3/CALGRID output was used, but as constant in time and space. The last case (set 4) is the base case where IC and BC were taken from REM3/CALGRID output and the data is variable in time and space. Results of these tests are shown in Figure 8 for Lugano (south) and Zurich (north). It is clearly seen that use of constant values from measurements (set 2, red) and models (set 3, green) lead to overestimation. On the other hand, results of simulations using space and time invariant, but very low particle concentrations (set 1, blue) are closer to the base case where IC and BC were taken from the REM3/CALGRID output and variable in time and space. These results indicate the importance of IC, BC definition in model simulations.

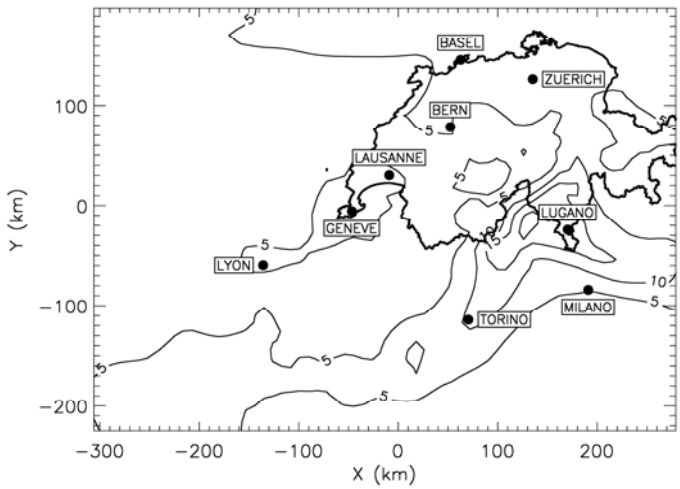


Figure 4. Modelled secondary PM2.5 aerosol mass concentrations (μg $m^{-3}$) on 5 August, 2003, 14:00-15:00 UTC.

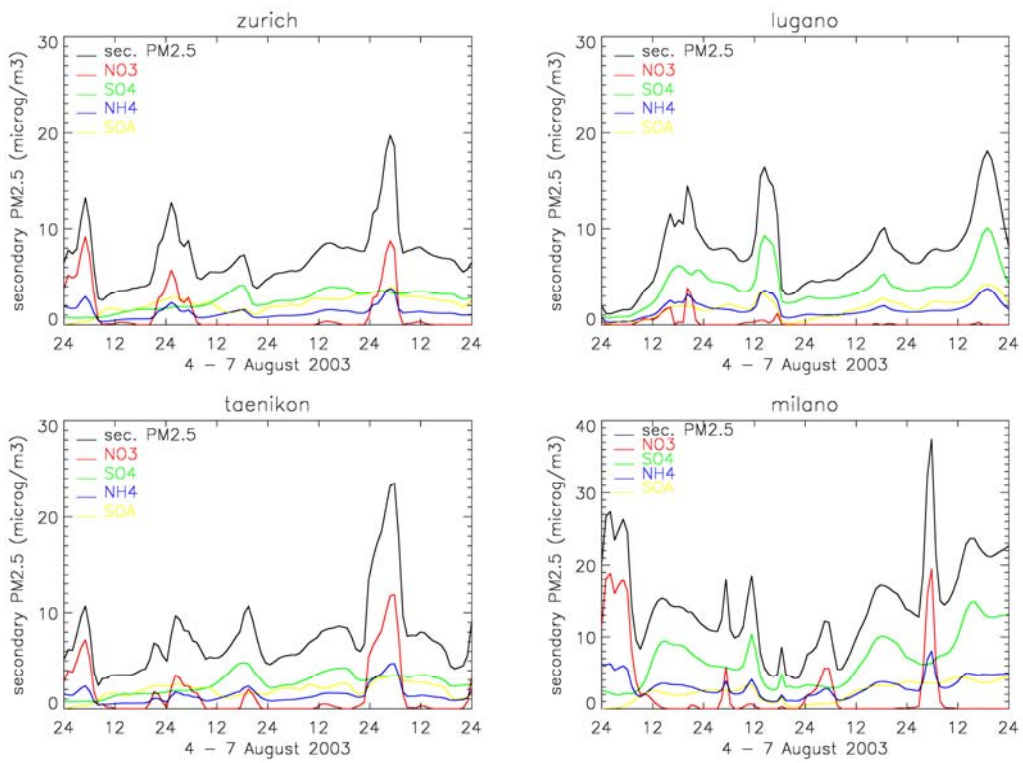


Figure 5. Diurnal variation of modelled particulate nitrate, sulfate, ammonium, secondary organic aerosols and the total secondary PM2.5 particles (μg $m^{-3}$) in Zurich (urban, north), Lugano (urban, south), Taenikon (suburban), Milan (urban, Italy).

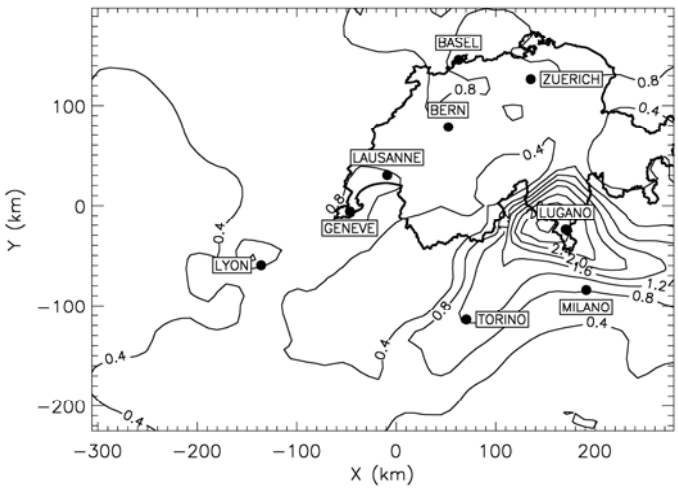


Figure 6. Modelled anthropogenic SOA (PM2.5) concentrations (μg $m^{-3}$) on 5 August, 2003, 14:00-15:00 UTC.

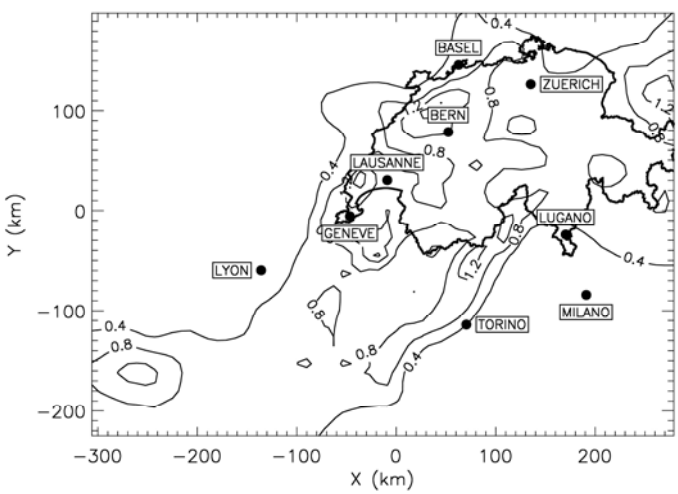


Figure 7. Modelled biogenic SOA (PM2.5) concentrations (μg $m^{-3}$) on 5 August, 2003, 14:00-15:00 UTC.

Sensitivity tests using reduced $NH_3$ and $NO_x$ emissions suggest that secondary aerosol formation is unlikely to be limited by $NH_3$ in northern Switzerland as seen in Figure 9, but rather by $HNO_3$ (therefore by $NO_x$ emissions). The blue color in the figure indicate the $HNO_3$ sensitive areas over the Swiss Plateau, especially around Zurich. On the other hand, aerosol formation in the southern part of Switzerland and northern Italy was predicted to be limited by $NH_3$. However, such sensitivity analyses strongly depend on $NH_3$ emissions which have high uncertainties.

Table 1. Comparison of model results with measurements in Zurich (Szidat et al., 2004).

| species | measurements<br>16 Aug. - 8 Sept. 2002 | model predictions<br>4 – 7 Aug. 2003 |
|---|---|---|
| $SO_4$ (μg $m^{-3}$) | 1.6 – 4.8 | 1.1 – 3.3 |
| $NO_3$ (μg $m^{-3}$) | 0.5 – 2.0 | 0.1 – 2.3 |
| $NH_4$ (μg $m^{-3}$) | 0.7 – 2.3 | 1.1 – 1.7 |
| SOA (μg $m^{-3}$) | 1.0 – 3.1 | 1.3 – 2.9 |
| Biogenic SOA (%) | 65 - 82 | 60 - 67 |

Table 2 . Model runs with various IC (initial conditions) and BC (boundary conditions)

| Run | IC, BC | Variability in time and space |
|---|---|---|
| Set 1 | low default values given in CAMx | constant |
| Set 2 | $NO_3$, $SO_4$, $NH_4$, EC from Hüglin et al. (2005) | constant |
| Set 3 | $NO_3$, $SO_4$, $NH_4$, EC from REM3/CALGRID output | constant |
| Set 4 (base case) | $NO_3$, $SO_4$, $NH_4$, EC from REM3/CALGRID output | variable |

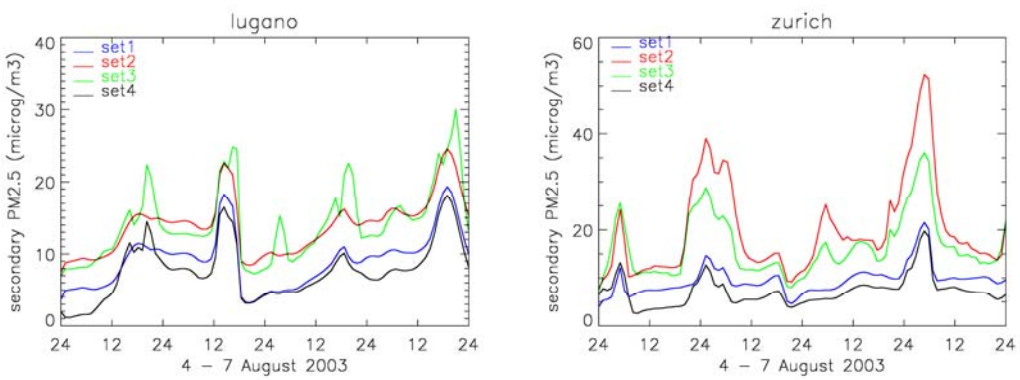


Figure 8. Sensitivity of modelled secondary aerosols to IC and BC. Description of various cases is given in Table 1. Set 4 (black) corresponds to base case.

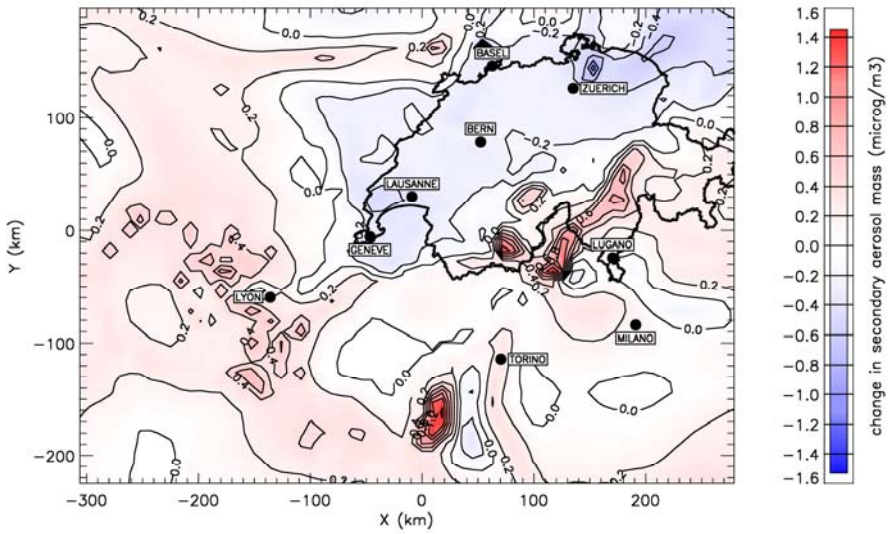


Figure 9.: Sensitivity of secondary aerosol formation to $HNO_3$ and $NH_3$ on 5 August 2003, 14:00-15:00 UTC. This figure shows the difference of two simulations with 50% reduction of $NO_x$ and $NH_3$ emissions. Blue colour indicates $HNO_3$ sensitive and red indicates $NH_3$ sensitive areas.

## 4. CONCLUSION

The formation and transport of ozone and secondary aerosols were simulated by a three-dimensional air quality model during an exceptionally hot and dry period in August 2003. The influence of the traffic speed reductions from 120 km $h^{-1}$ to 80 km $h^{-1}$ was predicted to be low, about 1 %. Although the speed reduction in Switzerland for a short period of time is not enough to reduce ozone levels significantly, it should be noted that the $NO_x$ and primary particle concentrations would decrease in such a traffic scenario. The predicted secondary PM2.5 mass concentrations are higher in southern Switzerland and model results are in a reasonable agreement with measurements. Sensitivity tests showed that initial and boundary conditions have a strong influence on the modelled particle concentrations. Results suggest that there is enough $NH_3$ in the northern part of Switzerland and therefore aerosol formation is rather limited by $HNO_3$. On the other hand, aerosol formation in southern Switzerland and northern Italy was predicted to be more sensitive to $NH_3$. The model results show a high contribution of biogenic sources (about 70%) to SOA formation in the northern part of Switzerland. This result is in agreement with the values obtained in another study using $^{14}C$ measurements for the source apportionment in Zurich. On the other hand, the biogenic contribution to SOA is relatively lower, about 40% in the south.

## 5. ACKNOWLEDGEMENTS

This work was financially supported by BUWAL. MeteoSwiss, FUB, TNO, J.Flemming are gratefully acknowledged for providing various data.

## REFERENCES


Andreani-Aksoyoglu, S., C.-H. Lu, J.Keller, A.S.H.Prévôt, J.S.Chang (2001). "Variability of indicator values for ozone production sensitivity: a model study in Switzerland and San Joaquin Valley (California)." Atmospheric Environment **35/32**: 5593-5603.

Andreani-Aksoyoglu S., J. K., J.Dommen,A.S.H.Prévôt (2003). "Modelling of air quality with CAMx: A case study in Switzerland." Water, Air & Soil Pollution : FOCUS **3**(5-6): 281-296.

Bessagnet, B., A. Hodzic, et al. (2004). "Aerosol modeling with CHIMERE--preliminary evaluation at the continental scale." Atmospheric Environment **38**(18): 2803-2817.

BUWAL, (2003) Ozonsommer 2003 im Vergleich mit 1993-2002, http://www.umwelt-schweiz.ch/buwal/de/fachgebiete/fg_luft/luftbelastung/publikat/nabel/index.html

Castro, L. M., C.A.Pio, R.M. Harrison, D.J.T. Smith (1999). "Carbonaceous aerosol in urban and rural European atmospheres: estimation of secondary organic carbon concentrations." Atmos. Environ **33**: 2771-2781.

Cousin, F., C. Liousse, et al. (2005). "Aerosol modelling and validation during ESCOMPTE 2001." Atmospheric Environment **39**(8): 1539-1550.

Environ (2004) Users's guide, Comprehensive Air Quality Model with Extensions (CAMx). Version 4.10s, ENVIRON International Corporation, Novato.

Gehrig, R. and B. Buchmann (2003). "Characterising seasonal variations and spatial distribution of ambient PM10 and PM2.5 concentrations based on long-term Swiss monitoring data." Atmospheric Environment **37**(19): 2571-2580.

Held, T., Q. Ying, et al. (2004). "Modeling particulate matter in the San Joaquin Valley with a source-oriented externally mixed three-dimensional photochemical grid model." Atmospheric Environment **38**(22): 3689-3711.

Hueglin, C., R. Gehrig, et al. (2005). "Chemical characterisation of PM2.5, PM10 and coarse particles at urban, near-city and rural sites in Switzerland." Atmospheric Environment **39**(4): 637-651.

Keller, J., S. Andreani-Aksoyoglu, M. Tinguely, A.Prevot (2004). Influence of reducing the highway speed limit to 80 km/h on ozone in Switzerland, Paul Scherrer Institute.

Kuebler, J., A.G.Russell, A.Hakami, A.Clappier, H.van den Bergh (2002). "Episode selection for ozone modelling and control strategies analysis on the Swiss Plateau." Atmos. Environ. **36**: 2817-2830.

PSU,NCAR (2004) MM5 Version 3 Tutorial Presentations, http://www.mmm.ucar.edu/mm5/mm5v3/tutorial/presentations/tut-presentations.html

Szidat, S., Jenk T.M., Gäggeler H.W., Synal H-A. Fisseha R., Baltensperger U., Kalberer M., Samburova V., Wacker L., Saurer M., Schwikowski M., Hajdas I. (2004). "Source apportionment of aerosols by $^{14}C$ measurements in different carbonaceous particle fractions." Radiocarbon **46**(1): 475-484.

Yin, D., W. Jiang, et al. (2004). "Improvement of biogenic emissions estimation in the Canadian Lower Fraser Valley and its impact on particulate matter modeling results." Atmospheric Environment **38**(4): 507-521.

*Proceedings of the Third International Symposium on Air Quality Management at Urban, Regional and Global Scales. 26-30 September 2005, Istanbul – Turkey*

# MODELING OF EUROPEAN AIR POLLUTION AND LONG-RANGE TRANSPORT TO THE EAST MEDITERRANEAN REGION

**Muwaffaq Freiwan[a,b], Selahattin Incecik[b] and Umit Anteplioglu[c]**

[a] Jordan Meteorological Department, P.O. Box: 341011, Amman – 11134, Jordan, mfreiwan@yahoo.com
[b] Istanbul Technical University, Aeronautics and Astronautics Faculty, Meteorological engineering Department, Maslak – 34469, Istanbul, Turkey, incecik@itu.edu.tr
[c] Kandilli Observatory, Bosphorus University, Cengelkoy, Istanbul, Turkey, anteplio@boun.edu.tr

## ABSTRACT

Measurements of some air pollution species, mainly $SO_4^{2-}$ in some rural locations in the Eastern Mediterranean revealed high concentrations which are comparable or higher than those of Central and Eastern Europe. Since the area is free of any source of pollution, it is believed that such high concentration of various pollution species are transported from other regions, such as Eastern or Southeastern Europe. The Antalya measurement station (36.47N, 30.34E) which is located on the Mediterranean coasts has recorded high concentrations of $SO_4^{2-}$ during the years 1992 – 2000. Of these a 4 day episode 26 – 29 August 1998 was selected to investigate the long range transport of European air pollution to the east Mediterranean region. Mesoscale Meteorological Model, MM5 was applied to forecast the three dimensional meteorological data. Backward trajectory simulations were also produced by MM5/RIP and HYSPLIT models. Consequently, three main sectors of air mass trajectory originated from Europe were found. Coupled with MM5, the three-dimensional Eulerian photochemical model CAMx is used to simulate the concentration, deposition and the long range transport of the air pollution species $PSO_4^{2-}$ and $SO_2$. CAMx air quality model simulations have revealed a great agreement with the air mass trajectory simulations produced by HYSPLIT and RIP/MM5 models and demonstrated that sulfate transport from central and southeastern Europe to the eastern Mediterranean has two main paths. The modeling system which is used for the first time in Turkey exhibited a good performance.

**Key Words:** Long Range Air Pollution Transport, Backward Trajectory, MM5, CAMx, HYSPLIT.

## 1. INTRODUCTION

The last two decades have been characterized by a growing interest in long-range transport of biogenic and anthropogenic aerosols and other air pollutants, mainly because of serious public health risks for human beings and to ecosystems in local, regional or either in global scales (Draxler, 1987; Galperin, 1991; Syrakov and prodnova, 2002; Chen et al., 2002; Sciare et al., 2002; Park and Lee, 2003; Cakmur and Miller, 2004; Kallos et al., 2004).

Because of its unique topographic and climatic diversity and its location in the mid-latitudes, the Mediterranean region is considered as one of the most attractive regions in the world for studying mesoscale and long-range transport of dust (Kubilay et Al., 2000; Israelevic et al., 2002), aerosol (Dogan and Tuncel, 2003; Kocak et al., 2004a) and other pollutants such as acidic sulfate and nitrate deposition (Gullu et al., 2000; Ozturk et al., 2003).

In Turkey, there are many studies handled aerosol concentrations and investigated their sources using observed wind field (Tuncel and Erduran, 2001), statistical back trajectory method (Tuncel, 2002), by analyzing the air mass trajectories (Kubilay et al., 2002) or by applying a trajectory model to a limited region, such as Izmir city, where Dincer et al. (2003) applied HYSPLIT back trajectory model to determine the pathway of $SO_2$ pollution in the city. But the transboundary long range air pollution transport modeling is still an absent topic in the Turkish literature. One of the major drawbacks that restrict modeling regional air pollution is the absence of the national emission inventories. Numerous European countries have their own emission models. Using the EMEP national annual emission inventories they can calculate the hourly gridded emission inventories of various pollutant emitting sources in the desired domain. Development of a national inventory model will pave the way for excessive air quality modeling researches.

In this study a modeling system consists of Mesoscale Meteorological Model, MM5, Comprehensive Air Quality Model with Extension, CAMx and the Hybrid Single Particle Lagrangian Integrated Trajectory (HYSPLIT) model was used to predict the atmospheric condition in large domain that includes the European continent, Turkey and the Mediterranean region, to predict the gridded concentrations and depositions of $PSO_4$ and $SO_2$ species, and to simulate their trajectories using the gridded wind field predicted by MM5 during the episodic period 26 – 29 August 1998. This modeling system is used for the first time in Turkey to handle the probable long range air pollution transport phenomenon from Europe to the eastern Mediterranean region represented by Antalya.

## 2. BRIEF DESCRIPTION OF THE MODELING SYSTEM

The PSU/NCAR **M**esoscale **M**odeling System, **5**$^{th}$ generation (**MM5**) version 3.61 is a limited-area, nonhydrostatic, terrain-following sigma-coordinate model designed to simulate or predict mesoscale and regional-scale atmospheric circulation. The model is widely used in forecasting the meteorological circumstances those are used in air pollution modeling. Details about the model are available in numerous publications including the MM5 community home page. In this study MM5 model was used to predict the meteorological conditions to be used firstly in the air quality model, CAMx. The model has been applied in a domain of 35° Lat. x 40° Lon. dimensions which lies between 25 – 60° N and 5 – 45° E in a horizontal spatial resolution of 50 km x 50 km and 89 x 78 grid-points in the E-W and in the N-S directions respectively vertical resolution of 34 layers. And secondly in the Hybrid Single Particle Lagrangian Integrated Trajectory (HYSPLIT) model to simulate the backward trajectories. Furthermore MM5/RIP (Read/Interpolate/Plot) has also been used to calculate and plot trajectories. Three-dimensional Eulerian air quality model CAMx (Comprehensive Air Quality Model with Extension) version 4.11s was applied to simulate the predicted concentration, deposition, transport and source origins of anthropogenic pollutants in the study domain during the selected episodic period 26 – 29 August 1998. The photochemical model, CAMx was applied to a mesoscale domain of 89 x 78 grid points with a horizontal resolution of 0.59° x 0.45° in the E-W and N-S directions respectively, and 14 layers vertical resolution. The first layer is 50 m AGL and the highest level is 4000 m AGL.

## 3. MODELS SIMULATIONS AND RESULTS

### 3.1. MM5 Model

The MM5 model simulations include hourly gridded predictions for both 2-dimensional and 3-dimensional meteorological variables during the 5 day period 25 – 29 August 1998. The visualization program RIP was used to plot the desired predicted charts of temperature, wind vectors and pressure or geopotential height fields for each time step in the episodic period at the mandatory levels. Additionally a NW – SE vertical cross section of the wind circulation, potential vorticity and potential temperature fields through the domain was predicted for each time step. Furthermore a Skew-T plot for Antalya is also predicted for each time step. Figure 1 shows the MM5 model predicted versus observed 700 hpa level plot of temperature, wind velocity and geopotential height. It is apparently seen from the figure that the model accomplished not only to predict the general pattern of the pressure systems, but also to produce a highly accurate forecast all over the episodic period. The 96 and 120 hours forecasts are as accurate as the 24 and 48 hours, which mean that the model has succeeded to prevent its accuracy and to maintain its performance level during the whole forecast period.

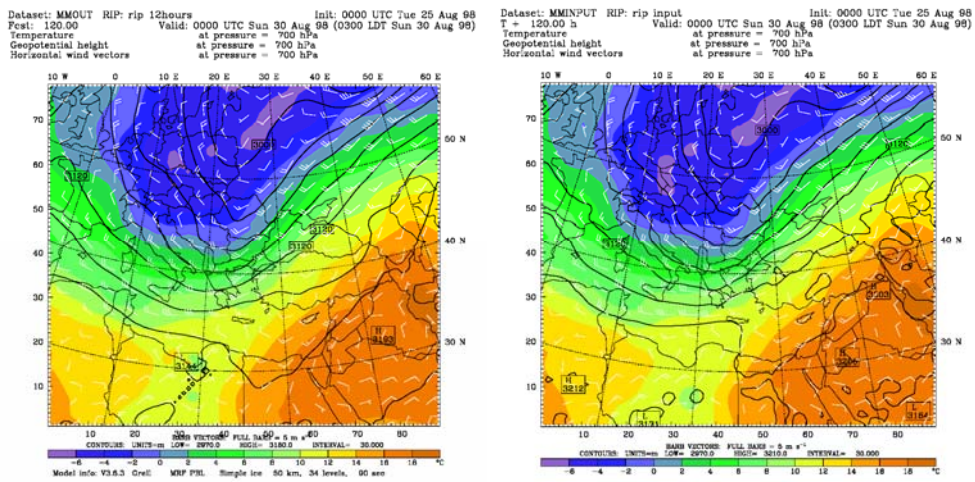


Figure 1. 120 hours forecast (left) and observed (right) of 700 hpa geopotential heights in gpm (black contours), temperature in °C (color shading) and horizontal wind velocity (white vectors), valid at 0000UTC, 30 – 08 – 1998.

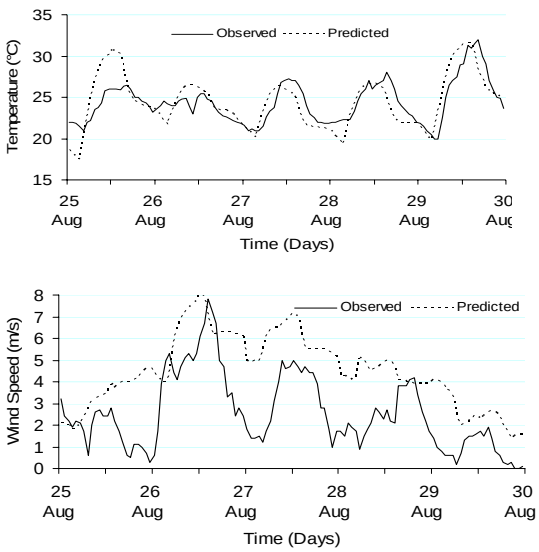

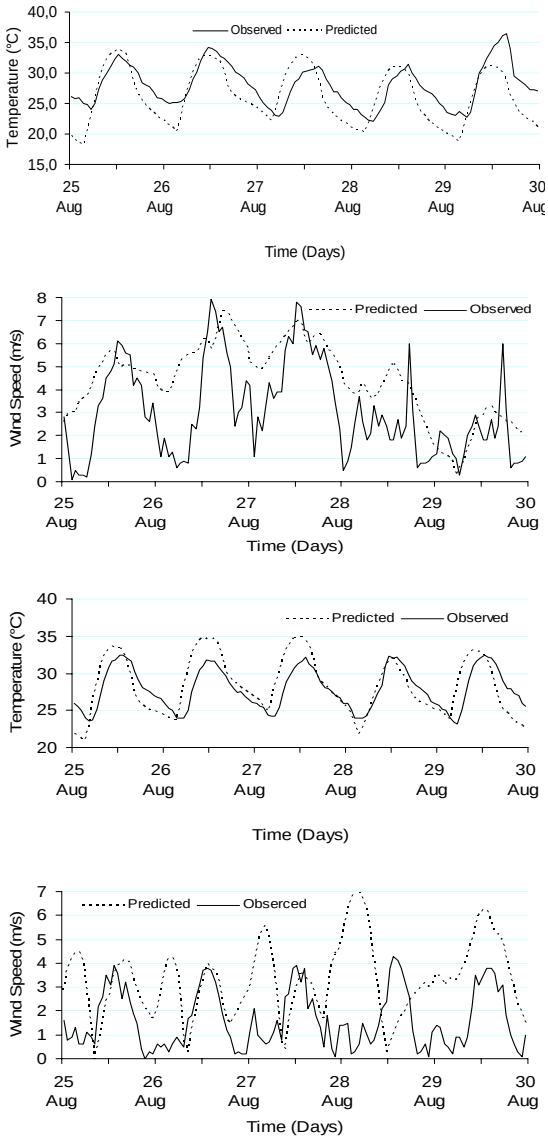


Figure 2. Hourly temperatures (left) and wind speed (right) observed in meteorological stations of Istanbul (upper), Izmir (middle) and Antalya (lower) versus predicted by MM5 model from 25 Aug. 00 Z to 30 Aug 00 Z.

The MM5 model performance was found to be superior in forecasting temperature and wind fields. A comparison between the model predicted and the observed hourly 5 day time series of air temperature and 10 m wind speed at three locations (Istanbul, Izmir and Antalya) have been illustrated in Figure 2. Furthermore scattered diagram of observed values versus MM5 model prediction values for both temperature and wind speed are also plotted for the same stations in Figure 3. It is obvious from the both figures that the model revealed a high accuracy in forecasting the temperature in each of the three stations. The correlation coefficient ($R^2$) is relatively high for temperature (0.59, 0.55, 0.57) and wind speed (0.47, 0.46. 0.05) in the three stations respectively except in Antalya.

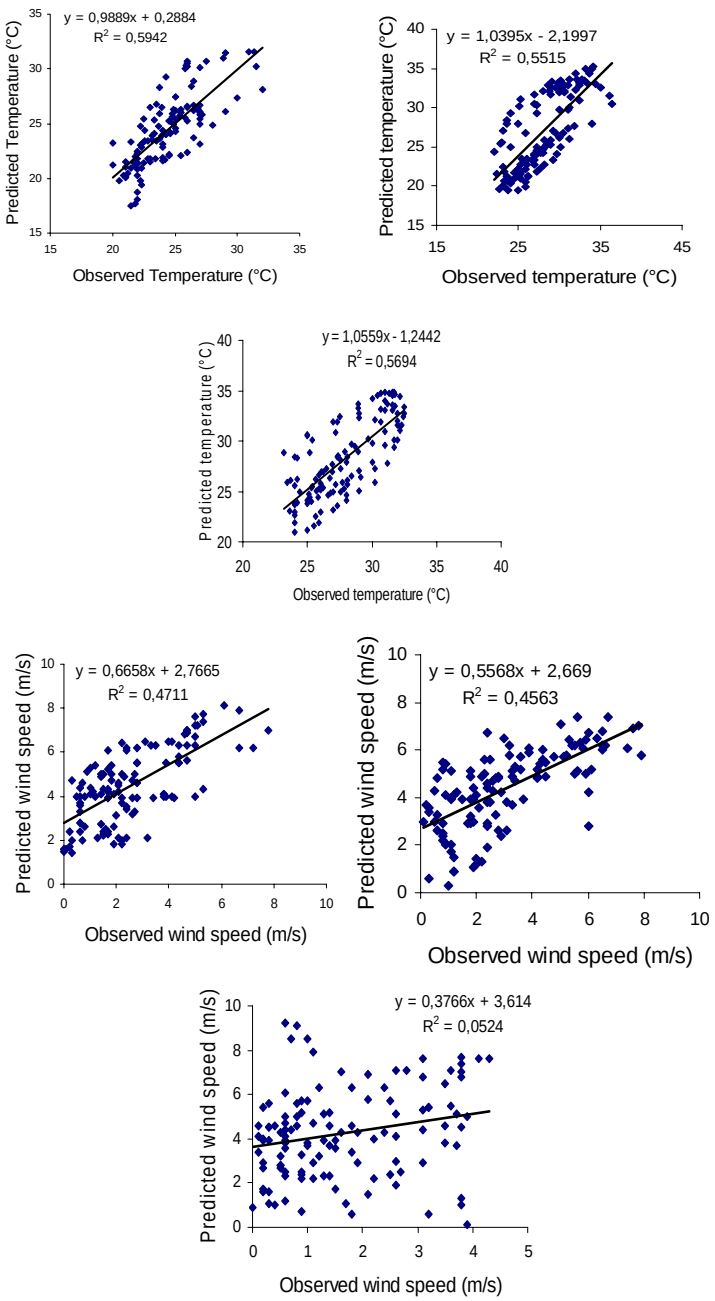


Figure 3. Model predicted versus observed hourly temperature (upper) and 10m wind speed (lower) in Istanbul (left), Izmir (middle) and Antalya(right) meteorological stations for the period from 25 Aug. 00 Z to 30 Aug 00 Z.

### 3.2. HYSPLIT and RIP Trajectory Model

The prognostic hourly wind field produced by the Mesoscale Meteorological Model, MM5 in 50km x 50km horizontal resolution was used to calculate air pollution trajectories to the eastern Mediterranean region. Two models were employed to calculate and simulate the trajectories using MM5 forecast data through a 96 hour period between 00 UTC, 26 – 08 – 1998 and 00 UTC, 30 – 08 – 1998.

1- The first model is the plot software RIP (Read/Interpolate/Plot).

2- The second is HYSPLIT (the Hybrid Single Particle Lagrangian Integrated Trajectory) model.

Backward trajectories at four sigma levels (0.998, 0.990, 0.900 and 0.850) were plotted for selected 13 points in the Eastern Mediterranean region and western Turkey. It is found that the trajectories are originated from three main sectors taking in account their tracks to the eastern Mediterranean as follows:

1. Sector A: Turkey and Eastern Europe, which includes trajectories originated from Ukraine, Moldavia and Romania through the Black Sea and Turkey to the eastern Mediterranean that is represented by Antalya.

2. Sector B: Turkey and central Europe, which has trajectories originated mainly from Bulgaria, Macedonia, Albania, the former Yugoslavia, Croatia and Slovenia through the western part of Turkey and then the eastern Mediterranean.

3. Sector C: Southern Europe and the Mediterranean Sea, the trajectories in this sector are originated mainly from the central and western Mediterranean Sea, Spain, the southern parts of France, Italy, Greece and the southwestern parts of Turkey to the eastern Mediterranean, which is represented by Antalya.

These results are in a great agreement with the findings of Sciare et al. (2001) regarding to the backward trajectories to Finokalia in the eastern Mediterranean.

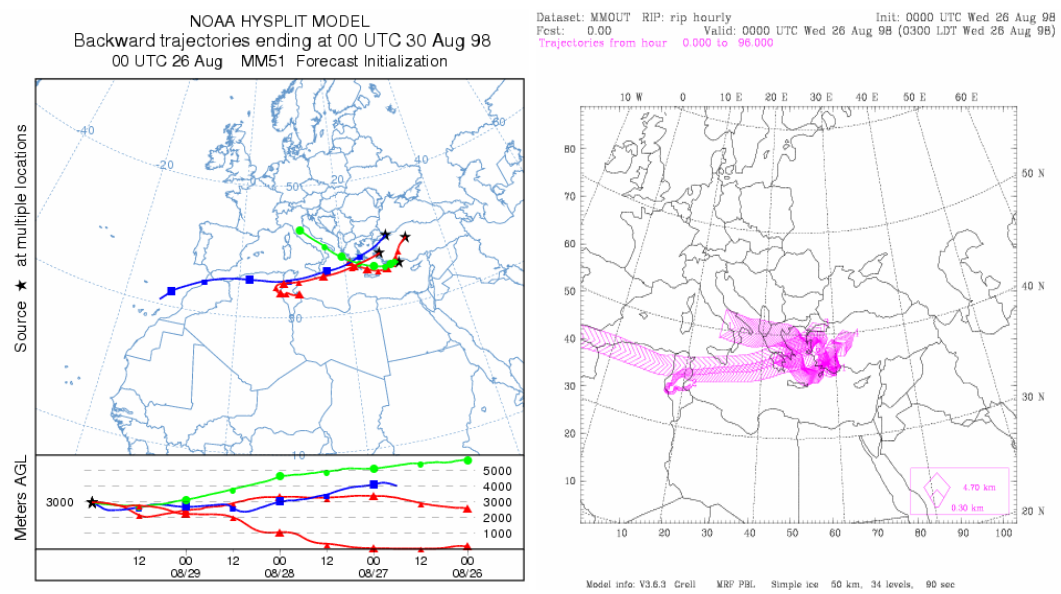


Figure 4. 96 hours backward trajectories at 3000 m AGL for Antalya, Izmir, Istanbul and Ankara plotted by HYSPLIT (left) and RIP (right) using the meteorological data predicted by MM5 model. Trajectories start at 0000 UTC, 30 Aug. 1998 and end at 0000 UTC, 26 Aug. 1998.

Figure 4 shows a simulation of 96 backward trajectory plots produced by both models; RIP and HYSPLIT for Antalya, Izmir, Istanbul and Ankara at 3000 m AGL.

The results are superior; trajectories produced by the two models are completely identical. The figure indicates that the trajectories to the eastern Mediterranean and western parts of Turkey are originated from southeastern Europe and the Mediterranean Sea through Greece and the Aegean Sea.

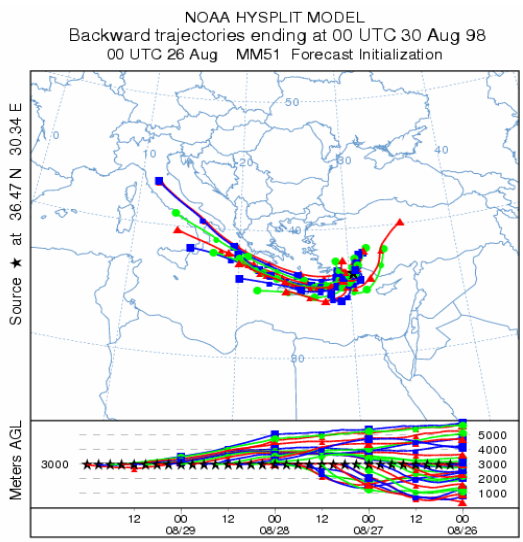


Figure 5. A multiple backward trajectory plot for Antalya at 3000 m AGL. Trajectories are lotted at 3 hour interval between 00 UTC, 30 Aug. 1998and 00 UTC, 26 Aug. 1998.

Furthermore multiple backward trajectory plots for Antalya at several levels are simulated by the HYSPLIT model ( one of these simulation is given in Figure 5 ). In these simulations trajectory generation is renewed every 3 hours all over the entire period that starts at 00:00 Z 30 Aug. 1998 and ends at 00:00 Z 26 Aug. 1998. As a result 32 trajectories are produced during 96 hour period, the first trajectory starts at Antalya at 00:00 Z 30 Aug. 1998 while the last one starts at 0300 Z 26 Aug. 1998 and all trajectories end at the origin source at 0000 Z 26 Aug. 1998.

Backward trajectory plots for Antalya station at 3000 m AGL (Fig.5) indicate that there are few short range trajectories originated from closed areas to Antalya, such as the southern parts of Turkey at levels below 3000 m AGL. Whereas the medium and long range transport is chiefly originated from Italy and Mediterranean Sea through the southern parts of Greece to Antalya within a layer ranges between 3000 – 6000 m AGL.

### 3.3. Air Quality Model, CAMx

CAMx air quality model, version 4.11s has been applied to simulate the predicted concentration, deposition, transport and source origins of anthropogenic pollutants in the study domain during the selected episodic period 26 – 29 August 1998. The

photochemical model, CAMx grid domain is of 89 grids in the east-west and 78 grids in the north-south directions with a horizontal resolution of 0.59° x 0.45° in the E-W and N-S directions respectively, and 14 layers vertical resolution. The first layer is 50 m AGL and the highest level is 4000 m AGL. To solve the pollutant continuity equation including the terms of: horizontal advection/diffusion, vertical transport/diffusion, chemistry, dry deposition and wet deposition, the CAMx model requires a set of input data that include: (i) Temperature, u, v wind components, pressure, geopotential height, cloud cover rain and other meteorological parameters are predicted by the mesoscale model MM5. (ii) The average default values of time/space constant top concentrations of all the species were selected to be used in a preprocessor to generate the initial and boundary concentration gridded data files. (iii) To generate the gridded landuse/surface vegetation cover inputs, the 30 sec., 24 categories USGS landuse / surface vegetation data were converted to CAMx 11 categories at 0.59° x 0.45° resolution. (iv) The UV albedo codes were calculated by a preprocessor depending on the landuse and vegetation distribution. (v) Gridded haze opacity codes, gridded ozone column codes and photolysis rates lookup tables are calculated by the radiative model, TUV assuming clear sky conditions as a function of 5 parameters: solar zenith angle, altitude, total ozone column, surface albedo and atmospheric turbidity. (vi) Emissions: The EMEP annual emission data were used to prepare the hourly gridded emission inventories of various anthropogenic pollutant emitting sources in the study domain. In this study CB-IV gas-phase chemical mechanism (mechanism 4) is used to invoke the aerosol chemistry which includes the gas-phase chemistry that governs the transformation of $SO_2$ to sulfate via the homogenous gas-phase reaction. The dry deposition of gases is based on the resistance model of Wesely (1989).

CAMx has been run for the 4 day episodic period, 26 – 29 Aug. 1998. Hourly gridded concentration and deposition distribution of the gaseous species $SO_2$ and the aerosol species $PSO_4$ were generated and the **P**ackage for **A**nalysis and **V**isualization of **E**nvironmental data (**PAVE**) software was used to simulating and mapping the gridded binary outputs of the CAMx model. Figure 6 shows the concentration simulations of $PSO_4$ and $SO_2$ on the first and last days of the study period. The figure indicates that the high sulfate concentrations exist over the southern parts of Italy on 26 Aug. 1200 Z have moved eastward and started to cross the western borders of Turkey on 29 Aug. 1200 Z. the high concentrations of sulfate over central Europe that were simulated in later hours (not seen in the figure) have also moved eastward and taken place over eastern Europe (lower part of the figure). The $SO_2$ concentration distribution was predicted to be identical through the study period. This means that the $SO_2$ concentration reveals large values only near sources and $SO_2$ is not transported to long distances from the origin sources.

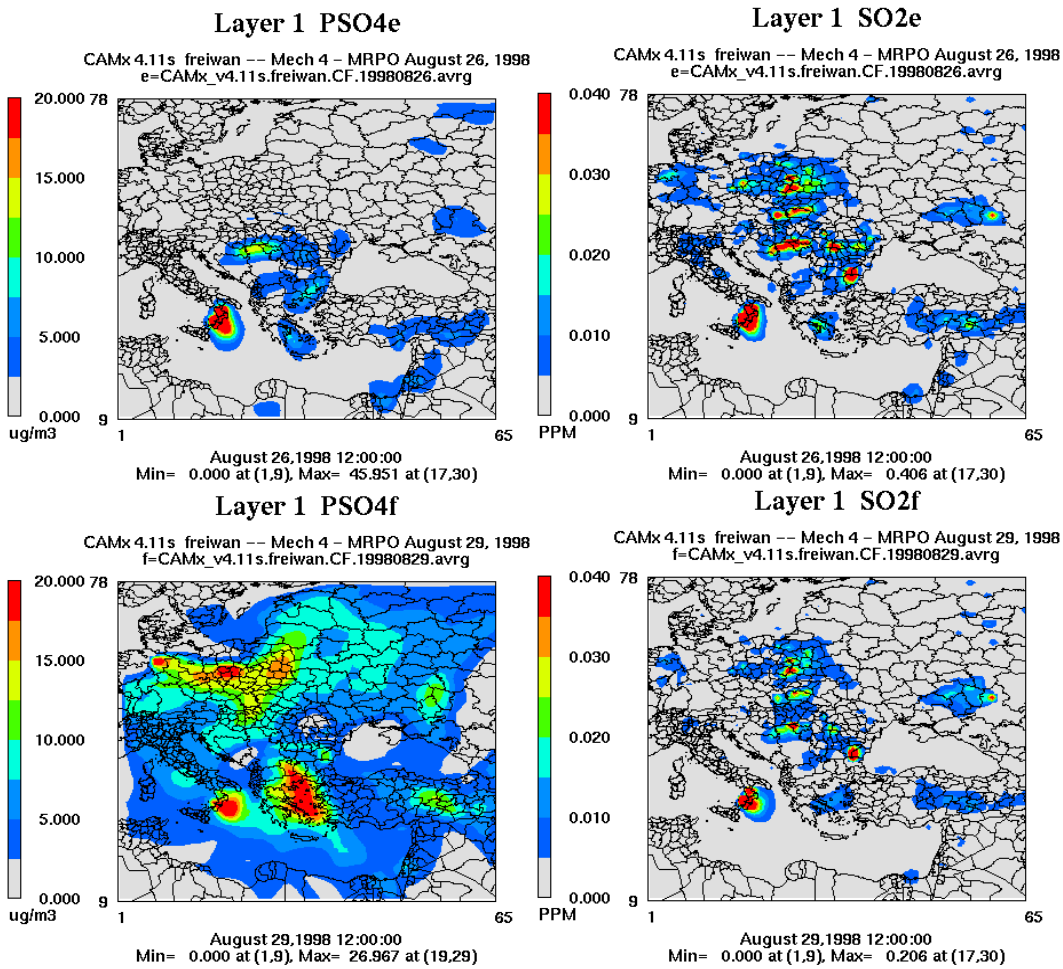


Figure 6. Concentration Simulations of $PSO_4$ (left) and $SO_2$ (right) on 26 Aug. 1200 Z (upper) and 3 days later on 29 Aug. 1200 Z (lower).

This result is unexpected, since several studies have reported that most of the $SO_2$ over the eastern Mediterranean originates from central and eastern Europe. The same findings were derived by Sciare et al. (2002). This can be probably attributed to the active oxidation of $SO_2$ to $SO_4$ in the fume of the power plant and to the rapid transformation of the $SO_2$ to aerosol sulfate in the troposphere which may occur within a short time (may be several hours). In the other hand the $PSO_4$ concentration simulations indicate obvious evidence to the sulfate transformation from central and southeastern Europe to the eastern Mediterranean region. Two main tracks are identifiable:

1- The first track is the transport of sulfate originated from Italy through Greece and the Aegean Sea to the southeastern Mediterranean. This result is also emphasized by the backward trajectories discussed in section 3.2 and illustrated in Fig. 3 and 5. In this case the transport taking place at high levels ranging between 3000 – 6000 m AGL may explain the long range transport of sulfate rather than $SO_2$.

2- The second one is the sulfate transport track which is apparently originated from central and Eastern Europe through the northwestern part of Turkey. This track is also identical to sector B of the backward trajectory distributions discussed in section 3.2.

Similar results related to transport and origin source determination of $PSO_4$ are reported by Kouvarakis et al. (2000), Sciare et al. (2002) and Kallos et al. (2004).

There is no internationally or regionally established methodology for the routine observation of dry deposition. Moreover, research on dry deposition is still limited in comparison with the many research projects and ongoing measurements of wet deposition in Europe.

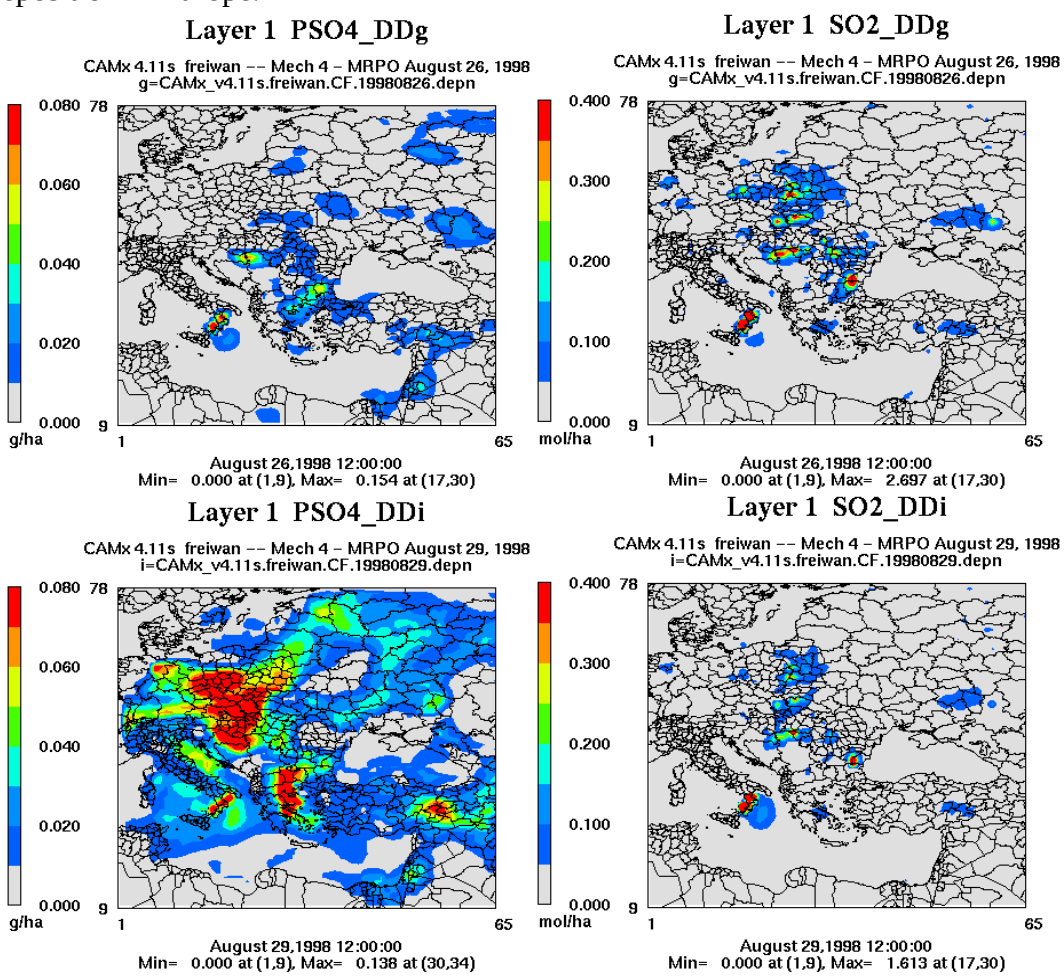


Figure 7. Deposition Simulations of $PSO_4$ (left) and $SO_2$ (right) on 26 Aug. 1200 Z (upper) and 3 days later on 29 Aug. 1200 Z (lower).

In this study gridded hourly deposition velocity, wet and dry deposition rates are predicted by CAMx model.The deposition outputs produced by CAMx include: (i) Two-dimensional dry deposition velocity (m/s), (ii) Two-dimensional dry deposited mass (mol/ha for gaseous species and g/ha for aerosols), (iii) Two-dimensional wet deposited mass (mol/ha for gaseous species and g/ha for aerosols) and (iv) Two-dimensional precipitation liquid concentration for species (mol/l for gasses, g/l for aerosols).

The downward flux and consequently the deposition rates are proportional to the concentration of the species near the ground. The eastern Mediterranean region was free of rainfall during the study period and so was a large portion of the domain. Accordingly the wet deposition and the liquid concentration of the both species will not be discussed in this study. Figure 7 shows the deposition simulations of $PSO_4$ and $SO_2$ on the first and last days of the study period. It is apparently seen from the concentration and the dry deposition figures 6 and 7 that the areas of high concentration of $SO_2$ and $PSO_4$ are also areas of large deposition of the same species and vice versa. Accordingly we can say that the deposited sulfate in the eastern Mediterranean region is originated from central and southeastern Europe.

## 4. CONCLUSIONS

In this study a modeling system consists of the Mesoscale Meteorological Model MM5, a three-dimensional Eulerian model CAMx (Comprehensive Air Quality Model with Extension) and the Hybrid Single Particle Lagrangian Integrated Trajectory model (HYSPLIT) was used to predict the atmospheric condition in large domain that includes the European continent, Turkey and eastern Mediterranean region, to estimate the gridded concentrations of various air pollution species and to simulate their trajectories using the gridded wind field predicted by MM5. This modeling system is used for the first time in Turkey to investigate the long range air pollution transport phenomenon through such large domain to southwestern Turkey and the east Mediterranean region, represented by Antalya. The air mass backward trajectory simulations by MM5/RIP and HYSPLIT have demonstrated three main sectors of air mass origins and tracks as follows:
**Sector A:** Turkey and Eastern Europe, which includes trajectories originated from Ukraine, Moldavia and Romania through the Black Sea to the central and western parts of Turkey and then the eastern Mediterranean.
**Sector B:** Turkey and central Europe, this sector includes trajectories originated mainly from Bulgaria, Macedonia, Albania, the former Yugoslavia, Croatia and Slovenia to the western part of Turkey and then the eastern Mediterranean.
**Sector C:** Southern Europe and the Mediterranean Sea, the trajectories in this sector are originated mainly from the central and western Mediterranean Sea, Spain, the southern parts of France, Italy and Greece through the Aegean Sea to the southwestern parts of Turkey and then to the eastern Mediterranean.
The air quality model simulations of sulfate concentration and deposition have revealed a great agreement with the air mass trajectory simulations produced by HYSPLIT and RIP/MM5 models. Simulations have demonstrated that sulfate transport from central and southeastern Europe to the eastern Mediterranean has two main paths: (i) the first is the transport of sulfate originated from Italy through Greece and the Aegean Sea to the southwestern parts of Turkey. (ii) The second is the track which is apparently originated from central and Eastern Europe through the northwestern part of Turkey.
Simulations of $PSO_4$ and $SO_2$ indicate a remarkable coincidence between concentration and deposition of the both species. The areas of high concentration of $SO_2$ and $PSO_4$ are also areas of large deposition of the same species and vice versa. Both $SO_2$ concentration and deposition have revealed large values only near sources

which indicate that $SO_2$ is not transported to long distances from the origin sources and deposited on the same areas. In contrast to $SO_2$, the deposited sulfate in the eastern Mediterranean region is mostly originated from central and southeastern Europe.

The performance of the mesoscale meteorological model, MM5 was found to be superior. The model exhibited a higher accuracy in the forth and fifth days of the forecast period. CAMx model also revealed a good performance in estimating $PSO_4$ in Ankara, but it underestimated the sulfate in Antalya by a factor of about 8. The model also overestimated $SO_2$ by a factor of 6. The overestimation of $SO_2$ concentration may be caused either by boundary conditions or emissions and it may be avoided by sensitivity analysis.

## 5. ACKNOWLEDGEMENT

The authors would like to thank Dr. Marina Astitha who has prepared the emission inventories that are used in CAMx model.

## REFERENCES

Camkur, R. V., and Miller, R. L., 2004: Incorporating the effect of small-scale circulations upon dust emission in an atmospheric general circulation model. *J. Geophys. Res.*, 109, D07201, doi: 10.1029/2003JD004067.

Chen, L.-W. A., Doddridge, B. G., Dickerson R. R., Chow, C. C., and Henry, R. C., 2002: Origins of fine Aerosol mass in Baltimore – Washington corridor: implications from observation, factor analysis and ensemble air particle back trajectory. *Atmospheric Environment*, 36, pp. 4541–4554

Dincer, F., Elbir, T., and Muezzinoglu, A., 2003: Analyzing the impacts of environmental air pollution the air quality in Izmir region using HYSPLIT back trajectory model. *The 6th national symposium on: combustion and air pollution control*, 10 – 12 September, Izmir, Turkey, pp. 161 – 168 (in Turkish).

Dogan G., and Tuncel, G., 2003: Comparison among aerosol concentrations in various regions of Turkey. *The 6th national symposium on: combustion and air pollution control*, 10 – 12 September, Izmir, Turkey (in Turkish).

Draxler, R. R., 1987: Sensitivity of a trajectory model to the spatial and temporal resolution of the meteorological data during CAPTEX. *Journal of Climate and Applied Meteorology*, Vol. 26, No: 11, pp. 1577 – 1588.

Galperin, M., 1991: Routine model for long-range transport calculations of sulfur and nitrogen compounds from continuous sources allowing for non-linear effects. Air Pollution modeling and its Application VIII, Edited by H. Van Dop and D.G. Steyn, *Plenum Press*, New York USA.

Gullu H.G., Olmez I., and Tuncel G., 2000: Temporal variability of atmospheric trace element concentrations over the eastern mediterranean Sea. *Spectrochimica Acta, Part B*, 55, pp. 1135–1150.

Israelevic, P. L., Levin, Z., Joseph, J. H., Ganor, E., 2002: Desert aerosol transport in the Mediterranean region as inferred from the TOMS aerosol index. *J. Geophys. Res.*, 107(D21), 4572, doi: 10.1029/2001JD002011.

Kallos, G., Astitha, M., Gofa, F., O'Connor, M., Mihalopoulos, N., and Zlatev, Z., 2004: "Transport and Deposition Patterns of Ozone and Aerosols in the Mediterranean Region". *27th NATO/CCMS International TechnicalMeeting on Air Pollution Modeling and its Applications*, October 2004, Banff, Canada.

Kocak, M., Nimmo, M., Kubilay, N., and Herut, B., 2004a: Spatio-temporal Aerosol trace metal concentrations and sources in Levantine basin of the Eastern Mediterranean. *Atmospheric Environment,* Vol. 38, pp, 2133 – 2144.

Kouvarakis, G., Tsigaridis, K., Kanakidou, M., and Mihalopoulos, N., 2000: Temporal Variation of Surface Regional Background Ozone over Crete Island in the Southeast Mediterranean. *J. Geophys. Res.* Vol. 105, No. D4. pp. 4399 – 4407.

Kubilay N., Nickovic S., Moulin C., and Dulac F., 2000: An illustration of the transport and deposition of mineral dust onto the eastern Mediterranean. *Atmospheric Environment,* Vol. 34, 8 , pp, 1293-1303.

Miller, M. J., 1974: On the use of pressure as vertical coordinate in modeling conversion. *Quart. J. Roy. Meteor. Soc.*, 100, 155 – 162.

Ozturk, F., SOULTANOV, L., and TUNCEL, G., 2003: Determination of the observed high sulfate concentrations in the Eastern Mediterranean Region. *The 6th national symposium on combustion and air pollution control*, 10 – 12 September Izmir, Turkey. pp. 298 – 309 (in Turkish).

Sciare, J., Bardouki, H., Moulin, C., and Mihalopoulos, N, 2002: Aerosol Sources and their Contribution to the Chemical Composition of Aerosols in the Eastern Mediterranean Sea during Summertime. *Atmos. Chem. Discuss*., 2, pp. 1287 – 1315.

Syrakov, D., and Prodanova, M., 2002: Transboundary exchange of sulfur pollution in region southeastern Europe. Air Pollution and its Application XV, Edited by Borrego and Schayes, *Kluwer Academic / Plenum Publissers*, New York, USA.

Tuncel, G., *2002:* Wet and dry deposition of natural and anthropogenic aerosol components to the Eastern Mediterranean. *Bi-National Israeli-Turkish workshop on: Atmospheric deposition of aerosols and gases in theEastern Mediterranean*, Golden Tulip Hotel, Dead Sea, Israel.

Tuncel, S. G., and Erduran, M. S., 2001: Characteristics of air pollutant in the Eastern Mediterranean coast. *The 2nd international symposium on: Airquality management at: urban, regional and global scales*. Istanbul, Turkey.

Wesely, M.L., 1989: Parameterization of Surface Resistances to Gaseous Dry Deposition in Regional-Scale Numerical Models. *Atmos. Environ.*, 23, 1293-1304.

*Proceedings of the Third International Symposium on Air Quality Management at Urban, Regional and Global Scales. 26-30 September 2005, Istanbul – Turkey*

# AIR POLLUTION IMPACT ASSESSMENT OF A COMPLEX INDUSTRIAL-URBAN AREA BY MEANS OF A LAGRANGIAN PARTICLE MODEL

**[1*] C. Gariazzo, [3] V. Papaleo, [1]A. Pelliccioni, [2]G. Calori, [2]P. Radice and [2]G. Tinarelli**

[1]ISPESL – DIPIA, Via Fontana Candida,1 00040 Monteporzio Catone (RM) Italy; **cgariazzo@tiscali.it*
[2]ARIANET, via Gilino 9, 20128 Milano, Italy
[3]Università degli Studi di Roma "La Sapienza" - Dipartimento di Idraulica, Trasporti e Strade, Via Eudossiana, 18 00184 Roma, Italy

## ABSTRACT

Taranto hosts one of the most relevant industrial districts of Italy adjacent to an urban area. An impact assessment study has been conducted to evaluate the effect produced by the main emission sources on the local air quality. A local emission inventory has been developed taking into account industrial sources, traffic, domestic heating, fugitive and harbor emissions. A 3D Lagrangian particle dispersion model (SPRAY) has then been applied on the study area using meteorological data collected in seasonal field campaigns. 3D short term hourly concentrations have been calculated for both total and specific sources. Results show that the model is able to reproduce the measured $SO_2$ and $NO_x$ concentrations. Industrial activities are confirmed to be the main contributor to $SO_2$. Industry and traffic are the main responsible for $NO_x$ simulated concentrations. CO concentrations are found to be mainly related with traffic emissions, while primary $PM_{10}$ simulated concentrations seem to be linked with industrial and fugitive emissions. Model source contributions at selected monitoring stations predict on average 87% and 41% of industrial contribution to the total concentration of $SO_2$ and $NO_x$ respectively. Traffic emissions account for 45% of the total $NO_x$ and for 89% of the total CO concentrations on average.

**Key Words:** Air pollution, Industrial, Urban, Particle Model, SODAR.

## 1. INTRODUCTION

The city of Taranto is a populated-industrialized areas in Italy. In this city the typical urban emissions are superimposed on the industrial ones located in proximity of city. Among the industrial activities we can find: a large steel plant, being the biggest one in terms of both emissions quantity and extension of working areas; the third most important oil refinery in Italy; a cement facility. Other smaller emission sources can also be found in this territory mainly related with both the above industries and with the local economy. All these industrial activities use the harbor of Taranto to

download primary materials and to delivery final products. These tasks are often related with emissions of particulate matter. Ships also produce pollutants emission during wharf operations.
According to this frame, an air pollution impact assessment study has been conducted to provide information on the impact produced by the main emission sources on the local air quality and to quantify their contributions.

## 2. MATERIALS AND METHODS

### 2.1 Modeling system

The modeling system used in this study is composed by three codes: the MINERVE meteorological model, the SURFPRO turbulence pre-processor and the SPRAY Lagrangian particles dispersion model. SPRAY 3.0 (Tinarelli et al., 1994; Gariazzo et al., 2004) was used to reproduce the concentration fields generated by the pollutants emitted by the considered sources. SPRAY is a 3-D model able to simulate air pollution dispersion in the atmosphere in non homogenous and non stationary conditions. The 3D fields of wind and temperature have been calculated using the diagnostic code MINERVE (Aria, 2001) using a mass-consistent objective analysis scheme.
The random turbulent fluctuation of wind components ($\sigma_u$, $\sigma_v$, $\sigma_w$ and skewness $w'^3$) are used by SPRAY to determine the random motion causing the dispersion. They are calculated by means of parameterization codes (Hanna, 1982) based on scaling variables derived by SURFPRO code on the basis of the Monin-Obukhov similarity theory and surface energy budget evaluation (Van Ulden and Holtslag, 1985), starting from two dimensional arrays of surface parameters (albedo, Bowen ratio, $z_0$) and ground meteorological parameters given as input.

### 2.2 Field campaign description

Two field campaigns were conducted in winter and summer seasons to feed the model with real data and to validate the modeling results. To provide meteorological data to the modeling system, different stations were used (figure 1). Among the local monitoring network, five stations (Garibaldi, Peripato, Orsini, Paolo VI and Dante) were used, located both downtown and in the city neighborhoods. Pollutants concentration measurements were also carried out in the above stations. In addition three mobile laboratories were located in the studied area. A Mobile Meteorological Laboratory (MML) was placed in the harbor of Taranto. It calculates averaged values of the main standard meteorological data and turbulence parameters starting from data collected by sonic anemometers. Two mobile chemical-meteorological laboratory were located respectively, in a rural area of Palagiano about 30 Km west the city of Taranto, and in the urban area of Statte, nearly 15 Km north of Taranto. To get information on meteorological parameters in the east and north parts of the territory, two other meteorological stations were placed in the S. Giorgio and Monte Mesola villages. In order to provide upper air measurements, a SODAR/RASS system was used. Wind, turbulence and temperature profiles up to 400 m a.g.l were measured close to the MML station. Such data were completed by wind and

temperature profiles up to 24 km collected every 6 hours at Brindisi by means of radiosoundings.


Figure 1. Satellite image of the study area with location of monitoring stations.

## 2.3 Emission inventory

The inventory set up for this study contains yearly emissions of five chemical species ($SO_2$, $NO_x$, CO, $PM_{10}$ and VOC) concerning the most significant anthropic activity sectors: industrial sources, road transport, domestic heating, maritime activity.

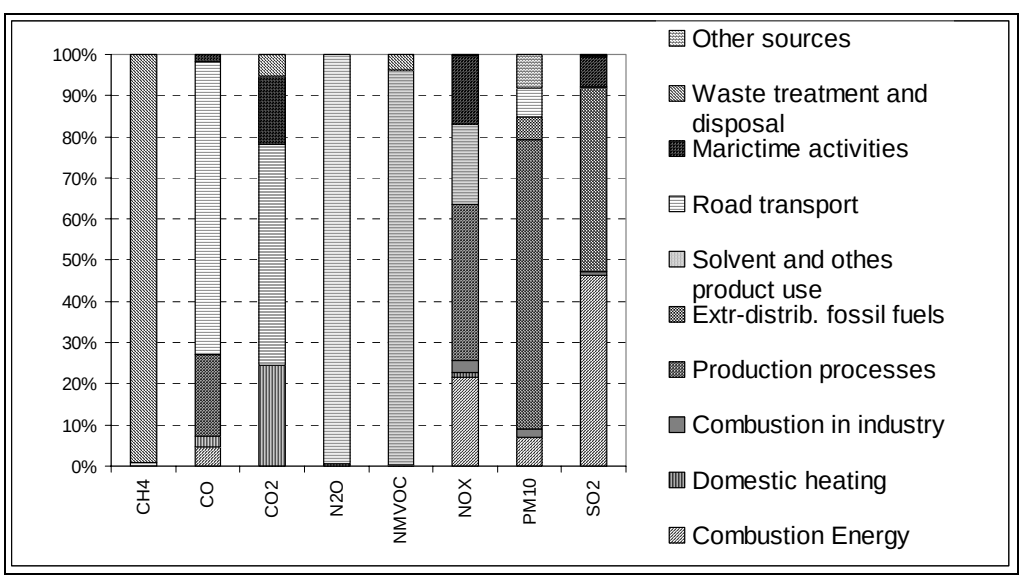


Figure 2. Sources contribution to the total emissions of some considered pollutants.

In figure 2 area and point sources emissions, considered as a whole and referred as SNAP categories, are shown in order to underline the importance of various activities

to the total emissions of specific pollutants; in most cases road traffic has the greatest relevance, it represents more than 50% of CO, $CO_2$, $N_2O$ and NMVOC emissions, and less than 20% $NO_X$ ones. For $CH_4$ the largest emissions are due to activities linked to solid waste disposal, while emission data concerning industrial sources are by far the major source of $SO_2$, $NO_x$ and $PM_{10}$.

Road traffic emissions are considered in two ways: as line and area sources. The geography of the road networks, with associated vehicular flows, are available for Taranto city, highways, provincial and state roads. Vehicle emissions estimation is based upon the COPERT III methodology integrated with more detailed emission factors for particulate emissions from brakes and tire wear (IIASA, 2001). The calculation is extended to cover all kinds of driving conditions (highway, rural, urban), taking into account mean speeds and slopes. Traffic emissions for all other populated places are treated as area sources and surrogated from the previous ones, using the number of registered vehicles.

The estimation of emissions from Taranto residential heating is based on yearly fuel consumption, while for all other cities, emissions are surrogated from Taranto ones, using the number of inhabitants. This activity causes about the 25% of the $CO_2$ emissions considered in this study and a little bit less than 1% of $NO_x$ emissions.

Harbour emissions from loading/unloading activities and combustion processes during wharf operations are estimated from mercantile fleet data, average in-port idling time and kind of transported goods. Emissions linked to the quays were derived from detailed information on goods handling. Ship emissions take into account three different stages: maneuvering, hotelling and cruising. Shipping movements in the studied area, vessel data (engine power, fuels,..) (Entec, 2002) were used for emissions estimation. Basing on these data, Lloyd's emission factors (Lloyd, 1999) and elaboration of fuel consumption data at full power (Trozzi et al., 1998), ship emissions in different phases are evaluated.

To feed the dispersion model, yearly emissions are temporally and spatially disaggregated using as possible specific information related to the area. Area emissions from the considered activities are allocated according to the spatial distributions of the related classes of soil usage (residential, industrial, etc.), while time disaggregation is based on the typical patterns of the different activities (production cycles for industries and harbour, vehicle passages, etc.).

### 2.4 Models set-up

A 35x35 $km^2$ model domain was considered to cover all possible impacts on the surrounding areas and all relevant towns. The domain has been horizontally divided into 71 x 71 grid cells with 500 m resolution and vertically splitted from the ground level to the top, set to 1500 m, using layers of variable thickness. Surface parameters were estimated on the basis of the Corine land cover maps. A total of 33 days were selected to simulate air pollution dispersion around the studied area. Fourteen of them were related to the winter season and nineteen to summer one. Their selection was based on both typical local atmospheric circulations/synoptical conditions in the considered season and on the occurrence of pollutants concentration peaks. The 3-D

wind and temperature fields generated by the MINERVE meteorological model, the atmospheric turbulence produced by SURFPRO and the emission data were provided as input to the dispersion model. 3D hourly concentrations of $NO_x$, $SO_2$, CO and primary $PM_{10}$ were calculated as total concentration and in terms of contributions of specific sources.

## 3. RESULTS

### 3.1 Comparison with monitoring data

To evaluate model performances the observed $NO_x$, $SO_2$, CO and primary $PM_{10}$ hourly concentrations were compared with the corresponding modeled values. Figure 3 shows a comparison of $NO_x$ observed and modeled concentrations at Orsini monitoring station in winter and summer seasons. The model results exhibits a good reproduction of observed values both in time and concentration value. A few peaks are underestimated but the average values on both seasons are well matched.

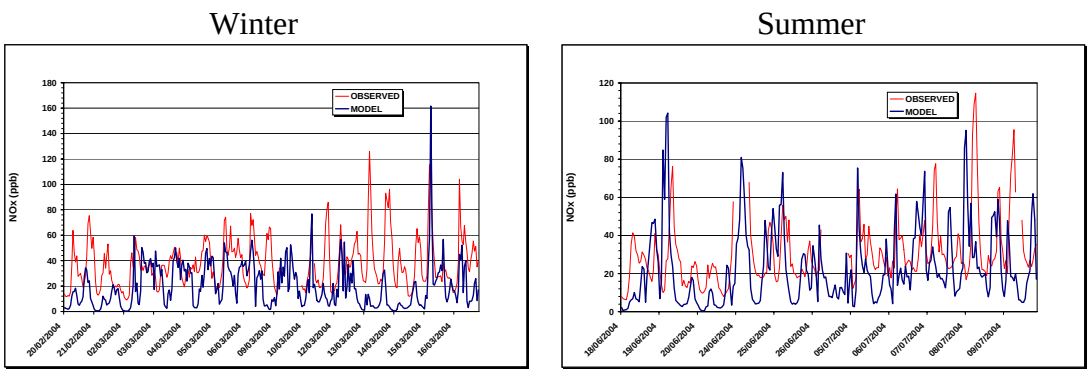


Figure 3. Comparison of observed and modeled $NO_x$ concentrations at Orsini monitoring station.

The $SO_2$ model results in general exhibit peaks higher than observed, with sometimes modeled peaks not revealed by observations. The primary $PM_{10}$ model results indicate an overall underestimation of measured concentrations. This result might be due to possibly missing sources or to an incorrect evaluation of the actual emission factors. A revising of the emission inventory is so required for this pollutant. Background value also needs improvement, but according to the fact that boundary conditions are not used in Lagrangian models, this can only be obtained by enlarging the model domain and including more emission sources. CO model results indicate a general underestimation of the overall average value. The model is able to reproduce the typical morning and evening peaks especially for the urban stations.

### 3.2 Seasonal averaged concentration maps

The 3D hourly concentrations results have been used to calculate daily average maps for each modeled pollutant. To summarize results, overall average winter and summer concentration maps have been calculated starting from daily maps calculated for the corresponding season. Figure 4 shows winter and summer averaged maps of

$NO_x$, $SO_2$, CO and primary $PM_{10}$ concentrations. During wintertime $NO_x$ averaged values up to 50 $\mu g/m^3$ are foreseen, while at summertime higher peak concentrations (70 $\mu g/m^3$) are predicted due to a greater mixing of the local atmosphere which drops down pollutants emitted by elevated stacks. The highest winter $NO_x$ peak is located in the urban area of Taranto and a secondary peak is also placed in the Tamburi district close to the industrial area. Other hot spot $NO_x$ peaks can also be observed in the nearby towns. At summertime a large $NO_x$ peak (up to 50 $\mu g/m^3$) is located around the industrial area, whilst the predicted concentration in the city of Taranto is lower (30$\mu g/m^3$). Hot spots on the surrounding towns are clearly visible as for winter results. The effect of land/sea breeze on concentrations is also clear visible on summer results. A greater part of the inland territory is influenced by the $NO_x$ concentrations, which extent up to 15 Km from the coastline . The spatial dispersion of $NO_x$ concentrations over the sea is also greater in summer than in winter.
The $SO_2$ winter averaged concentration map shows three peaks with averaged value of 25 $\mu g/m^3$, located close to industrial area and in the urban area of Taranto. During summertime the averaged concentration map of $SO_2$ shows a maximum located, as for winter results, in the industrial area, with values up to 60 $\mu g/m^3$, and spreading over the urban area of Taranto with concentrations between 10 and 20 $\mu g/m^3$. As for $NO_x$ results, the spatial distribution of summer and winter $SO_2$ concentration maps are rather different due to different meteorological conditions.
The winter and summer CO concentration maps both show a traffic related origin, with peaks located in the urban areas and in the connecting roads. Summer concentration values are foreseen to be higher than winter one (200 vs. 100 $\mu g/m^3$) due to the frequent low wind speed conditions during summer time. The spatial distribution of the predicted concentrations seems not to be affected by the different seasonal meteorological conditions as for $NO_x$ and $SO_2$ results. The concentrations are confined around the emission areas as a consequence of the soil level emission height.
Primary $PM_{10}$ seasonal concentration maps both exhibit an impact area restricted to the industrial district and its surrounding with an extension of 4x4 $Km^2$. The city of Taranto is only partially influenced by this kind of emission. As far as the low accuracy on $PM_{10}$ results is concerned, this estimation needs to be verified. According to the model prediction, the summer concentration are higher (120 $\mu g/m^3$) than the winter one (70 $\mu g/m^3$).

### 3.3 Evaluation of source contribution

In order to evaluate the contribution of specific sources to the predicted concentrations, six monitoring stations were selected: three of them are located in the urban area of Taranto (Orsini, Dante and Peripato), two in the city surrounding (Palagiano and Statte) and one in the new urban district of Paolo VI. Results are shown in table 1 for the considered pollutants, in terms of percent source contribution to the total estimated ground concentration (expressed $\mu g/m^3$) as at each selected monitoring station. Contributions from industry as a whole, traffic, domestic heating, fugitive and harbour activities were considered for contribution analysis.

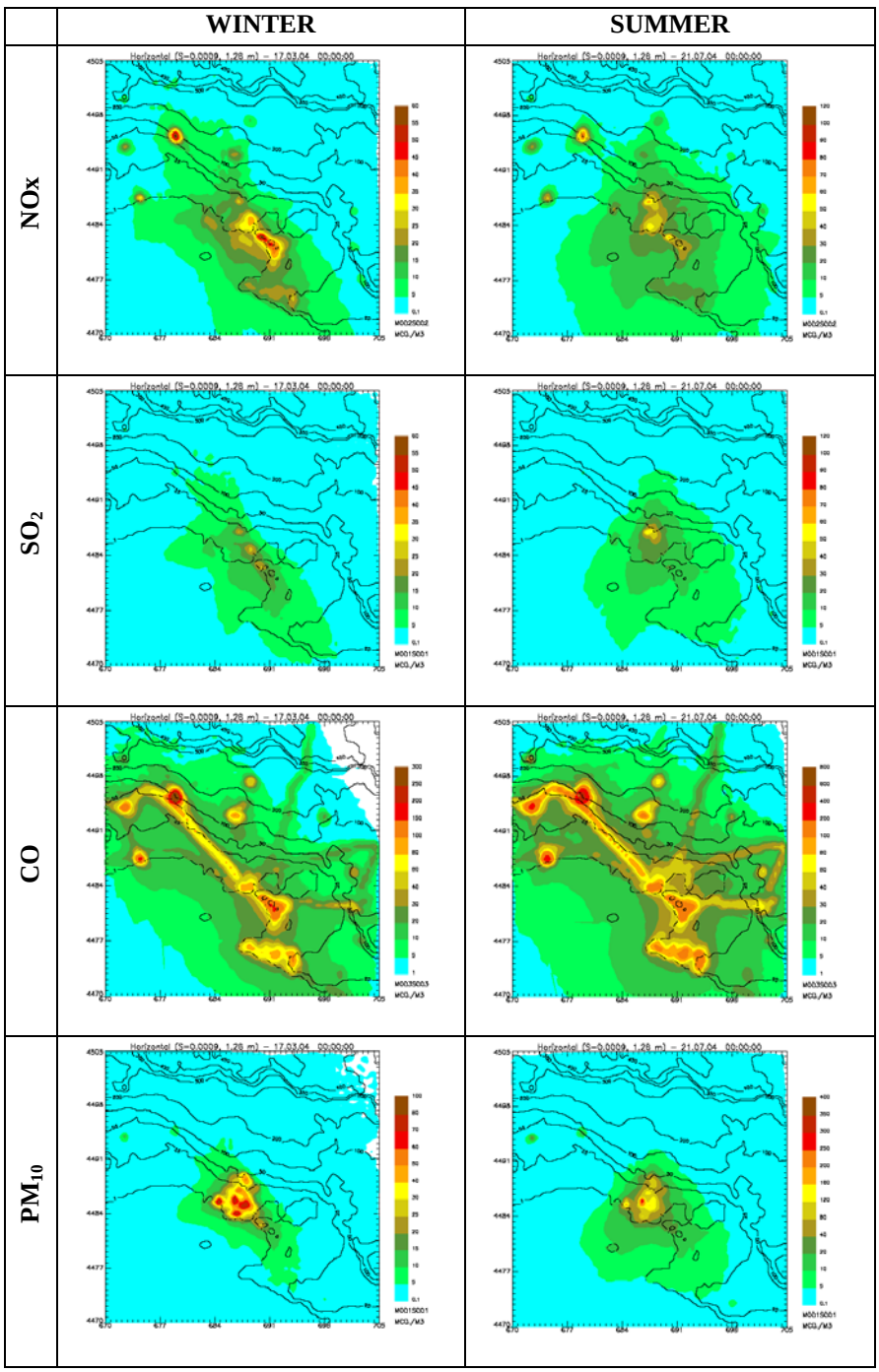

Figure 4. Average concentration maps in winter and summer seasons.

It can be shown industry activities mainly contributes to the total $SO_2$ concentrations (up to 97%) regardless of both station and season. The harbour activities exhibit the second larger contribution with percent values among 3-11%, not considering the result at Palagiano station (23-15%) due to the low total $SO_2$ concentrations (1 $\mu g/m^3$). Low or negligible contributions are instead foreseen for both traffic and domestic heating. The $NO_x$ contributions show some differences among both sources

and stations. Industry and traffic emissions are the two main contributors to the estimated total ground concentrations with 41% and 45% respectively on average.

Table 1. Estimation of seasonal pollutants sources contributions at selected monitoring stations (WI (winter); SU (summer)).

| | **Dante** | | **Orsini** | | **Palagiano** | | **Paolo VI** | | **Peripato** | | **Statte** | |
|---|---|---|---|---|---|---|---|---|---|---|---|---|
| | **$SO_2$ (%)** | | | | | | | | | | | |
| | WI | SU | WI | SU | WI | SU | WI | SU | WI | SU | WI | SU |
| **Industry** | 92 | 86 | 97 | 89 | 70 | 71 | 91 | 92 | 95 | 89 | 94 | 91 |
| **Traffic** | 2 | 3 | 1 | 1 | 7 | 14 | 2 | 1 | 1 | 2 | 2 | 2 |
| **Domestic heating** | 0 | N.A | 0 | N.A | 0 | N.A | 0 | N.A | 0 | N.A | 0 | N.A |
| **Harbour activities** | 6 | 11 | 3 | 10 | 23 | 15 | 7 | 7 | 4 | 9 | 4 | 7 |
| **Total concen. ($\mu g/m^3$)** | **15** | **14** | **25** | **26** | **1** | **1** | **2** | **9** | **22** | **19** | **4** | **6** |
| | **NOx (%)** | | | | | | | | | | | |
| | WI | SU | WI | SU | WI | SU | WI | SU | WI | SU | WI | SU |
| **Industry** | 38 | 30 | 65 | 53 | 15 | 16 | 47 | 62 | 64 | 54 | 23 | 22 |
| **Traffic** | 43 | 59 | 24 | 30 | 66 | 74 | 28 | 24 | 24 | 35 | 65 | 73 |
| **Domestic heating** | 13 | N.A | 6 | N.A | 7 | N.A | 15 | N.A | 7 | N.A | 9 | N.A |
| **Harbour activities** | 6 | 11 | 5 | 17 | 12 | 10 | 10 | 14 | 5 | 11 | 3 | 5 |
| **Total concen. ($\mu g/m^3$)** | **40** | **38** | **36** | **41** | **6** | **3** | **4** | **12** | **44** | **43** | **18** | **21** |
| | **CO (%)** | | | | | | | | | | | |
| | WI | SU | WI | SU | WI | SU | WI | SU | WI | SU | WI | SU |
| **Industry** | 7 | 3 | 7 | 9 | 1 | 1 | 7 | 14 | 12 | 5 | 3 | 2 |
| **Traffic** | 78 | 97 | 80 | 90 | 97 | 99 | 79 | 85 | 77 | 94 | 93 | 98 |
| **Domestic heating** | 15 | N.A | 13 | N.A | 2 | N.A | 14 | N.A | 11 | N.A | 4 | N.A |
| **Harbour activities** | 0 | 0 | 0 | 1 | 0 | 0 | 0 | 1 | 0 | 1 | 0 | 0 |
| **Total concen. ($\mu g/m^3$)** | **131** | **139** | **59** | **76** | **39** | **41** | **15** | **27** | **94** | **108** | **84** | **105** |
| | **$PM_{10}$ (%)** | | | | | | | | | | | |
| | WI | SU | WI | SU | WI | SU | WI | SU | WI | SU | WI | SU |
| **Industry** | 72 | 73 | 62 | 62 | 78 | 65 | 58 | 74 | 82 | 80 | 65 | 69 |
| **Traffic** | 14 | 15 | 2 | 2 | 18 | 33 | 11 | 7 | 6 | 6 | 14 | 18 |
| **Domestic heating** | 4 | N.A | 0 | N.A | 1 | N.A | 2 | N.A | 1 | N.A | 2 | N.A |
| **Harbour activities** | 0 | 0 | 0 | 0 | 0 | 0 | 0 | 0 | 0 | 0 | 0 | 0 |
| **Fugitive** | 10 | 12 | 36 | 36 | 3 | 2 | 29 | 19 | 11 | 14 | 19 | 13 |
| **Total concen. ($\mu g/m^3$)** | **14** | **18** | **51** | **78** | **3** | **2** | **2** | **7** | **22** | **29** | **3** | **4** |

Both domestic heating and harbour activities contribute for about 9% on average. Results at the selected monitoring stations show some difference among source contributions. The urban stations of Dante, Orsini and Peripato indicate a different impact from industry and traffic. Whilst the Dante station, located downtown, shows a dominant traffic contribution (43-59%), with an industry influence up to 30-38%, the Orsini station, located close to the industrial area, exhibits a prevailing industry impact (53-65%). The same effect can also be observed at the Peripato urban station, located in a urban park close to Mar Piccolo with an open area facing the industry facilities. The urban district of Paolo VI, located north to Mar Piccolo, seems to be mainly affected by industrial sources (47-62%), while traffic contribution at this station can be accounted for 24-28% of the total $NO_x$ concentration. The town of Statte, located north to the industrial area, reveals an industry contribution of up to 23%, whereas traffic is estimated to be main contributor source in this area. The rural area of Palagiano also show a dominant traffic influence (66-74%) but the total estimated $NO_x$ concentration is very low (3-6 $\mu g/m^3$). The harbour NOx contributions exhibit higher values at summertime due to the influence of sea breeze. In particular the Orsini station, closest to the harbour, exhibits the greatest values (17%), followed by Paolo VI (14%). The urban stations of Dante and Peripato both show an harbour contribution at summertime of about 11%. The $NO_x$ summer harbour contribution at Statte is instead about 5%.

CO source contributions are dominated by traffic emission (89% on average) regardless of season and station. The remain contributions can be ascribed to the domestic heating and industries emissions for about the same amount.

Primary $PM_{10}$ concentrations can mainly be attributed to industry emissions (70%). Traffic and fugitive emissions are the two other contributing sources. Among the results obtained in the considered monitoring stations, it is worth to notice the fugitive and traffic contributions at the Orsini station. Here fugitive contributions up to 36% are predicted, being the second largest value, while the traffic one is nearly negligible (2%). This result can be explained with its proximity to the industrial area. The urban stations of Dante show a traffic influence of about 14-15% and fugitive contribution of 10-12%. A lower traffic $PM_{10}$ contribution (6%) is estimated at the Peripato station, in agreement with the lower NOx contributions predicted at the same station for this source. The $PM_{10}$ contribution results at Palagiano, Paolo VI and Statte stations are nearly of the same order of magnitude or lower than other stations, but the total estimated concentrations is significantly low (2-7 $\mu g/m^3$), due to distance from the industrial area, considered as the main emission source for this pollutant.

## 4. CONCLUSIONS

A modeling system based on a Lagrangian Particle dispersion model (SPRAY) has been used to evaluate the impact of the most relevant emission sources located in the city of Taranto and its surrounding areas. Three dimensional $SO_2$, $NO_x$, CO and primary $PM_{10}$ concentration fields have been calculated for the studied area in selected periods covering both winter and summer seasons. The model system has been fed up with both ground and upper air meteorological data and with an on purpose emission inventory taking into account industrial, traffic, domestic heating,

fugitive and harbour activities as emission sources. Modeled concentrations have been validated with observed data collected during a proper field campaign.
Results show the impact area of the emitted pollutants extends to a large area of the local territory depending from the pollutant. Typical industrial contaminant, such as $NO_x$ and $SO_2$, locate their concentration peaks around the industrial areas but significant concentrations are found in the surrounding urban and rural areas. The CO concentrations are mainly confined around the emission areas located on urban and motorway roads. Primary $PM_{10}$ peak concentrations are mostly limited in the proximity of industrial areas. A seasonal effect on the ground concentration fields is observed mainly caused by the different meteorological conditions. In particular the summer breeze seems to produce a larger spread of the concentration fields in particular for $SO_2$, $NO_x$ and $PM_{10}$ pollutants.
Source contributions for the modeled pollutants have been calculated at selected monitoring stations. Results indicate a prevailing contribution of industrial activities on the estimated ground concentrations of $SO_2$ and $PM_{10}$. Fugitive particulate emission source is evaluated to be the second larger contributor to the estimated primary $PM_{10}$ concentrations together with traffic. The latter is mainly responsible for the predicted CO concentration. $NO_x$ contribution results point out a more diffuse responsibility, with industry and traffic sources mainly involved with the concentrations of this pollutant, followed by domestic heating and harbour activities with a much lower contribution. The harbour activities have been evaluated to account for mainly $NO_x$ and $SO_2$ ground concentrations, while negligible contributions are foreseen for CO and $PM_{10}$.

## REFERENCES


Aria Technologies, (2001). Minerve Wind Field Models version 7.0, General Design Manual. ARIA Report, May 2001, Aria Technologies 2001.
Entec UK limited, (2002). European Commission - Quantification of emissions from ships associated with ship movements between ports in the European Community, July 2002.
Gariazzo, C., Pelliccioni, A., Bogliolo, M. P., Scalisi, G., (2004). Evaluation of a Lagrangian Particle Model (SPRAY) to assess environmental impact of an industrial facility in complex terrain. Water, Air and Soil Pollution 155: 137-158.
Hanna, S. R., (1982). Applications in Air Pollution Modeling. In. Atmospheric Turbulence and Air Pollutin Modelling, F.T.M. Nieuwstadt and H. Van Dop, Reidel, Dordrecht, Chapter 7.
IIASA, (2001). RAINS-Europe http://www.iiasa.ac.at/~rains/home.html.
Lloyd's Register, (1999). Marine exhaust emission quantification study – Mediterranean Sea. Prepared for European Commission, DG XI Environment, Nuclear Safety and Civil protection. Report n. 99/EE/7044.
Tinarelli, G., Anfossi, D., Brusasca, G., Ferrero, E., Giostra, U., Morselli, M.G., Moussafir, J., Tampieri, F., and Trombetti, F., (1994). Lagrangian particle simulation of tracer dispersion in the Lee of a schematic two-dimensional hill. Journal of Applied Meteorology, 33, pp. 744-756.

Trozzi, C., Vaccaro, R., (1998). Methodologies for estimating air pollutant emissions from ships. TECHNE Report MEET RF98), March 1998.
Van Ulden, A. P., Holtslag, A. A. M., (1985). Estimation of atmospheric boundary layer parameters for diffusion application. Journal of Climate and Applied Meteorology, 24, pp. 1196-1207.

*Proceedings of the Third International Symposium on Air Quality Management at Urban, Regional and Global Scales. 26-30 September 2005, Istanbul – Turkey*

# EMISSION MODELING IN THE ASSESSMENT OF PM2.5 FROM TRAFFIC AND RESIDENTIAL WOOD COMBUSTION

**Niko Karvosenoja[1], Petri Porvari[1], Arjen Raateland[1], Jouni T. Tuomisto[2], Marko Tainio[2], Matti Johansson[3] and Anu Kousa[4]**

[1] Finnish Environment Institute (SYKE), Research Department, P.O.Box 140, FIN-00251 Helsinki, Finland, Firstname.Lastname@ymparisto.fi
[2] National Public Health Institute (KTL), Department of Environmental Health, P.O.Box 95, FIN-70701 Kuopio, Firstname.Lastname@ktl.fi
[3] United Nations Economic Commission for Europe (UNECE), Bureau 350, Palais des Nations, CH-1211 Geneva 10, Switzerland, Matti.Johansson@unece.org
4 Helsinki Metropolitan Area Council (YTV), P.O.Box 521, FIN-00520 Helsinki, Finland, Anu.Kousa@ytv.fi

## ABSTRACT

Fine particulate matter (PM) concentrations in ambient air have been cause severe health effects. The highest primary fine PM emissions in Finland are caused by sources with low emission height, such as traffic and residential combustion, which enable immediate exposure near the source. The Finnish Regional Emission Scenario (FRES) model calculates primary PM emissions in several size classes with $1 \times 1$ $km^2$ spatial resolution. In this study the importance of PM2.5 emissions from road traffic and residential wood combustion, and their relation to population densities in Finland were studied. The statistical comparison involved no atmospheric dispersion modelling, instead relative differences between sectors in potential human exposure were estimated. Preliminary results show that more population lives adjacent to PM2.5 emissions from road traffic than from residential wood combustion. The national total emissions from road traffic are lower. However, when only effects near the source are considered, PM2.5 emissions from road traffic are relatively more important to human health. The study gave new insight on the relative importance of the two main sectors on the potential PM2.5 exposure near the emission source. The results supplement PM health risk information that will be obtained from spatially more coarse regional PM assessment modeling.

**Key Words**: Traffic, Wood Combustion, Emission, Fine Particles, Population

## 1. INTRODUCTION

The ambient particulate matter (PM) has been associated with multiple adverse health effects worldwide. The adverse health effects have been seen for both short-term (daily variations) and long-term (chronic) studies (e.g. Stieb et al. 2003, Hoek et al 2002). The most consistently association has been found between ambient PM and increased cardiopulmonary mortality, lung cancer mortality and reduced lung function (WHO 2003).

The average $PM_{2.5}$ concentrations in Finland are relatively low compared to those in central and southern Europe. The highest concentrations occur in southern Finland, where for the Helsinki metropolitan area Pakkanen et al. (2001) have measured fine particle concentrations during October 1996 – May 1997 both at an urban and at a regional background site, and the average concentrations were 11.8 and 8.4 $\mu g/m^3$, respectively. It was estimated that at the background site, less than 10% of the measured concentration originates from local sources. For the urban site, long range transported (LRT) contribution to $PM_{2.5}$ concentration was estimated at 60-63% (Ojanen et al., 1998). These contributions are supported by computational values of Karppinen et al (2005), who estimate the LRT contribution to the measured $PM_{2.5}$ concentration in urban air in Helsinki at 64-76%.

The highest primary fine PM emissions in Finland originate from residential wood combustion and road traffic. Based on national emission statistics submitted to the Convention on Long-range Transboundary Air Pollution (CLRTAP) and its secretariat at the United Nations Economic Commission for Europe (UNECE) (Finnish Environment Institute 2005) residential wood combustion emitted 15.9 Gg(PM2.5) $a^{-1}$ in 2003, which contributed 41% of the Finnish total PM2.5 emissions. However, emission factor estimates are under revision at the moment. Road traffic caused 3.0 Gg(PM2.5) $a^{-1}$ direct exhaust and 1.7 Gg(PM2.5) $a^{-1}$ indirect dust emissions. Emissions from these sources are released into the atmosphere from low height, and therefore enable immediate exposure near the source.

The health effects of fine particulate matter have recently been recognized in Europe and North America. International and national air quality guidelines set limits to daily and annual average concentrations, but the emissions are currently not included in the protocols of the Convention on Long-range Transboundary Air Pollution (LRTAP) or in the national emission ceilings directive (NECD) of the European Union (EU). Intensive research work is onging to address potential health effects (UNECE 2004a) and methods to include them in integrated assessment models (IAM). The possibilities for their inclusion in forthcoming emission reduction agreements under LRTAP Convention or within EU work, including the Clean Air for Europe (CAFE) thematic strategy, is being explored (UNECE 2004b). These assessments mostly cover transboundary air pollution, however, recently there have been attempts to link regional concentrations to urban background levels. The first results indicated that the relative share of local PM emission was generally below 50% and highly variable. However, need for studies focusing on primary PM effects at fine spatial resolution has been identified (Forsberg et al. 2005).

Finnish regional IAM of PM is in development in KOPRA project (www.fmi.fi/research_air/air_47.html). The aim is to integrate PM emission and reduction cost estimates, atmospheric modeling and health risk modeling. The emissions at $1 \times 1$ $km^2$ resolution and the reduction costs of technical control measures are estimated in the Finnish Regional Emission Scenario (FRES) model. Atmospheric dispersion modeling have been done with the modelling system SILAM (Sofiev & Siljamo, 2003) for two grids: 30 km resolution was selected for the European computations based on official EMEP emission data and 5 km grid cell

size was taken for Finnish regional simulations. In both runs, the output of meteorological model HIRLAM was used for the complete year 2000 with 30 km meteorological data resolution. The health risk model combines the emission and dispersion data with the background population data. The dose-response semi-model will be used to estimate the relationship between particles and associated health effects in Finland.

This study concentrated on primary PM2.5 emissions from residential wood combustion and road traffic in $1 \times 1$ km$^2$ grid, and their relation to population densities in adjacent grid cells. Emission calculation and spatial allocation are presented. Population densities are weighted with emissions for various distances from emission grid cells, and relative human exposure potential is estimated. The study involved no atmospheric dispersion modelling.

## 2. METHODOLOGY

### 2.1 Emission calculation and spatial allocation

The Finnish Regional Emission Scenario (FRES) model is a part of the integrated assessment model (IAM) system of air pollution (Johansson et al. 2001) which have lately been extended to PM (www.fmi.fi/research_air/air_47.html). FRES consists of coherent emission calculation from all anthropogenic sources with spatial allocation of emissions. The pollutants include primary particles in different sizes and the main precursor gases of secondary PM. Large energy production and industrial plants are described as point sources. Area emissions are calculated at country level, and spatially allocated at two steps to municipality and $1 \times 1$ km$^2$ level. A more detailed model description can be found from Karvosenoja and Johansson (2003a).

A summary on the spatial dimensions of road traffic and residential wood combustion is presented in Table 1. For road traffic the spatial allocation to municipality level is based on fuel consumption values from the Finnish road traffic emission calculation system LIISA (Mäkelä *et al.* 2002). Allocation to $1 \times 1$km$^2$ level was carried out based on national SLICES land use element (Mikkola et al. 1999). SLICES is a combination of different national land use GIS databases, of which output is raster databases in $10 \times 10$ and $25 \times 25$ m$^2$. The allocation that is based on road surface area does not take into account traffic volumes in different roads. As a basis for the municipality allocation of domestic combustion of different fuels, degree-day weighted gross-floor areas of different types of buildings from national building and dwelling register were used. Building and dwelling register is a part of SLICES and includes all Finnish buildings with information on e.g. gross floor area, heating types and fuels, building date and resident. Degree-day weighting was assumed to represent the differences in room heating needs in different parts of the country. Gross-floor area data from building and dwelling register were used also in $1 \times 1$km$^2$ level allocation of domestic wood combustion. Population data used in this study was also based on building and dwelling register. The spatial allocation of area emissions is described in detail in Karvosenoja et al. (this issue).

Table 1. The spatial allocation of road traffic and residential wood combustion in FRES model

| Main sectors at country level; Number of subsectors and fuels | Sectors at municipality level; Data used as a basis for emission allocation | Sectors at 1 × 1km$^2$ level; GIS data used as a basis for emission allocation from municipality to 1x1km2 level |
|---|---|---|
| Road traffic; 10 subsectors, 3 fuels | Light-duty gasoline exhaust; Annual LD gasoline consumption[1] | Road traffic; Road surface area[2] |
| | Light-duty diesel exhaust; Annual LD diesel consumption[1] | |
| | Heavy-duty diesel exhaust; Annual HD diesel consumption[1] | |
| | Light-duty dust emissions; Annual LD fuel consumption[1] | |
| | Heavy-duty dust emissions; Annual HD diesel consumption[1] | |
| Residential combustion; 16 subsectors, 3 fuels | Wood comb. in boiler-heated residential buildings (RsB); Degree-day weighted gross-floor area (DWGA) of wood boiler -heated RsB[3] | Wood comb. in wood-heated RsB; Gross-floor area (GA) of wood-heated RsB[3] |
| | Wood comb. in stove-heated RsB; DWGA of wood stove -heated RsB[3] | |
| | Wood comb. in RsB heated primarily with other than wood; DWGA of detached RsB built after 1979 and heated primarily with other than wood[3] | Wood comb. in RsB heated primarily with other than wood; GA of detached RsB built after 1979 and heated primarily with other than wood[3] |
| | Wood comb. in recreational buildings (RcB); DWGA of all RcB[3] | Wood comb. in RcB; GA of all RcB[3] |

1) Mäkelä et al. 2002; 2) SLICES (Mikkola et al. 1999); 3) Building and dwelling register (Mikkola et al. 1999)

The emission calculation of road traffic and residential wood combustion at country level are presented in Tables 2 and 3. Traffic exhaust emission factors and reduction efficiencies are based on the RAINS model of IIASA (Klimont et al. 2002). The emission factors of traffic induced dust are based on international literature reported in Karvosenoja et al. (2002). Annual activity (i.e. fuel consumption) and technology utilization rate (i.e. age profile of vehicle fleet) values in year 2000 are based on the Finnish road traffic emission calculation system LIISA (Mäkelä *et al.* 2002).

Residential wood combustion activities (i.e. wood combustion amounts in different types of combustion appliances) are based on several questionnaire studies (Sevola et al. 2003, Tuomi 1990) and expert estimates (*e.g.* S. Tuomi, Finnish Work Efficiency Institute, 28.8.2003). The emission factors are based on the results of a Nordic project (Sternhufvud et al. 2004) and recent Finnish measurements (Raunemaa et al. in press).

### 2.2 Emission weighted population

For the two studied sectors s, residential wood combustion and road traffic, emission weighted population EWP values were calculated for various distance zones from the emission sources. EWPs describe sector specific emission weighted average populations at various distance zones over all Finnish emission grid cells. For emission grid cells n (i.e. grid cells where emission $EM_n > 0$), population grid cells p (i.e. grid cells where population $POP_p > 0$) in various distances adjacent to emission grid cells are explored. EWPs are calculated for each distance zone d from 0 to 16 km in 1 km steps (see Figure 1).

$$EWP(s,d) = \frac{\sum_n (EM_n(s) \cdot \sum_p POP_p(d))}{\sum_n EM_n(s)} \quad (1)$$

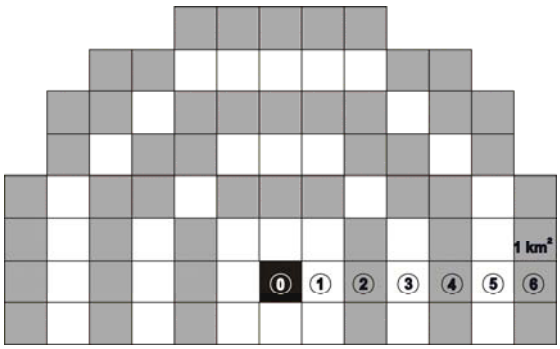


Figure 1. The schematic presentation of distance zones (circled numbers) from emission grid cell (black). The distance was from 0 to 16 km in the calculations.

**2.3 Average exposure concentration**

Without dispersion modeling it is not possible to quantitatively assess human exposure to emissions. However, relative differences between sectors in potential human exposure can be estimated. If the dilution and transport of emissions in the atmosphere (here described with dilution function DF) is assumed equal to all geographical directions and in all parts of Finland, PM concentration caused by a primary PM emission source at certain distance from the emission source is relative to emission quantity. For one emission grid cell n', average exposure concentration EC at a particular distance from the source can be calculated:

$$EC^{n'}(s,d) = EM_n{}^{n'}(s) \cdot DF(s,d) \cdot \sum_p POP_p{}^{n'}(d) \quad (2)$$

Since DF is assumed constant, average exposure concentration over all Finnish grid cells is:

$$EC(s,d) = DF(s,d) \cdot \sum_n (EM_n(s) \cdot \sum_p POP_p(d)) = DF(s,d) \cdot \sum_n EM_n(s) \cdot EWP(s,d) \quad (3)$$

i.e. relative to EWP multiplied by the total Finnish emission of the sector. This is a useful simplification for sector comparison, although the full utility can only be obtained if dilution functions are estimated as well.

## 3. RESULTS AND DISCUSSION

Country level PM2.5 emission calculation of road traffic and residential wood combustion in 2000 are presented, and FRES emissions compared to statistics (Finnish Environment Institute 2005) in Tables 2 and 3. Residential wood combustion country total emissions are higher than road traffic emissions. When FRES results are compared to statistics, the difference is large in residential wood combustion. Considerable uncertainties in the activities and especially emission factor estimates of residential wood combustion have been identified (Karvosenoja and Johansson 2003b). The emissions submitted to CLRTAP and its secretariat at UNECE (Finnish Environment Institute 2005) and earlier FRES estimates have been calculated using relatively old emission factor estimates that are based mainly on international measurements. Since that the emission factors have been revised in the light of recent Nordic (Sternhufvud et al. 2004) and Finnish (Raunemaa et al. in press) measurements. However, the uncertainties are still large because of the nature of residential wood combustion. Residential wood combustion appliances are relatively simple and poorly controllable, and emission factors are strongly dependent on user's habits.

Biggest uncertainties in traffic emission calculation lie on indirect dust emission factor estimates. So far there were very little Finnish road dust measurements available, and the current estimates used in FRES are based on international measurements (presented in Karvosenoja et al. 2002). The estimates are relatively conservative describing average emissions from clean paved roads. Indirect dust emissions may, however, be considerably higher, especially during spring time because of winter sanding dust resuspension. Statistics (Finnish Environment Institute 2005) do not include estimate on indirect traffic emissions for the year 2000. Indirect emissions in current statistics 2003 are calculated using the same emission factors than in the FRES model.

Table 2. PM2.5 emissions in 2000 from road traffic and comparison to statistics.

| | Activity | Unabated PM2.5 emission factor | Control technology; utilization rate; reduction efficiency | PM2.5 emission (Gg $a^{-1}$) |
|---|---|---|---|---|
| Motorcycles & mopeds, 2-stroke, exhaust | 0.2 PJ $a^{-1}$ | 95 mg $MJ^{-1}$ | EURO1, 9%, 30% | 0.02 |
| Passenger cars, vans & 4-stroke motorcycles, gasoline, exhaust | 72 PJ $a^{-1}$ | 6.0 mg $MJ^{-1}$ | EURO1, 16%, 45%<br>EURO2, 31%, 45%<br>EURO3, 4%, 82% | 0.3 |
| Passenger cars & vans, diesel, exhaust | 32 PJ $a^{-1}$ | 111 mg $MJ^{-1}$ | EURO1, 14%, 35%<br>EURO2, 30%, 74%<br>EURO3, 4%, 81% | 2.4 |
| Trucks, buses & other heavy duty, diesel, exhaust | 45 PJ $a^{-1}$ | 58 mg $MJ^{-1}$ | EURO1, 20%, 36%<br>EURO2, 47%, 74%<br>EURO3, 7%, 82% | 1.4 |
| Buses, natural gas, exhaust | 0.05 PJ $a^{-1}$ | 1.8 mg $MJ^{-1}$ | - | 0.0001 |
| Light-duty resuspension and tyre wear dust | 43 $10^9$ km $a^{-1}$ | 18 mg $km^{-1}$ | - | 0.8 |
| Light-duty break wear dust | 43 $10^9$ km $a^{-1}$ | 2.8 mg $km^{-1}$ | - | 0.1 |
| Heavy-duty resuspension and tyre wear dust | 3.4 $10^9$ km $a^{-1}$ | 180 mg $km^{-1}$ | - | 0.6 |
| Heavy-duty break wear dust | 3.4 $10^9$ km $a^{-1}$ | 59 mg $km^{-1}$ | - | 0.06 |
| **Road traffic TOTAL** | **149 PJ $a^{-1}$ / 47 $10^9$ km $a^{-1}$** | | | **5.8** |
| Road traffic exhaust in statistics in 2000 (Finnish Environment Institute 2005) | | | | 3.6 |

Table 3. PM2.5 emissions in 2000 from residential wood combustion and comparison to statistics.

| | Activity (PJ $a^{-1}$) | Unabated PM2.5 emission factor (mg $MJ^{-1}$) | Control tech.; util rate; red. eff. | PM2.5 emission (Gg $a^{-1}$) |
|---|---|---|---|---|
| Residential buildings, manual feed boilers with accumulator tank | 5.4 | 80 | - | 0.4 |
| Residential buildings, manual feed boilers without accumulator tank | 2.7 | 700 | - | 1.9 |
| Residential buildings, automatic feed wood chip boilers | 1.4 | 80 | - | 0.1 |
| Residential buildings, automatic feed pellet boilers | 0.1 | 30 | - | 0.003 |
| Residential buildings, iron stoves | 0.3 | 1000 | - | 0.3 |
| Residential buildings, other stoves and ovens[1] | 24 | 100 | - | 2.4 |
| Residential buildings, open fireplaces | 0.4 | 800 | - | 0.3 |
| Recreational buildings, iron stoves | 0.8 | 1000 | - | 0.8 |
| Recreational buildings, other stoves and ovens[1] | 4.0 | 100 | - | 0.4 |
| Recreational buildings, open fireplaces | 0.3 | 800 | - | 0.2 |
| **Residential wood combustion TOTAL** | **39** | | | **6.8** |
| Residential wood combustion in statistics in 2000 (Finnish Environment Institute 2005) | | | | 15 |

1) incl. masonry heaters, masonry ovens, kitchen ranges and sauna stoves

$1 \times 1$ km$^2$ resolution PM2.5 emissions from road traffic and residential wood combustion, and population are presented as $10 \times 10$ km$^2$ maps for the whole Finland, and as $1 \times 1$ km$^2$ maps for south-western Finland (Figure 2). Traffic emissions occur in population centers in south-western Finland. Residential wood combustion emissions are relatively evenly distributed to the whole southern and central Finland.

Spatial top-down emission allocation may add uncertainty. In residential combustion allocation is done using building and dwelling register (Mikkola et al. 1999) that contains information on primary heating devices of all Finnish buildings. The building and dwelling register data has been analyzed for this part and is considered relatively certain. However, 25% of the residential wood combustion emissions is caused by wood use in electricity and oil heated houses as supplementary heat source. The building and dwelling register does not contain information on supplementary heating devices. In this study, supplementary wood heating was spatially allocated using the time of inauguration in the building and dwelling register, with the assumption that detached houses commissioned in 1980 or later use supplementary wood heating, and older houses do not. This assumption is based on the fact that vast majority of residential buildings built in 1980s, 90s and 2000s are equipped with supplementary wood heaters. This part of the spatial allocation retain considerable uncertainty, but it was the best practical basis considering data availability.

For road traffic the spatial allocation to municipality level in FRES model is based on national road traffic emission calculation system LIISA (Mäkelä *et al.* 2002) that is considered relatively certain. The allocation from municipality to $1 \times 1$km$^2$ level was based on road cover land use information in SLICES land use element (Mikkola et al. 1999). It does not include small private or residential roads. Furthermore, the allocation does not take into account traffic volumes in different roads. Therefore emission allocation inside municipalities should be considered uncertain.

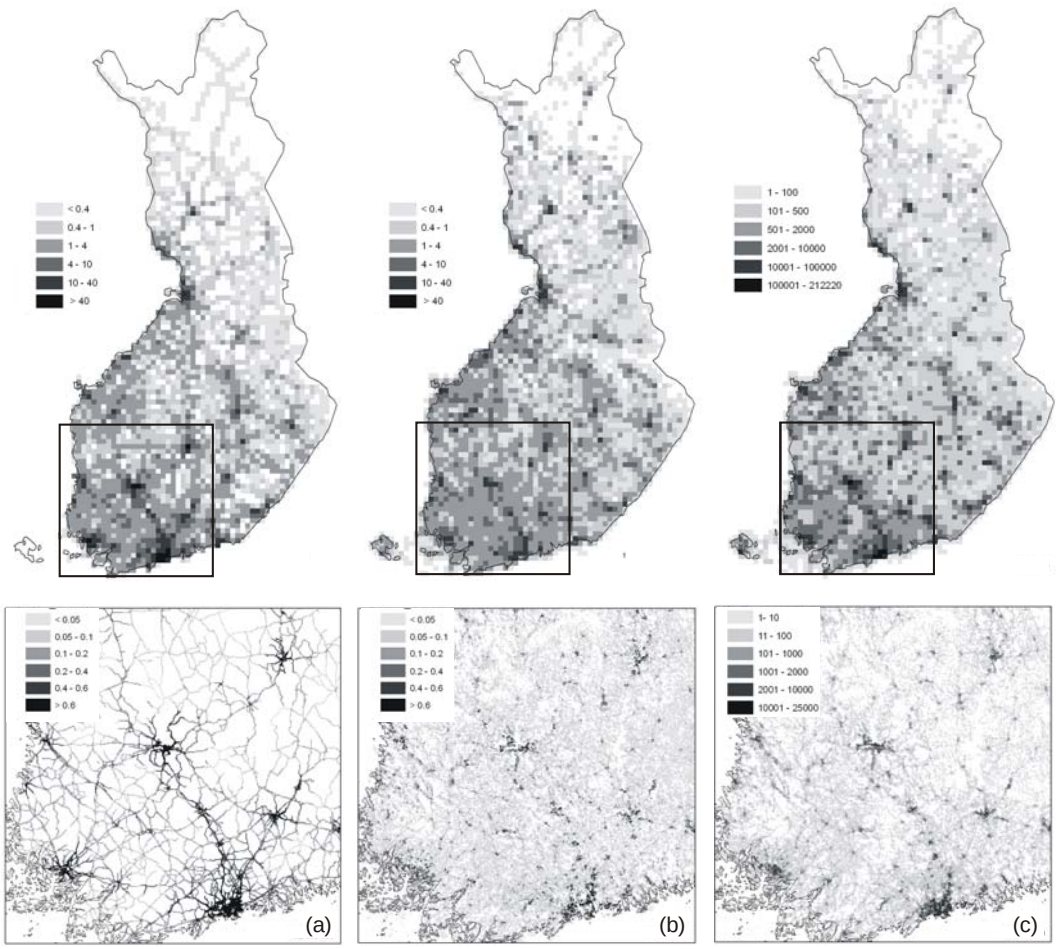


Figure 1. Finnish PM2.5 emissions (Mg $a^{-1}$) from (a) road traffic and (b) residential wood combustion in 2000 presented in 10 × 10 $km^2$ grid (upper) and 1 × 1 $km^2$ grid (lower). Population is presented in (c).

Table 5. Emission weighted population (EWP) and average exposure concentration divided by dilution function (EC/DF) in different distance zones. Inh = inhabitant.

| Distance zone | EWP [inh.] | EWP per grid cell [inh $km^{-2}$] | EC/DF [inh Gg $a^{-1}$] | EC/DF per grid cell [inh Gg $a^{-1}$ $km^{-2}$] | EWP [inh.] | EWP per grid cell [inh $km^{-2}$] | EC/DF [inh Gg $a^{-1}$] | EC/DF per grid cell [inh Gg $a^{-1}$ $km^{-2}$] |
|---|---|---|---|---|---|---|---|---|
| | Road traffic | | | | Residential wood combustion | | | |
| 0 | 562 | 562 | 3260 | 3260 | 276 | 276 | 1877 | 1877 |
| 1 | 3361 | 420 | 19494 | 2437 | 1401 | 175 | 9527 | 1191 |
| 2 | 4163 | 347 | 24145 | 2012 | 1617 | 135 | 10996 | 916 |
| 3 | 4849 | 303 | 28124 | 1758 | 1817 | 114 | 12356 | 772 |
| 4 | 8514 | 266 | 49381 | 1543 | 3071 | 96 | 20883 | 653 |
| 5 | 6651 | 238 | 38576 | 1378 | 2376 | 85 | 16157 | 577 |
| 6 | 8552 | 214 | 49602 | 1240 | 3097 | 77 | 21060 | 526 |
| 7 | 7879 | 197 | 45698 | 1142 | 2864 | 72 | 19475 | 487 |
| 8 | 8664 | 181 | 50251 | 1047 | 3220 | 67 | 21896 | 456 |
| 9 | 11025 | 162 | 63945 | 940 | 4273 | 63 | 29056 | 427 |
| 10 | 8218 | 147 | 47664 | 851 | 3270 | 58 | 22236 | 397 |
| 11 | 9550 | 133 | 55390 | 769 | 3870 | 54 | 26316 | 366 |
| 12 | 8360 | 123 | 48488 | 713 | 3432 | 50 | 23338 | 343 |
| 13 | 9951 | 113 | 57716 | 656 | 4204 | 48 | 28587 | 325 |
| 14 | 9052 | 103 | 52502 | 597 | 4029 | 46 | 27397 | 311 |
| 15 | 8016 | 95 | 46493 | 553 | 3711 | 44 | 25235 | 300 |
| 16 | 9607 | 86 | 55721 | 498 | 276 | 276 | 31518 | 281 |

Table 5 presents the values of emission weighted population (EWP) and average exposure concentration divided by dilution function (EC/DF) in different distance zones for the two studied sectors. Dilution function was assumed constant in this study. EWP values for road traffic are more than twice as high as for residential wood combustion for all the distance zones, i.e. more population lives adjacent to PM2.5 emissions from road traffic. Road traffic emissions take for large extent place in urban areas, while residential wood combustion is more common in sparsely populated areas. Also EC/DF values are higher for road traffic than for residential wood combustion. This indicates that, when only effects near the source are considered, PM2.5 emissions from road traffic are relatively more important to human health.

## 5. CONCLUSIONS

This study provided a useful method to analyze the relative importance of two emission sectors with comparable emission heights without dispersion modeling. It indicated that road traffic is more important in potential health risks than residential wood combustion. The results in $1 \times 1$ km$^2$ grid supplement PM health risk information that will be obtained from the regional integrated assessment modeling project KOPRA, that will be carried out in $5 \times 5$ km$^2$ for Finland.

## ACKNOWLEDGEMENTS

The development of the Finnish Regional Emission Scenario (FRES) model has mainly been carried out in two projects aiming at national integrated assessment modelling of PM in Finland. The authors gratefully acknowledge the financial support from the Ministry of the Environment and the KOPRA project in the technological programme "FINE Particles - Technology, Environment and Health 2002-2005" of the National Technology Agency of Finland (Tekes). All the members of the KOPRA project group are acknowledged.

## REFERENCES

Finnish Environment Institute 2005. Air pollutant emissions in Finland 1990-2003 – National inventory report to the Secretariat of the UNECE CLRTAP, 13 May 2005.

Forsberg B., Hansson H.-C., Johansson C., Areskoug H., Persson K. and Järvholm B. 2005. Comparative health impact assessment of local and regional particulate air pollutants in Scandinavia. Ambio 34:1,.pp. 11-19.

Hoek, G, Brunekreef, B, Goldbohm, S, Fischer, P, & van den Brandt, P. A. (2002). Association between mortality and indicators of traffic-related air pollution in the Netherlands: a cohort study. Lancet, 360 (9341), 1203-1209.

Johansson M, Alveteg M, Amann M, Bak J, Bartnicki J, Ekqvist M, Forsius M, Frohn L, Geernaert G, Gimeno B, Guardans R, Karvosenoja N, Martín F, Posch M, Suutari R. and Syri S. 2001. Integrated assessment modeling of air pollution in four European countries. Water, Air, and Soil Pollution **130**(1-4): 175-186.

Karppinen A., Härkönen J., Kukkonen J., Aarnio P., Koskentalo T., 2005. Statistical model for assessing the portion of fine particulate matter transported regionally and long range to urban air. Scand J Work Environ Health, in press.

Karvosenoja N., Porvari P., Raateland A., Kupiainen K., Johansson M. this issue. The spatial allocation of air pollutants in Finnish regional emission model.
Karvosenoja N. and Johansson M. 2003a. The Finnish Regional Emission Scenario model – a base year calculation. Proceedings of Air Pollution XI Conference, Catania, Italy, pp. 315-324.
Karvosenoja N. and Johansson M. 2003b. Primary particulate matter emissions and the Finnish climate strategy. Boreal Environment Research 8:125-133.
Karvosenoja N., Johansson M. and Kupiainen K. 2002. The importance of primary particulate emissions from non-combustion sources in Finland. Proc of the 16th Intnl Clean Air and Env Conf of the Clean Air Soc of Australia & NZ, pp. 393-398.
Klimont Z., Cofala J., Bertok I., Amann M., Heyes C. and Gyarfas F., 2002. Modelling Particulate Emissions in Europe A Framework to Estimate Reduction Potential and Control Costs. Interim Report IR-02-076.
Mäkelä K., Laurikko J. and Kanner H. 2002. Road traffic exhaust gas emissions in Finland. LIISA 2001.1 calculation model. VTT Research Notes 2177. Finland.
Mikkola A., Jaakkola O., Sucksdorff Y. 1999. The Slices project: National classification of land use, land cover and soil, and the production of databases. Finnish Environment 342. Helsinki, Finland.
Ojanen C., Pakkanen T., Aurela M., Mäkelä T., Meriläinen J., Hillamo R., Aarnio P., Koskentalo T., Hämekoski K., Rantanen L., Lappi M., 1998. Size distribution, chemical composition and sources on inhalable particles in the Helsinki Area. Helsinki Metropolitan Area Council, Pääkaupunkiseudun julkaisusarja C1998:7.
Pakkanen T.A., Loukkola K., Korhonen C.H., Aurela M., Mäkelä T., Hillamo R.E., Aarnio P., Koskentalo T., Kousa A., Maenhaut W., 2001. Sources and chemical composition of atmospheric fine and coarse particles in the Helsinki area. Atmospheric Environment 35: 5381-5391.
Raunemaa et al. in press. Project report "Fine particle emissions from small-scale wood combustion".
Sevola Y., Peltola A. and Moilanen J. 2003. Fuelwood use in detached houses 2000/2001. Bulletin of Finnish Forest Research Institute 894.
Sofiev, M., Siljamo, P. (2003) Forward and inverse simulations with Finnish emergency model SILAM. Air Pollution Modelling and its Applications XVI, eds. C.Borrego, S.Incecik, Kluwer Acad. / Plenum Publ. pp.417-425.
Sternhufvud C., Karvosenoja N., Illerup J., Kindbom K., Lükewille A., Johansson M. and Jensen D. 2004. Particulate matter emissions and abatement options in residential wood burning in the Nordic countries. Copenhagen, ANP 2004:735.
Tuomi S., 1990. Heating devices fired by indigenous fuels used in detached houses in Finland. Helsinki, Finland, TTS-Institute's Publications Series 312. 95 pp.
Stieb,D.M.; Judek,S.; Burnett,R.T. 2003. Meta-analysis of time-series studies of air pollution and mortality: Update in relation to the use of generalized additive models. Journal of the Air & Waste Management Association, 53 (3), 258-261.
UNECE 2004a., Modelling and assessment of the health impact of particulate matter and ozone, EB.AIR/WG.1/2004/1, UNECE, Geneva.
UNECE 2004b. Integrated assessment modelling, EB.AIR/GE.1/2004/7, UNECE
WHO 2003. Health Aspects of Air Pollution with Particulate Matter,Ozone and Nitrogen Dioxide, Report on a WHO Working Group. Report on a WHO working group, Bonn, Germany, January 13-15 2003.

*Proceedings of the Third International Symposium on Air Quality Management at Urban, Regional and Global Scales. 26-30 September 2005, Istanbul – Turkey*

# THE SPATIAL ALLOCATION OF AIR POLLUTANTS IN FINNISH REGIONAL EMISSION MODEL

**Niko Karvosenoja[1], Petri Porvari[1], Arjen Raateland[1], Kaarle Kupiainen[1] and Matti Johansson[2]**

[1] Finnish Environment Institute (SYKE), Research Department, P.O.Box 140, FIN-00251 Helsinki, Finland, Firstname.Lastname@ymparisto.fi
[2] United Nations Economic Commission for Europe (UNECE), Bureau 350, Palais des Nations, CH-1211 Geneva 10, Switzerland, Matti.Johansson@unece.org

## ABSTRACT

Human health effects caused by fine particulate matter (PM) have raised a need for estimation tools, such as integrated assessment models (IAMs). The Finnish Regional Emission Scenario (FRES) model has been developed as part of the Finnish IAM of air pollution. FRES calculates the annual emissions of primary PM in different sizes and the main precursor gases of secondary PM from 1990 to 2020. Recently the model has been extended to include chemical speciation, i.e., climate and health relevant, black and organic carbon as well as sulphates. Emissions are calculated as point and area sources. Area sources are aggregated to 8 main sectors and more than 100 subsectors. The spatial resolution of area emissions has recently been refined to 1 × 1 $km^2$ grid. This paper presents the spatial allocation of area emissions in FRES. The emission estimates of FRES were convergent compared to other emission inventories. The spatial allocation procedure in two steps: (i) first from country to municipality level in more sectoral detail, and (ii) second from municipality to 1 × 1 $km^2$ level, was found useful. Municipality level weighting surrogates were available for the most important emission sources at adequate aggregation level. At 1 × 1 $km^2$ level weighting surrogates were available for the two most important area emission sources, road traffic and domestic wood combustion.

**Key Words**: Emission, Area Sources, Fine Particles, GIS

## 1. INTRODUCTION

The health risk of fine particulate matter (PM) can be assessed with integrated assessment models (IAMs), which include spatially allocated emission estimates, atmospheric modeling and health risk modeling. Earlier Finnish regional IAM system has been used to assess acidification (Syri et al. 2002, Johansson et al. 2001). PM assessment has so far included emission scenario (Karvosenoja and Johansson 2003a, Karvosenoja et al. 2003) and qualitative health implication estimates (Johansson et al. 2003). The extension of IAM for PM assessment to include atmospheric dispersion and health risk modeling is in development in a KOPRA project (www.fmi.fi/research_air/air_47.html).

The Finnish Regional Emission Scenario (FRES) model has been used as an emission estimation tool in the Finnish IAM system. In acidification assessment relatively coarse spatial resolution of area emissions at municipality level has been found adequate. In order to better meet the requirements of PM health risk assessment, the spatial description of area source emissions in FRES has recently been refined to $1 \times 1$ km$^2$ grid. There are two main arguments for the need of high resolution emission estimates. First, atmospheric models, into which FRES emission data are fed in the IAM system, requires more and more high resolution emission data while computer data processing capacity increases. The regional atmospheric model system that is used with FRES in the KOPRA project is SILAM (Sofiev & Siljamo, 2003) of Finnish Meteorological Institute with $30 \times 30$ km$^2$ grid size for Europe and $5 \times 5$ km$^2$ for Finland. Second, high spatial resolution allows the assessment of the relative importance of different low-height emission sources on PM concentrations in the vicinity of the sources.

This paper presents the spatial allocation of area emissions in FRES, including recent refinement to $1 \times 1$ km$^2$ grid. In addition, sectoral country-total emissions of fine primary particles (PM2.5), sulphur dioxide ($SO_2$), nitrogen oxides ($NO_x$), ammonia ($NH_3$) and non-methane volatile organic compounds (NMVOCs), as well as black and organic carbon fractions in fine particles (BC and OC) are presented. The respective emissions at $1 \times 1$ km$^2$ grid are graphically presented as maps.

## 2. METHODOLOGY

The Finnish Regional Emission Scenario (FRES) model works as a part of the integrated assessment model (IAM) system of PM. FRES consists of coherent emission calculation from all anthropogenic sources with spatial allocation of emissions. The pollutants include primary total suspended particles (TSP) and finer size fractions (PM10, PM2.5 and PM1), and the main precursor gases of secondary PM, *i.e.* sulphur dioxide ($SO_2$), nitrogen oxides ($NO_x$), ammonia (NH3) and non-methane volatile organic compounds (NMVOCs). Primary particle estimate includes partition to different chemical compounds: black carbon (BC), organic carbon (OC) and sulphates. Large energy production and industrial plants are described as point sources (*i.e.* the plants utilizing boilers with thermal capacity exceeding 50 $MW_{th}$, and the plants with TSP, $SO_2$ or $NO_x$ emissions higher than 20 Mg/a, respectively). Other sources are described as area sources. A more detailed model description can be found from Karvosenoja and Johansson (2003b). The spatial allocation of area emissions at two steps (municipality and $1 \times 1$km$^2$ level) is described in detail in the following.

Area emissions are described at three different spatial level: country, municipality and $1 \times 1$km$^2$ level. Emission calculation takes place at country level. Area emissions $EM^{cou}$ are calculated from country level annual activity data $A^{cou}$, unabated emission factors EF and removal efficiencies $\eta$ of various emission control technologies which can be applied to each source sector (*i.e.* sector-fuel type combination) with certain utility rates X. The country level emission $EM^a$ from an area source sector is:

$$EM^{cou}{}_{i,j,k,l}(t) = \sum_{l} A^{cou}{}_{j,k}(t) \cdot EF_{i,j,k} \cdot X_{i,j,k,l}(t) \cdot (1 - \eta_{i,j,k,l}) \quad (1)$$

where t = time, i = pollutant, j = fuel, k = sector and l = control technology. The base year 2000 activity data is mainly based on national statistics (Statistics Finland 2003). The emission factors, control technology removal efficiencies and utilization rates are based on literature and other sources reported in Karvosenoja (2001), Karvosenoja and Johansson (2003b) and Karvosenoja *et al.* (2002). The emission factors for chemical species, black carbon, organic carbon, and sulphates, are calculated from source specific chemical emission profiles (as percentages in $PM_{2.5}$) that have been estimated based on national and international literature.

Country level area emissions are allocated to 448 municipalities using the respective relative fractions $RF^{mun}$ of municipality level allocation data B in base year 2000 in 25 emission source sectors (see Table 1). Area source emission $EM^{mun}$ in a municipality m is:

$$EM^{mun}{}_{i,j,k,l,m}(t) = EM^{cou}{}_{i,j,k,l}(t) \cdot RF^{mun}{}_{j,k,m} \quad (2)$$

where

$$RF^{mun}{}_{j,k,m} = \frac{B^{mun}{}_{j,k,m}}{B^{cou}{}_{j,k}} \quad (3)$$

Municipality level emissions are further allocated to 1 × 1km$^2$ grid at four main emission sectors: road traffic, domestic wood combustion, agriculture and other sources. Because of high national interest in studying the importance of domestic wood combustion in health effects, its allocation takes place in 6 subsectors (see Table 1). Emission $EM^{1\times1}$ in an emission grid cell n is:

$$EM^{1x1}{}_{i,j,k,l,m,n}(t) = EM^{mun}{}_{i,j,k,l,m}(t) \cdot RF^{1x1}{}_{j,k,m,n} \quad (4)$$

where

$$RF^{1x1}{}_{j,k,m,n} = \frac{C^{1x1}{}_{j,k,m,n}}{C^{mun}{}_{j,k,m}} \quad (5)$$

where C is geographical allocation information at 1 × 1km$^2$ level. Municipality and 1 × 1km$^2$ level sectoral division and allocation data used in the determination of the relative fractions are presented in Table 1. For road traffic at municipality level fuel consumption values were based on the Finnish road traffic emission calculation system LIISA (Mäkelä *et al.* 2002). For the municipality allocation of animal-related PM and ammonia emissions from agriculture, municipality level animal numbers weighted with country-level PM and ammonia emissions, respectively, of different

animal types were used as weighting factors. The animal number data were taken from agricultural databases of Finnish Environment Institute (Grönroos et al. 1998). Agricultural field area information from national SLICES land use element (Mikkola et al. 1999) was used at municipality level as a basis for agricultural machinery and field-origin PM emissions. In addition, SLICES data at $1 \times 1km^2$ level was used for all agricultural non-combustion emissions. SLICES data on road surface area was used in road traffic emission allocation to $1 \times 1km^2$ level. SLICES is a combination of different national land use GIS databases, of which output is raster databases in $10 \times 10$ and $25 \times 25$ $m^2$. For example, relative fraction $RF^{1\times1}$ for road traffic emission is road surface area in a grid cell divided by road surface area in respective municipality.

As a basis for the municipality allocation of domestic combustion of different fuels, degree-day weighted gross-floor areas of different types of buildings from national building and dwelling register were used. Building and dwelling register is a part of SLICES land use element, and includes all Finnish buildings with information on e.g. gross floor area, heating types and fuels, building date and resident. Degree-day weighting was assumed to represent the differences in room heating needs in different parts of the country. For the allocation of domestic peat and coal combustion, however, population was used as allocation basis instead of heating information. Domestic peat and coal combustion are rare in Finland, and building and dwelling register was noticed not to include adequate information on peat and coal heating. Population data used in this study was also based on building and dwelling register. The building and dwelling register gross-floor area data were used also in $1 \times 1km^2$ level allocation of domestic wood combustion. Allocation to $1 \times 1km^2$ level was not done with building and dwelling register on domestic oil combustion, which contributes to less than 5% of the total PM2.5 emissions of domestic combustion, and therefore was not considered relevant in terms of potential health risks.

Other data used in municipality emission allocation included managed forest area (8th nation-wide forest inventory data base), annual fuel combustion in energy production boilers below 50 $MW_{th}$ (Korkia-Aho et al. 1995) and annual milled peat production values (VAPO Group data base).

Table 1. Spatial area source emission allocation in the FRES model

| Main sectors at country level;<br>Number of subsectors and fuels | Sectors at municipality level;<br>Data used as a basis for emission allocation | Sectors at 1 × 1km$^2$ level;<br>GIS data used as a basis for emission allocation from municipality to 1x1km2 level |
|---|---|---|
| Road traffic;<br>10 subsectors, 3 fuels | Light-duty gasoline exhaust;<br>Annual LD gasoline consumption[1] | Road traffic;<br>Road surface area[3] |
| | Light-duty diesel exhaust;<br>Annual LD diesel consumption[1] | |
| | Heavy-duty diesel exhaust;<br>Annual HD diesel consumption[1] | |
| | Light-duty dust emissions;<br>Annual LD fuel consumption[1] | |
| | Heavy-duty dust emissions;<br>Annual HD diesel consumption[1] | |
| Agricultural non-combustion activities (primary PM and $NH_3$);<br>6 subsectors | PM from animal husbandry;<br>Animal numbers weighted with PM emissions of animals[2] | Agriculture;<br>Agricultural field area[3] |
| | NH3 from animal husbandry;<br>Animal numbers weighted with $NH_3$ emissions of animals[2] | |
| | PM from field preparation and harvesting;<br>Agricultural field area[3] | |
| Residential and other small-scale combustion;<br>23 subsectors, 6 fuels | Wood comb. in boiler-heated residential buildings (RsB);<br>Degree-day weighted gross-floor area (DWGA) of wood boiler -heated RsB[4] | Wood comb. in wood-heated RsB;<br>Gross-floor area (GA) of wood-heated RsB[4] |
| | Wood comb. in stove-heated RsB;<br>DWGA of wood stove -heated RsB[4] | |
| | Wood comb. in RsB heated primarily with other than wood;<br>DWGA of detached RsB built after 1979 and heated primarily with other than wood[4] | Wood comb. in RsB heated primarily with other than wood;<br>GA of detached RsB built after 1979 and heated primarily with other than wood[4] |
| | Wood comb. in recreational buildings (RcB);<br>DWGA of all RcB[4] | Wood comb. in RcB;<br>GA of all RcB[4] |
| | Wood comb. in agricultural buildings (AB);<br>DWGA of wood-heated AB[4] | Wood comb. in aAB;<br>GA of wood-heated AB[4] |
| | Wood comb. in public buildings (PB);<br>DWGA of wood-heated PB[4] | Wood comb. in PB;<br>GA of wood-heated PB[4] |
| | Wood comb. in industrial buildings (IB);<br>DWGA of wood-heated IB[4] | Wood comb. in IB;<br>GA of wood-heated IB[4] |
| | Oil combustion;<br>DWGA of all oil-heated buildings[4] | Other sources;<br>Population[4] |
| | Peat and coal combustion;<br>Population[4] | |
| Off-road traffic and machinery;<br>14 subsectors, 4 fuels | Forestry machinery;<br>Managed forest area[5] | |
| | Agricultural machinery;<br>Agricultural field area[3] | |
| | Other off-road and machinery (incl. domestic navigation and air traffic);<br>Population[4] | |
| Power plants and industrial comb. in boilers <50 $MW_{th}$;<br>8 subsectors, 10 fuels | Power plants and industrial comb.;<br>Annual fuel consumption in boilers below 50 $MW_{th}$[6] | |
| Industrial non-comb. processes, em. <20 Mg $a^{-1}$;<br>14 subsectors | Industrial processes;<br>Population[4] | |
| Other primary PM related non-combustion sources;<br>19 subsectors | Milled peat production;<br>Annual milled peat production[7] | |
| | Other sources;<br>Population[4] | |
| Other NMVOC related non-comb. sources; 8 subsectors | Other NMVOC related sources;<br>Population[4] | |

1) Mäkelä et al. 2002, 2) Grönroos et al. 1998, 3) SLICES (Mikkola et al. 1999), 4) building and dwelling register (Mikkola et al. 1999), 5) 8th nation-wide forest inventory data base, 6) Korkia-Aho et al. 1995, 7) VAPO data base

## 3. RESULTS AND DISCUSSION

### 3.1 Country level

Emissions in main emission sources in the base year 2000 are presented in Table 2. The major contributors to fine primary PM emissions were small-scale wood combustion and traffic sources. These sources were predominant also in particulate black (BC) and organic carbon (OC) emissions. Stationary industrial activities, *i.e.* power plants, and combustion and processes in industry, were the main contributors to $SO_2$ emissions. Traffic sources caused the biggest $NO_x$ and NMVOC emissions. Ammonia ($NH_3$) originated mainly from agriculture. Area sources contributed to 77, 37, 71, 97, 96, 98 and 98% of PM2.5, $SO_2$, $NO_x$, NH3, NMVOCs, BC and OC emissions, respectively, of the total emissions.

The results of the FRES model were convergent compared to other inventories. The biggest difference is in PM2.5, where FRES estimate for residential wood combustion is 8.2 Gg $a^{-1}$ lower than in other inventories. The PM2.5 emission factors of residential wood combustion have been lately revised in the light of recent Nordic (Sternhufvud et al. 2004) and Finnish (Raunemaa et al. in press) measurements. This review is reflected to FRES results, but not yet to other inventories. Residential wood combustion emissions are discussed in more detail in Karvosenoja et al. (this issue).

Table 2. FRES emissions in 2000 and comparison to national inventories (Gg $a^{-1}$)

| **Main area sources at country level** | **PM2.5** | **SO2** | **NOx** | **NH3** | **NMVOC** | **BC in PM2.5** | **OC in PM2.5** |
|---|---|---|---|---|---|---|---|
| Road traffic | 5.5 | 0.2 | 75 | | 42 | 1.9 | 1.3 |
| Agricultural non-combustion activities (primary PM and $NH_3$) | 0.4 | | | 32 | | 0.0 | 0.2 |
| Residential and other small-scale combustion | 8.0 | 3.2 | 8.0 | | 28 | 1.4 | 3.9 |
| Off-road traffic and machinery | 3.8 | 3.8 | 43 | | 27 | 1.3 | 1.1 |
| Power plants and industrial comb. in boilers below 50 $MW_{th}$ | 2.4 | 17 | 14 | | 1.9 | 0.6 | 0.3 |
| Industrial non-comb. processes with emissions below 20 Mg $a^{-1}$ | 0.0 | 4.5 | 4.8 | | 15 | 0.0 | 0.0 |
| Other primary PM related non-combustion sources | 3.1 | | | | | 0.0 | 1.6 |
| Other NMVOC related non-combustion sources | | | | | 37 | | |
| **TOTAL area sources** | **23** | **29** | **145** | **32** | **151** | **5.3** | **8.3** |
| Point sources | 6.8 | 49 | 58 | 1.0 | 7.1 | 0.1 | 0.2 |
| **TOTAL** | **30** | **78** | **203** | **33** | **158** | **5.5** | **8.5** |
| TOTAL in national inventories | 38[a] | 74[a]/76[b] | 210[a]/206[b] | 33[a] | 160[a] | - | - |

a) Finnish Environment Institute 2005, b) Statistics Finland 2004

### 3.2 1 × 1km$^2$ level

The total Finnish emissions of PM2.5, $SO_2$, $NO_x$, NMVOC, BC and OC spatially allocated to 1 × 1km$^2$ are presented in 10 × 10km$^2$ grid (Figure 1). Primary PM emissions, including BC and OC, are relatively evenly distributed to the whole southern and Central Finland, while NOx and NMVOC emissions are more weighted to population centers in southern and south-western Finland. Sulphur emissions take place mainly in large point sources, such as power plants and industrial processes.

The total number of grid cells in the Finnish land, lake and coastal sea area is 365 980, of which 102 393 are inhabited. Spatially allocated sectoral emissions are presented in 10 × 10km$^2$ maps for the whole Finland and 1 × 1km$^2$ for south-western Finland. The emissions of road traffic occur in population centers in south-western Finland (Figure 2a). Residential wood combustion emissions are relatively evenly distributed to the southern and central Finland (Figure 2b). Agricultural emissions take place in rural areas mainly in western Finland. (Figure 2c). Source sector other area emissions are presented in Figure 2d and point source emissions in Figure 2e.

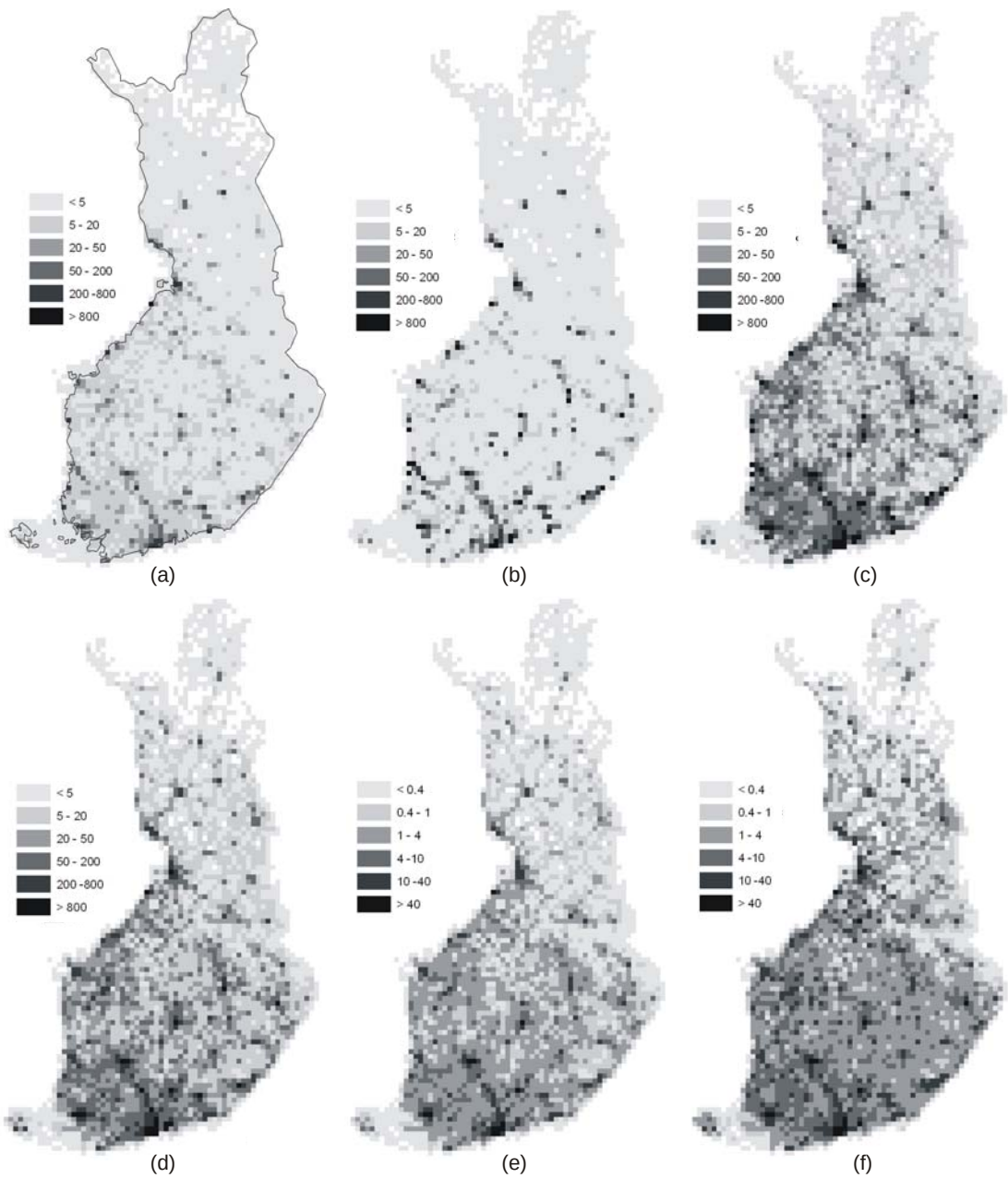


Figure 1. Total emissions of (a) PM2.5, (b) $SO_2$, (c) $NO_x$, (d) NMVOC, (e) BC and (f) OC in 2000 presented in 10 × 10km$^2$. Unit Mg a$^{-1}$.

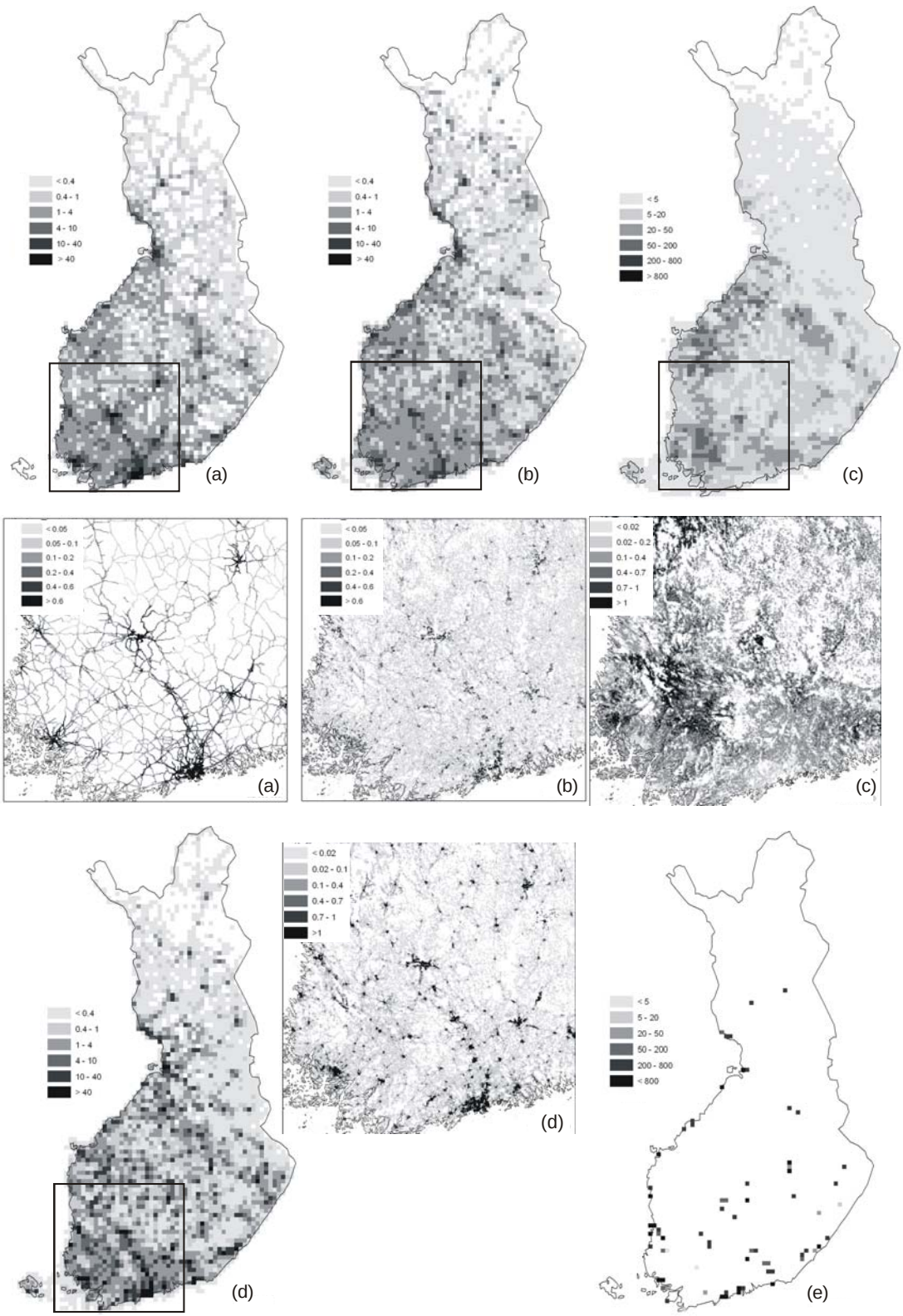


Figure 2. The sectoral emissions of (a) road traffic, (b) residential wood combustion, (c) agriculture, (d) other area sources and (e) point sources in 2000 presented in 10 × 10km$^2$ and (a) – (d) in 1 × 1km$^2$. Unit Mg(PM2.5) a$^{-1}$, except (c) Mg($NH_3$) a$^{-1}$ and (e) Mg($SO_2$) a$^{-1}$.

## 4. CONCLUSIONS

This paper presents the emission calculation of Finnish Regional Emission Scenario (FRES) model a which combines a top-down approach of aggregated emission source sector description with more detailed bottom-up calculation of large point sources. The spatial allocation of area emissions at two steps to municipality and 1 × 1km$^2$ level is presented.

The country total emissions of fine primary particles (PM2.5), sulphur dioxide ($SO_2$), nitrogen oxides ($NO_x$), ammonia ($NH_3$), non-methane volatile organic compounds (NMVOCs), particulate black carbon (BC) and organic carbon (OC) were presented and compared to official national emission inventories. The results were convergent, except for residential wood combustion where the latest emission factor estimates have not yet been implemented in official emission inventories.

The top-down spatial allocation from country level was carried out successfully using municipality and 1 × 1km$^2$ level weighting surrogates. Municipality level weighting surrogates were available for the most important emission sources at adequate aggregation level. At 1 × 1 km$^2$ level weighting surrogates were available for the two most important area emission sources, road traffic and domestic wood combustion.

## 5. ACKNOWLEDGEMENTS

The development of the Finnish Regional Emission Scenario (FRES) model has mainly been carried out in two projects aiming at national integrated assessment modelling of PM in Finland. The authors gratefully acknowledge the financial support from the Ministry of the Environment and the KOPRA project in the technological programme "FINE Particles - Technology, Environment and Health 2002-2005" of the National Technology Agency of Finland (Tekes).

## REFERENCES

Finnish Environment Institute 2005. Air pollutant emissions in Finland 1990-2003 – National inventory report to the Secretariat of the UNECE CLRTAP, 13 May 2005.

Grönroos, J.; Nikander, A.; Syri, S.; Rekolainen, S.; Ekqvist, M. 1998. Agricultural ammonia emissions in Finland. Part 1: Emission assessment. Part 2: Emission reduction and reduction costs. The Finnish Environment 206, Helsinki, Finland, 65 pp (in Finnish with English abstract).

Johansson M., Karvosenoja N., Porvari P. and Kupiainen K. 2003. Emission scenarios for particulate matter research and policy assessment in Finland. Proceedings of the 12th International USEPA Emission Inventory Conference "Emission Inventories – Applying New Technologies", San Diego, USA 29.4.-1.5.2003, 14 pp.

Johansson M, Alveteg M, Amann M, Bak J, Bartnicki J, Ekqvist M, Forsius M, Frohn L, Geernaert G, Gimeno B, Guardans R, Karvosenoja N, Martín F, Posch M,

Suutari R. and Syri S. 2001. Integrated assessment modeling of air pollution in four European countries. Water, Air, and Soil Pollution **130**(1-4): 175-186.
Karvosenoja N., Porvari P., Raateland A., Tuomisto J. T., Tainio M., Johansson M. and Kousa A. this issue. Emission modeling in the assessment of PM2.5 from traffic and residential wood combustion.
Karvosenoja N. and Johansson M. 2003a. Primary particulate matter emissions and the Finnish climate strategy. Boreal Environment Research 8:125-133.
Karvosenoja N. and Johansson M. 2003b. The Finnish Regional Emission Scenario model – a base year calculation. Proceedings of Air Pollution XI Conference, Catania, Italy, pp. 315-324.
Karvosenoja N., Johansson M. and Kupiainen K. 2003. SIZE-FRACTIONED PARTICULATE MATTER EMISSIONS IN FINLAND IN 1990-2020. Proceedings of the 14th International IUAPPA Conference "Air Quality – Assessment and Policy at Local, Regional and Global Scales" 6.-10.10.2003, Dubrovnik, Croatia, pp. 97-104.
Karvosenoja N., Johansson M. and Kupiainen K. 2002. The importance of primary particulate emissions from non-combustion sources in Finland. Proceedings of the 16th International Clean Air and Environment Conference of the Clean Air Society of Australia & New Zealand, 19 - 22 August 2002. pp. 393-398.
Karvosenoja N. 2001. Primary particulate emissions from stationary combustion processes in Finland. Finnish Environment Institute Mimeograph 232. Helsinki, Finland, Finnish Environment Institute.
Korkia-Aho S., Koski O., Meriläinen T. and Nurmio M. 1995. VAHTI description. West Finland Regional Environmental Centre 29.9.1995 , Memorandum, 35 pp. (In Finnish.)
Mäkelä K., Laurikko J. and Kanner H. 2002. Road traffic exhaust gas emissions in Finland. LIISA 2001.1 calculation model. VTT Research Notes 2177. Espoo, Finland. (in Finnish with English abstract.)
Mikkola A., Jaakkola O., Sucksdorff Y. 1999. The Slices project: National classification of land use, land cover and soil, and the production of databases. Finnish Environment 342. Helsinki, Finland.
Raunemaa et al. in press. Project report "Fine particle emissions from small-scale wood combustion".
Sofiev, M., Siljamo, P. (2003) Forward and inverse simulations with Finnish emergency model SILAM. Air Pollution Modelling and its Applications XVI, eds. C.Borrego, S.Incecik, Kluwer Acad. / Plenum Publ. pp.417-425.
Statistics Finland 2004. Energy Statistics 2003. Helsinki, Finland, Energy 2004:2.
Sternhufvud C., Karvosenoja N., Illerup J., Kindbom K., Lükewille A., Johansson M. and Jensen D. 2004. Particulate matter emissions and abatement options in residential wood burning in the Nordic countries. Nordic Council of Ministers, Copenhagen, ANP 2004:735.
Syri S., Karvosenoja N., Lehtilä A., Laurila T., Lindfors V. and Tuovinen J.-P. 2002. Modeling the impacts of the Finnish climate strategy on air pollution. Atmospheric Environment 36: 3059-3069.

*Proceedings of the Third International Symposium on Air Quality Management at Urban, Regional and Global Scales. 26-30 September 2005, Istanbul – Turkey*

# LISBON AIR QUALITY FORECAST USING STATISTICAL METHODS

**Jorge Neto[1], Pedro Torres[2], Francisco Ferreira[2] and Filomena Boavida[3]**

[1] Instituto de Meteorologia / Departamento de Observação e Redes
[2] Faculdade de Ciências e Tecnologia da Universidade Nova de Lisboa
[3] Instituto do Ambiente
Faculdade de Ciências e Tecnologia da Universidade Nova de Lisboa
Departamento de Ciências e Engenharia do Ambiente
Quinta da Torre,
2829-516 Caparica, Portugal, jorge.neto@meteo.pt

## ABSTRACT

Ozone and particulate matter levels in Southern European countries are particularly high, exceeding the established limit values, and the information and alert thresholds (in the case of ozone). Therefore, it is relevant to develop a good prediction methodology for the concentrations of these pollutants. Statistical models based on multiple regression analysis and classification and regression trees analysis were developed successfully. The models were applied in forecasting the average daily concentrations for particulate matter and average maximum hourly ozone levels, for next day, for the group of existing air quality monitoring stations in the Metropolitan Area of North Lisbon in Portugal.

**Key Words:** Statistical Forecast, Particles, Ozone

## 1. INTRODUCTION

An important commitment of Portugal in the area of air quality is the fulfillment of the Portuguese and European legislation. Since ozone and particulate matter levels in Southern European countries are particularly high, exceeding the established limit values and the information and alert thresholds (in the case of ozone), it is relevant to develop a good prediction methodology for the concentrations of these pollutants. The forecasting of air pollutant concentrations is very important for areas with air quality problems. Predictions can be developed through the integration of physico-chemical relationships from both meteorology and pollutants behaviour, or by using stochastic methods based on the analysis of data series. A combination of standard statistical methods was the selected process described in this paper. Statistical models based on multiple regression analysis (MR) and classification and regression trees analysis (CART) were developed successfully applied in forecasting the average daily concentrations for both particulate matter ($PM_{10}$) and average maximum hourly ozone ($O_3$) levels for next day, for the existing air quality monitoring stations in the Metropolitan Area of North Lisbon in Portugal.

## 2. METHODOLOGY

Using past information on studies to understand the variability of $O_3$ and $PM_{10}$ (Clapp and Jenkinb, 2001; Ferreira *et al*., 2000; Ferreira *et al*., 2004; Neto *et al*., 2004; Wang *et al*., 2003) was the first step to start to build a highly detailed data base using all the existing data. The data base is based on a detailed analysis of both historical and expert knowledge involving meteorology and air quality aspects with data from the years 2000 to 2002. Air quality data was obtained from the Commission for Regional Development of Lisbon and the Tagus River Valley Region (CCDR-LVT) network, and from one station of the Institute for the Environment. Surface meteorological parameters such as maximum temperature, relative humidity, and stations pressure differences were collected from seven stations of the Meteorology Institute. Geopotential heights, temperature, relative humidity, maximum mixing layer height by the Holzworth method (1964), and the inversion layer height, and thickness were also collected from the daily radio soundings of Lisbon Gago-Coutinho station. Synoptic situations at surface and 500 mb level from the forecast global model of European Centre for Medium-Range Weather Forecasting (ECMWF, 2003; IM, 2003) were classified in seven and five classes (Tables 1 and 2). A future objective is to use ten automatic weather types using pressure points centered in Portugal from the ECMWF forecast (Mendes et al., 2002; Trigo and DaCamara, 2000). The weather types are the eight typical circulations (NE, E, SE, S, SW, W, NW and N) and the pure high and low pressure systems.

Table 1.Classification of surface synoptic situations

| | |
|---|---|
| Front systems | 1 Front systems |
| Low pressure systems | 2 Deepening low pressure (instability)<br>3 Low pressure influence |
| High pressure systems | 4 Surface calm<br>5 N/NW circulation<br>6 Building high pressure ridge or zonal flow<br>7 NE/E circulation |

Table 2. Classification of 500 hPa synoptic situations

| |
|---|
| 1 Cut off low |
| 2 Low pressure trough |
| 3 Approaching trough or ridge breakdown |
| 4 Building high pressure ridge or zonal flow |
| 5 High pressure ridge |

The variables used are:

- Daily maximum temperature and average relative humidity for Lisbon, Santarém, Évora and Beja (both absolute values and the difference between yesterday and today's values);
- Pressure difference between Lisbon and others cities (Porto, Portalegre, Évora and Faro) at 12UTC (the difference between yesterday and today's values);
- 12UTC geopotential height at 1000, 850, 700 e 500 mb. 12UTC temperature and relative humidity at 925, 850 and 700 mb;
- Daily average values of air quality data for all the stations in the area of study: $PM_{10}$, $O_3$ maximum, $O_3$ and carbon monoxide eight hour average, nitrogen dioxide, sulphur dioxide (the difference between today and yesterday values; all the air quality values are calculated as in the existing air quality index for Lisbon);
- Others variables like duration of the solar day, day of week and type of day (if week-day or week-end).

Some variables initially selected were substituted afterwards by better descriptors. One of the examples is the wind direction which was substituted by the pressure difference between stations in order to have the synoptic wind, and not the local one.

Using the techniques already used for the case of Los Angeles by Casmassi (1987) presented also by EPA (2003), the statistical models were first built using CART analysis, and then MR analysis. The next step was to perform the MR analysis using each one of the final four groups obtained in the CART analysis for both pollutants. The MR used backward stepwise analysis with a significance level of 0.15.

For daily prediction, each pollutant value is transformed in terms of an index from very good to very bad (five levels). The worst index calculated from the two pollutants is the one chosen to represent our predicted index value for the next day.

## 3. RESULTS AND DISCUSSION

Figure 1 represents the CART analysis for both pollutants predicted. In both cases persistence is very important. The most determinant variable was the value of the pollutant obtained in the day before (PM10_1 and O3_1). In the $O_3$ model for higher values a good relationship exists with the maximum temperature observed in Santarém (TX734). This result may indicate that the air masses that come from East in the summer are related with high values $O_3$.

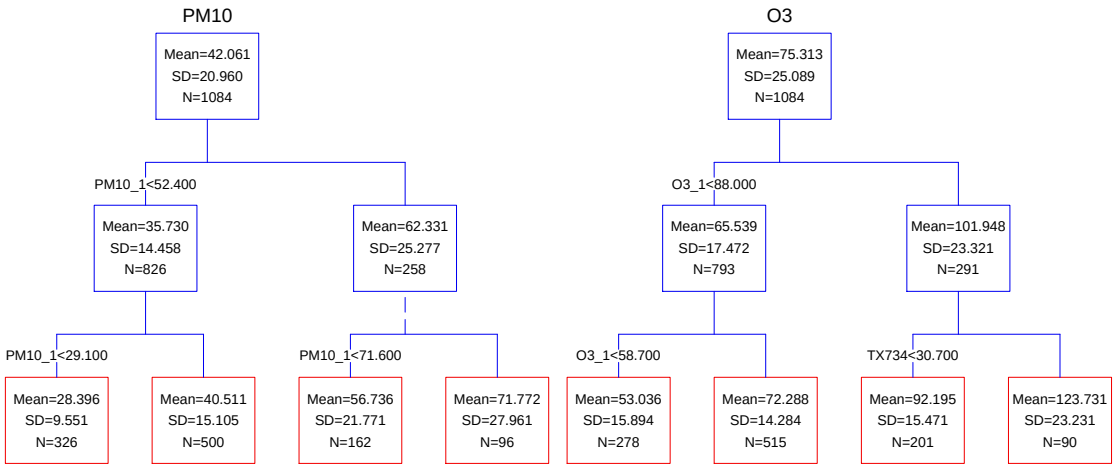


Figure 1. CART models for $O_3$ e $PM_{10}$ for the period 2000-2002

The results obtained RM models constructions for both pollutants perform correlations between 0.964 and 0.996. Tables 3 and 4 represent the results from the development of the different models for both pollutants.

Table 3. Results from the several MR models for $PM_{10}$

| | PM10_1<52.4 | | PM10_1>=52.4 | |
|---|---|---|---|---|
| | PM10_1<29.1 | PM10_1>=29.1 | PM10_1<71.6 | PM10_1>=71.6 |
| r | 0.976 | 0.964 | 0.982 | 0.975 |
| $r^2$ | 0.953 | 0.930 | 0.965 | 0.950 |
| Std.error | 6.731 | 11.715 | 12.359 | 21.845 |
| N | 322 | 498 | 159 | 96 |

Table 4. Results from the several MR models for $O_3$

| | O3_1<88 | | O3_1>=88 | |
|---|---|---|---|---|
| | O3_1<58.7 | O3_1>=58.7 | T734<30.7 | T734>=30.7 |
| r | 0.985 | 0.992 | 0.994 | 0.996 |
| $r^2$ | 0.970 | 0.984 | 0.989 | 0.993 |
| Std.error | 10.223 | 9.725 | 11.018 | 13.645 |
| N | 278 | 512 | 201 | 90 |

Then models were tested with other periods (winter and summer data from year 2003). The results show a high correlation, statistically significant at a 95% confidence level. Variance explained between predicted and measured concentrations were up to 88% for $O_3$, and 74% for $PM_{10}$, in best cases. The selected models allow a better understanding of each synoptic situation, and its relation with air quality leading to a forecast with considerable certainty for the majority of the identified scenarios. Figures 2 and 3 show an example of the test for the 2003 summer (June to August). The results are always better for $O_3$ because this pollutant has a very good

relationship with temperature, mostly in summer, when both variables are very high. For $PM_{10}$ no meteorological variable has the same explanatory impact. In the figure 2 two significant differences exists, due the existence of intense fires in Portugal in this days.

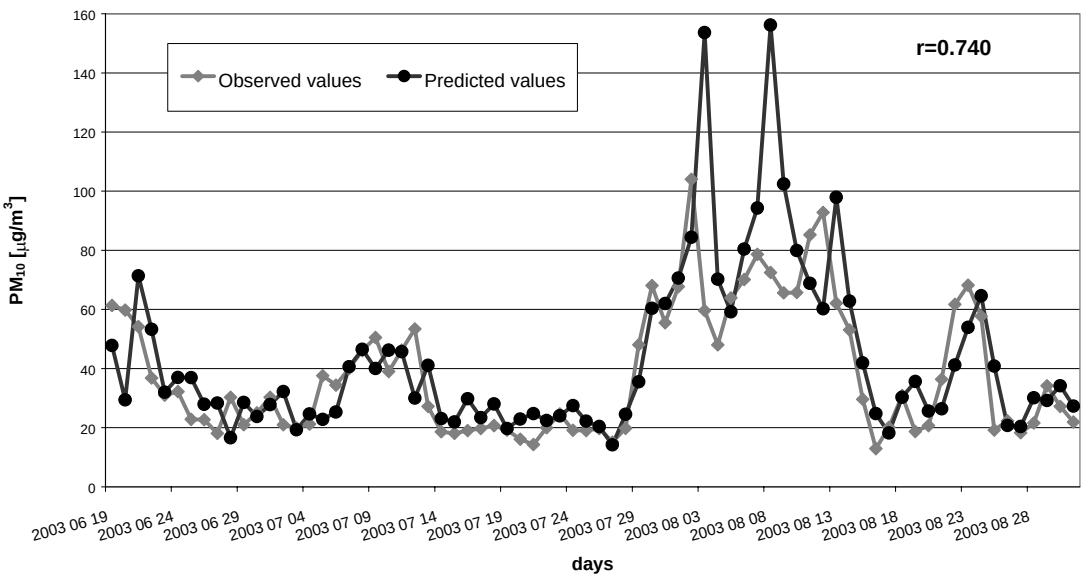


Figure 2. Observed and predicted $PM_{10}$ concentrations values using CART+MR models (July 1st to August 31st 2000)

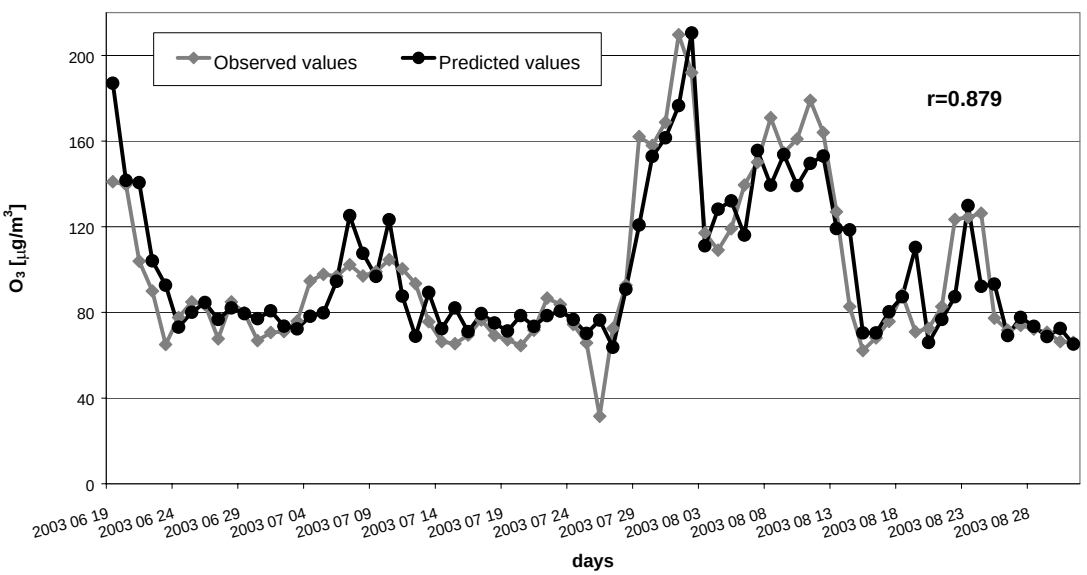


Figure 3. Observed and predicted $O_3$ concentrations values using CART+MR models (July 1st to August 31st 2000)

The models are already in daily use since January 2005. Since then in 67% of days the final predicted index corresponds to the observed one. In all the other situations the predicted index is only one level worst above the observed one.

## 4. CONCLUSIONS

The work presented is a statistical attempt based on a detailed analysis of both historical and expert knowledge involving meteorology and air quality aspects concerning ozone and particulate matter. The final goal was to develop a daily air quality forecast using statistical methods for the Lisbon region. A 3-year period (2000-2002) was selected as the fitness period for the models, while another period was select for the validation of the model. The use of statistical models based on MR and CART analysis was very successful in forecasting the average daily concentrations for both particulate matter and average maximum hourly ozone levels for next day in the Lisbon area in Portugal. The models developed also enabled a better understanding of the role of the different variables involved and their relationships.

## 5. ACKNOWLEDGEMENTS

The work developed was supported by Instituto do Ambiente and by Instituto de Meteorologia. The authors also wish to acknowledge the Comissão de Coordenação e Desenvolvimento Regional de Lisboa e Vale do Tejo for the data provided.

## REFERENCES

Casmassi, J., 1987 Development of an objective ozone forecast model for the south coast air basin. 80th Annual Meeting of APCA (The Association Dedicated to Air Pollution Control and Hazardous Waste Management). New York – June 21-26, 1987.

Clapp, L.J. and Jenkinb, M.E., 2001 Analysis of the relationship between ambient levels of $O_3$, $NO_2$ and NO as a function of $NO_x$ in the UK, Atmospheric Environment, 35, 6391-6405.

ECMWF 2003 Analyses Charts, European Centre for Medium-Range Weather Forecasts, 2000 - 2002.

EPA 2003 Guidelines for Developing an Air Quality (Ozone and PM2.5) Forecasting Program, U.S. Environmental Protection Agency, Office of Air Quality Planning and Standards, North Carolina, EPA-456/R-03-002.2

Ferreira, F., Tente, H., Torres, P., Cardoso, S., Palma-Oliveira, J.M., 2000 Air Quality Monitoring and Management in Lisbon, Environmental Monitoring and Assessment 2000, 65, 443-450.

Ferreira, F., Torres, P., Neto, J., Tente, H., 2004 Ozone Levels in Portugal: the Lisbon Region Assessment. Em Proceedings of Air & Waste Management's 97th Annual Conference & Exhibition. June 22-25, 2004, Indianapolis, Indiana. CD-ROM, pp. 18.

Holzworth, G.C., 1967 Mixing depths, wind speeds and air pollution potential for selected locations in the United States, J. Appl. Meteor., 1967, 5, 1039-1044.

Instituto de Meteorologia 2003 Boletim diário, Instituto de Meteorologia. 2000 a 2002

Mendes, M.T., Trigo, R.M. & DaCamara, C.C., 2002 Padrões de circulação atmosférica para Portugal Continental (1881-1995) in: Garcia, F.G. & Valero, J.L.B. (Ed.), 3ª Assembbleia Luso Espanhola de Geodesia e Geofísica – Valencia 2002. UPV, Valência. pp. 961-964.

Neto, J., Torres, P. & Ferreira, F., 2004 Previsão da qualidade do ar para Lisboa – a abordagem estatística. In 8ª Conferência Nacional de Ambiente. 27-29 Outubro de 2004, Lisboa. CD-ROM, pp. 11.

Trigo R.M. and DaCamara C.C., 2000 Circulation Weather Types and their influence on the Precipitation Regime in Portugal. Int. J. Climatol, 20, 1559-1581.

Wang, W., Weizhen, L., Wang, X., Leung, A., 2003 Prediction of maximum daily ozone level using combined neural network and statistical characteristics. Environment International 29, 555–562.

*Proceedings of the Third International Symposium on Air Quality Management at Urban, Regional and Global Scales. 26-30 September 2005, Istanbul – Turkey*

# ON SOME NEW ADVECTION SCHEMES FOR AIR POLLUTION MODELLING APPLICATION

**Hristina Kirova-Galabova, Silvia Petrova,**
**Dimiter Syrakov, Maria Prodanova,**

National Institute of Meteorology and Hydrology, 66, Tzarigradsko chaussee, Sofia 1784, Bulgaria, Hristina.Kirova@meteo.bg, Silvia.Petrova@meteo.bg, Dimiter.Syrakov@meteo.bg. Maria.Prodanova@meteo.bg

## ABSTRACT

The advection scheme TRAP is Bott type one. It is explicit, positively definite and conservative with limited numerical dispersion and good transport ability. Instead of integrating the polynomial fit over the neighboring grid values as in the Bott scheme, the flux area is supposed trapezoidal, here. The flux is determined as a product of the Courant number and a single value of the approximating polynomial referring the middle of the passed distance. Displaying the same properties as the Bott scheme, the TRAP scheme turns out to be faster. Some new and faster schemes built on the base of TRAP scheme are presented. They are obtained by optimization of the so called "normalization" procedure. The performance quality of these schemes is determined exploiting the rotational test. A set of criteria is established for quantitative estimates of schemes' properties.

**Key words:** Air Pollution Modelling, Dispersion models, Advection Schemes

## 1. INTRODUCTION

The description and prediction of local and transboundary air pollution is one of the key environmental problems. A state-of-the-art method for this is the numerical modeling which is able to account for a great number of dispersion processes like transport (advection), diffusion, wet and dry deposition, physical and chemical transformations. Very often such kind of numerical models incorporate one or more advection schemes.

Many advection schemes are described in the literature (WMO, 1979) but none of them possesses all properties of the exact solution of the advective equation. One of the most widely used schemes is developed by Bott (1989). It is an explicit flux scheme. The leftmost and rightmost edge fluxes are calculated for each grid cell and the change of concentration is determined as their difference. In the Bott scheme, the advective fluxes are computed utilizing the integrated flux concept of Tremback et al. (1987). Upper and lower limitation and **normalization** are applied as well. The produced scheme is conservative and positively definite with small numerical diffusion. These properties make the Bott scheme very attractive for further improvements and optimizations. The TRAP scheme (Syrakov, 1995, Syrakov and Galperin, 1997) is a kind of a daughter scheme to Bott's one. It is built supposing that the shape of the so called "flux area" is trapezoidal and its magnitude is

calculated as a product of the Courant number and the concentration in the middle of the trapezium. The last one is determined from the polynomial fitting over the concentrations in the neighboring grid points. Some variants of TRAP scheme are elaborated and tested, decreasing the order of the fitting polynomial (Syrakov, 2003). In this paper, four new variants of the TRAP scheme are presented. They are obtained by optimization of the Bott's normalization procedure. Two of these schemes are self-normalizing modifications of the best third order TRAP scheme (***Trb***), denoted as ***Tr3_n1*** and ***Tr3_n2***. The other two are modifications of the second order TRAP scheme (***Tr2***) and are denoted as ***Tr2_n1*** and ***Tr2_n2***. The new created schemes are tested and compared with mother ones using the two-dimensional rotational test of Smolarkiewicz (1982), their transport abilities demonstrated on a number of initial concentration shapes.

## 2. DESCRIPTION OF TRAP-SCHEME (*Trb*)

The one-dimensional case will be considered here. In multi-dimensional case the splitting technique can be applied. The one-dimensional advection equation in non-divergent and in divergent form is

$$\frac{\partial C}{\partial t}+u\frac{\partial C}{\partial x}=0\,, \qquad \frac{\partial C}{\partial t}+\frac{\partial uC}{\partial x}=0\,, \tag{1}$$

where $C(x,t)$ is the concentration of the tracer, $u(x,t)$ – the transport velocity, $x$, $t$ – space and time. The simplest way to solve Eq.(1) is to replace the derivatives with some differential approximations. Let's introduce a homogeneous grid: $x\rightarrow x_i=i\Delta x$, $i=1,N_x$, $t\rightarrow t_n=n\Delta t$, $n=0,N_t$, $\Delta x$ and $\Delta t$ being the space and time steps. The corresponding values of speed and concentration are $u(x_i,t_n)=u_i^n$ and $C(x_i,t_n)=C_i^n$. The discrete form of (1) for cell $i$ is

$$C_i^{n+1}=C_i^n-\left(F_{i+1/2}-F_{i-1/2}\right)\Delta t/\Delta x \quad \text{or} \quad C_i^{n+1}=C_i^n-\left(Fr_i-Fl_i\right) \tag{2}$$

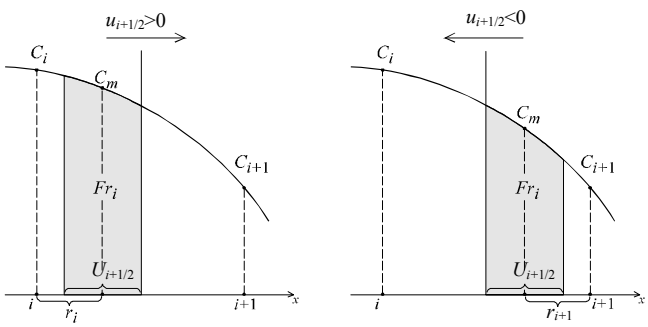


**Fig.1** Flux trough the right edge of cell $i$ at positive and negative transport velocity

where $F_{i\pm1/2}=F(u,C)$ are the mass-fluxes trough the edges of the cell, $Fr$ и $Fl$ being masses transported trough the right and left edges of the $i^{\text{th}}$ cell for one time step, respectively. $Fr$ and $Fl$ can be positive or negative depending on the transport direction: $Fm=\text{sign}(u_m)A_m$, $(m=r,l)$, where $A_m$ is the so-called ***flux area*** – the shadowed shapes in **Fig.1**. The problem can be normalized by introducing the Courant number $U_i^n=u_i^n\Delta t/\Delta x$ and setting $\Delta x=\Delta t=1$.

The schemes are *explicit* when the fluxes $F_{i\pm1/2}$ are calculated for the moment $t_n$. Here, such type of schemes will be discussed; therefore the upper index $^{(n)}$ will be omitted further on. Practically, all schemes can be re-formulated and written in the form of Eq.(2). They differ in the way of determining the fluxes. A scheme is *mass conservative* if it is constructed in such a way that the condition $Fl_i = Fr_{i\text{-}1}$ is fulfilled during the whole integration period. Because this condition is fulfilled for all schemes here, only the right edge fluxes of each cell will be considered further.

Let us assume a staggered grid, i.e. the concentrations $C_i$ are defined in the points $i$, and the velocities (Courant numbers) $U_i$ – in the points $i$+1/2. According to the TRAP concept, the flux area is approximated by rectangular trapezium laying on its height (**Fig.1**) and its magnitude $Ar_i$ can be calculated as a product of this height (i.e. the Courant number) and the half-sum of the concentrations representing both bases. Estimates for these bases can by obtained using the proper approximating polynomial. In TRAP, instead of calculating the two bases, a single estimate for the point in the middle of the passed distance (the trapezium height) is obtained exploiting the same polynomial, thus achieving additional acceleration of the scheme.

$$Ar_i = C_m.|U_i| \qquad C_m = C_i^p(r), \tag{3}$$

where $C_m$ is the value of the concentration in point $r$, $C_i^p(r)$ - interpolation polynomial of proper order and $r$ is the non-dimensional distance from point $i$ to the centre of the trapezium height. According to Fig.1, this distance is

$$r = (1\text{-}\ U_{i+1/2})/2, \tag{4}$$

and it is the same in both cases of positive and negative transport velocity.

Bott recommended the 4th order Lagrangean polynomial as best fit of concentration profile. In the ***Trb***-variant of the TRAP scheme (Syrakov and Galperin, 1997) a Bessel type polynomial of 3rd order is applied instead:

$$C^b(r) = b_0 + b_1 r + b_2 r^2 + b_3 r^3, \tag{5}$$

In order to determine the coefficients $b_k$ a local coordinate system (4-point pattern) is introduced with origin in point $i$ as shown in Scheme 1. Known the grid values of the concentration, a system of four ordinary algebraic equations results:

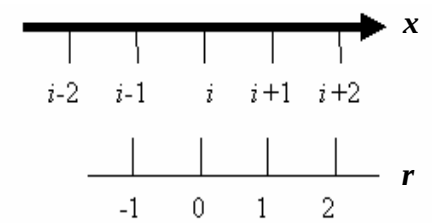


**Scheme 1**

$$\begin{aligned}
&at\quad r=-1:\quad C_{i-1} = b_0 - b_1 + b_2 - b_3\\
&at\quad r=\ 0:\quad C_i = b_0\\
&at\quad r=\ 1:\quad C_{i+1} = b_0 + b_1 + b_2 + b_3\\
&at\quad r=\ 2:\quad C_{i+2} = b_0 + 2b_1 + 4b_2 + 9b_3
\end{aligned} \tag{6}$$

Its solution gives the polynomial coefficients:

$$\begin{aligned}
b_0 &= C_i\\
b_1 &= \left(-2C_{i-1} - 3C_i + 6C_{i+1} - C_{i+2}\right)/6\\
b_2 &= \left(C_{i-1} - 2C_i + C_{i+1}\right)/2\\
b_3 &= \left(-C_{i-1} + 3C_i - 3C_{i+1} + C_{i+2}\right)/6
\end{aligned} \tag{7}$$

This local approach of polynomial fitting (separate coefficients for each cell) leads to a small numerical diffusion, but in case of strong gradients in the concentration field, the values of the polynomial can become negative or unrealistically high. That is why the next step is to introduce upper and lower limits for the flux area (Bott).

$$\begin{aligned} 0 \le Ar_i < C_i, \quad & at \quad U_{i+1/2} > 0 \\ 0 \le Ar_i < C_{i+1}, \quad & at \quad U_{i+1/2} < 0 \end{aligned} \tag{8}$$

In the above described operations, the mass transported trough the cell edge is determined using an interpolation polynomial, derived assuming that the concentration in the points *i, i*±1 etc. is $C_i$, $C_{i\pm1}$ etc. This is not fully correct, because $C_i$, $C_{i\pm1, \ldots}$ are the average concentrations in respective cells, and not the values in the specific points (the centers of the cells). In order to correct this, Bott introduces a **normalization** of the fluxes multiplying the flux area by the factor $C_i/A_i$ when $U_{i+1/2} > 0$ and $C_{i+1}/A_{i+1}$ when $U_{i+1/2} < 0$, where $A_i$ is the whole area of the cell *i* (total mass in the cell) determined through the same polynomial as

$$A_i = \int_{-1/2}^{1/2} C_i^b(x)dx \text{, i.e. } \begin{aligned} A_i &= (C_{i-1} + 22C_i + C_{i+1})/24, \quad at \quad U_i > 0 \\ A_{i+1} &= (C_i + 22C_{i+1} + C_{i+2})/24, \quad at \quad U_i < 0 \end{aligned} \tag{9}$$

Finally, the change of concentration in the cell is determined after Eq.(2). At every time step the procedure recurs for each cell consecutively, starting from the first one.
The introduction of Bessel polynomial leads to some important results. Firstly, the lower order leads to a smaller number of coefficients, so the computations are less. Secondly, the number of the boundary points (points in which it is necessary to introduce boundary conditions) decreases. Finally, it is well known that the Lagrangean polynomials give the best interpolation quality for the interval $|r| \le 0.25\Delta x$, i.e. close around the central point *i*, while the highest order of accuracy of the Bessel polynomial is for the region $0.25 \le r \le 0.75$, i.e. around the cell edge ($r$=1/2), where the flux area is usually located.
The results from the experiments made with the Bott's scheme and some variants of TRAP scheme, exposed in Syrakov (2003), show that Bott's scheme and the 3rd order TRAP schemes (with both Bessel and Lagrange polynomials) possess practically equal simulation abilities, but TRAP schemes are faster. As a final conclusion the Bessel variant of TRAP scheme (***Trb***) was recommended for practical use, there.

## 3. TIRD-ORDER SELF-NORMALIZING TRAP SCHEMES (*Tr3_n1*, *Tr3_n2*)

Further optimization of the TRAP scheme can be achieved applying the so called self-normalizing proposed by Galperin (1998). It was mentioned above that the **normalization** is a necessary step because the fitting polynomial is built assuming that grid values $C_i$, $C_{i\pm1}$ etc. are the values in points *i, i*±1 etc. It is clear *a priori* that $C_i$ is the average concentration in the $i^{th}$ cell, not the concentration in the centre of the cell. It is possible to account for this during the calculation of the polynomial coefficients. As a result, the necessity of normalization step fells out. The coefficients of polynomials must be determined in such a way that the integral of the polynomial over the whole cell is equal to the mass in the respective cell. This is

achieved if in Eq.(6) the polynomial values are not equalized to $C_i$, $C_{i\pm1}$, but to the integrals of the polynomial in the respective boundaries.

### 3.1. Description of the scheme *Tr3_n1*

This modification of TRAP is realized on the same 4-point pattern [-1,0,1,2] with origin in point *i* as shown in **Scheme 1**. It means that a polynomial of third order will be used again:

$$C^3(x) = p_0 + p_1 x + p_2 x^2 + p_3 x^3 \tag{10}$$

In accordance with Galperin's approach, the next system of equations is derived:

$$\begin{aligned}
&at \quad r=-1: \quad C_{i-1} = \int_{-3/2}^{-1/2} C^3(x)dx = p_0 - p_1 + \frac{13}{12}p_2 - \frac{5}{4}p_3 \\
&at \quad r=\ 0: \quad C_i = \int_{-1/2}^{1/2} C^3(x)dx = p_0 + \frac{1}{12}p_2 \\
&at \quad r=\ 1: \quad C_{i+1} = \int_{1/2}^{3/2} C^3(x)dx = p_0 + p_1 + \frac{13}{12}p_2 + \frac{5}{4}p_3 \\
&at \quad r=\ 2: \quad C_{i+2} = \int_{-3/2}^{-1/2} C^3(x)dx = p_0 + 2p_1 + \frac{49}{12}p_2 + \frac{17}{2}p_3
\end{aligned} \tag{11}$$

The solution of the system gives the unknown coefficients of the polynomial Eq.(10):

$$\begin{aligned}
p_0 &= \left(-C_{i+1} + 26C_i - C_{i-1}\right)/24 \\
p_1 &= \left(-5C_{i+2} + 27C_{i+1} - 15C_i - 7C_{i-1}\right)/24 \\
p_2 &= \left(C_{i+1} - 2C_i + C_{i-1}\right)/2 \\
p_3 &= \left(C_{i+2} - 3C_{i+1} + 3C_i - C_{i-1}\right)/6
\end{aligned} \tag{12}$$

After calculating the rightmost flux area for cell *i* according to

$$Ar_i = |U_{i+1/2}|C^3(r_i), \qquad r_i = (1 - U_{i+1/2})/2, \tag{13}$$

the Bott limiters, Eq.(8), are applied and the flux with its sign is determined. Finally, the new time level concentration is calculated after Eq.(2).

### 3.2. Description of the scheme *Tr3_n2*

***Tr3_n2*** is realized using the same polynomial Eq. (10) and the same 4-point pattern but shifted a half step right, so its origin matches the point *i*+1/2 (**Scheme2**). Using the same approach as Eq. (11) similar system of equations for the coefficients of the polynomial is obtained. Its solution gives:

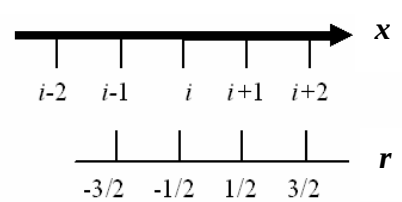

**Scheme 2**

$$\begin{aligned}
p_0 &= \left(-C_{i+2} + 7C_{i+1} + 7C_i - C_{i-1}\right)/12 \\
p_1 &= \left(-C_{i+2} + 15C_{i+1} - 15C_i + C_{i-1}\right)/12 \\
p_2 &= \left(C_{i+2} - C_{i+1} - C_i + C_{i-1}\right)/4 \\
p_3 &= \left(C_{i+2} - 3C_{i+1} + 3C_i - C_{i-1}\right)/6
\end{aligned} \tag{14}$$

The rightmost flux area for the $i^{th}$ cell is calculated as $Ar_i = |U_{i+1/2}|C^3(r_i)$, but that time, because the origin of the pattern is in point *i*+1/2

$$r_i = -U_{i+1/2}/2. \quad (15)$$

The other steps (Bott limiting, flux calculation, etc.) are as in the case of ***Tr3_n1***.

## 4. SECOND ORDER TRAP-SCHEMES (*Tr2, Tr2_n1, Tr2_n2*)

It was shown in Syrakov (2003) that the decrease of the order of approximation from 4 to 3 leads to acceleration of computations without considerable change for the worse. Further decrease of this order and applying a pattern like those in **Scheme 1** and **Scheme 2** is worth to be checked: The interpolation polynomial has the form:

$$C^2(x)=d_0+d_1x+d_2x^2 \quad (16)$$

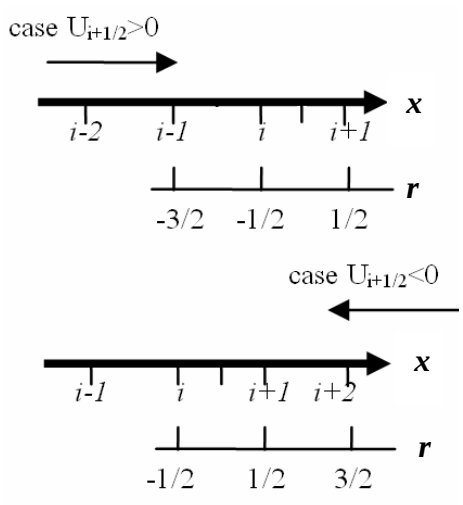


**Scheme 3**

The 3-point grid pattern has its origin in point $i+1/2$, its orientation depending on the transport direction as shown in **Scheme 3**. In such a way, two points in upstream direction and one - in downwind one are used. The polynomial coefficients are:

$$\text{at } U_{i+1/2} > 0$$
$$d_0 = (-C_{i-1} + 6C_i + 3C_{i+1})/8$$
$$d_1 = -C_i + C_{i+1} \quad (17a)$$
$$d_2 = (C_{i-1} - 2C_i + C_{i+1})/2$$

$$\text{at } U_{i+1/2} < 0$$
$$d_0 = (3C_i + 6C_{i+1} - C_{i+2})/8$$
$$d_1 = -C_i + C_{i+1} \quad (17b)$$
$$d_2 = (C_i - 2C_{i+1} + C_{i+2})/2$$

The flux area is calculated by multiplying the Courant number by the value of Eq.(16) at $r_i = -U_{1+1/2}/2$. Bott's limiters, Eq.(8), and **normalization** procedure are applied, mass-in-cell determined as

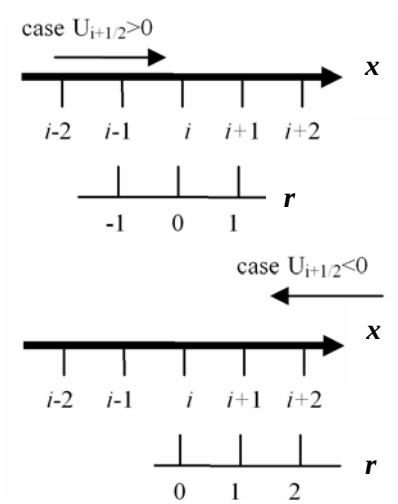


**Scheme 4**

$$A_i=d_0-d_1/2+d_2/3 \text{ at } U_{i+1/2}>0 \quad (18)$$

$$A_{i+1}=d_0+d_1/2+d_2/3 \quad \text{at } U_{i+1/2}<0$$

### 4.1. Description of the scheme *Tr2_n1*

A 3-point pattern with origin in point $i$ is applied (**Scheme 4)**. The coefficients in Eq.(16) are derived after the approach in Eq. (11). They are:

$$\begin{aligned} &at \quad U_{i+1/2} > 0 \\ &d_0 = \left(-C_{i-1} + 26C_i - C_{i+1}\right)/24 \\ &d_1 = \left(-C_{i-1} + C_{i+1}\right)/2 \\ &d_2 = \left(C_{i-1} - 2C_i + C_{i+1}\right)/2 \end{aligned} \tag{19a}$$

$$\begin{aligned} &at \quad U_{i+1/2} < 0 \\ &d_0 = \left(23C_i + 2C_{i+1} - C_{i+2}\right)/24 \\ &d_1 = \left(-3C_i + 4C_{i+1} - C_{i+2}\right)/2 \\ &d_2 = \left(C_i - 2C_{i+1} + C_{i+2}\right)/2 \end{aligned} \tag{19b}$$

Next, the rightmost flux area for the $i^{th}$ cell is calculated:

$$Ar_i = |U_{i+1/2}|C^2(r_i), \qquad r_i = (1- U_{i+1/2})/2. \tag{20}$$

The Bott limiters, Eq.(8), are applied and the flux with its sign is determined. Finally, the new time level concentration is calculated after Eq.(2).

### 4.2. Description of the scheme *Tr2_n2*

This modification of TRAP uses the same 2nd order polynomial realized on the same 3-point pattern as in **Scheme 3**. The approach from Eq.(11) leads to the coefficients:

$$\begin{aligned} &at \quad U_{i+1/2} > 0 \\ &d_0 = \left(-C_{i-1} + 5C_i + 2C_{i+1}\right)/6 \\ &d_1 = -C_i + C_{i+1} \\ &d_2 = \left(C_{i-1} - 2C_i + C_{i+1}\right)/2 \end{aligned} \quad \text{and} \quad \begin{aligned} &at \quad U_{i+1/2} < 0 \\ &d_0 = \left(2C_i + 5C_{i+1} - C_{i+2}\right)/6 \\ &d_1 = -C_i + C_{i+1} \\ &d_2 = \left(C_i - 2C_{i+1} + C_{i+2}\right)/2 \end{aligned} \tag{20}$$

The flux is calculated like in Eq. (20) but $r_i$ = - $U_{i+1/2}/2$. The other steps (Bott limiting, flax calculation, etc) are as in the first case (***Tr2_n1***).

Table 1 Estimates for simulation quality of numerical advection schemes (rotational test)

| **Estimate** | **Meaning** |
|---|---|
| **Cmax** = max( $C_{ij}$ )/max( $C^o_{ij}$ ) | **Cmax**<1 – presence of numerical diffusion |
| **Cmin** = min( $C_{ij}$ )/max( $C^o_{ij}$ ) | **Cmin**<0 absence of positive definiteness |
| **CM** = $(\sum_{ij} C^o_{ij} - \sum_{ij} C_{ij}) / \sum_{ij} C^o_{ij}$ | **CM** - normalized difference of masses.<br>**CM**≠0 denotes absence of conservativeness |
| **CM2** = $(\sum_{ij} C^{o\,2}_{ij} - \sum_{ij} C_{ij}{}^2) / \sum_{ij} C^{o2}_{ij}$ | **CM2** reflects the second moment conservativeness of the scheme. The ideal advection scheme has **CM2**=0. |

| | |
|---|---|
| $\mathbf{DXc} = \sum_{ij} iC_{ij} / \sum_{ij} C_{ij} - \sum_{ij} iC^o_{ij} / \sum_{ij} C^o_{ij}$<br>$\mathbf{DYc} = \sum_{ij} jC_{ij} / \sum_{ij} C_{ij} - \sum_{ij} jC^o_{ij} / \sum_{ij} C^o_{ij}$ | **DXc** and **DYc** estimate the displacement of the mass centre due to numerical effects. **DXc** = **DYc** = 0 after a full rotations indicate ideal transport ability |
| $\mathbf{DD} = (\mathbf{D} - \mathbf{D}^0) / \mathbf{D}^0$, where<br>$\mathbf{D} = \sum_{ij} C_{ij} \left[ (x - \mathbf{Xc})^2 + (y - \mathbf{Yc})^2 \right] / \sum_{ij} C_{ij}$ | **D** - dispersion around the mass centre<br>**DD** shows the degree of deconcentration of masses due to the numerical diffusion |
| $\mathbf{T} = \Delta T_{calc} / \Delta T^{ref}$, | relative speed of performance, $\Delta T^{ref} = \Delta T^{\mathbf{Trb}}$ |

## 3. NUMERICAL EXPERIMENTS

### 3.1. Description of the rotational test, estimates

The described variants of TRAP scheme have passed the two-dimensional rotational test (*Smolarkiewicz*, *1982*). Instantaneous releases with different initial profiles have been rotated with constant angular velocity. The computational domain is a grid field with 101×101 points and horizontal steps $\Delta x = \Delta y = 1$. Following Smolarkiewicz, a rotational wind field is imposed on this domain with a constant angular velocity $\omega \approx 0.1$ (~600 time steps per rotation) and centre at point (51, 51). Setting $u = -\omega y$ and $v = \omega x$ a counter-clockwise rotation is achieved. Keeping in mind that the initial field of concentration $C^0_{ij}$ is the exact solution of the advection equation after one or several full rotations, the following criteria for estimation of the quality of the numerical simulation are established (Table 1).

The simulation quality of the six schemes described above is examined using different types of sources. The values of the estimates are shown in Table 2.

Table 2 Values of the simulation quality estimates after **six** rotations.

| **Persents (%)** | | ***TrB*** | ***Tr3_n1*** | ***Tr3_n2*** | ***Tr2*** | ***Tr2_n1*** | ***Tr2_n2*** |
|---|---|---|---|---|---|---|---|
| **Cone shape (6 rotations)** | **Cmax** | 85.9 | 89.1 | 89.1 | 81.3 | 80.8 | 80.8 |
| | **Cmin** | 0.0 | 0.0 | 0.0 | 0.0 | 0.0 | 0.0 |
| | **CM** | -0.8 | -0.2 | -0.2 | -1.2 | -0.8 | -0.8 |
| | **CM2** | -3.8 | -0.6 | -0.6 | -9.5 | -8.6 | -8.6 |
| | **DXc** | -15.8 | -15.8 | -15.8 | -14.8 | -14.8 | -14.8 |
| | **DYc** | 51.5 | 51.9 | 51.9 | 51.8 | 51.8 | 51.8 |
| | **DD** | -27.7 | -30.2 | -30.2 | -26.2 | -26.5 | -26.5 |
| | **T** | 100 | 43.4 | 41.5 | 48.2 | 35.1 | 34.6 |
| **Gauss shape (6 rotations)** | **Cmax** | 93.2 | 98.7 | 98.7 | 77.0 | 76.6 | 76.6 |
| | **Cmin** | 0.0 | 0.0 | 0.0 | 0.0 | 0.0 | 0.0 |
| | **CM** | -0.6 | -0.4 | -0.4 | -0.4 | -0.2 | -0.2 |
| | **CM2** | -6.5 | 0.0 | 0.0 | -17.3 | -15.9 | -15.9 |
| | **DXc** | -24.6 | -24.8 | -24.8 | -23.1 | -23.4 | -23.4 |
| | **DYc** | 51.7 | 51.9 | 51.9 | 51.9 | 51.9 | 51.9 |
| | **DD** | -41.3 | -46.1 | -46.1 | -37.3 | -38.4 | -38.4 |
| | **T** | 100 | 42.2 | 43 | 50 | 37.8 | 37.6 |
| **Point source** | **Cmax** | 1.6 | 2.2 | 2.2 | 0.9 | 0.9 | 0.9 |
| | **Cmin** | 0.0 | 0.0 | 0.0 | 0.0 | 0.0 | 0.0 |
| | **CM** | 1.9 | 0.0 | 0.0 | 0.0 | 0.0 | 0.0 |
| | **CM2** | -99.2 | -98.8 | -98.8 | -99.5 | -99.5 | -99.5 |

| | | | | | | | |
|---|---|---|---|---|---|---|---|
| | **DXc** | -48.9 | -47.1 | -47.1 | -48.9 | -49.5 | -49.5 |
| | **DYc** | 52.5 | 53.0 | 53.0 | 52.3 | 52.2 | 52.2 |
| | **T** | 100 | 42.7 | 41.5 | 48.7 | 36 | 35.9 |

Several conclusions can be made from the values shown in the table above. First of all, no one of these schemes describes the point source rotation well. As far as the point source is an absolute discontinuity, there is no difference scheme able to do this. All schemes give their best results on gauss shape (absolute smoothness) and more or less good ones on the cone shape (intermediate case). One can see that the two normalized versions of the TRAP-scheme exploiting Lagrange polynomial of 3rd degree (***Tr3_n1*** and ***TR3_n2***) perform the rotations best, considering all criteria. The conservation of mass characteristics are very satisfying, especially for the second one, ***Tr3_n2*** (with shifted pattern). Moreover, they show high speed of performance – more than twice faster than the ***Trb*** scheme.

In the pictures presented below, cases with background concentration are shown exhibiting additional properties of the tested schemes. The initial shape and the shape after ¾ rotations are shown in every graph. In Fig.2, the performance of two 3rd order schemes is presented. The ***Trb*** scheme describes better the shapes with discontinuities (cone) and steep gradients, while its normalized versions form several Gibbs's waves lugging after the main shape. On the other hand, the two self-normalizing schemes are faster and obtain better simulation qualities concerning the movement of smooth shapes (gauss shape).

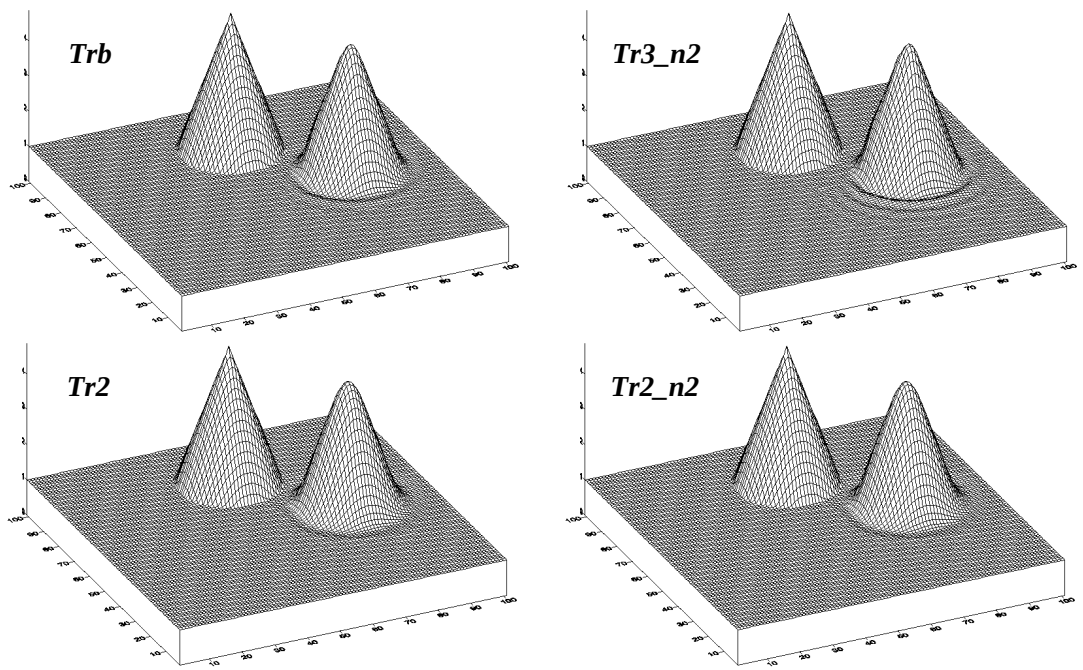


Fig.2 Initial and ¾ rotation shapes as described by 3rd and 2nd order TRAP schemes

Analyzing the schemes using polynomial of 2nd degree, slightly worse results than the 3rd order schemes can be noticed. They, especially the self-normalizing variants, are the fastest ones and do not form Gibbs's waves like the higher order schemes.

The reason for this is, possibly, the limited variability of polynomial when fitted over smaller number of points. They can be recommended for use in case of convection (vertical advection), all the more so since they can be easily modified to account for non-homogeneous grids.

## DISCUSSION AND CONCLUDING REMARKS

The tests over background are very important in proving the positive definiteness of a numerical scheme. In case of zero background, an option for checking for and neglecting the negative concentrations can keep the positive definiteness of a scheme. This limiter does not work when background tests are made. The undershooting and overshooting of the schemes usually dig "holes" in the background or produce picks to avoid the discontinuity, i.e. waves appear. ***Tr2*** and its normalized versions demonstrate better quality in this sense, but ***Trb*** and its version transport the smooth forms better than the 2nd order schemes.
It must be noted also, that in the reality discontinuities are produced by the intensive point sources and the wet removal processes. Turbulent diffusion works in direction of smoothening of these discontinuities, so, as a whole, the concentration fields are smooth enough and ***Tr3_n2*** can be used with certainty. It is up to the modeler to decide what property of a scheme is more valuable for the specified task.

## ACKNOWLEDGEMENTS

This study is made under the financial support of European Commission – 5thFP project BULAIR (Contract Nr. EVK2-CT-2002-80024) and the 6thFP Network of Excellence ACCENT (Contract Nr. GOCE-CT-2002-500337). The contacts within the framework of NATO Collaborative Linkage Grant EST.CLG 979794 were extremely stimulating, as well.

## REFERENCE

Bott, A., 1989. A positive definite advection scheme obtained by nonlinear renormalization of the advective fluxes, *Mon.Wea.Rev*., 117, pp. 1006-1015.

Galperin, M, 1997. Two numerical advection schemes for atmospheric models: development and comparison testing, in *Proceeding from Swedish- Bulgarian Workshop*, 1997, Sozopol, Bulgaria, pp 49- 61, Pensoft

Smolarkiewicz, P.K., 1982. The multidimensional Crowley advection scheme, *Mon.Wea.Rev*., 113, pp. 1109-1130.

Syrakov, D., 1995. On a PC-oriented Eulerian Multi-Level Model for Long-Term Calculations of the Regional Sulphur Deposition, in *Air Pollution Modelling and its Application XI, NATO/CMSS*, 21, Gryning S.E. and Schiermeier F.A., ed., Plenum Press, N.Y. and London, pp. 645-646.

Syrakov, D., 2003. Once more on the advection schemes: description of TRAP-schemes, in *Proceedings of the 26th ITM, 26-30 May 2003,* Istanbul, Turkey, pp 225-258.

Syrakov, D., M. Galperin, 2000. On some explicit advection schemes for dispersion modelling applications, *Intrnational Journal of Environment and Pollution*, 14, pp. 267-277.

Tremback, C.J., J. Powell, W.R. Cotton and R.A. Pielke, 1987. The forward-in-time upstream advection scheme: Extension to higher orders, *Mon.Wea.Rev*., 115, pp. 540-555.

WMO-TCSU, 1979. Numerical methods used in atmospheric models, Vol. I and II, *GARP Publication series*, No 17, Sept. 1979.

*Proceedings of the Third International Symposium on Air Quality Management at Urban, Regional and Global Scales. 26-30 September 2005, Istanbul – Turkey*

# ESTIMATION OF THE EXCHANGE OF SULPHUR POLLUTION OVER THE BALKAN REGION IN 1995-2000

**Hristo Chervenkov, Dimiter Syrakov* and Maria Prodanova***

National Institute of Meteorology and Hydrology - branch Plovdiv, "Ruski" 139, Plovdiv, Bulgaria, hristo.tchervenkov@meteo.bg
National Institute of Meteorology and Hydrology, "Zarigradsko Shausee" 66, Sofia, Bulgaria, dimiter.syrakov@meteo.bg, maria.prodanova@meteo.bg

## ABSTRACT

The Bulgarian dispersion model EMAP is used to estimate the sulphur pollution over the Balkan region for the period 1995-2000. A sub-domain of the EMEP grid is chosen containing 12 countries. As meteorological driver the operational DWD "Europa-Model" is used. The source input is the official EMEP emission data. Monthly calculations are made having the last moment fields from the previous month as initial conditions for the next. The boundary conditions are set to zero so the influence of the other European sources is not accounted for. According to the EMEP methodology multiple runs are made setting every time the sources of various countries to zero. The impact of every country in the pollution of all others is estimated.

**Key Words:** Dispersion Modelling, Sulphur Dioxide, Blame matrix, Multi-year estimates.

## 1. INTRODUCTION

The Bulgarian dispersion model EMAP is used to estimate the concentration in air and in precipitation water and the total deposition of oxidized sulphur over southeast Europe for the six-year period 1995 - 2000 due to sources from 12 countries (Table 1). As only sources from these countries are handled, the results can be considered as an estimate of their impact on the acid pollution of the region as well as an estimate of the reciprocal pollution.

Table 1. List of countries and their notations.

| Albania | Bosnia and Herzegovina | Bulgaria | Croatia | Serbia and Montenegro | The FYR Macedonia |
|---|---|---|---|---|---|
| AL | BH | BG | HR | YU | MK |
| Moldavia | Romania | Turkey[1] | Slovenia | Greece | Hungary |
| MO | RO | TR | SL | GR | HU |

(1) The part inside the model domain.

## 2. SHORT DESCRIPTION OF THE EMAP MODEL

EMAP (Syrakov, 1995) is a simulation model that allows describing the dispersion of multiple pollutants. The processes of horizontal and vertical advection, horizontal

and vertical diffusion, dry deposition, wet removal, gravitational settling (aerosol version) and the simplest chemical transformation (sulphur version) (Seinfeld, 1986) are accounted for in the model. Within EMAP, the semi-empirical diffusion-advection equation for scalar quantities is treated. The governing equations are solved in terrain-following coordinates. Non-equidistant grid spacing is settled in vertical directions. The numerical solution is based on discretization applied on staggered grids using the splitting approach. Conservative properties are fully preserved within the discrete model equations. Advective terms are treated with the TRAP scheme, which is a Bott-type one. Displaying the same simulation properties as the Bott scheme (explicit, conservative, positive definite, transportability, and limited numerical dispersion), the TRAP scheme proves to be several times faster (Syrakov, 1996; Syrakov and Galperin, 1997). The advective boundary conditions are zero at income flows and "open boundary" - at outcome ones. Turbulent diffusion equations are digitized by means of the simplest schemes – explicit in horizontal, and implicit in vertical direction. The bottom boundary condition for the vertical diffusion equation is the dry deposition flux, the top boundary condition is optionally "open boundary" and "hard lid" type. The lateral boundary conditions for diffusion are "open boundary" type. In the surface layer (SL), a parameterization is applied permitting to have the first computational level at the top of SL. It provides a good estimate for the roughness level concentration and accounts also for the action of continuous sources on the earth surface (Syrakov and Yordanov 1996). A similarity theory based PBL model (Syrakov and Yordanov 1997) is built in the model producing 3D velocity and turbulence fields on the base of minimum meteorological information – the wind and temperature at geostrophic level and the surface temperature.
The model is evaluated and validated during the ETEX-II intercalibration study - ranged 9th among 34 models (Syrakov and Prodanova, 1998). It is validated on the database of 1996 EMEP/MSC-E intercalibration of heavy metal models (Syrakov and Galperin, 1997).

## 3. MODEL DOMAIN, PARAMETERIZATION AND INPUT DATA

The aim of this modeling is to estimate the sulphur pollution in the region of Southeast Europe, taking a territory of 38×28 EMEP 50×50 $km^2$ grid cells with Bulgaria in the center (see figure 1). Every cell is divided to four 25×25 $km^2$ cells. The chosen territory includes entirely all 11 countries of interest and partly other territories. In the created versions of EMAP, a 5-layer vertical structure is used. The first four layers have representative levels at 50, 200, 650 and 1450 m with layer boundaries 20-100, 100-375, 375-995, 995-1930 m. The 5th layer accounts parametrically for the free atmosphere. The volume of this layer is so big that the concentration tends to be zero there, although it can contain some mass.
Two kinds of input are necessary for EMAP performance: sources and meteorological data.

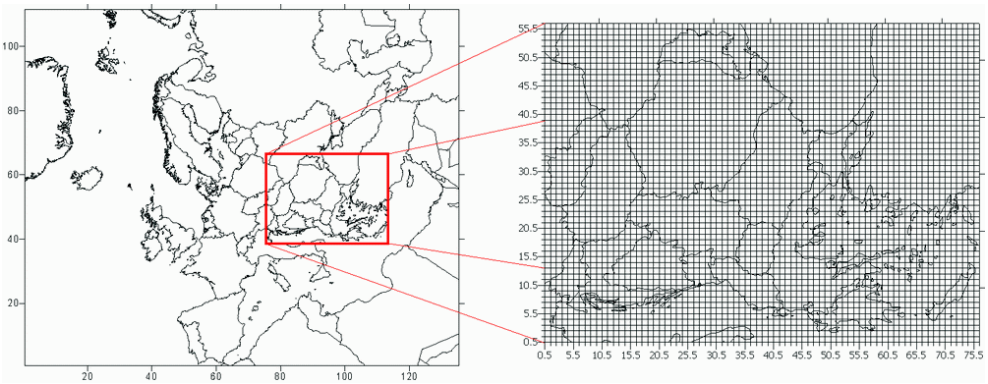


Figure 1. Nesting the model domain in the EMEP-domain

### 3.1 EMISSIONS

The sources (stationary, monodisperse - $SO_2$ only) are determined through an emission inventory based on the CORINAIR methodology. They correspond to the official 50x50 $km^2$ data reported by the corresponding governmental authorities to EMEP's MSC-West and can be downloaded from its web site (http://www.emep.int/). Additional mass-conservative redistribution of these data is made over the finer grid of 25-km space resolution. The emissions are provided in mass units per second. All sources are divided in two classes: high sources (like high and very strength industrial stacks etc.) called Large Point Sources (LPS) and area sources (AS) –the sum of all low and diffusive sources in the given grid cell. As all LPS are supplied with high stacks, the emission of these sources is prescribed to be released in layer 2, i.e., between 100 and 375 m.. In this paper the present scheme of EMEP has been applied. In it the sources are divided in 11 SNAP (Selected Nomenclature for reporting of Air Pollutants) sectors and the data gaps (in former schemes) are filled. The study of the contribution of the each sector is not a subject of this research, therefore each sector is treated as AS or LPS, according to table 3. The annual emission trend is shown on table 2. According the inventory the number and the strength of the sources are changed in the years. It can be seen that by the most of the countries the emitted quantities with a few exceptions decreased during the period of the study. By 9 countries (Albania, Bulgaria, Bosna&Herzegovina, Greece, Hungary, Croatia, Moldova, Slovenia and Serbia&Montenegro) these quantities for 2000 are smaller then for 1995, by 2 countries (Macedonia and Hungary) there is no significant change and only by Turkey the emitted mass for 2000 is greater than for 1995. Generally, the total released mass of sulphur dioxide decreased from 55456 $10^2$t to 46531 $10^2$t., i.e. with 16%. This rate is much smaller in comparison with other regions of Europe for the same period (Lövblad et al., (Eds.) 2004)

Table 2. Annual trend of the emission strength (unit: 100t/year). The boxes where the values are greater then the values for the previous year are shown in orange.

| year | source | AL | BG | BH | GR | HR | HU | MK | MO | RO | SL | TR | YU | all countr. |
|---|---|---|---|---|---|---|---|---|---|---|---|---|---|---|
| 1995 | ARS | 290.7 | 2334.9 | 1776.0 | 1303.2 | 452.8 | 2587.0 | 388.5 | 14.4 | 2758.1 | 197.3 | 2021.8 | 670.0 | 14794.8 |
| | LPS | 429.3 | 12425.1 | 3024.0 | 3976.8 | 251.2 | 4462.6 | 661.5 | 626.2 | 6361.9 | 1052.7 | 3439.9 | 3950.0 | 40661.1 |
| | Total | 720.0 | 14760.0 | 4800.0 | 5280.0 | 704.0 | 7049.6 | 1050.0 | 640.6 | 9120.0 | 1250.0 | 5461.7 | 4620.0 | 55455.9 |
| 1996 | ARS | 290.7 | 2242.5 | 1776.0 | 1404.9 | 449.2 | 2360.0 | 388.5 | 13.0 | 2758.1 | 152.4 | 2201.8 | 520.0 | 14557.3 |
| | LPS | 429.3 | 11957.5 | 3024.0 | 3775.1 | 212.8 | 4372.3 | 661.5 | 657.3 | 6361.9 | 967.6 | 3746.1 | 3820.0 | 39985.3 |
| | Total | 720.0 | 14200.0 | 4800.0 | 5180.0 | 662.0 | 6732.3 | 1050.0 | 670.3 | 9120.0 | 1120.0 | 5947.9 | 4340.0 | 54542.5 |
| 1997 | ARS | 290.7 | 2216.3 | 1776.0 | 1384.0 | 446.3 | 1947.7 | 388.5 | 8.7 | 2758.1 | 138.9 | 2271.0 | 580.0 | 14206.3 |
| | LPS | 429.3 | 11433.7 | 3024.0 | 3726.0 | 357.7 | 4637.4 | 661.5 | 352.6 | 6361.9 | 1041.1 | 3863.9 | 4640.0 | 40529.0 |
| | Total | 720.0 | 13650.0 | 4800.0 | 5110.0 | 804.0 | 6585.1 | 1050.0 | 361.3 | 9120.0 | 1180.0 | 6135.0 | 5220.0 | 54735.4 |
| 1998 | ARS | 290.7 | 2192.0 | 1776.0 | 1512.8 | 424.1 | 1290.9 | 388.5 | 7.2 | 2758.1 | 109.2 | 2417.4 | 690.0 | 13857.1 |
| | LPS | 429.3 | 10318.0 | 3024.0 | 3667.2 | 470.9 | 4627.0 | 661.5 | 313.6 | 6361.9 | 1120.8 | 4113.0 | 4520.0 | 39627.1 |
| | Total | 720.0 | 12510.0 | 4800.0 | 5180.0 | 895.0 | 5917.9 | 1050.0 | 320.8 | 9120.0 | 1230.0 | 6530.4 | 5210.0 | 53484.1 |
| 1999 | ARS | 355.3 | 618.4 | 342.3 | 1020.9 | 446.7 | 865.1 | 205.7 | 48.7 | 916.4 | 138.5 | 2545.7 | 633.0 | 8136.6 |
| | LPS | 214.7 | 8811.6 | 3727.7 | 4379.1 | 463.3 | 5034.9 | 844.3 | 71.3 | 8203.6 | 901.5 | 3940.5 | 2917.0 | 39509.5 |
| | Total | 570.0 | 9430.0 | 4070.0 | 5400.0 | 910.0 | 5900.0 | 1050.0 | 120.0 | 9120.0 | 1040.0 | 6486.2 | 3550.0 | 47646.2 |
| 2000 | ARS | 361.6 | 644.0 | 352.4 | 913.1 | 284.7 | 712.6 | 205.7 | 52.7 | 916.4 | 131.9 | 2555.3 | 690.1 | 7820.4 |
| | LPS | 218.4 | 9176.0 | 3837.6 | 3916.9 | 295.3 | 4147.4 | 844.3 | 77.3 | 8203.6 | 858.1 | 3955.5 | 3179.9 | 38710.4 |
| | Total | 580.0 | 9820.0 | 4190.0 | 4830.0 | 580.0 | 4860.0 | 1050.0 | 130.0 | 9120.0 | 990.0 | 6510.8 | 3870.0 | 46530.8 |

Table 3. SNAP Sectors and their description

| SNAP | Description | assumed |
|---|---|---|
| S1 | Combustion in energy and transformation industries (stationary sources) | LPS |
| S2 | Non-industrial combustion plants (stationary sources) | AS |
| S3 | Combustion in manufacturing industry (stationary sources) | AS |
| S4 | Production processes (stationary sources) | AS |
| S5 | Extraction and distribution of fossil fuels and geothermal energy | AS |
| S6 | Solvent use and other product use | AS |
| S7 | Road transport | AS |
| S8 | Other mobile sources and machinery | AS |
| S9 | Waste treatment and disposal | AS |
| S10 | Agriculture | AS |
| S11 | Other sources and sinks | Not incl. |

The monthly emissions are obtained using the following dimensionless annual variation coefficients, recommended by MSC-E (Table 4):

Table 4. Annual variation coefficients

| J | F | M | A | M | J | J | A | S | O | N | D |
|---|---|---|---|---|---|---|---|---|---|---|---|
| 1.34 | 1.30 | 1.18 | 1.00 | 0.73 | 0.69 | 0.69 | 0.73 | 0.83 | 1.00 | 1.17 | 1.34 |

## 3.2 METEOROLOGICAL DATA

An important advantage of the used model is that, due to the built in PBL model, it utilizes only numerical analysis and forecast data from the world weather centers, distributed via the Global Telecommunication System of the World Meteorological Organization. For this task the meteorology input has a time resolution of 6 hours. It consists of the sequence of analyzed $U_{850}$, $V_{850}$, $T_{850}$ and $T_{surf}$ fields and 6-hour forecast for precipitation from the standard 50×50 km$^2$ output of the former "Europa-Model" of the German Met. Service (DWD). On this base, the PBL model calculates *U*-, *V*-, *W*- and $K_z$-profiles at each grid point. It provides also $u_*$ and SL universal profiles necessary in SL parameterization. The roughness and the Coriolis parameter fields are pre-set additional input to the PBL model. Orography height, surface type (sea-land mask) and roughness height are to be provided for each grid location. Initial concentration field is optionally introduced (spin-up fields).

## 3.3 SULPHUR PARAMETRISATION AND OTHER MODEL PARAMETERS

Two species of sulphur in the air are considered: gaseous sulphur dioxide $SO_2$ and particulate sulfate $SO_4^=$. Sources emit $SO_2$ only, in the air it is transformed to sulfate. The pollutant specific model parameters used are given in Table 4.

Table 5. Specific model parameters

| Pollutant | $SO_2$ | | $SO_4^=$ | |
|---|---|---|---|---|
| Transformation rate constant $\alpha_{tr}$ [h$^{-1}$] | 0.01 (winter) - 0.04 (summer) | | | |
| Wet removal constant $\gamma$ [mm$^{-1}$], | 0.3 | | 0.2 | |
| surface type | sea | land | sea | land |
| Dry deposition velocity $V_d$ [m/s] | 0.01 | 0.03 | 0.002 | 0.006 |

The other model parameters are: horizontal diffusion coefficients Kx= Ky= 5.10$^4$ m$^2$/s and time step Du= 0.25 h.

## 4. CALCULATION RESULTS

Monthly runs with the above mentioned sources are performed. The output consists of the following fields: monthly dry (DD), wet (WD) and total (TD) depositions, monthly concentration mean in air (CA) and, from the meteorological driver, monthly sum of the precipitation (SP). Additionally is calculated the concentration in the precipitation (CP) for each month. Then, the mean annual value of each of the above mentioned fields $\overline{p}$ is calculated according to the formula:

$$\overline{p} = \frac{\sum_1^n m_i p_i}{\sum_1^n m_i}, \; i = 1, n, \qquad (1)$$

where $m_i$ is the duration of the month $i$, and $p_i$ is the corresponding monthly value of the parameter. Finally, using (1) again, where $m_i$ is the duration of each year 1995 - 2000, and $p_i$ is the corresponding mean annual value, the average of the

concentration in air, concentration in precipitation water and the total deposition in the whole period is obtained. The spatial distribution of these parameters is shown on figure 2, figure 3 and figure 4.

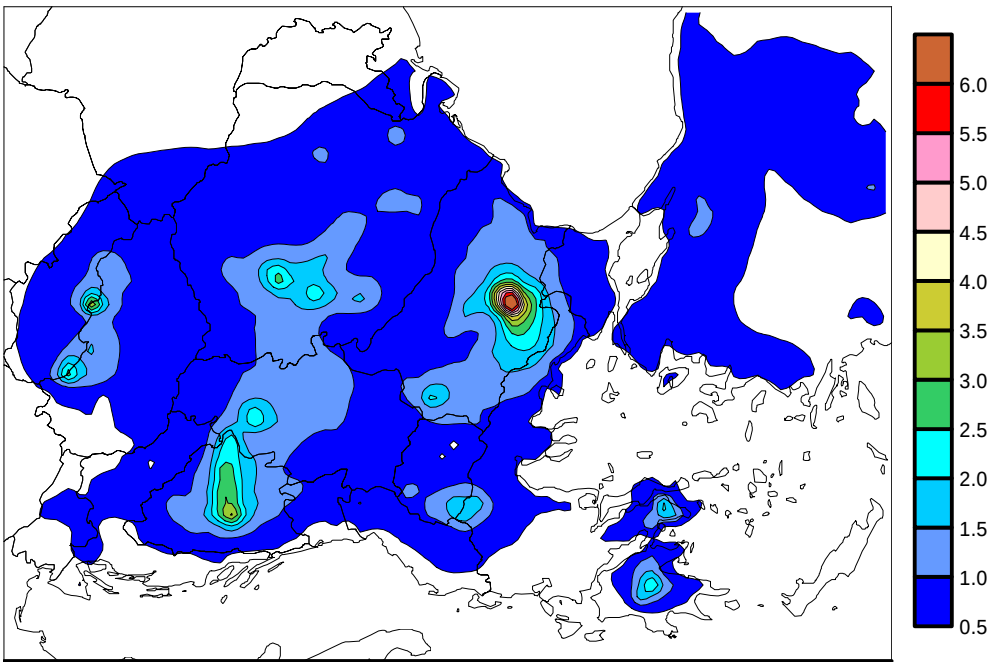


Figure 2. Mean annual concentration in air (unit: μg (S)/$m^3$) of oxidized sulphur in 1995-2000.

In figure 2, it is shown that in the main part of the model domain the concentration in surface air is below 1 μg/$m^3$; over a part of Northern Greece, Bulgaria, Romania, Serbia and Montenegro and Hungary it is between 1 and 2 μg/$m^3$ and only over small areas in Bosnia and Herzegovina, Romania, northern Hungary, in Bulgaria (the region of Sofia) and in Greece (Athens) it is over 3 μg/$m^3$. The most polluted region is that of Southeast Bulgaria, the place around the most powerful source in the region - "Maritsa Iztok" Thermal Power Plant. This TPP is a set of 3 neighboring coal-burning plants. They are so close to each other that they occupy a single 25-km cell. In its vicinity the total the concentration reaches 7 μg/$m^3$.

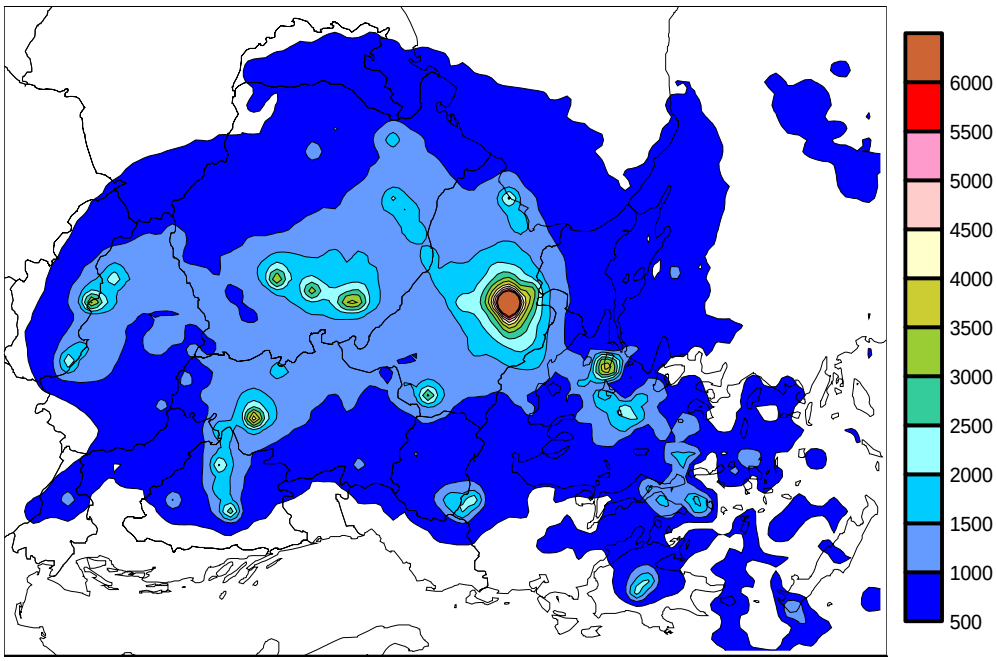


Figure 3. Mean annual total deposition (unit: mg (S)/m$^2$) of oxidized sulphur in 1995-2000.

The shape of isopleths of the mean annual total deposition is similar. Over the main part of the model domain it is below 2 g/m$^2$ only over small areas ("hot spots") in Bosnia and Herzegovina, Bulgaria, Romania and Hungary it is between 3 and 4 g/m$^2$. Again, the most polluted region is that of Southeast Bulgaria, the place around "Maritsa Iztok" TPP, where the deposition reaches 13.5 g/m$^2$.
The picture of the distribution of the concentration in the precipitation is more irregular then the others. In the main part of the model domain it is below 2 mg/l and over a few "hot spots", mainly near the strength sources, it is between 2 and 5 mg/l. In spite of the irregular field of the precipitation, the highest concentration is again in the region of "Maritsa Iztok" TPP where it reaches 13.6 mg/l.
In Table 6, the time-averaged deposition budget matrix for oxidized sulphur is presented. It is obtained from the annual matrixes with the above-mentioned procedure. Every-year matrix is calculated after multiplication of the total deposition field to array containing the distribution of the territory of each country in the model domain. The deposition budget matrix shows the impact of each country to the sulphur pollution of the other countries. The last three rows show respectively the medium values of the total deposited quantity due to the sources from the country in the column header, the total emitted sulphur for this country and the percentage of deposited quantities from the yearly emitted ones. The last value can be treated as the relative part of the sulphur that remained in the domain. It can be noticed that the main part of the sulphur pollution emitted by each country is deposited over the country itself. It can be seen also that the percentage of the total deposited quantity is between 19% and 30%, the rest goes out of the model domain.

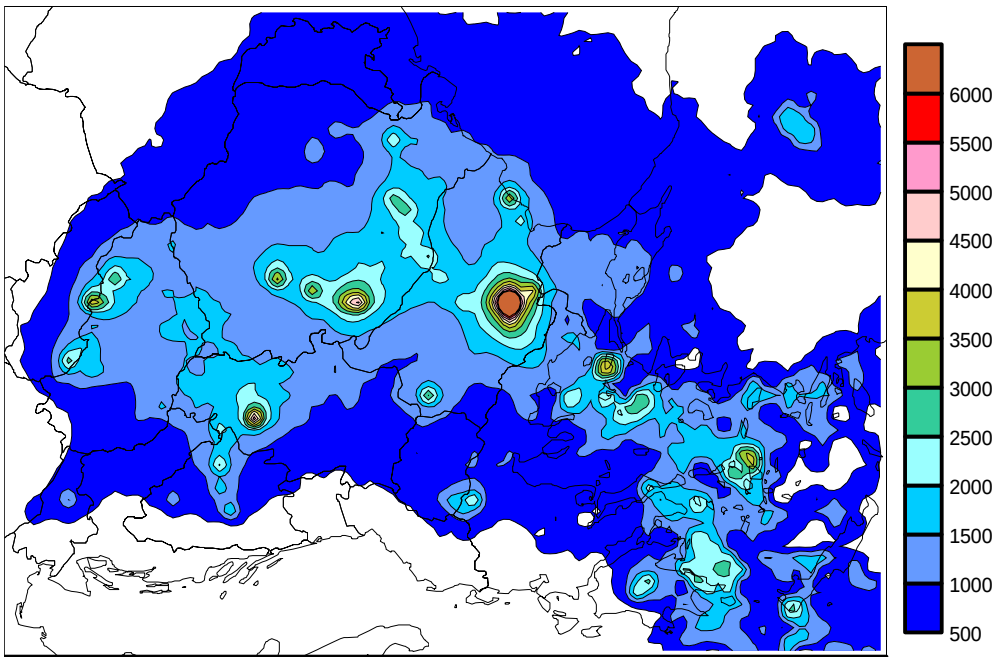


Figure 4. Mean annual concentration in the precipitation (unit: µg (S)/l) of oxidized sulphur in 1995-2000.

Table 6. Deposition budget matrix (unit 100 t). The shaded elements show the deposition quantity for each country due to its own sources.

| emitter / receiver | AL | BG | BH | GR | HR | HU | MK | MO | RO | SL | TR | YU |
|---|---|---|---|---|---|---|---|---|---|---|---|---|
| **AL** | 67.03 | 18.66 | 11.52 | 42.55 | 0.87 | 3.82 | 29.71 | 0.09 | 4.62 | 0.70 | 1.13 | 18.96 |
| **BG** | 8.30 | 1582.90 | 35.04 | 56.36 | 2.92 | 36.73 | 34.31 | 3.15 | 313.58 | 3.71 | 21.83 | 100.50 |
| **BH** | 3.43 | 11.13 | 483.66 | 4.88 | 22.66 | 41.75 | 2.80 | 0.13 | 11.21 | 10.69 | 0.48 | 67.50 |
| **GR** | 20.38 | 254.72 | 13.24 | 443.69 | 1.06 | 7.70 | 34.20 | 0.79 | 28.93 | 1.16 | 20.52 | 20.18 |
| **HR** | 1.30 | 7.80 | 102.95 | 2.58 | 70.90 | 44.54 | 1.26 | 0.09 | 8.98 | 33.47 | 0.34 | 26.98 |
| **HU** | 1.61 | 21.33 | 91.05 | 3.73 | 27.33 | 476.05 | 2.77 | 0.37 | 53.84 | 31.52 | 0.73 | 70.78 |
| **MK** | 17.93 | 58.67 | 7.55 | 65.18 | 0.53 | 4.96 | 77.65 | 0.14 | 9.41 | 0.54 | 1.81 | 20.70 |
| **MO** | 0.49 | 33.24 | 6.33 | 2.30 | 0.72 | 13.37 | 1.06 | 21.52 | 87.40 | 1.03 | 2.23 | 9.98 |
| **RO** | 8.32 | 392.07 | 152.43 | 26.77 | 15.45 | 274.30 | 19.22 | 17.07 | 1544.81 | 17.66 | 14.05 | 278.92 |
| **SL** | 0.18 | 1.99 | 8.20 | 0.56 | 15.80 | 9.48 | 0.22 | 0.03 | 2.51 | 68.05 | 0.09 | 4.89 |
| **TR** | 4.50 | 279.57 | 10.70 | 130.37 | 1.00 | 11.59 | 8.44 | 1.99 | 65.14 | 1.53 | 1037.56 | 18.72 |
| **YU** | 23.84 | 117.56 | 226.53 | 31.05 | 13.56 | 98.64 | 39.22 | 0.62 | 84.07 | 9.57 | 2.76 | 509.05 |
| total dep. | 198.42 | 3627.10 | 1346.59 | 1300.49 | 224.44 | 1651.32 | 293.86 | 74.79 | 2717.93 | 274.14 | 1347.22 | 1331.71 |
| total em. | 671.65 | 12394.65 | 4576.59 | 5163.19 | 759.04 | 6173.81 | 1050.00 | 373.86 | 9120.00 | 1134.93 | 6178.71 | 4468.00 |
| % | 29.55 | 29.04 | 29.31 | 25.16 | 29.56 | 26.65 | 27.99 | 19.69 | 29.80 | 24.16 | 21.82 | 29.89 |

The minimum of this value is for Moldova - the possible explanation is that this territory is close to the east border of the model domain and the main tropospheric transport is west east in these latitudes.

In the figure 5, the diagram of the annual trend of the deposition over each country due to the activity of all sources in the domain is shown. Generally, the trend is descending - for all countries, except Turkey, the deposed quantities for the last year

are smaller then for the first year. Especially significant is the abatement in the deposition over the most polluted countries - Romania and Bulgaria. The ascending trend in Turkey can be explained with the increasing of the emissions there.

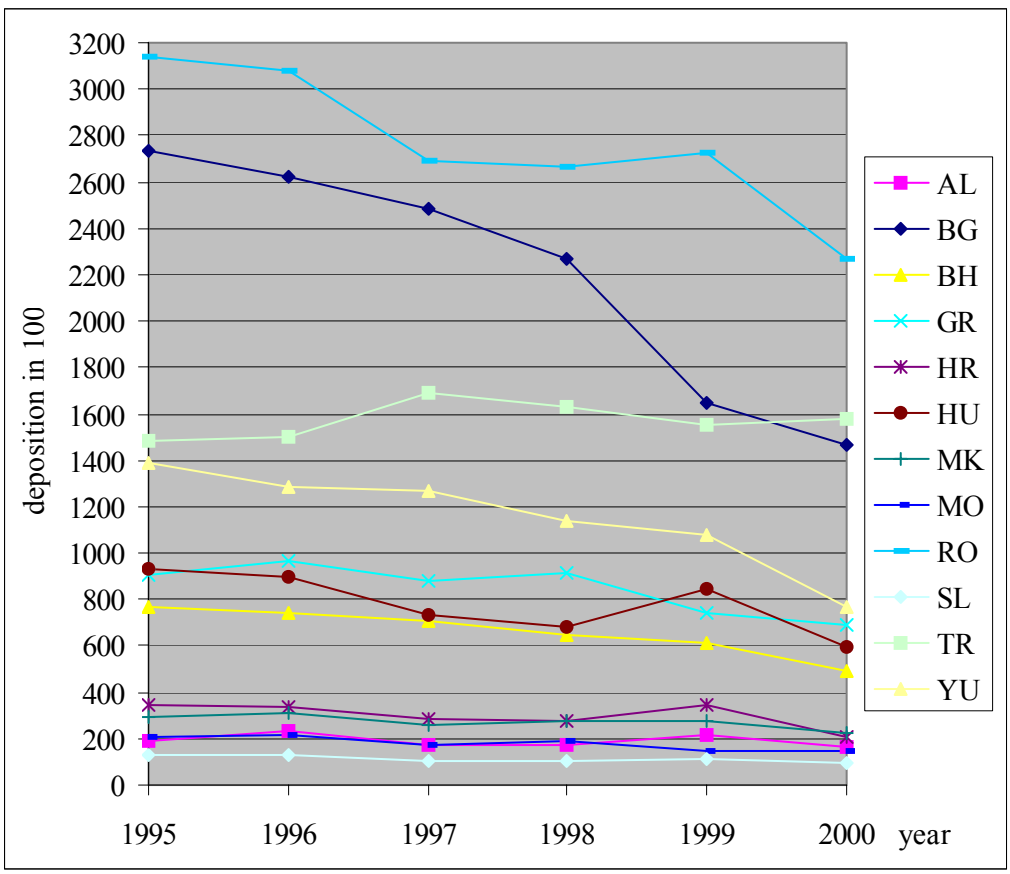


Figure 5. Annual deposition trend of the total deposition.

## 5. CONCLUSION

The paper shows that for long periods of time the part of sulphur pollution, released in one and deposed over other countries and territories in Southeast Europe is significant. The obtained results are in good agreement with former calculations by other authors (Ganev and Syrakov, 2002). In the comparison with officially published results from the status report of EMEP/MSC-W that the exchange of sulphur pollution between these countries is estimated in the correct order of magnitude, giving at the same time much more details in the time and space distribution of deposed quantities. Generally, the emissions, respectively the concentrations and depositions, decreased during the period, although with relative small rate. The author's conclusion is that the model produces a reasonable picture of the concentrations and depositions in the 25-km grid for the sulphur components in the region of Balkans.

The results of such calculations can be used in decision-making, negotiating and contamination strategies development.

## 6. ACKNOWLEDGEMENTS

The present work is supported by the BULAIR project (EVK2-CT-2002-80024) under FP5, ACCENT Network of Excellence (GOCE-CT-2002-500337) under FP6 and NATO Collaborative Linkage Grant EST.CLG 979794.

## REFERENCES

Barret, K., Berge, E., (Eds.) 1996, Transboundary Air Pollution in Europe, EMEP/MSC-W status report 1997, Part One and Two: Numerical Addendum, Norwegian Meteorological Institute, Oslo, Norway, pp. B3-B46.

Ganev K., Syrakov D., 2002 On some cases of extreme sulphur pollution in Bulgaria or Northern Greece. Bulg. Geoph. J.XXVIII № 1-4

Lövblad et al., (Eds.) 2004 EMEP Assessment Report, Part I,

Seinfeld, J. Athmospheric Chemistry and Physics of Air Pollution, 1986

Syrakov, D., 1995, On a PC-oriented Eulerian Multi-Level Model for Long-Term Calculations of the Regional Sulphur Deposition, in Gryning S. E. and Schiermeier F. A. (eds), Air Pollution Modelling and its Application XI, NATO - Challenges of Modern Society, Vol. 21, Plenum Press, N.Y. and London, pp. 645-646.

Syrakov, D., 1996, On the TRAP advection scheme - Description, tests and applications, in Geernaert G., Walloe-Hansen A. and Zlatev Z., Regional Modelling of Air Pollution in Europe. Proceedings of the first REMAPE Workshop, Copenhagen, Denmark, September 1996, National Environmental Research Institute, Denmark, pp. 141-152.

Syrakov, D., and Galperin, M., 1997a A model for airborne poli-dispersive particle transport and deposition, Proc. of 22nd NATO/CCMS International Technical Meeting on Air Pollution Modelling and its Application, 2-6 June 1997, Clermont-Ferrand, France, pp. 111-118.

Syrakov, D., and Galperin, M., 1997b On a new Bott-type advection scheme and its further improvement, in Hass H. and Ackermann I. J. <Eds.>, Proc. of the first GLOREAM Workshop, Aachen, Germany, September 1997, Ford Forschungszentrum Aachen, pp. 103-109.

Syrakov, D., and Prodanova, M., 1998, Bulgarian Emergency Response Models - Validation against ETEX First Release, Atmos. Environ., **32**, No. 24, pp. 4367-4375.

Syrakov, D., and Yordanov, D., 1996, On the surface layer parameterization in an Eulerian multi-level model, Proceedings of the 4th Workshop on Harmonisation within Atmospheric Dispersion Modelling for Regulatory Purposes, 6-9 May 1996, Ostende, Belgium, v.1

*Proceedings of the Third International Symposium on Air Quality Management at Urban, Regional and Global Scales. 26-30 September 2005, Istanbul – Turkey*

# RELATIVE IMPACT OF MOBILE SOURCE EMISSIONS ON A SEMI-ARID COASTAL URBAN AIRSHED

**Kuruvilla John[1], Zuber Farooqui[2] and Ronald K. Brown[3]**

1. Frank H. Dotterweich College of Engineering, Texas A&M University-Kingsville, MSC 188, Kingsville, Texas 78363, k-john@tamuk.edu
2. Department of Environmental and Civil Engineering, Texas A&M University-Kingsville, MSC 213, Kingsville, Texas 78363, zfarooqui@even.tamuk.edu
3. Department of Environmental and Civil Engineering, Texas A&M University-Kingsville, MSC 213, Kingsville, Texas 78363, rbrown@even.tamuk.edu

## ABSTRACT

A regional photochemical modeling was performed for a high ozone episode of September 1999 to evaluate the effectiveness of ozone control strategies in four near non-attainment areas (NNAs) of Texas. The Comprehensive Air quality Model with extensions (CAMx) was used as the photochemical model in this study. The Fifth-Generation NCAR/Penn State Mesoscale Model (MM5) was used for prognostic meteorological inputs, the Emissions Preprocessing System (EPS 2.0) was used for emission inputs, and MOBILE6.2 for mobile source emission inputs to the photochemical model. The NONROAD model was used for developing the non-road source emissions inputs to the EPS, while the marine vessel emissions were computed using EPA-approved methodology developed by Environ, Inc. A thorough analysis of the non-road source category revealed significant dock-side emissions from the hotelling of large ships and marine vessels at the Port of Corpus Christi. This study presents various sensitivity analyses using the photochemical model with respect to mobile source emissions. First, the sensitivity of modeled ozone to various emission sources was evaluated for the Corpus Christi urban airshed by zeroing out on-road and non-road mobile sources to assess mobile source impact on ozone formation as compared to other emission source categories. Mobile source emissions including on-road and non-road had the most impact on the ozone air quality within the Corpus Christi urban airshed. Additional sensitivity analysis related to on-road mobile source emissions were performed for various Reid Vapor Pressures (RVPs) and vehicle travel miles (VMTs) using MOBILE 6.2 coupled with the photochemical model. This study also evaluated the impact of spatial reallocation of on-road and non-road mobile sources. The analyses conducted in this study will allow local air quality planners to identify and develop innovative emissions control strategies for the region.

**Keywords:** Ozone, photochemical model, mobile emissions, MOBILE6.2, NONROAD, semi-arid, coastal urban airshed

*Proceedings of the Third International Symposium on Air Quality Management at Urban, Regional and Global Scales. 26-30 September 2005, Istanbul – Turkey*

# A FIRST APPROACH TO ESTIMATING AIR POLLUTANTS IN TURKEY USING AN AIR QUALITY MODEL

**Tayfun Kindap[a], Shu-Hua Chen[b], Alper Unal[c], M. Talat Odman[c] and Mehmet Karaca[a,d]**

[a] Eurasia Institute of Earth Sciences, Istanbul Technical University, 34469, Istanbul,TURKEY, kindap@itu.edu.tr
[b] Dept. of Atmospheric Science University of California, Davis, CA 95616, USA, shachen@ucdavis.edu
[c] School of Civil and Environmental Engineering, Georgia Institute of Technology, Atlanta, USA, talat.odman@itu.edu.tr
[d] Faculty of Mining, Istanbul Technical University, 34469, Istanbul, TURKEY, karaca@itu.edu.tr

## ABSTRACT

Most of the European countries have their own emission inventories, which gives them a chance to carry out detailed and more accurate research of air pollutants. However, we do not witness any activity in preparing a national emission inventory for Turkey. In the absence of such an inventory, regional-scale studies to depict the concentration of air pollutants have to rely on the EMEP/CORINAIR emission inventory. This inventory provides data covering all of Europe with a 50-km resolution. Recently, Kindap et al., (2005) used this inventory to show the long-range aerosol transport from Europe to Turkey.

In this study, we aim to estimate various air pollutant levels in the city of Istanbul during a specific winter episode. The city has the largest population and is one of the most polluted cities of Turkey. However, there has not been any comprehensive study, nor any regulation to fix and solve the air quality problem. This study may call Turkish authorities' attention to the problem. We developed a framework to model air quality in Europe using MM5 (i.e., for meteorological modeling) and CMAQ (i.e., for transport and chemistry modeling). It should be noted that we developed our own emission modeling techniques to process EMEP emissions. Model results underestimate the concentration of air pollutants over Istanbul as expected. A high-resolution national emission inventory is necessary to get more accurate results.

**Key Words:** Emission Inventory, Air Pollutants, MM5T, CMAQ.

## 1. INTRODUCTION

Air quality has become an important issue to societies since it strongly affects human health, and plays an important role in climate change. Since local emission of pollutants can be augmented significantly by long-distance transport, it is important

to take into account the transport effect when considering new policies aimed at improving air quality.

Numerous studies have examined the transport of gases and airborne pollutants (e.g., Lelieveld et al. 2002; Rodriguez et al. 2001; Kubilay et al. 2000; Toon et al. 1988; Westphal et al. 1988; Nickovic, and Dobricic, 1996; Kallos, et al. 1998; Hacisalihoglu et al. 1992), but the problem of pollutant transport from Europe to Northern and Western Turkey has received relatively little attention. Recently, a comprehensive study about this transport has already been carried out for PM10 and highly polluted cities in Eastern Europe have been demonstrated, which could be partially responsible for pollution events in Istanbul (Kindap et al., 2005). Yet, such a transport has contributed to two high pollution events that occurred in Istanbul, Turkey on 7-8 and 10-11 January, 2002 (Fig. 1). During these events, the atmospheric circulation over central Europe was dominated by a cold-core surface anti-cyclone, a climatologically favored feature during the cold season (Kallos et al. 1998). Air trajectories associated with this anti-cyclone were capable of transporting high concentrations of pollutants over long distances to Istanbul.

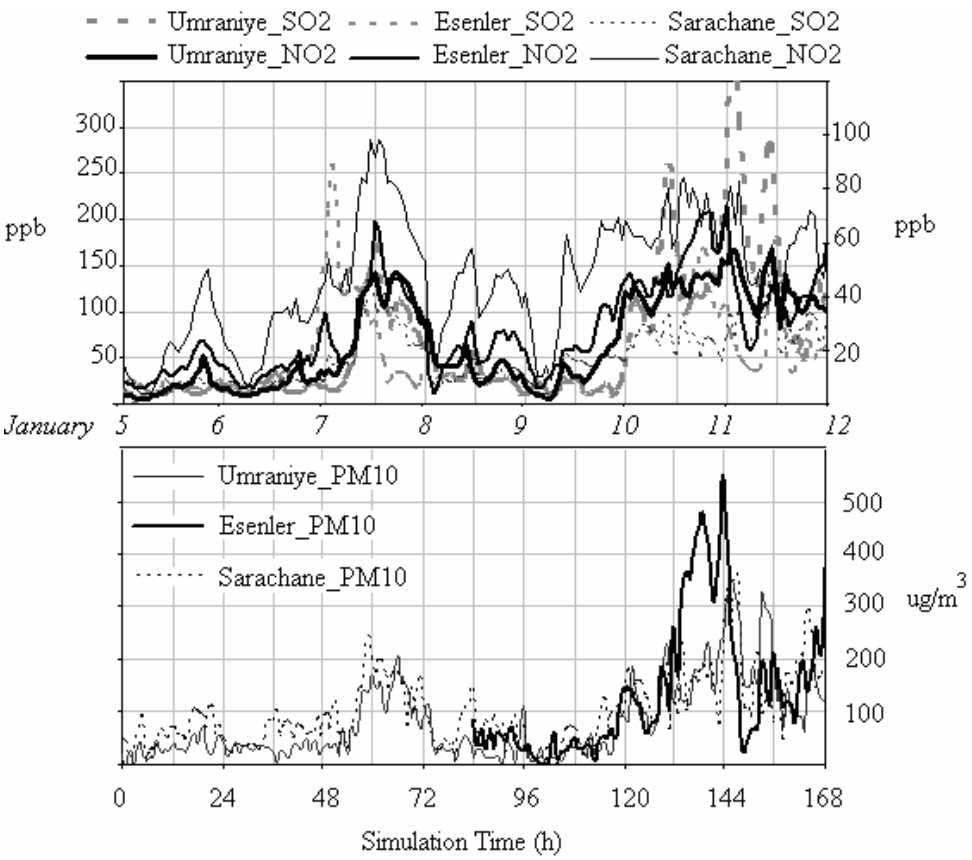


Figure 1. Time series of measured SO2 (left axis) and NO2 (right axis) concentration on the upper panel and PM10 concentrations (right axis) on the bottom panel at Umraniye, Esenler and Sarachane observation stations in Istanbul from 00 UTC January 5 to 00 UTC January12, 2002.

In the present case study, an episode of trans-boundary transport of nitrogen dioxide and sulfur dioxide was investigated. Ground-based measurements of NO2 and SO2 were compared with an air quality model and tracer studies. In this manner, the convective transport of gases and particulate matter within Eastern Europe and the resulting impact over the city of Istanbul was identified. The above mentioned long-range PM10 transport from Europe to Istanbul had already been investigated and the sensitivity analysis had put forward some quantitative results for consideration (Kindap et al., 2005).

It is observed that the lifetime of NO2 in the middle and upper troposphere is several days (Jaegl´e et al., 1998; Seinfeld and Pandis, 1998), which means that it is maintained even in the long-range transport (Stohl et al., 2002). On the other hand, NO2 has a relatively short (about one day) lifetime in the boundary layer (Jaegl´e et al., 1998). Leue et al. (2001) used vertical tropospheric NO2 column densities observed in the Global Ozone Monitoring Experiment over the eastern coast of North America to estimate a NO2 lifetime of 27 h in the PBL and following the plume leaving the coast of India, Kunhikrishnan et al. (2004) estimated a lifetime of 18 h. The lifetime of sulphur dioxide molecules in the troposphere is a few days. It is removed from the troposphere in gas phase by formation of sulfuric acid or directly by way of an uptake on aerosols and clouds.

## 2. METHODS

### Tracer Studies

To prove our hypothesis, we used an on-line tracer model to generate qualitative evidence of pollutant transport during these two pollution events. Furthermore, we used the meteorological parameters of the model to document the favorable weather conditions associated with these events.

The Fifth-Generation NCAR / Penn State Mesoscale Model (MM5; Grell et al. 1994) V3.6 on-line tracer model (MM5T) was used here. A single domain with grid-spacing of 30 km was configured, and it covered the entire European continent and nearby seas and countries. There were 176 x 227 x 38 grids in the east-west, north-south, and vertical directions, respectively. Tracers in MM5T were carried in a 4D array and the transport of tracers due to advection, MRF boundary layer mixing (Hong and Pan 1996), and Kain-Fritsch cumulus convection (Kain 2004) was taken into account. Other chosen physics options were the RRTM (Rapid Radiative Transfer Model) radiation scheme (Mlawer et al. 1997) and simple ice microphysics scheme (Dudhia 1989).

Two tracer simulations were conducted, experiment 1 (EXP1) and experiment 2 (EXP2), corresponding to the two peak events of pollutant concentration in Istanbul, 7-8 and 10-11 January 2002. Model integration run from 00 UTC 5 to 00 UTC 8 January for EXP1 and from 00 UTC 8 to 0 UTC 11 January for EXP2. The National Centers for Environmental Prediction (NCEP) Global Data Assimilation System (GDAS) data (with 2.5° latitude/longitude resolution) were used for MM5T boundary and initial conditions. To mimic emission characteristics, tracers were

released at the lowest model level from selected cities at time-varying rates. The selected cities were Warsaw, Silesia, and Krakow in Poland; Kiev in Ukraine; Moscow in Russia; Sofia and Plovdiv in Bulgaria; and Bucharest in Romania. These cities were chosen because they were potentially significant local sources of pollutants and they were positioned upstream of Istanbul on the dates in question.

Several characteristics of the simulated tracer emission are important to note. The emission was specified to vary over a daily cycle according to a half sine curve, with a maximum of about 0.1 units s-1 at 5 p.m. and a minimum of 0 units s-1 at 5 a.m. local time. The area of emission in each city had a radius of 100 km. To further understand the transport characteristics, tracers from the same city but different days (i.e., 00 UTC to 00 UTC next day) were tracked separately. Note that tracers released from Silesia and Krakow were not distinguished.

**Air Quality Model**

**Emission inventory:**
When the study was started, the best available emission datasets for this region was the 2001 EMEP, where the data were available as annual averages for each European country. The available data must, therefore, be processed to produce the inputs required by the air quality model, normally as hourly averaged gridded values. As a result, an emission processing module should be developed for this purpose. This kind of study was performed in a PhD thesis (Kindap, 2005). As a result of this study, the time series of PM10 over Istanbul for 3 days can be seen in figure 2 with an accompanying example of the emission model result.

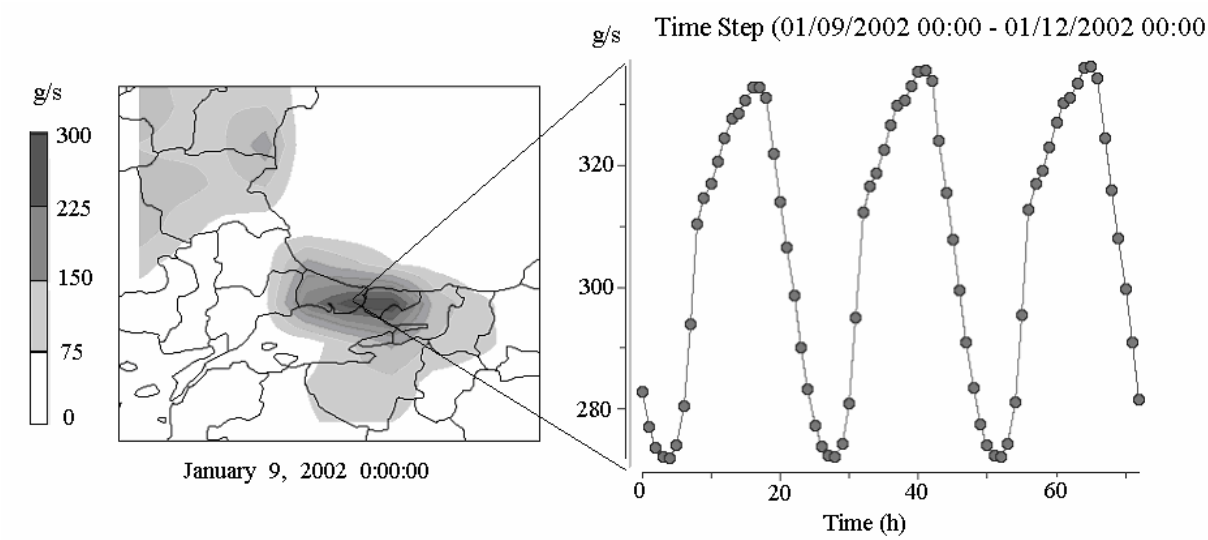


Figure 2. Time series of PM10 (g/s) over Istanbul according to the emission model (Adapted by Kindap, 2005).

Note that at present, the big part of the EMEP/CORINAIR (CO-oRdination d'Information Environnementale) Emissions Inventory is filled with expert

information from the main source categories of energy, transport, agriculture, production and processes. Furthermore, this dataset provides emissions for sole anthropogenic sources and a 50-km resolution.

**CMAQ Model:**
The CMAQ horizontal grid size was set to 50 km with 132 cells along the east-west direction and 111 cells in the north-south direction covering all of Europe. There were 20 layers in the vertical direction. The initial and boundary conditions were set to background concentrations starting from 00:00 UTC January 5, 2002 to 00:00 UTC January 12, 2002.

## 3. CASE STUDY – RESULTS AND DISCUSSION

After 24 h of integration in EXP1, a synoptic-scale circulation pattern that favors pollutant transport into Turkey is quite evident (Fig. 3). Specifically, a surface high-pressure center is positioned over central Europe while a surface low is located over western Russia. The pressure gradient between these two centers induces a strong boundary-layer flow into Turkey from the north-northwest, creating a mechanism for the transport of pollutants from upstream cities to Istanbul.

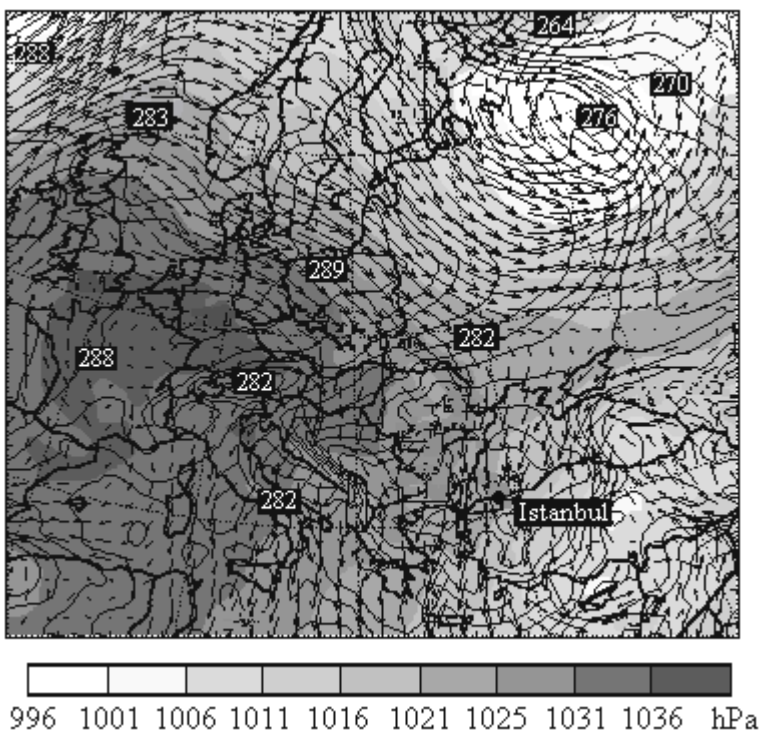


Figure 3. 24 h forecast from EXP1, showing sea level pressure (shaded; hPa), 1.5 km height potential temperature (solid lines; K), and 950-mb height wind vectors at 00 UTC 6 January, 2002. Large dot indicates the location of Istanbul.

Simulated tracer transport from various source cities can be seen in Fig. 4. For the first simulation period (00 UTC 5 January to 00 UTC 8 January), the tracer released from Bucharest on the first day (not shown) had little impact in Istanbul during the

first one and a half days. But the tracer released in Bucharest on the second day first reaches Istanbul at 18 UTC 6 January (about 18-h transport time) and gave the maximum pollution impact on the city at 00 UTC 7 January (dashed lines in Fig. 4a). Tracer released from Plovdiv, Bulgaria on the first day moved southward and did not pass over Istanbul, while the edges of the plumes released in Plovdiv on the second and third days skirted Istanbul and contributed relatively small concentrations of pollutants to the city.

Silesia and Krakow in Poland are relatively far away from Istanbul, yet tracers released from both cities on the first day reached Istanbul after about 42 h of transport (by 18 UTC 6 January). Silesia and Krakow tracers from the second day reached the city as well, arriving around at 12 UTC 7 with a higher concentration than the first day's plume. In our simulation, tracers released from other selected cities, such as Kiev, Sofia, and Warsaw, did not reach Istanbul due to the directions of low-level winds. For the second simulation period (00 UTC 8 January to 00 11 January), the evolution of tracers predicted by MM5T was also similar (Figs. 4b), however, tracers take slightly longer to propagate to Istanbul in this second period.

a) b)

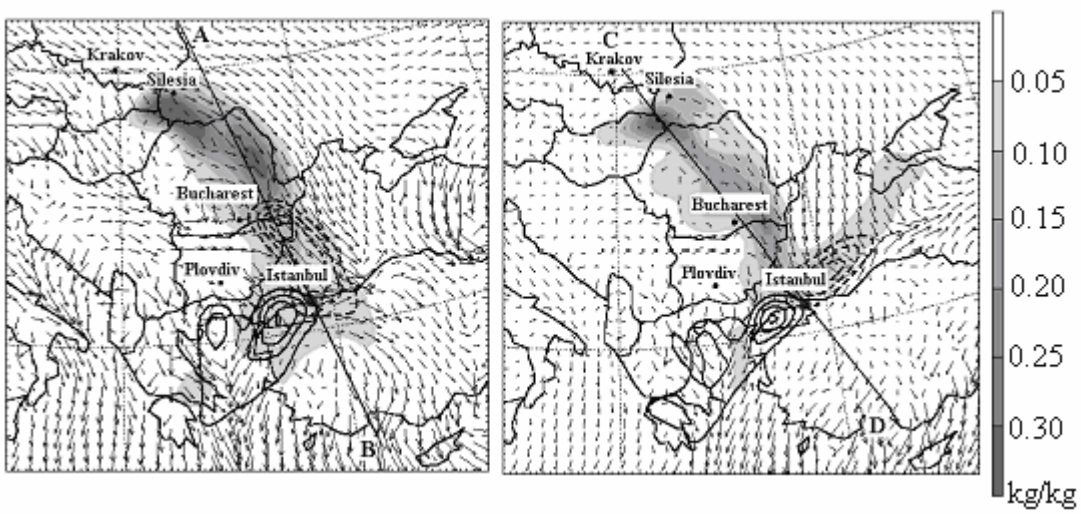


Figure 4. Simulated tracers and wind vectors at the 100 m height at (a) 48-h simulation from EXP1 and (b) 54-h simulation from EXP2. Tracers from Bucharest (dashed lines; 0.05 unit of interval) and Plovidiv (solid lines; 0.1 unit of interval) are released during the 2nd day and from Silesia and Krakow (shaded) are released during the first 2 days.

As for CMAQ Model, model simulated NO2 and SO2 concentrations were compared with those measured at three stations in Istanbul (Fig. 5). The locations of these stations have been chosen on road or industry area of the city without any scientific approach by the authorities. As a result, high concentrations of pollutants could be observed from time to time by the stations. It is worth to mention that there are 10 stations in Istanbul, but only three of them have complete data for the simulation period.

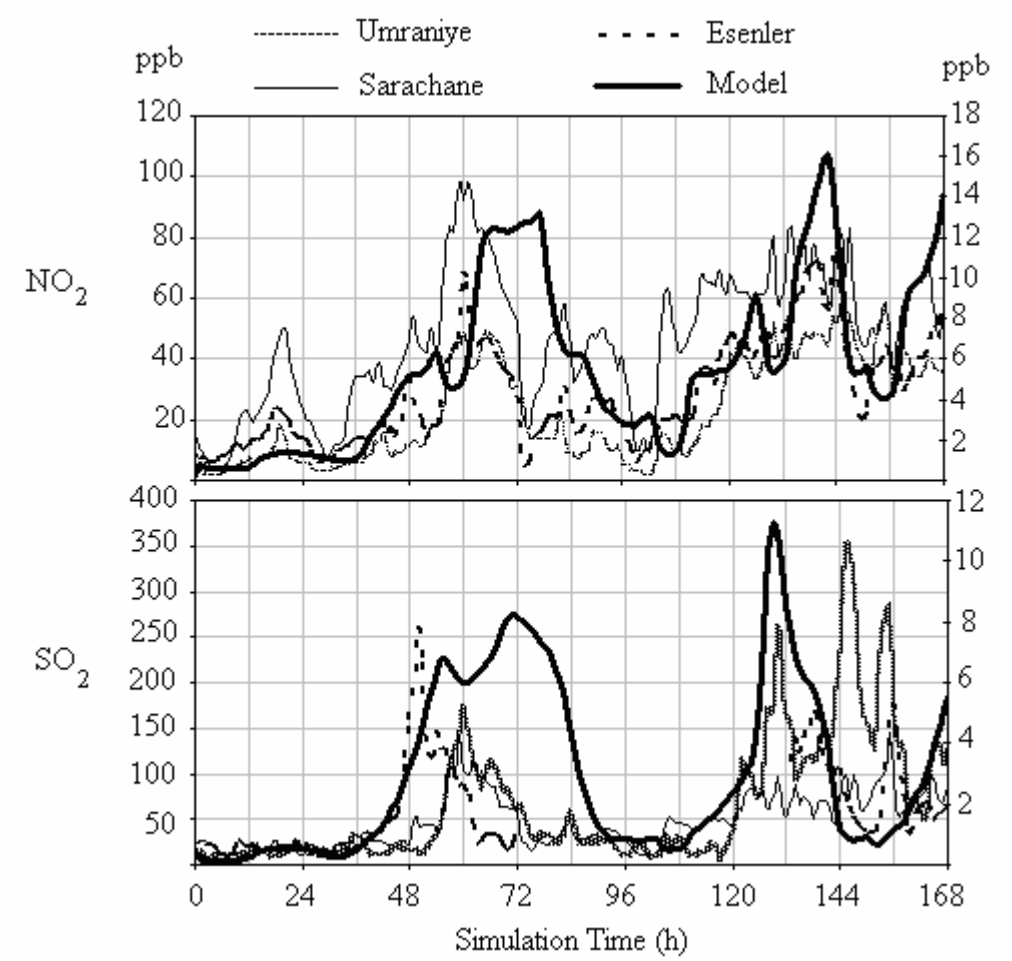


Figure 5. Time series of observed NO2 and SO2 concentrations at Umraniye, Sarachane and Esenler stations in Istanbul (left axis) and model simulated concentrations (right axis) for the 50×50km2 Istanbul cell from 00 UTC January 5 to 00 UTC January12, 2002.

It can be clearly seen in the figure that the trend is captured reasonably well by the air quality model. On the other hand, it is not possible to put forward the similar outcome for the comparison of concentrations of the model and the stations. The difference between the simulated and observed concentrations, which is expected, is noticed at the first glance. The primary reason for this discrepancy is most likely the coarse grid resolution. The first model layer above the ground is 92m and the horizontal resolution is 50 km.

This coarse resolution can substantially dilute the concentration of pollutants. The discrepancies may also be due to the deficiencies in EMEP emission data. The annual emission inventory data are based on data reported from the European countries, and these data are filled with experts' estimates when they are incomplete or inconsistent. Such interpretations may introduce errors. Furthermore, natural emissions are absent in EMEP database. In addition, the use of 2001 emission data

(instead of 2002 data, which were not available during the study) in combination with a January 2002 meteorological episode resulted in added uncertainty when comparing the CMAQ model results to monitoring data. For the most part, CMAQ correctly reproduces the trends in observed NO2 and SO2 values for Istanbul. For example, the model is able to catch the relatively high-pollution episodes on January 7 and January 10.

## 4. CONCLUDING REMARKS

Two high-pollution events that occurred in Istanbul, Turkey on 7-8 and 10-11 January, 2002 were studied qualitatively using the MM5 on-line tracer model (MM5T). Different tracers were used to represent pollutants released from selected cities on different days, using a diurnal cycle of emission rates that maximized at 5 p.m. and approached zero at 5 a.m. local time.

The first step in analyzing model results was to verify accurate simulation of meteorological fields, especially the low-level wind fields that play a crucial role in transport calculations. Time-series of low-level wind and temperature fields in the vicinity of Istanbul had showed a good agreement with local observations of the previous study (Kindap et al., 2005). Furthermore, the model also reproduced the larger-scale patterns well. In particular, it simulated a surface high-pressure system over central Europe and a surface low over western Russia, with a substantial pressure gradient between these two systems. This gradient induced strong north-northwesterly low-level flow, capable of transporting upstream pollutants towards Istanbul. Moreover, the model reproduced a strong frontal inversion over the path of tracer transport, a feature that suppressed mixing at the top of the planetary boundary layer and effectively trapped low-level pollutants near the ground. These weather conditions created a favorable environment for limited dilution and long-range transport of pollutants.

The simulated tracer evolution provided qualitative proof that transport of pollutants emitted from Bucharest in Romania, Plovdiv in Bulgaria, and Silesia and Krakow in Poland could have contributed to two high-pollutant events on 7-8 and 10-11 January, 2002 in Istanbul. Our model suggests that pollutant transport to Istanbul took about one day from Bucharest and Plovdiv and about two days from Silesia and Krakow during these events.

Results obtained from this tracer study are very reasonable and qualitatively support our hypothesis that the long-range transport from the north and northwest played an important role in both high pollutants events in Istanbul in January 2002. Transports nearby from the cities like Odessa, Sevastopol of Ukraine have been studied by various researchers (Kallos et al. 1998). But there is no work done on transports from Central Europe to the vicinity that we are concerned with, yet. This work is the first study on this matter. This study is a very preliminary, qualitative work to understand the causes of these two high pollution events.

Having in mind that a fine emission inventory for the area of interest is difficult to find, it is not entirely reliable. Therefore, these types of qualitative studies are quite useful to understand transports of gases or aerosols in the region.

A quantitative study of pollution arising from local emissions and long-range transports for both pollution events has also been studied using an air pollution model. It is a well-known fact that a regional air quality approach will not give any details of air quality over a city. As a result, the large model underestimation of Istanbul NO2 and SO2 is not surprising for the regional model which is not designed to simulate urban concentration.

Although Istanbul has the largest population and is one of the most polluted cities of Turkey, there has not been any comprehensive study nor any regulation to fix and solve the air quality problem. Using the EMEP emission inventory which is the only available data, we aim to estimate various air pollutant levels in the city of Istanbul during a specific winter episode. Model results underestimate the concentration of air pollutants over Istanbul as expected, but the trend is captured reasonably well. A high-resolution national emission inventory is necessary to get more accurate results. This study may call Turkish authorities' attention to the problem.

## 5. ACKNOWLEDGEMENTS

The authors (Kindap T. and Karaca M) appreciate ITU Scientific Research Fund and TUBITAK for their support.

## REFERENCES

Dudhia, J., 1989: Numerical study of convection observed during the winter monsoon experiment using a mesoscale two-dimensional model. J. Atmos. Sci., 46, 3077-3107.

Grell, G. A., J. Dudhia, and D. R. Stauffer, 1994: A description of the fifth-generation Penn State/NCAR mesoscale model (MM5). NCAR/TN-398+STR, National Center for Atmospheric Research, Boulder, CO, 122 pp.

Hong, S.-Y., and H.-L. Pan, 1996: Nonlocal boundary layer vertical diffusion in a medium-range forecast model. Mon. Wea. Rev., 124, 2322-2339.

Kain, J. S., 2004: The Kain-Fritsch convective parameterization: An update. J. Appl. Meteor., 43, 170-181.

Hacisalihoglu, G., Eliyakut, F., Olmez, I., Balkas, T. I., Tuncel, G., 1992. Chemical composition of particles in the Black Sea atmosphere. Atmospheric Environment 26A, 3207-3218.

Jaegl´ e, L., Jacob, D. J., Wang, Y., Weinheimer, A. J., Ridley, B. A., Campos, T. L., Sachse, G. W., and Hagen, D. E.: Sources and chemistry of NOx in the upper troposphere over the United States, Geophys. Res. Lett., 25, 1705–1708, 1998.

Kubilay, N., S. Nickovic, C. Moulin, and F. Dulac, 2000: An illustration of the transport and deposition of mineral dust onto the eastern Mediterranean. Atmos. Environment, 34, 1293-1303

Kunhikrishnan, T., Lawrence, M. G., von Kuhlmann, R., Richter, A., Ladst¨atter-Weissenmayer, A., and Burrows, J. P.: Analysis of tropospheric NOx over Asia using the model of atmospheric transport and chemistry (MATCH-MPIC) and GOME-satellite observations, Atmos. Envir., 38, 581–596, 2004.
Kallos, G., V. Kotroni, K. Lagouvardos, and A. Papadopoulos, 1998: On the long-range transport of air pollutants from Europe to Africa. Geophysical Research Letters, 25, 619-622.
Kindap, T., 2005. Long-range Aerosol Transport from Europe to Istanbul, Turkey, 2005, PhD Thesis, Istanbul Technical University, Turkey.
Kindap, T., Unal, A., Chen, S. H., Tao, Y., Odman, M. T., Karaca, M., Long-Range Aerosol Transport from Europe to Istanbul, Turkey, Atmospheric Environment, In review.
Lelieveld, J., Berresheim, H., Borrmann, S., Crutzen, P. J., Dentener, F. J., Fischer, H., Feichter, J., Flatau, P. J., Heland, J., Holzinger, R., Korrmann, R., Lawrence, M. G., Levin, Z., Markowicz, K. M., Mihalopoulos, N., Minikin, A., Ramanathan, V., de Reus, M., Roelofs, G. J., Scheeren, H. A., Sciare, J., Schlager, H., Schultz, M., Siegmund, P., Steil, B., Stephanou, E. G., Stier, P., Traub, M., Warneke, C., Williams, J., Ziereis, H., 2002. Global Air Pollution Crossroads over the Mediterranean. Science 298: 794-799
Leue, C., Wenig, M., Wagner, T., Klimm, O., Platt, U., and Jahne, B.: Quantitative analysis of NOx emissions from Global Ozone Monitoring Experiment satellite image sequences, J. Geophys. Res., 106, 5493–5505, 2001.
Mlawer, E. J., S. J. Taubman, P. D. Brown, M. J. Iacono, and S. A. Clough, 1997: Radiative transfer for inhomogeneous atmosphere: RRTM, a validated correlated-k model for the long-wave. J. Geophys. Res., 102 (D14), 16663-16682.
Nickovic, S., and S. Dobricic, 1996: A model for long-range transport of desert dust. Mon. Wea. Rev., 124, 2537–2544
Rodriguez, S, X. Querol, A. Alastuey, G. Kallos, and O. Kakaliagou, 2001: Saharan dust contributions to PM10 and TSP levels in Southern and Eastern Spain. Atmos. Environment, Vol. 35, no. 14, pp. 2433-2447. 2001.
Seinfeld, J. H. and Pandis, S. N.: Atmospheric chemistry and physics – from air pollution to climate change, John Wiley & Sons, New York, 1998.
Stohl, A., Eckhardt, S., Forster, C., James, P., and Spichtinger, N.: On the pathways and timescales of intercontinental air pollution transport, J. Geophys. Res., 107, art. no. 4684, 2002.
Toon, O.B., R. P. Turco, D. Westphal, R. Malone, M. Liu, 1988: A multidimensional model for aerosols: Description of computational analogs. J. Atmos. Sci., 45, 2123–2144
Westphal, D.L., O. B. Toon, and T. N. Carlson, 1988: A case study of mobilisation and transport of Saharan dust. J. Atmos. Sci., 45, 2145–2175

*Proceedings of the Third International Symposium on Air Quality Management at Urban, Regional and Global Scales. 26-30 September 2005, Istanbul – Turkey*

# DAILY FORECAST OF AIR QUALITY OVER EUROPE WITH THE EURAD MODEL SYSTEM

**Hermann Jakobs, Michael Memmesheimer and Adolf Ebel**

Rhenish Institute for Environmental Research at the University of Cologne, EURAD project, Aachenerstr. 201-209, 50931 Cologne, Germany,
Hermann.Jakobs@eurad.uni-koeln.de

## ABSTRACT

A real-time forecast system for atmospheric pollutants is presented. The forecast system is based on the EURAD Model (European Air Pollution Dispersion Model). The daily updated forecast of atmospheric constituents for Europe, Central Europe and the German State of Northrhine-Westfalia was tested and is quasi operational since June 2001. The whole forecast system includes the meteorological forecast (MM5) and an updated Emission data base for the above mentioned regions. The results of the forecasts on the different regions are published and are updated every day on the EURAD homepage **www.eurad.uni-koeln.de**.

**Key Words:** Air Quality Forecast, Air Quality Modeling, Ozone Concentration, Suspended Particulate Matter

## 1. INTRODUCTION

Regional and local air quality models have become an important tool for environmental research and application to environmental assessment and policy questions. On one hand it is important to use air quality models as a tool to understand the simulations carried out with them, and on the other side, evaluated, highly improved models should be used to forecast atmospheric pollutants in an operational state.
Since summer 2001 a real-time forecast system based on the EURAD Model was tested and established to predict the main atmospheric pollutants on different scales in Europe. Fig. 1 describes the forecast system as it was used for these purposes. The EURAD Air Quality Forecast System consists mainly of the mesoscale meteorological model MM5 (PennState/NCAR mesoscale model Version 5), the emission processor EEM (EURAD Emission Model) and the EURAD Chemistry Transport Model (EURAD-CTM). The initial and boundary data for MM5 are obtained from the global GFS forecast (NCEP) at the start of the forecast cycle (00 UTC). The emission data are interpolated from the EMEP data base in time and space for 3 different regions of interest: Europe (N0), Central Europe (N1) and the German state Northrhine-Westfalia (N2) (Fig. 2). In addition to the predicted gas phase concentrations, aerosol particles are also forecasted during the cycle.

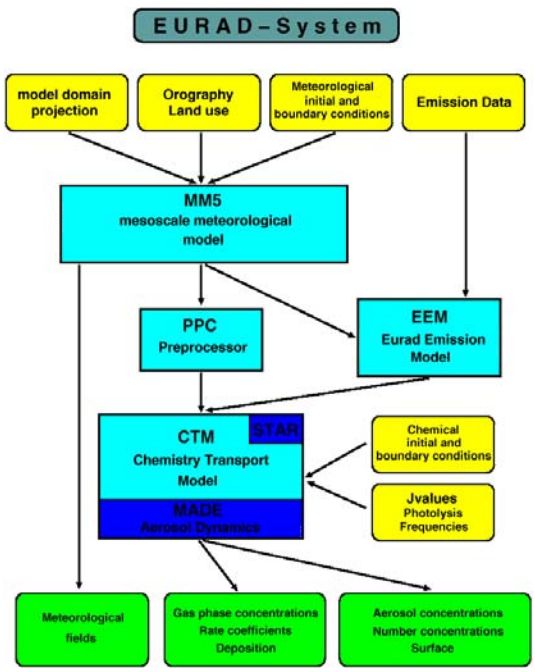


Figure 1. The flowchart of the EURAD Air Quality Forecast System

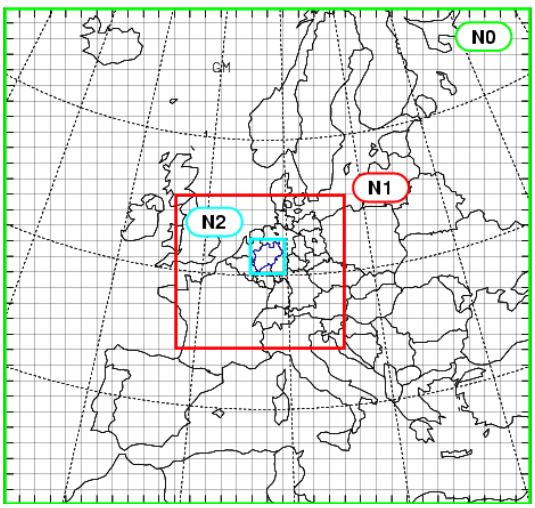


Figure 2. Domains of the EURAD Air Quality Forecast System

## 2. OBJECTIVES AND ACTIVITIES

During the last few years, one major goal in environmental research is to establish a forecast system to predict atmospheric pollutants (Jakobs et al., 2002). Since about 15 years the EURAD model was developed and improved for applications within numerous case studies on the regional scale in Europe (e.g. Jakobs et al., 1995; Ebel et al., 1997, Elbern and Schmidt, 2001). The main purpose of the predictions was to answer the following questions: How reliable are the predictions and how can they be improved? Can short-term measures on a local scale confirm an excess of the ozone concentration and other major constituents limits, if such an excess is predicted?

The EURAD air pollution forecast system starts with first tests in spring 2001. It becomes quasi operational in June 2001. The system starts automatically with the download of the GFS global meteorological forecast via ftp at around 03:30 UTC every morning. Then the initial and boundary conditions are prepared for the meteorological model MM5 for the coarse domain (Europe) to predict the meteorological variables for a forecast cycle of 72 hours. Together with the selected emission data for the selected time and domain, the EURAD-CTM predicts the concentrations for the atmospheric constituents. Then the forecast for the first nested domain (Central Europe) continues. A second nested domain, which covers the region of the German state Northrhine-Westfalia, was included in the forecast cycle. In addition, the full aerosol option of the EURAD-CTM was applied for the

chemistry transport calculations and the integrated prognostic variable $PM_{10}$ (particle matter with diameter less than 10 micrometer) was included as displayed variable. With all these improvements it is now possible to predict every day the concentration of atmospheric pollutants within a sufficient time range, e.g. the whole forecast starts at 03:30 UTC and is finished at around 08:30 UTC every morning and the results are updated and displayed on the EURAD web side (www.eurad.uni-koeln.de).

## 3. RESULTS

Every day, an extensive amount of data is produced by the EURAD forecast system. This includes the meteorological prediction variables and the concentrations of the atmospheric constituents at all model levels as well. In order to compare later especially the concentrations of air pollutants main effort was done to visualize the near surface concentrations of the main air pollutants $O_3$, $NO_2$, $SO_2$, CO and $PM_{10}$ for the above mentioned domains. For assessment studies the ranges for the concentration thresholds were selected according to the EU directives. Since photo oxidant processes play no important role during winter, as an example the results for the near surface concentrations of $PM_{10}$ are displayed for February 09, 2002 (Figure 3). This date was characterized by a blocking high over Central Europe, which allow accumulating air pollution concentration up to critical levels (higher than 50 $\mu g/m^3$ for the maximum 24h running mean).

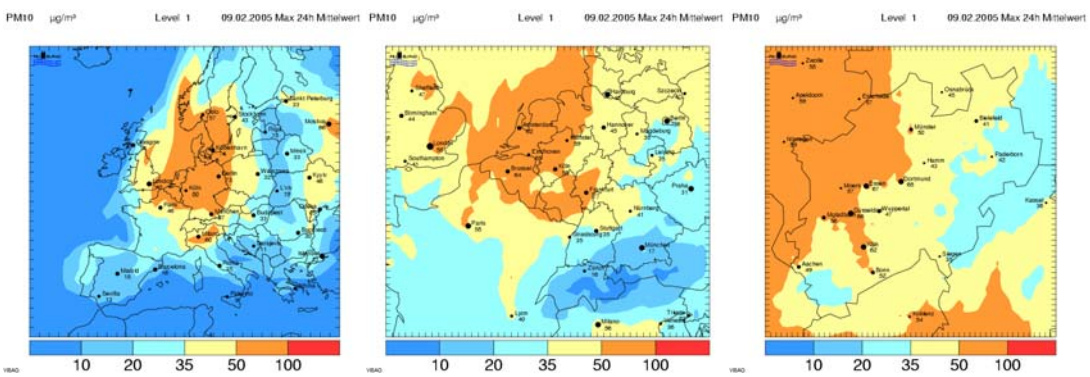


Figure 3. Near surface concentrations (maximum 24h running mean) of $PM_{10}$ ($\mu g/m^3$) for the different domains at 09 February 2005.

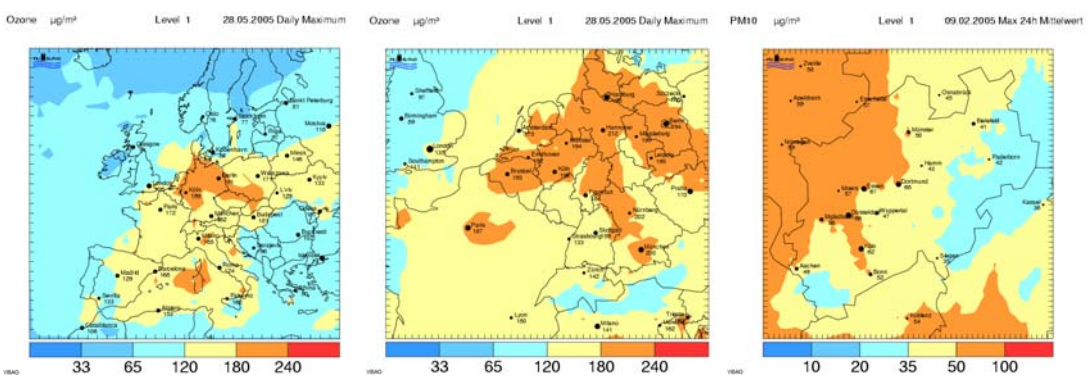


Figure 4. Near surface concentrations (daily maximum) of Ozone ($\mu g/m^3$) for the different domains at 28 May 2005.

During springtime, photo oxidant processes become more relevant and the first minor summer smog episodes were observed. Fig. 4 demonstrates one of these episodes, where relatively high ozone concentrations were forecasted. The thresholds for the information level according to EU directives (180 µg/m$^3$) were exceeded for main parts of Central Europe.

In order to evaluate the forecast system, we recently established a verification tool, where the predicted daily maxima and daily means of the concentrations in the domain N1 are compared with certain measuring sites of Germany. The forecast values are taken as first guess for a 2-d variational data assimilation procedure to calculate analyzed fields for the near surface concentrations. Fig. 5 displays the comparison of predicted, observed and analyzed concentrations in the region of Germany for a selected day with high ozone concentration.

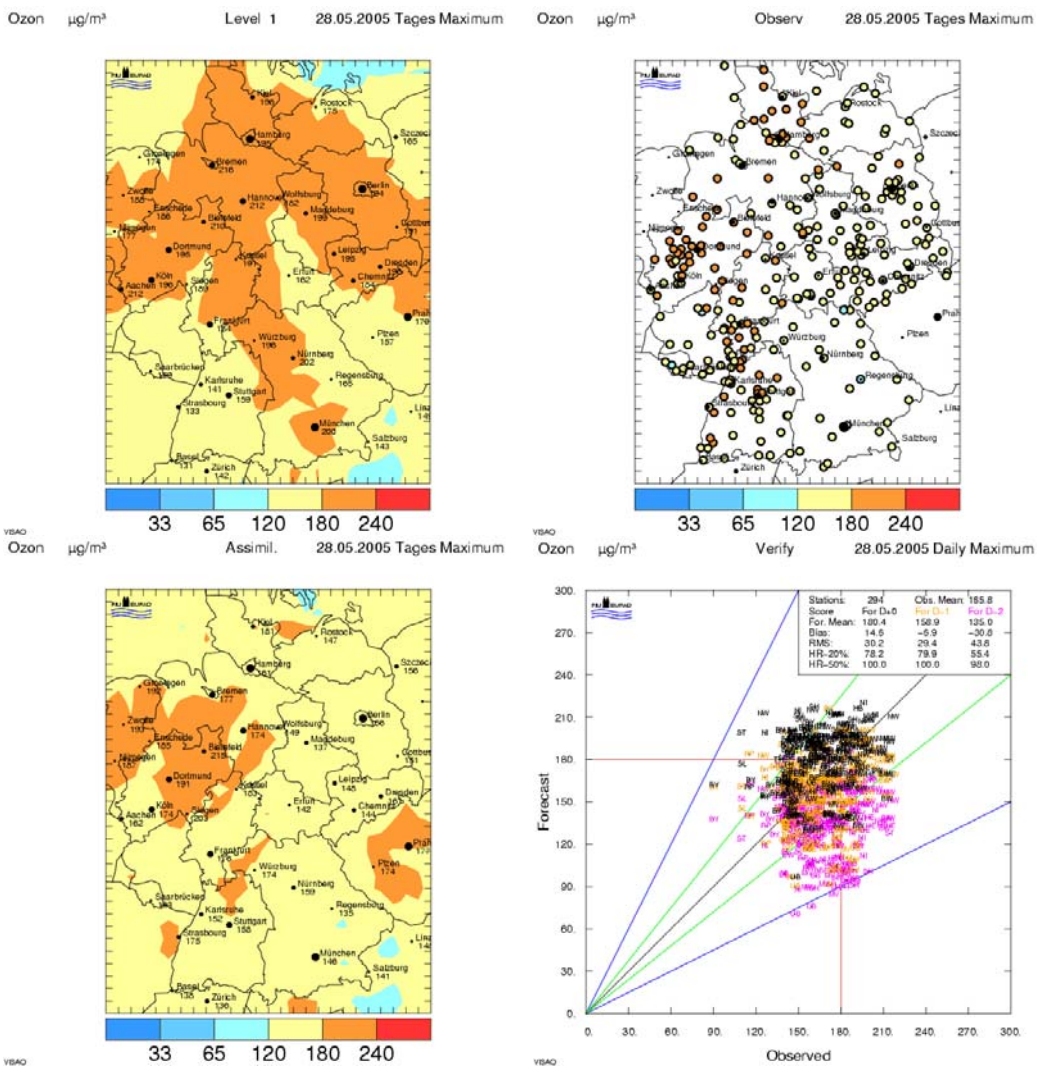


Figure 5. Validation of the forecast: Daily maximum of ozone for 28 May 2005. upper left, forecast; upper right, observation at stations; lower left, analysis; lower right, scatter diagram for forecast at the same day (D+0), a day before (D-1) and a 2 days before (D-2).

This Figure demonstrates the relative good performance of the prediction of the near surface ozone concentrations at days with high critical levels. In general, there is a relative good agreement between observations and predictions (e.g. almost 100 % of the predicted ozone concentration lay within a 50% interval of the observations and around 80% lay within a 20% interval of the observations). An intensive evaluation of the whole year 2005 will follow up in the near future.

## 4. CONCLUSION

A new air quality forecast system based on the EURAD model was established in order to predict every day the concentration of atmospheric pollutants over Europe, Central Europe and the German state of Northrhine-Westfalia. The fact, that such a complex model system was developed and established for operational purposes, including a complex aerosol model together with a relatively short computational time, was the main success of these developments. It can be easily used for assessment studies and good be an appropriate tool for policy making institutions.

## 5. ACKNOWLEDGEMENTS

We like to thank all the colleagues of the EURAD group, who contributed to the results of the implementation of the forecast model system. This project was partially funded by the Federal Ministry of Education and Research (BMBF). The forecast system was additionally supported by the State Environmental Agency (LUA) of the German state Northrhine-Westfalia and by the ESA GMES Service PROMOTE.

## REFERENCES

Ebel, A., H. Elbern, H. Feldmann, H.J. Jakobs, C. Kessler, M. Memmesheimer, A. Oberreuter, G. Piekorz, 1997. Air Pollution Studies with the EURAD Model System (3):EURAD - European Air Pollution Dispersion Model System. Mitteilungen aus dem Institut für Geophysik und Meteorologie, Universität zu Köln, Nr. 120.

Elbern, H., H. Schmidt, 2001. Ozone episode analysis by four-dimensional variational chemistry data assimilation. J. Geophys. Res., 106, No. D4, 3569-3590.

Jakobs, H.J., H. Feldmann, H. Hass, M. Memmesheimer, 1995. The use of nested models for air pollution studies: an application of the EURAD model to a SANA episode. J. Appl. Meteor., Vol. 34, No. 6, 1301-1319.

Jakobs, H.J., S. Tilmes, A. Heidegger, K. Nester and G. Smiatek, 2002. Short-term ozone forecasting with a network model system during Summer 1999. Journal of Atmos. Chem. 42, 23-40.

*Proceedings of the Third International Symposium on Air Quality Management at Urban, Regional and Global Scales. 26-30 September 2005, Istanbul – Turkey*

# SCALE INTERACTIONS IN LOCAL, URBAN AND REGIONAL AIR QUALITY MODELLING

**C. Mensink, K. De Ridder, F. Deutsch, F. Lefebre and K. Van de Vel**

VITO - Centre for Integrated Environmental Studies
Boeretang 200, B-2400 Mol, Belgium
clemens.mensink@vito.be

## ABSTRACT

Air quality modeling can help us to improve our understanding of scale interactions related to meteorology, transport, emissions, formation and removal and other processes taking place at local urban and regional scales. For the local scale we use a coupling of a street canyon model and the Gaussian dispersion model to study the interactions of emissions and concentrations in urban streets and surrounding urban neighborhoods. For the urban scale, the AURORA model has been applied successfully in assessments of urban air quality in the entire cities or urbanized areas like the Ruhr area in Germany. The model can calculate ozone and $PM_{10}$ concentrations for various land use scenario's revealing the impact of urban sprawl and the use of green areas. For the regional scale, the EUROS model is used to study the urban and regional scale interactions that are important in simulating concentrations of ozone, $PM_{2.5}$ and $PM_{10}$.

**Key Words:** Air Quality Modelling, Scale Interactions, Urban Air Pollution, Street Canyons, Particulate Matter.

## 1. INTRODUCTION

In Northwest Europe more than 80% of the population is living in cities or towns. Clean air is essential to this urban life. However, more than 70% of large European cities fail to meet air quality standards set by the World Health Organisation. It is obvious that people in urban areas are increasingly concerned about this, especially since the growing awareness of the possible health impacts of exposure to air pollution. Urban air quality is strongly related to other important elements that determine the quality of the urban environment, like accessibility and opportunities for economic activities, social interaction and recreation (green areas, open space). Air quality management is therefore a difficult and interdisciplinary task which often goes beyond the limits of the urban scale.

Scale interactions can also be found back in the physical context. Local emissions sources form traffic or industrial activities have a major impact on the urban air quality. Cities have a significant impact on urban and regional air quality up to 10-100 km because of their particular surface characteristics and because of high emissions of several pollutants. Atmospheric circulation created by the city itself (e.g. as an urban heat island) directly affect the dispersion of these pollutants. On the

other hand it is known that the majority of Europe's total urban population is exposed to high levels of ozone concentrations and particulate matter. These concentration levels are in many cases largely determined by regional scale processes.

The objective of this contribution is to show how we can improve our understanding of some of these scale interactions by studying the local emission control measures on pollutant concentrations in and around urban areas. Important questions that will be addressed are:

- How are the local urban concentrations affected by traffic emission reductions in surrounding street canyons and high ways?
- How does urban air quality benefit from green spaces and open spaces in the city?
- To what extend are PM concentrations in urban areas determined by regional processes?

## 2. METHODOLOGY

Over the past decade, we developed several modelling tools to assess air quality at various scales, ranging from the local scale to the continental scale with urban and regional scales in between. The models were developed, improved and implemented to estimate environmental risks and perform various assessment studies for the Flemish, Belgian and European administrations, as well as for industrial companies.

### 2.1 Local scale modeling

Gaussian models are widely accepted as tools for local air quality assessment. They are used in assessing the environmental impact of certain private or public initiatives. For regulatory purposes, environmental impact studies and more specific impact studies in Flanders, the IFDM model is used (Cosemans et al., 1997).

In order to study the interactions of emissions and concentrations in a specific urban street on one hand and the emissions and concentrations in the surrounding urban neighborhood on the other hand, a novel approach has been developed consisting in the coupling of a street canyon model (OSPM, Berkowicz, 1998) and the Gaussian IFDM model (Mensink and Cosemans, 2005). OSPM computes the contribution of the traffic emissions inside a particular street, whereas IFDM computes the background contributions, including the concentration levels caused by the surrounding streets, industrial stacks and domestic heating within a domain with a 20-30 km radius. Both models are interacting and have been integrated into an advanced computer program.

### 2.2 Urban scale modeling

On an urban scale the AURORA model (Mensink *et al.*, 2001) is used as an urban air quality management tool that can provide reliable answers to policy makers and traffic planners. This urban air quality management system has been designed for urban and regional policy support and reflects the state-of-the-art in air quality modelling, using fast and advanced numerical techniques. The model input consists of terrain data (orography, land use, road networks, remote sensing), meteorological fields and detailed emission data. Meteorological input data are provided with a resolution up to a few hundred meters by a separate meteorological model (ARPS). The emission input data are resulting from a detailed inventory and acquisition of existing emission data in combination with emission modelling (Mensink *et al.*, 2000). In this way the emissions are described as a function of space, time and temperature.

The AURORA model was successfully applied for assessment of urban air quality in the cities of Antwerp and Ghent in Belgium, and furthermore in Budapest in Hungary and in the Ruhr area in Germany. It also contributed to the EU 5$^{th}$ framework projects DECADE (http://www.cle.de/umwelt/decade/edecade.htm) and BUGS (Benefit of Urban Green Spaces) (http://www.vito.be/bugs/) (De Ridder *et al.*, 2004).

### 2.3 Regional scale modelling

On the regional scale the operational Eulerian air quality model EUROS was extended with two special modular algorithms for atmospheric particles. The first module is the Caltech Atmospheric Chemistry Mechanism (CACM, Griffin et al., 2002), being the first mechanism in describing the formation of precursors of secondary organic aerosols in the atmosphere in a mechanistic way. The second module is the Model of Aerosol Dynamics, Reaction, Ionization and Dissolution (MADRID 2, Zhang et al., 2004), which treats the formation of secondary aerosols through equilibrium calculations between the gas phase and the aerosol phase for inorganic (ISORROPIA) and hydrophilic and hydrophobic organic compounds (AEC-SOA-module). Also dynamic processes (e.g. nucleation) are included in MADRID 2. The chemical composition is expressed in terms of 7 components: ammonium, nitrate, sulphate, primary inorganic compounds, elementary carbon, primary organic compounds and secondary organic compounds (SOA).

The Caltech Atmospheric Chemistry Mechanisms (CACM) comprises 361 reactions among 122 components. CACM contains besides the complete ozone chemistry also the reactions of various generations of organic compounds during which semi-volatile reaction products are formed which can equilibrate into the solid phase. 42 of these condensable products are treated in CACM, all of them reaction products of anthropogenic and natural organic compounds, e.g. terpenes. Various routines of EUROS (e.g. VOC-split, background concentrations) were adjusted to CACM.

## 3. RESULTS

### 3.1 Local scale modeling

The coupled system OSPM/IFDM was applied to a city quarter in Ghent, Belgium. For this exercise, traffic emissions were obtained dynamically from the traffic simulation model Paramics. The dynamic emission allocation is derived by VITO from emissions measurements (Mensink et al., 2005) and is used to calculate for each time step and for each car, the emission of 5 pollutants (PM, CO, $NO_x$, VOC and $CO_2$) depending on the car's category, speed and acceleration. Figure 1 shows the yearly averaged $PM_{2.5}$ concentrations for 2003. Results show that the background contribution from a nearby highway exit is dominant in streets where low traffic is observed, but even in cases of moderate traffic, the local background concentration is substantial.

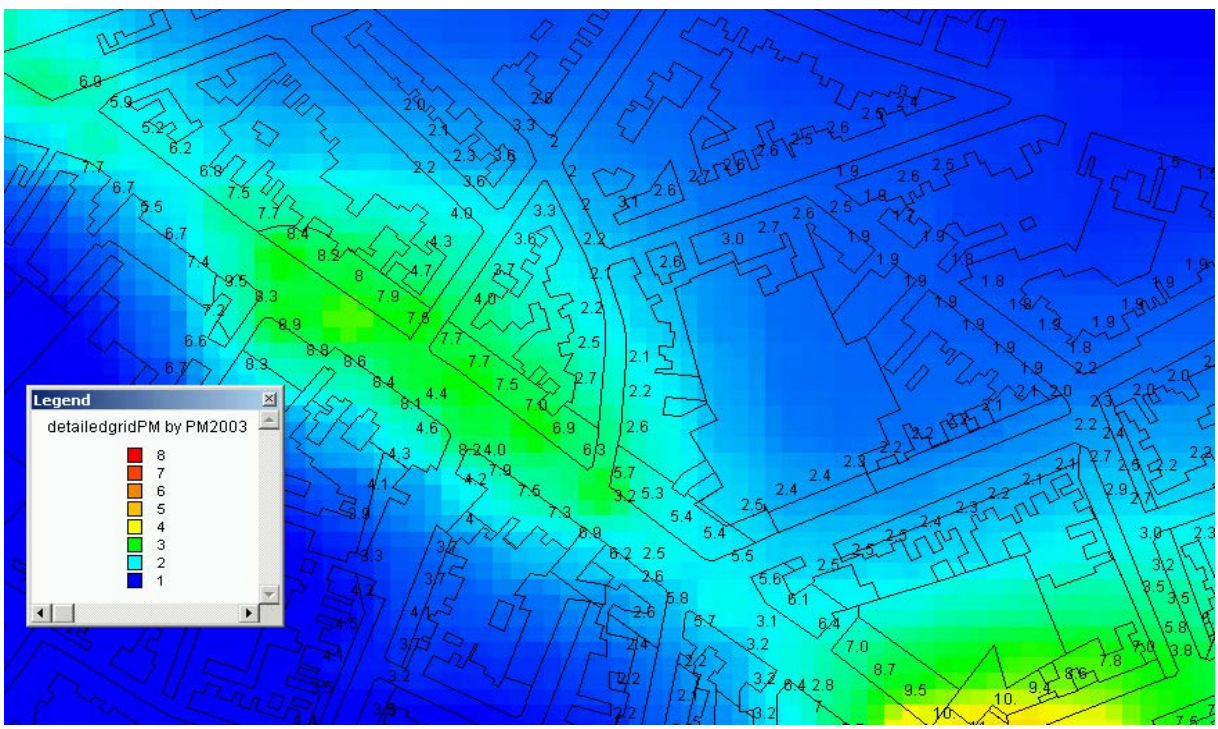


Figure 1. Predicted concentrations of $PM_{2.5}$ (2003) in the city quarter of Gentbrugge. Numbers show the $PM_{2.5}$ concentrations inside street canyons. Colours show the $PM_{2.5}$ concentrations outside street canyons.

### 3.2 Urban scale modeling

Application of the AURORA model to the German Ruhr area reveals that the re-distribution of green areas have a considerable impact. This was studied by comparing two different urban sprawl scenario's representing different developments in jobs,

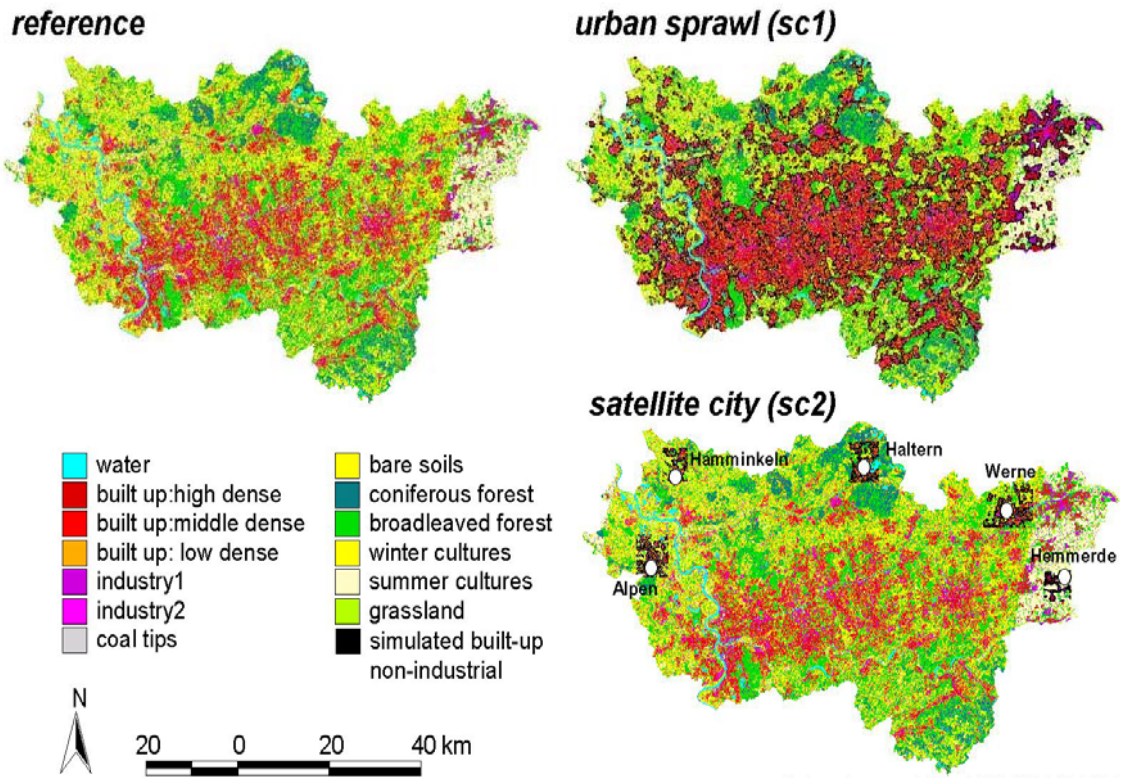


Figure 2. Land use categories of the reference state and the two scenarios urban sprawl (1) and satellite city (2). The red band extending in the east-west direction in the central portion of the domain corresponds with the urbanised areas.

mobility and land use. Figure 2 shows the land use categories of the reference state and two scenarios: a urban sprawl scenario (1) in which no controlled urban development is simulated and a satellite city scenario (2) in which the urban development is controlled by creating 5 concentrated urban development areas. The main result here is that, for the urban-sprawl situation, the urbanised area in the study domain increases by almost 75 %, hence land consumption is rather drastic. For the satellite-city scenario, urban land use changes are much lower, around 9 %. The resulting updated maps of the area were used as input for the traffic and atmospheric dispersion simulations, which showed that total traffic kilometres and associated emissions increased by up to almost 17 %. As a consequence, the domain-average pollutant concentrations also increased, though by a smaller amount.

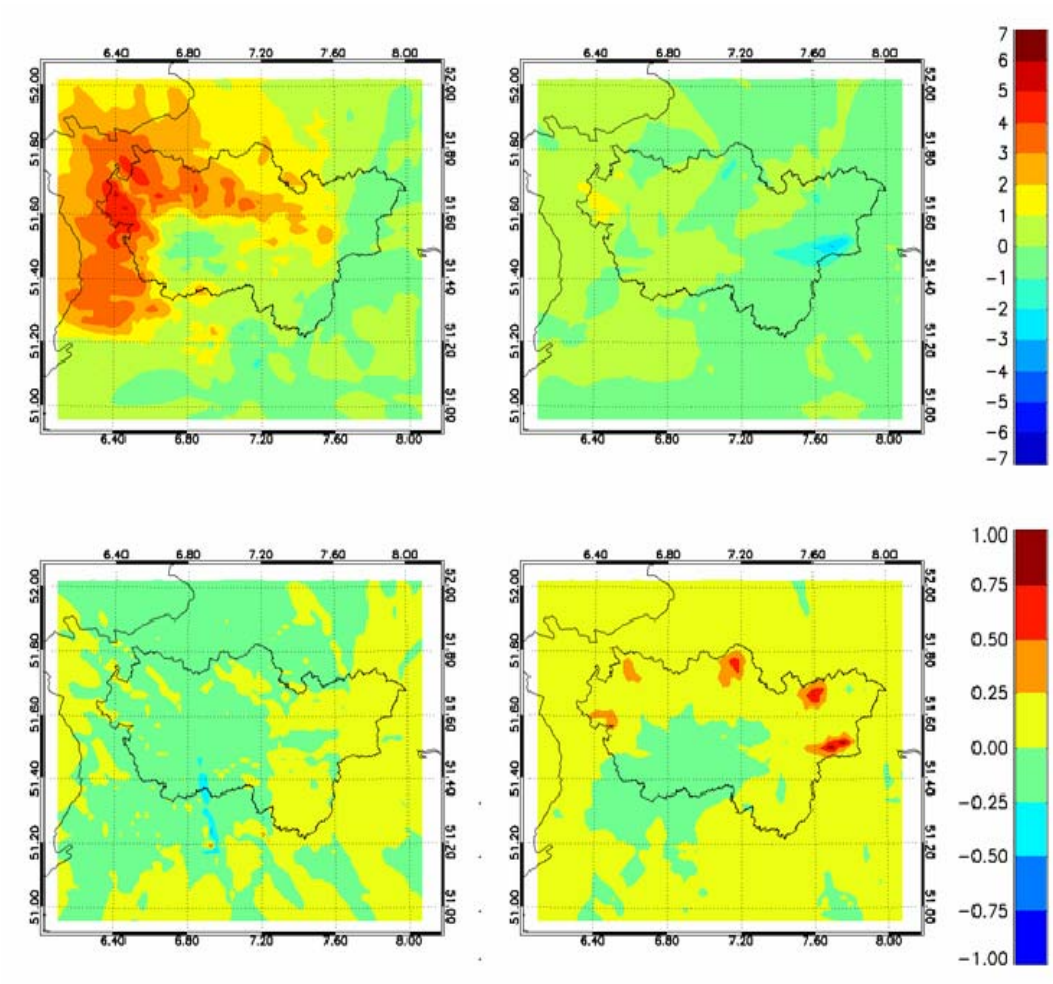


Figure 3. Concentration change (in µg $m^{-3}$) of ozone (upper panels) and $PM_{10}$ (lower panels) for scenario 1 (left panels) and scenario 2 (right panels). Positive values indicate an increase of the considered scenario compared to the reference situation.

For a three-week simulation period, 1-20 May 2000, the simulated change of ground-level ozone and of primary particulate matter is shown in Figure 3. With respect to ozone, the largest changes are seen to occur for the urban-sprawl scenario. Owing to the dominating south-easterly wind direction during this episode, an increased ozone plume is simulated north-west of the agglomeration. The titration effect, on the other hand, slightly depresses ozone concentrations in the central portion of the domain, i.e., where the highest population densities occur. As a result, the average exposure to ozone pollutants (calculated as the average of the concentrations, spatially weighted with population density) remained almost unchanged – they increased by 0.3 % – between the reference case and the urban-sprawl scenario. Also in the satellite-city scenario the changes are minimal (decrease by 0.45 %), despite the increased domain-average emissions.

With respect to fine particulate matter, the effect of the scenarios is perhaps not so clear (Figure **3**3). Whereas the satellite-city scenario clearly exhibits local spots of (a very modest) increase of this pollutant, the concentration patterns in the urban-sprawl

case appear almost unaltered. A detailed analysis shows that there is a slight overall increase of domain-average concentration. However, the effects on human exposure to this pollutant are not so straightforward: whereas one would intuitively associate increased emissions and the ensuing increased domain-average concentrations with increased human exposure values, the contrary is seen to occur. Indeed, a detailed analysis shows that the urban-sprawl scenario results in an exposure *reduction* of 5.7 %, and a reduction of 1.4 % for the satellite-city case. The dominant driver of these exposure changes appears to be the movement of people from locations with high to locations with lower particulate matter concentrations. Stated otherwise, the global exposure decreases when a portion of the population moves from the relatively polluted conurbation to less-polluted areas.

### 3.3 Regional scale modelling

The EUROS model has been applied to urban areas in the Flanders in order to study the formation and chemical composition of aerosols in an urban and regional context. The chemical composition of the aerosol showed a strong dependence on the season.

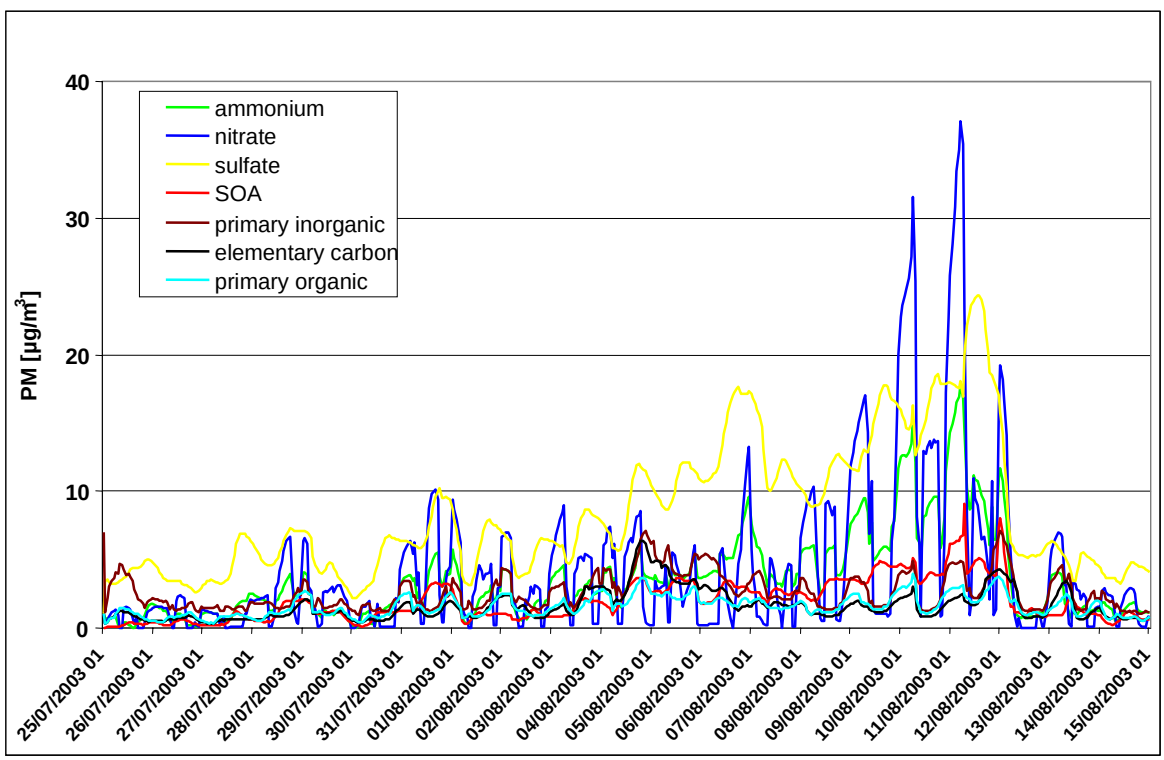


Figure 4. Composition of $PM_{2.5}$ during summer time conditions in 2003 in an urban monitoring station in Flanders (Borgerhout).

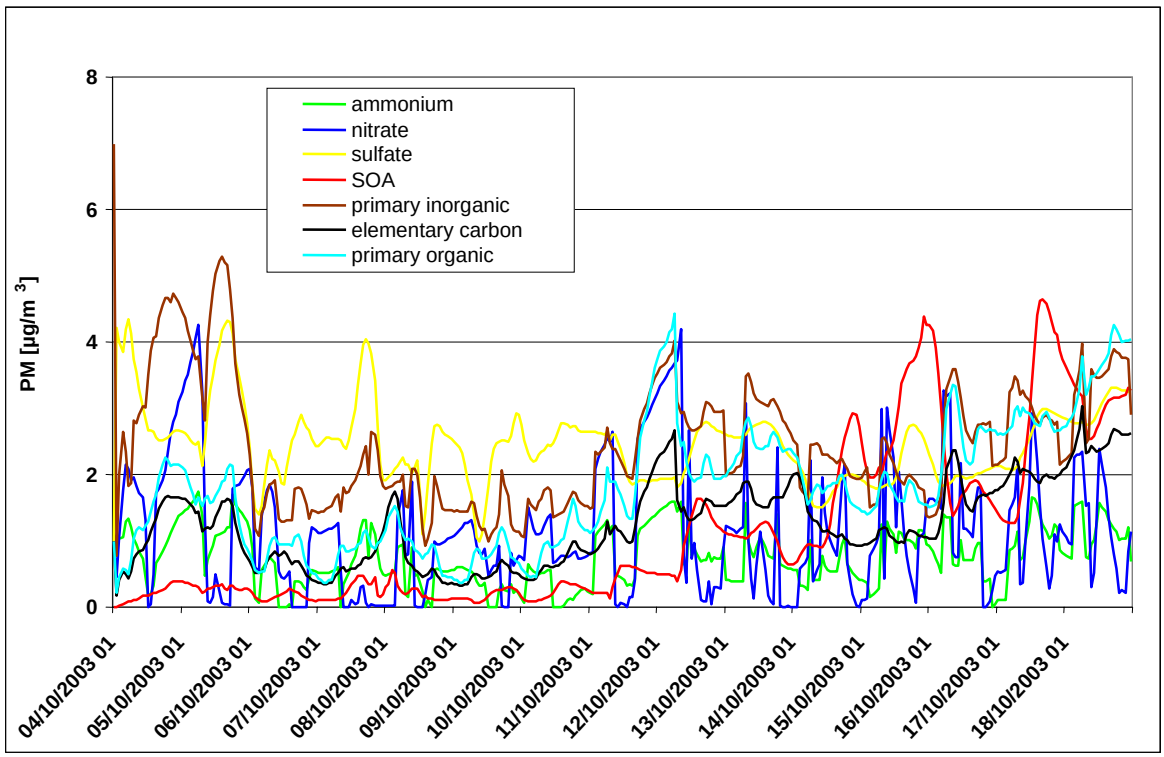


Figure 5. Composition of $PM_{2.5}$ during autumn time conditions in 2003 in an urban monitoring station in Flanders (Borgerhout).

Figure 4 shows the contributions to the composition of $PM_{2.5}$ during summer conditions in an urban monitoring station in Flanders (Borgerhout). Figure 5 shows the aerosol composition of $PM_{2.5}$ in autumn time conditions for this station.

High aerosol concentrations during the summer were mainly due to high concentrations of the secondary components nitrate, ammonium and SOA in the fraction $PM_{2,5}$, thus showing a dominant regional contribution. This shows again the importance of taking scale interactions into account. During the autumn and winter, lower concentrations of secondary aerosol were modeled and hence local or urban contributions of e.g. primary PM components were found to be more important.

## 4. CONCLUSIONS

A novel approach was demonstrated based on the coupling of the street canyon model OSPM and the Gaussian model IFDM. OSPM calculates the contribution of the traffic emissions inside a particular street canyon, whereas IFDM computes the background contributions, including the concentration levels caused by the surrounding streets, industrial stacks and domestic heating. The combined modelling tool can be applied to study these scale interactions within a domain with a 20-30 km

radius. Both models are interacting and have been integrated into an advanced computer program.

On an urban scale, urban sprawl and satellite-city scenarios were studied using spatial modelling techniques, traffic simulations and the air quality model AURORA. Despite the global concentration increases that were calculated by the model, an analysis of human exposure to atmospheric pollution revealed that both scenarios considered here lead to *lower* rather than higher exposure values. While not contesting the evident advantages of compact or polycentric cities with respect to a host of sustainability indicators, like e.g. land consumption, these results indicate that compact/polycentric cities may also induce adverse effects, which should be taken into account by policy makers when making choices regarding urban development scenarios.

The fine particulate matter version of the EUROS-model showed to be suited to determine the most important contributions to aerosol concentrations, including the percentage of secondary aerosols. It can be used to define sources and formation mechanisms of particulate matter and can be an important policy-supporting instrument for drawing up and evaluating reduction scenario's for fine particulate matter.

The chemical composition of the aerosol showed a strong dependence on the season. High aerosol concentrations during the summer were mainly due to high concentrations of the secondary components nitrate, ammonium and SOA in the size fraction $PM_{2,5}$. These secondary compounds are transported from outside the urban area that is considered (regional contribution). During other seasons, secondary components were less abundant in this size fraction, although SOA still contributed significantly to the total aerosol mass. For these cases local or urban contributions of e.g. primary PM components were found to be more important.

## REFERENCES

Berkowicz, R., 1998. 'Street scale models', in Urban Air Pollution – European Aspects, J. Fenger, O. Hertel and F. Palmgren (Eds.) Kluwer Academic Publishers, Dordrecht, pp. 223-251.

Cosemans, G., Dumont, G., Roekens, E . and Kretzschmar J.G., 1997. IFDM modelling for optimal siting of air quality monitoring stations around five oil refineries, Int. J.Environment and Pollution 8, 401-407.

De Ridder, K., F. Lefebre, A. Bañuelos, J.M. Pérez-Lacorzana, J.Dufek, V. Adamec, O. Damsgaard, A. Thierry, M. Bruse, M. Bürger, C. Weber, and J. Hirsch, 2004. An integrated methodology to assess the benefits of urban green space. Science of the Total Environment, 334-335, 489-497.

Griffin R.J., Dabdub D. and Seinfeld J.H., 2002. Secondary organic aerosol 1. Atmospheric chemical mechanism for production of molecular constituents, J. Geophys. Res. 107(D17), 4332, doi:10.1029/2001JD000541.

Mensink C. and Cosemans, G., 2005. Determination of urban background concentrations caused by traffic flows in city street canyons, Proceedings of the 14th International Scientific Symposium Transport and Air Pollution, in: P. J. Sturm, S. Minarik (eds.) VKM-THD Mitteilungen Volume 85/I, pp. 323-330, Technischen Universität Graz, Austria.

Mensink, C., Cosemans, G. and Pelkmans, L., 2005. Dynamic modelling of transient emissions and concentrations from traffic in street canyons, Int. J. Environment and Pollution (in press)

Mensink, C., Colles, A. Janssen, L and Cornelis, J., 2003. Integrated air quality modelling for the assessment of air quality in streets against the Council directives, Atmospheric Environment 37, 5177-5184.

Mensink, C., De Ridder, K., Lewyckyj, N., Delobbe, L. Janssen, L and Van Haver, Ph., 2001. Computational aspects of Air quality modelling in Urban Regions using an Optimal Resolution Approach, in: S. Margenov, J. Wasniewski and P. Yamalov (Eds.) Large-Scale Scientific Computing, Lecture Notes in Computer Science 2179, 299-308.

Mensink, C., De Vlieger, I. and Nys, J., 2000. An urban transport emission model for the Antwerp area. Atmospheric Environment, 34, 4594-4602.

Zhang Y., Pun B., Vijayaraghavan K., Wu S.-Y., Seigneur C., Pandis S.N., Jacobson M.Z., Nenes A. and Seinfeld J.H., 2004. Development and application of the Model of Aerosol Dynamics, Reaction, Ionization, and Dissolution (MADRID), J. Geophys. Res. 109, D01202, doi:10.1029/2003JD003501.

*Proceedings of the Third International Symposium on Air Quality Management at Urban, Regional and Global Scales. 26-30 September 2005, Istanbul – Turkey*

# MODELING $SO_2$ DISPERSION DURING 5-6 FEBRUARY 1997 EPISODE OVER IZMIT GULF, TURKEY

**Mete Tayanç and Aytuğ Berçin**

Marmara University, Faculty of Engineering, Department of Environmental Engineering, İstanbul, Turkey, mtayanc@eng.marmara.edu.tr, aytugbercin@mynet.com

## ABSTRACT

In this study $SO_2$ dispersion over İzmit Gulf is simulated by CALPUFF for the air pollution episode of 5-6 February 1997. This period is characterized by a dominant high pressure system with pressure values reaching 1033 mb, low wind speeds together with calm conditions at critical times, and low temperatures with a minimum of –4°C. Ambient $SO_2$ concentrations measured at 8 stations were obtained from Kocaeli Municipality. The emission inventory was formed by gathering plant emissions from 32 factories and town emissions from 24 sub-municipalities. Hourly meteorological data was bought from State Meteorological Office (DMI). After analyzing the measured $SO_2$ values, 5-6 February period was found to be highly critical with daily average $SO_2$ values greater than 200 $\mu g/m^3$. Hourly simulations during this period were carried out with CALPUFF and results revealed very high concentrations of $SO_2$ transported to the downwind regions of Tüpraş and Gebze, sometimes exceeding 1000 $\mu g/m^3$. Nighttime and morning simulations associated with inversion produced considerably higher values of $SO_2$ than the afternoon simulations associated with breeze. It was also found that, at certain hours, $SO_2$ concentration over and nearby of Kocaeli city is exceeding 500 $\mu g/m^3$, causing dangerous conditions for the inhabitants. Model verification was conducted by comparing the measured daily average values of 8 stations with the model predicted values at the same receptor points. Results showed that the model well predicted the values at stations Gebze, Körfez, Gölcük, Dilovası and Santral and generally underestimated the values at other receptor stations.

**Key Words**: Air Pollution Modeling, İzmit Gulf Region, $SO_2$ Dispersion, CALPUFF

## 1. INTRODUCTION

Transport and dispersion models are powerful tools for assessing the consequences resulting from routine residential and industrial emissions, and accidental releases of pollutants. This $SO_2$ simulation and evaluation of the model results with observations includes a meteorological model CALMET (Scire et al. 2000a) and the California Puff (CALPUFF) model (Scire et al. 2000b). The CALPUFF modeling system offers many advantages and capabilities beyond that in the current generation of straight-line, steady-state Gaussian models, both in terms of its range of applicability and use of recent advances in modeling techniques.

CALPUFF is a model recommended by the U.S. Environmental Protection Agency (EPA) for regulatory applications and is being widely used recently. Barna and Gimson (2002) modeled the inter-suburb dispersion of particulate air pollution in Christchurch, New Zealand, by the CALPUFF during a wintertime particulate

pollution episode. Levy et al. (2002a) applied the CALPUFF atmospheric dispersion model with meteorological data from NOAA's Rapid Update Cycle model to a set of nine power plants in Illinois to evaluate primary and secondary particulate matter impacts across a grid in the Midwest, USA. Cohen et al. (2005) developed a regression model to approximate the CALPUFF predicted concentrations and determine the impacts of roadway proximity on ambient concentrations of three hazardous air pollutants, benzene, 1,3-butadiene, and diesel PM. Jiang et al. (2003) employed a back trajectory method using the CALPUFF model in a reverse diffusion mode to investigate the details of ozone formation within the Puget Sound area of western Washington State, USA. The use of this modeling system for the simulation of the transport and the dispersion of pollutants, and evaluation purposes has become popular in 2000s worldwide such as the studies of Levy et al. (2002b) Chang et al. (2003), Villasenor et al. (2003), Zhou et al. (2003), Elbir (2004), and Lopez et al. (2005).

The aim of this work is to model the transport and the dispersion of $SO_2$ in İzmit Gulf for the air pollution episode 5-6 February 1997 by using CALMET/CALPUFF modeling system, and to evaluate the model results with observations. Section 2 of this paper describes study area, data and summarizes the models and how they were configured. Results of the modeling system and the evaluation appears in section 3. Section 4 gives conclusions and discussion.

## 2. STUDY AREA, DATA AND METHODOLGY

İzmit Gulf is one of the largest industrial regions of Turkey, including the giant petrochemical industry, Tüpraş and organized industrial settlement, Gebze. The region has special importance in terms of its close proximity to İstanbul and Kocaeli cities and the transportation of industrial raw material in and out of the area. Closely located factories surrounding the gulf provide financial income for local people. On the other hand, while being such an important part of the local industry, the surrounded factory establishments play a critical role in the ecological discipline of the region. Pollution of air, water and soil have been a problem since the industrialization of the region. Despite various precautions and regulations, which were adapted not to allow illegal discharge of pollutants, from time to time, pollution over the area reach levels that might be considered as 'very dangerous' for living organisms.

The pollutant emission and behavior in the atmosphere is one of the important subjects that must be studied carefully in order to understand air pollution over the region. In this study we used the plant emission inventory developed for the region by Anbar et al. (2003), produced a residential emission inventory for the cities and towns, and simulated the $SO_2$ distribution by CALPUFF in the light of meteorological, topographical and land-use data for the air pollution episode.

Ambient $SO_2$ concentrations measured at 8 stations were obtained from Kocaeli Municipality. The emission inventory for 32 factories that are almost homogeneously distributed over the area are obtained from Anbar et al. (2003). In the development of

residential emission inventory, city and town emissions in 24 sub-municipalities were used. Hourly meteorological data was bought from State Meteorological Office (DMİ) for Kocaeli and Göztepe stations. Figure 1 shows the location of stations with crosses as the factories and municipalities, triangles as the receptor points, and circles as the meteorology stations. After analyzing the measured $SO_2$ values, 5, 6 February 1997 days were found to be highly critical with daily average $SO_2$ values exceeding 200 $\mu g/m^3$. The CALMET diagnostic meteorological model is used to develop hourly three dimensional wind, temperature fields and various boundary layer parameters, and the CALPUFF dispersion model is to simulate the spatial $SO_2$ distribution over the region for the considered episode.

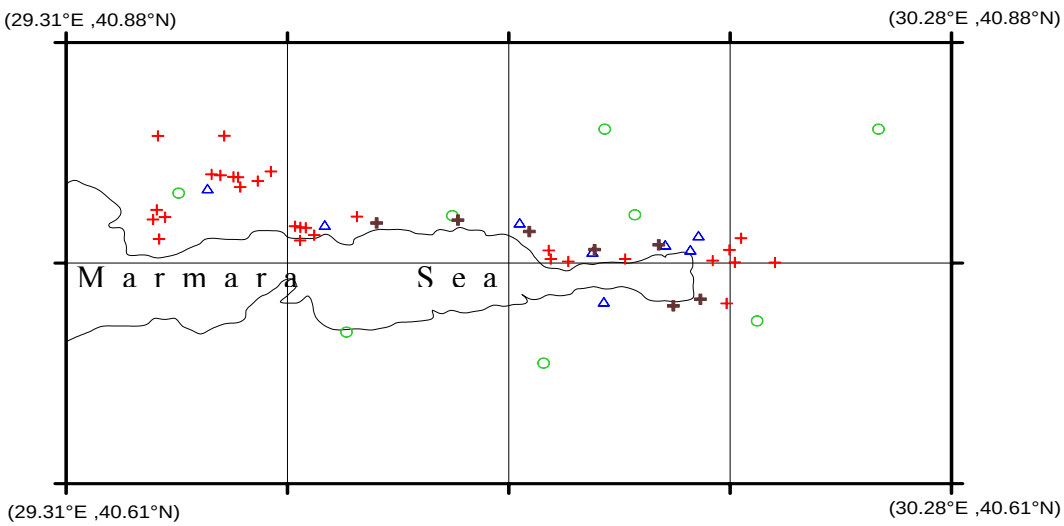


Figure 1. Location of stations in the İzmit Gulf (crosses: factories, triangles: ambient air pollution measurement points, circles: meteorology stations)

The CALPUFF model is a multi-layer, multi-species non-steady-state Gaussian puff dispersion model which can simulate the effects of time- and space-varying meteorological conditions on pollutant transport. The combination of CALMET and CALPUFF offers the potential to treat many important complex terrain effects, including the spatial variability of the meteorological fields, curved plume trajectories, and plume-terrain interaction effects, in a physically realistic manner. In this application most of the default values of the CALPUFF dispersion model have been used, including 1 hour time step, Gaussian distribution in the vertical near field, and use of the slug model in the near field.

## 3. RESULTS

### Day I: February 5, 1997

This day is characterized with wind directions as SE, S and SW over Göztepe and Kocaeli stations. Göztepe station records show wind speeds were varying between 0.5 m/s and 1.7 m/s until 09:00 am. Then until midnight, it did not drop under 1 m/s, while sometimes exceeding 3 m/s. Kocaeli measurements reveal that average wind

speed over the city did not exceed 1 m/s during entire day, while there were calm conditions at certain hours. Figure 2 illustrates the highest frequency of wind direction together with the maximum wind speed in that direction as generated by CALMET. It is clear from the figure that the western parts of the region has considerably much stronger dominant wind speeds than those of the region between Derince and Kocaeli city.

Mixing height was located at 1118 m at 00.00 GMT and 923 m at the 12.00 GMT according to the Göztepe radiosonde data. The region was under the effect of a high pressure field ranging from 1027mb in the morning, decreasing to 1022mb in the afternoon. Relative humidity was obtained as 80%, 46% and 66% at 07.00, 14.00 and 21 o'clock local time in Göztepe, respectively, and almost constant for Kocaeli with a value of 70. A property of high pressure systems is clear skies, with no exception for this case. Daily maximum temperatures for Göztepe and Kocaeli was lower than the long term normals as 5 and 7°C, in order.

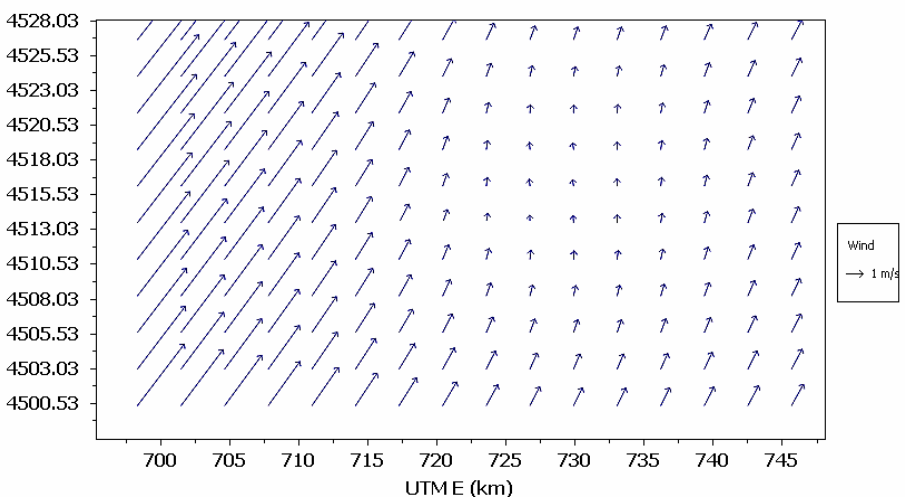

Figure 2. Maximum wind vector profile for February 5, 1997.

**Model Results**

Figure 3 shows the CALPUFF results of the distribution of $SO_2$ at the ground level as a) daily average, and hourly basis at b) 07.00, c) 14.00 and d) 21:00 on the first day of the episode, February 5, 1997. It is obvious that the southwesterly wind was carrying the pollutant cloud towards northeast to the north Derince region. The magnitude of the wind was low, enabling considerable dispersion over the region before the plume transported away. Maximum average concentration was estimated as over 500 $\mu g/m^3$, mainly originating from Tüpraş.

During all night, the ground surface was cooling by emitting infrared radiation and in the early morning minimum temperature was reached, in turn the most stable form of atmosphere formed during morning hours relative to the other times of the day, leading to the accumulation of emitted pollutants at the ground level. It is clear from the figure that the highest concentrations of $SO_2$ was at 07.00 and 21.00 o'clock, reaching to values of 1000 $\mu g/m^3$ over the north Derince region.

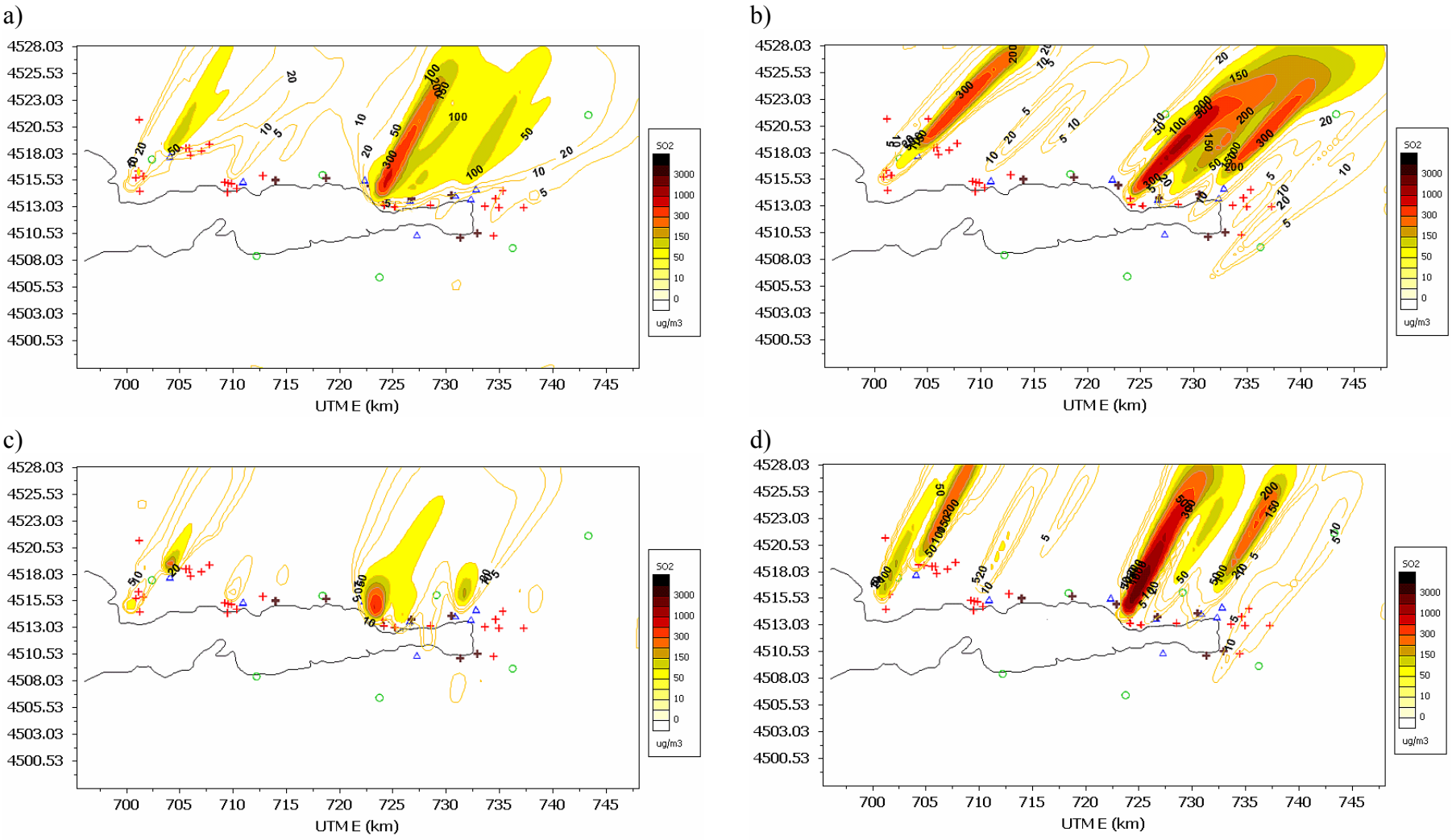


Figure 3. Model results of the spatial distribution of $SO_2$ as a) daily average, and hourly basis at b) 07.00, c) 14.00 and d) 21:00 on February 5, 1997

When the sun came up, it heated the ground surface, which heated the layer above it, by conduction, convection and radiation. That layer heated the next layer above it, and so on. After several hours, the surface temperature increased, a local low pressure area started to develop and the stability of the atmosphere changed into unstable form. Verifying the situation, the pressure at the ground decreased from 1027mb to 1022mb during 5$^{th}$ of February. Figure 3 c) shows considerably low values of $SO_2$ at the surface around 14.00 o'clock, suggesting that pollutants were carried high into the atmosphere.

With the sunset surface cooled down, again forming stable conditions and inversion. The breezes developed over the Gulf lost their strength and in turn horizontal transportation became dominant over the vertical one. Fig. 3d shows the transportation of $SO_2$ plume towards notheast with concentrations of $SO_2$ exceeding 1000 μg/m$^3$.

**Day II: February 6, 1997**

On second day of air pollution episode, dominant wind direction was determined to be southsouthwesterly over the İzmit Gulf. The highest frequency of wind direction together with the maximum wind speed in that direction is generated by CALMET and illustrated in Figure 4 for February 6. It is proved from the figure that the dominant wind blowed from southsouthwest direction with maximum speeds around 2 m/s. Wind shows variability between south and west directions throughout the day. According to the Göztepe measurements wind speed varied between 1 and 2.2 m/s in the interval of midnight - 09:00 am. Then until next midnight it did not decrease under 1 m/s, while exceeeding 4 m/s at instantaneous conditions in the afternoon. Kocaeli station records shows that wind speed increased up to 2.6 m/s until 09:00 am. After this time calm conditions prevailed over the region until midday. After 14:00 pm wind speed again increased and reached to 3.2 m/s by the time of 15:00 pm. Then again calm conditions were dominant.

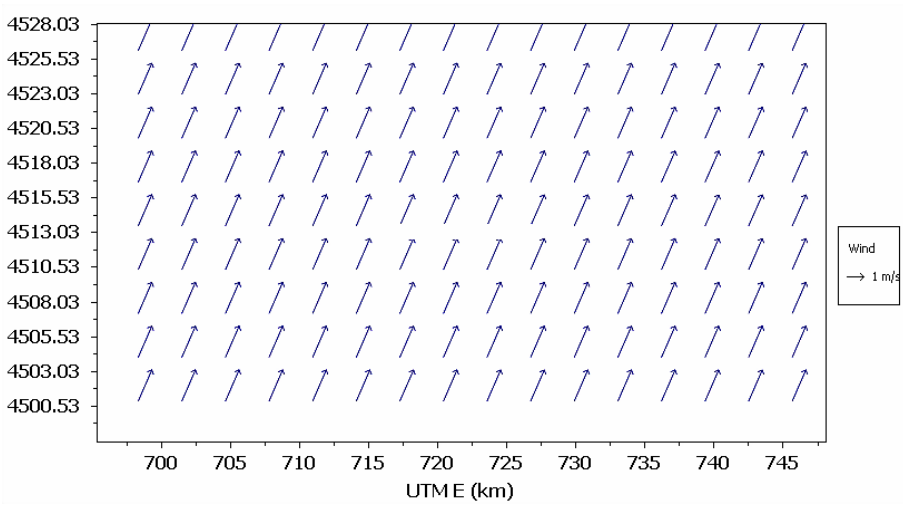

Figure 4. Maximum wind vector profile for February 6, 1997.

At 00.00 GMT radiosonde records, it is seen that the inversion was starting near ground, at an altitude of about 50 m. With the heating of the surface, mixing height raised to 1000 m in the afternoon. The İzmit Gulf was under the effect of a high-pressure field ranging from 1021 mb in the morning, increasing to 1024 mb in the afternoon and night. This suggests that pressure was increasing advectively over the region more than the local decrease due to surface heating.

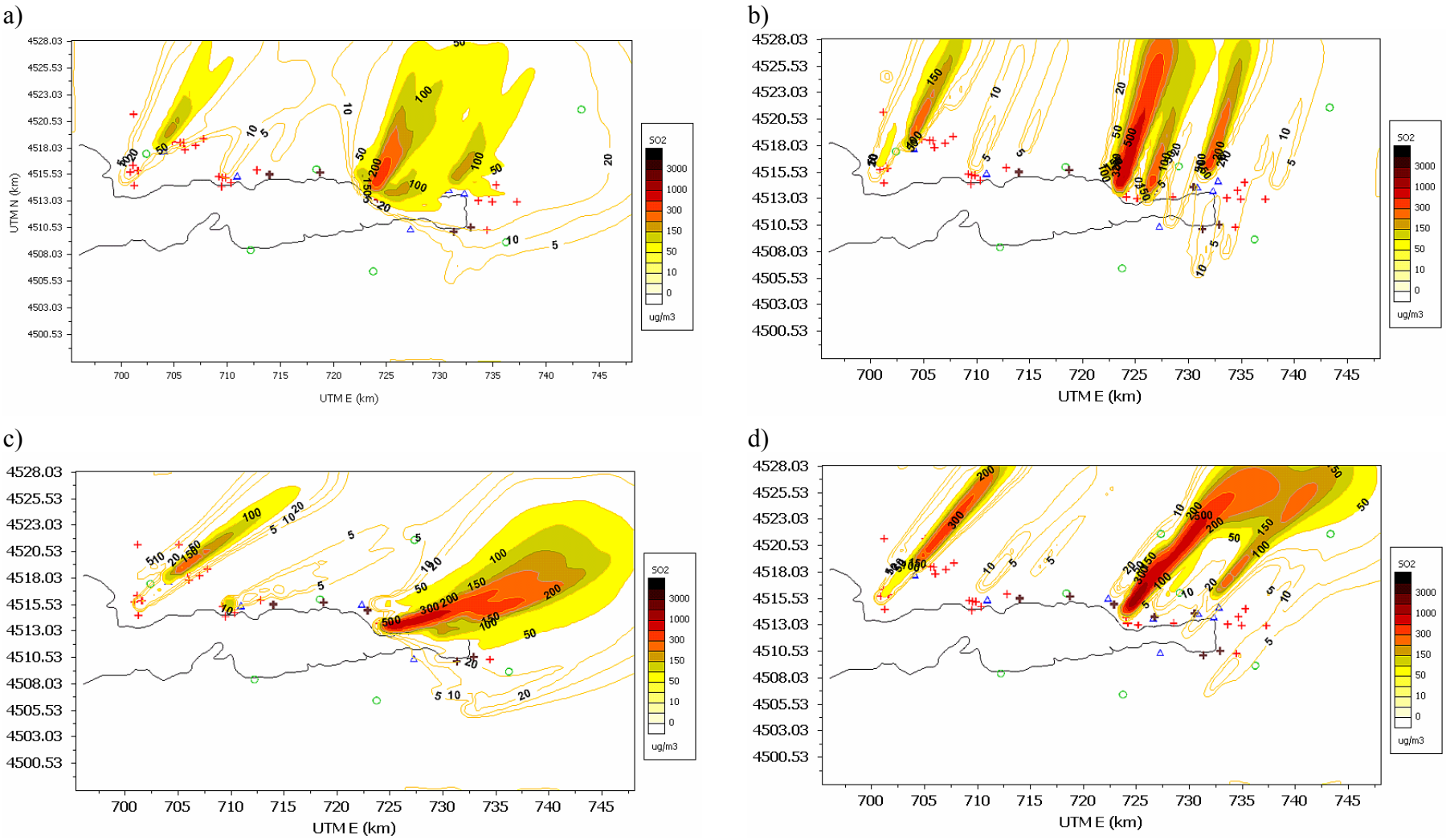


Figure 5. Model results of the spatial distribution of $SO_2$ as a) daily average, and hourly basis at b) 07.00, c) 14.00 and d) 21:00 on February 6, 1997

Daily average relative humidity was obtained as 60 % and 46 % in Göztepe and Kocaeli stations, respectively. Cloudiness was around 70% till 08.00 am in the morning, then clear atmosphere dominated between 08.00 and 16.00 o'clock, and again cloud cover was 70% in the last 8 hours of the day. During the second day of the episode temperature record of Göztepe showed a minimum of 3°C and a maximum of 9°C, which are higher than the first day's values of -4°C and 5°C, respectively.

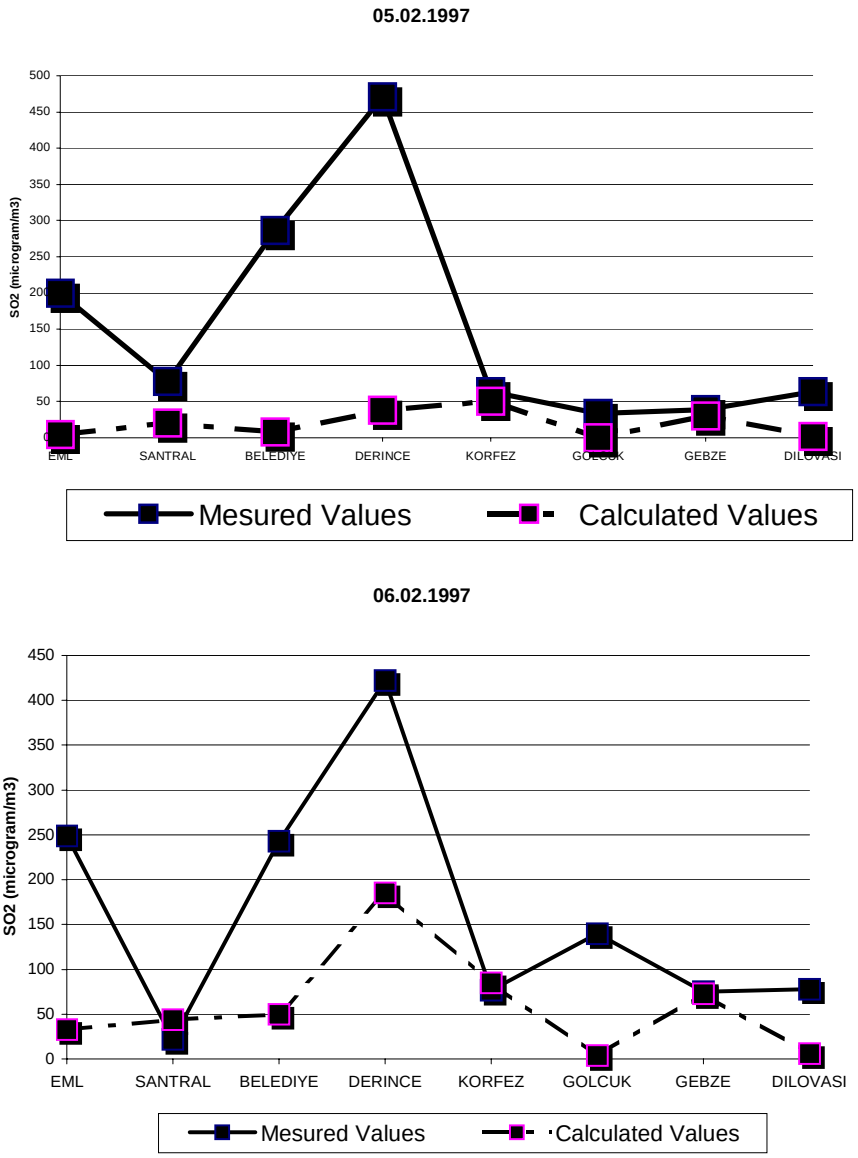


Figure 6. Comparison of measured values with the model results on a) February 5, 1997 and b) February 6, 1997

## Model Results

Figure 5 shows the CALPUFF results of the distribution of $SO_2$ at the ground level as a) daily average, and hourly basis at b) 07.00, c) 14.00 and d) 21:00 on February 6, 1997. The maximum ground level $SO_2$ values were lower than the previous day exceeding 500 $\mu g/m^3$ only on Derince and Kocaeli city at certain hours. The daily variation of pollutant dispersion with high concentrations in the morning, then low in the afternoon and again high levels in the evening disappeared in the second day of the episode. Thus, the dispersion of $SO_2$ in the morning, afternoon and evening showed almost similar patterns, with slight differences in the direction of the plume. At 14.00 o'clock the center of plume moved towards the Kocaeli city, with

concentrations reaching to 500 μg/m$^3$ threatening the life there. At 07.00 and 21.00 o'clock $SO_2$ carried towards north, northeast forming high concentrations in north Derince and north İzmit regions.

**Evaluation of Model Results with the Measurements**

Model verification was conducted by comparing the measured daily average values of 8 stations with the model predicted values at the same receptor points. Since those 8 stations only monitor cumulative $SO_2$, the evaluation was restricted to the daily average values. Results reveal that the model well predicted the values at Körfez and Gebze stations throughout the episode. There are slight differences in the values of Santral, Gölcük and Dilovası. But large differences exist between the recorded concentrations and predicted ones at EML, Belediye and Derince. The model underestimated those concentrations with several orders of magnitude.

The relatively more flat terrain of Gebze, Körfez, Santral, Gölcük and Dilovası, better formed emission inventory for theose sub-regions, and their considerable distance to Tüpraş may be the reasons of this success. On the other hand EML, Belediye and Derince are under the effect of large variation in the emissions together with the largest emission sources located in their proximity. This shows that there is a large possibility of some missing important emission sources in the area close to those three stations. Nevertheless, the trends were caught by the model, showing its sensitivity to changing meteorological conditions.

## 4. CONCLUSIONS

In this study $SO_2$ dispersion over İzmit Gulf is simulated by CALMET/CALPUFF system for the air pollution episode of February 5-6, 1997. On the first day the highest concentrations of $SO_2$ was obtained during morning and evening hours, where the stability was strong and the wind speeds were low or calm conditions prevail, with values exceeding 1000 μg/m$^3$ over the north Derince region. Afternoon hours were generally characterized by low concentrations of $SO_2$ with more unstable conditions and vertical mixing.

On the second day of the episode, it was found that the hourly maximum ground level $SO_2$ values were lower than the previous day, exceeding 500 μg/m$^3$ only on Derince and Kocaeli city at certain hours. At 14.00 o'clock the center of plume moved towards the Kocaeli city, with concentrations reaching to 500 μg/m$^3$ threatening the life there.

The model very well predicted the daily average values of $SO_2$ at stations Körfez and Gebze, and well predicted those at stations Santral, Gölcük and Dilovası during this episode. It underestimated the concentrations at EML, Belediye and Derince with several orders of magnitude. This shows that the model was not capable of simulating the large variability in the emissions and meteorological situation in the area close to those three stations. Tüpraş and Kocaeli city emissions were much larger than those of the other sources and had the lion's share in the formation of pollution in the region.

## 5. ACKNOWLEDGEMENTS

The authors thank Tamer Gürcan, Umut Aydın, Kerem Saka, Aziz Anbar and Mutlu Küpçü for their valuable assistance. This study is supported by TUBİTAK with project YDABÇAG-100Y062.

## REFERENCES


Anbar, A., Saka, K., Kupcu, M., 2003. Modeling air pollution dispersion by RIMPUFF over Gebze Kocaeli region, Graduation Thesis, Marmara University, Istanbul.

Barna, M.G., Gimson, N.R., 2002. Dispersion modelling of a wintertime particulate pollution episode in Christchurch, New Zealand. Atmospheric Environment, 36, 3531–3544.

Chang, J.C., Franzese, P., Chayantrakom, K., Hanna, S.R., 2003. Evaluations of CALPUFF, HPAC, and VLSTRACK with two mesoscale field datasets., Journal of Applied Meteorology, 42, 453-466.

Cohen, J., Cook, R., Bailey, C.R., Carr, E., 2005. Relationship between motor vehicle emissions of hazardous pollutants, roadway proximity, and ambient concentrations in Portland, Oregon. Environmental Modelling & Software, 20, 7-12

Elbir, T., 2004. A GIS based decision support system for estimation, visualization and analysis of air pollution for large Turkish cities. Atmospheric Environment, 38, 4509–4517.

Gürcan, T., 2002. A study on preparing an emission inventory for Gebze-Kocaeli industrial region, Graduation Thesis, Marmara University, Istanbul.

Jiang, G., Lamb, B., Westberg, H., 2003. Using back trajectories and process analysis to investigate photochemical ozone production in the Puget Sound region. Atmospheric Environment, 37, 1489–1502.

Levy, J.I., Spengler, J.D., Hlinka, D., Sullivan, D., Moon, D., 2002a. Using CALPUFF to evaluate the impacts of power plant emissions in Illinois: model sensitivity and implications. Atmospheric Environment, 36, 1063–1075.

Levy, J.I., Greco, S.L., Spengler J.D., 2002b. The importance of population susceptibility for air pollution risk assessment: a case study of power plants, Washington, DC. Environmental Health Perspectives, 110, 1253-1260.

Lopez, M.T., Zuk, M., Garibay, V., Tzintzun, G., Iniestra, R., Fernandez, A., 2005. Health impacts from power plant emissions in Mexico. Atmospheric Environment, 39, 1199–1209.

Scire, J.S., F.R. Robe, M.E. Fernau and R.J. Yarmartino, 2000a: A User's Guide for the CALMET Meteorological Model (Version 5). Earth Tech Inc., Concord, MA, 332 pp.

Scire, J.S., D.G. Strimaitis and R.J. Yarmartino, 2000b. A User's Guide for the CALPUFF Dispersion Model (Version 5.0). Earth Tech, Inc., Concord, MA, 521 pp.

Villasenor, R., Lopez-Villegas, M.T., Eidels-Dubovoi, S., Quintanar, A., Gallardo, J.C., 2003. A mesoscale modeling study of wind blown dust on the Mexico City Basin. Atmospheric Environment, 37, 2451–2462.

Zhou, Y., Levy, J.I., Hammitt, J.K., Evans, J.S., 2003. Estimating population exposure to power plant emissions using CALPUFF: a case study in Beijing, China. Atmospheric Environment, 37, 815–826.

*Proceedings of the Third International Symposium on Air Quality Management at Urban, Regional and Global Scales. 26-30 September 2005, Istanbul – Turkey*

# SIMULATION OF TEMPORAL AND SPATIAL DISTRIBUTIONS OF OZONE IN THE SEOUL METROPOLITAN AREA USING MODELS-3/CMAQ

**Chong Bum Lee and Mi Hee Lee**

Kangwon national university, ChunCheon 200-701,KOREA
cbl@kangwon.ac.kr , lmh306@kangwon.ac.kr

## ABSTRACT

In order to simulate hourly ozone levels, the photochemical model, CMAQ is applied to Seoul and down wind area. Horizontal grid of 30km, 10km and 3.3km have been employed for this study. Ozone episode periods in June 2004 were simulated and the results have been compared to several Air-quality Monitoring stations. Input data of emissions have been used to CAPSS. The CB-IV chemical scheme has been used to simulate the atmospheric reaction for ozone. The model performance has been evaluated with measured data through a range of statistical measures.

**Key Word:** Photochemical Model, Ozone Modeling

## 1. INTRODUCTION

Recently, high ozone concentration phenomenon is embossed as one of the air pollution problem in downtown and downwind side of Seoul metropolitan area.

It is difficult to simulate the photochemical reaction of various air pollutants such as ozone because production process is complicated. In this research, the simulation of photochemical pollutant was carried out especially ozone was performed by using Models-3/CMAQ. Temporal and spatial patterns of ozone concentration obtained by Models-3/CMAQ under various weather conditions were examined. Also we analyzed the contribution of the emission source in Seoul metropolitan and downwind area.

Together with a user interface the MM5. CMAQ system is referred to as Models-3 (Byun et al., 1998). MM5 (Fifth-Generation Penn State/NCAR Mesoscale Model)

was developed by Pennsylvania State University/National Centre for Atmospheric Research (PSU/NCAR) as a community mesoscale model. It is a limited-area, non-hydrostatic, terrain-following sigma coordinate model designed to simulate or predict mesoscale atmospheric circulation. The model is supported by several pre- and post-processing programs. CMAQ (Community Multiscale Air Quality Model) is a powerful third generation air quality modelling and assessment tool designed to support air quality modeling for various applications ranging from regulatory to research studies (Byun et al., 1998). The CMAQ system can simulate concentrations of tropospheric ozone, acid deposition, visibility, fine particulate and other air pollutants in the context of ‘‘one atmospheric’’ perspective involving complex atmospheric pollutant interactions on regional and urban scales.

## 2. METHODOLOGY

The nested grid system (grid sizes are 30km, 10km, 3.333km respectively) was used for CMAQ modeling (Fig.1). The domain for 30km grid covers important emission areas in the East Asia.

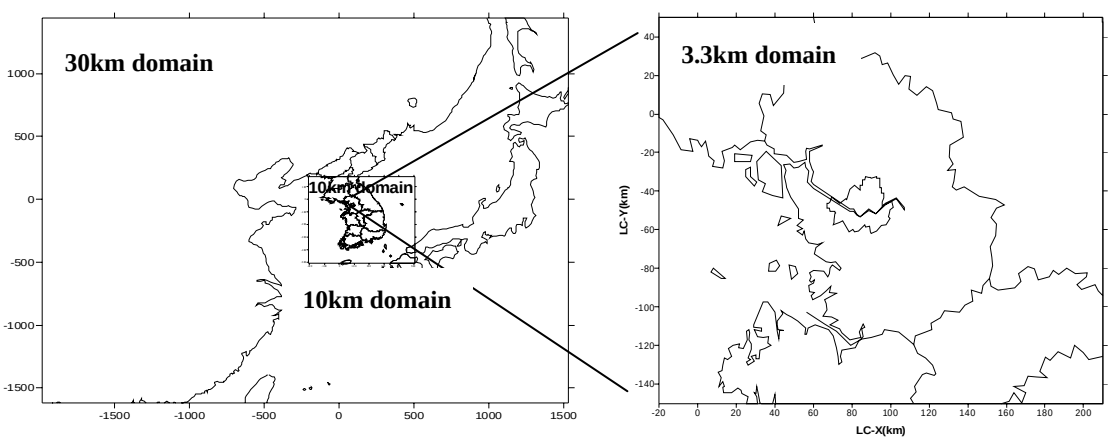


Figure 1. The 30km, 10km and the 3.3km domain in Korea.

The emission data prepared for ACE-ASIA project, which was conducted in North Pacific Ocean area and East Asia in 2000, were used as emission data for 30km grid simulation of CMAQ. The emission data of 2001 Clean Air Policy Support System(CPASS) is used for the modeling of 10km and 3.3km grid domain as emission data.

CAPSS is one of the most reliable and useful emission inventory in Korea. CAPSS

has a resolution of 1km*1km covering all the southern part of the Korean Peninsula. It has been used for air quality model as emission inventory. CAPSS data changed to L-C(Lambert Conformal) coordinate system to used by input data of Models-3/CMAQ because it is TM(Transverse Mercator) coordinate system. Also, it equalized according to 10km, 3.3km grid modeling and considered time factor about each material.

Meteorological data were generated by using MM5 model. The simulation was performed for 14 days from May 30 to June 12 when various meteorological events occurred.

Because of spin up time, the results of CMAQ for May 30, 31 were excluded in analysis and CMAQ result of 12 days were divided into 3 period(June 1-4, June 5-8, June 9-12) based on weather condition. The modeling results were evaluated spatially and temporally. The process analysis, included in CMAQ modeling system as a tool, was used to analyze the contribution of chemical reaction, diffusion, advection and deposition process. Figure 2 shows process analysis area. Process analysis divides upwind area(west), urban(center) and down wind area(east).

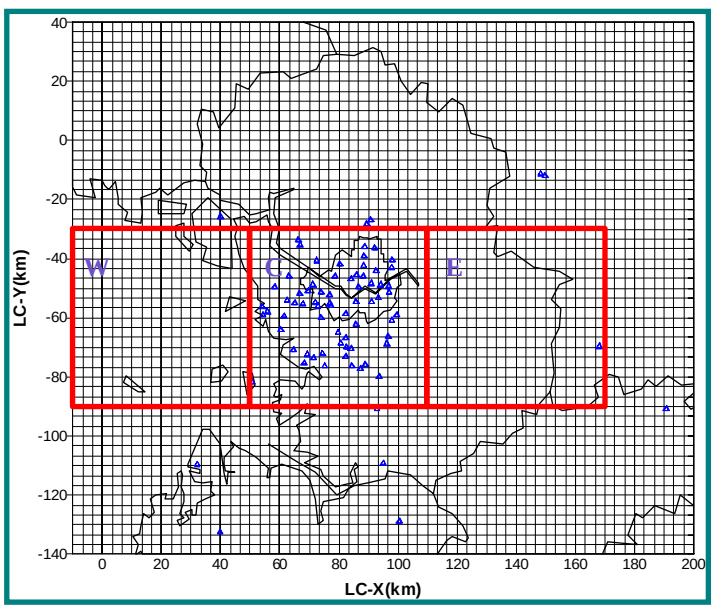


Figure 2. Process analysis area and Air-quality monitoring site in 3.3km modeling area.

## 3. RESULTS

Figure 3 shows MM5 results during the modeling period. Temperature and solar radiation are very high during the period from June 1 to 4. During the period from June 4 to 8, 'cloudy' and 'temperature' were low. After June 8, temperature rose again and solar radiation became strong.

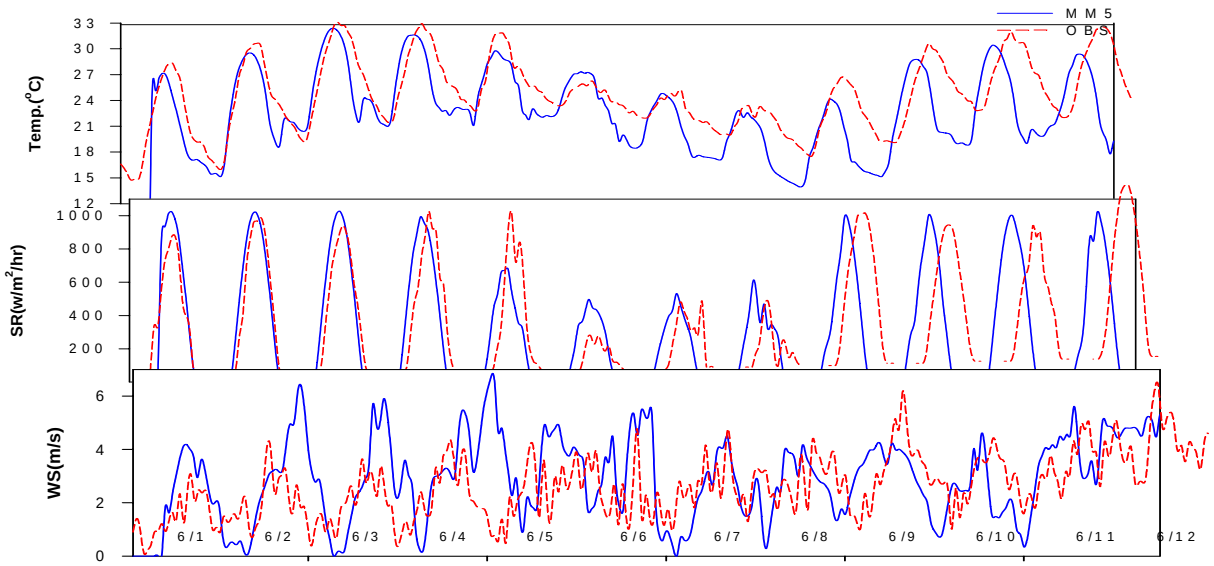


Figure 3. Comparison of observations and MM5 model results for 1-12 June 2004.

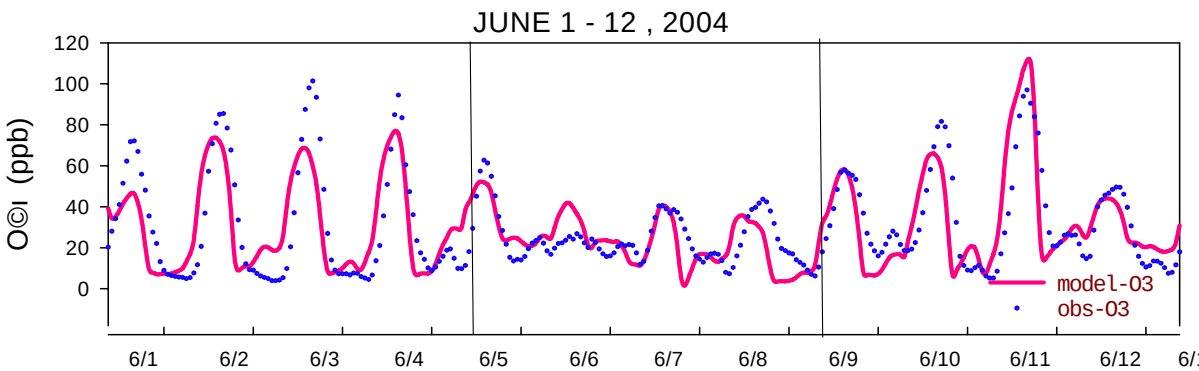


Figure 4. Ozone time series comparison between observed data form the Seoul monitoring station and CMAQ predictions for 1-12 June 2004.

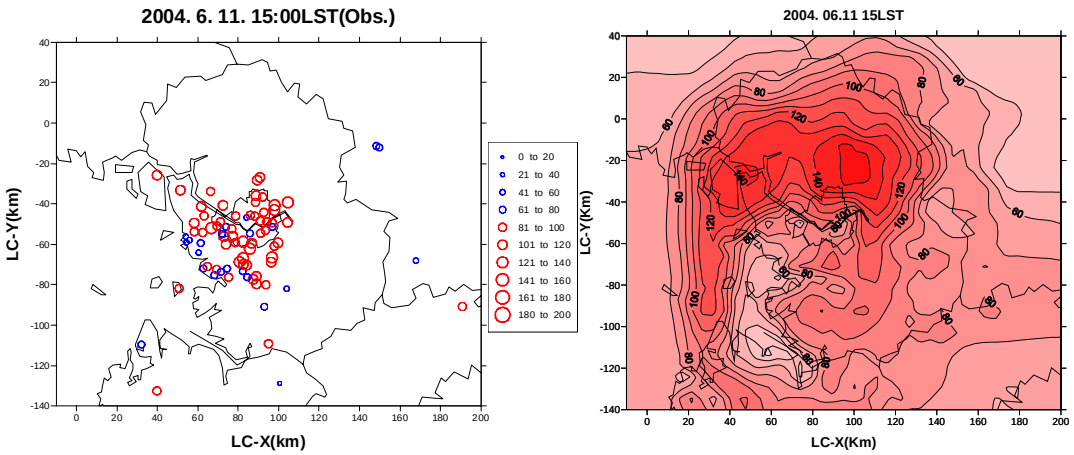


Figure 5. Ozone(ppb) distribution comparison between observed data(left) and CMAQ predictions(right) on June 11,2004, 15LST.

The model results were compared with the observational data during modeling periods (Fig.4). The high ozone concentration appeared on June 3 and 11 and modeling results were similar to observation.

Modeling result of horizontal distribution of ozone on June 11, 15LST shows the high concentration over 120ppb, in downtown of Seoul. As see in horizontal distribution of survey ozone concentration, showed high concentration more than 100ppb Seoul and its outskirts (Fig.5).

Figure 6 shows process analysis result of June 11 that showed the highest ozone concentration. Process analysis examined contribution of ozone creation from 09 LST to 15LST(left) and from 15LST to 18LST(right) about up wind area, urban and down wind area. As see result from 09LST to 15LST, it was chemical reaction that make the biggest contribution in ozone creation in up wind area, downtown area and down wind area. As see result from 15LST to 18LST, ozone concentration of upwind area and downtown area decreases by horizontal transport. But ozone concentration of down wind area increased by horizontal transport.

## 4. SUMMARY

The performance of CMAQ was evaluated using observed ozone concentration. The results show that the performance of CMAQ was quite good for simulation of ozone episode in the Seoul metropolitan area.

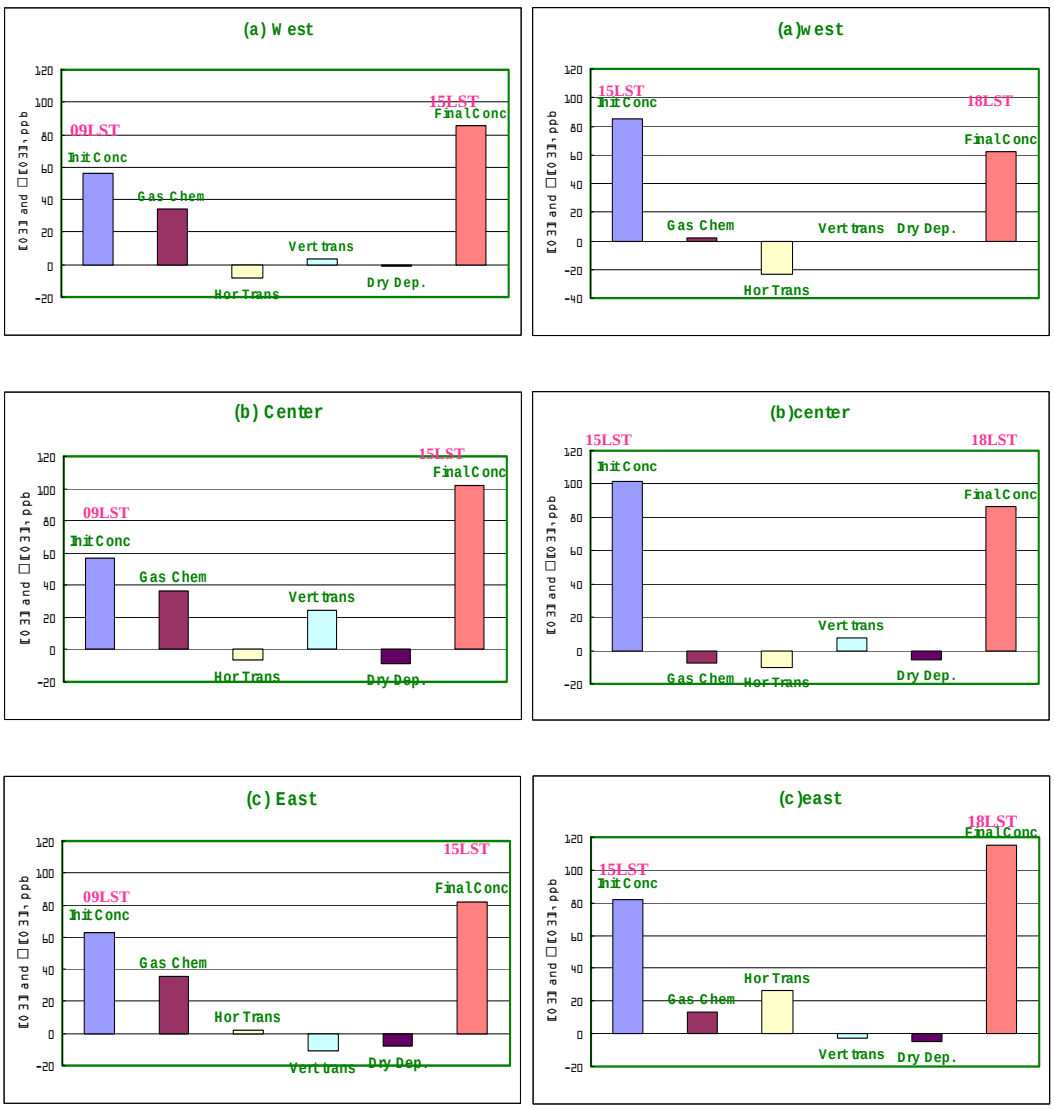


Figure 6. Mass balances of process contribution to O3 on June 11, 2004, 9LST-15LST(left) and 15LST-18LST(right).

## REFERENCES

Byun, D.W., Ching, J.K.S. (Eds.), 1999. Science Algorithms of the EPA Models-3/Community Multi-scale Air Quuality(CMAQ) Modeling System. US EPA Report No.EPA/600/R-99/030, Office of Research and Developement, Washington, DC.

R.S.Sokhi, R.San Jose, 2004. Prediction of ozone levels in London using the MM5-CMAQ modelling system. Environmental Modelling & Software.

*Proceedings of the Third International Symposium on Air Quality Management at Urban, Regional and Global Scales. 26-30 September 2005, Istanbul – Turkey*

# DETERMINATION OF TRANSPORT PROCESSES OF NOCTURNAL OZONE IN ISTANBUL ATMOSPHERE

**Kadir Alp[1] and Asude Özkan[2]**

[1]Department of Environmental Engineering, Faculty of Civil Eng., 34469, Maslak, Istanbul, Turkey, kalp@ins.itu.edu.tr
[2]Department of Environmental Engineering, Corlu Eng. Faculty, 59860, Corlu, Tekirdag, Turkey, aozkan@corlu.edu.tr

## ABSTRACT

Ozone, usually has a minimum value at nights, often increases its concentration level, depending on atmospheric movements especially in urban areas. This increased level of ozone at night is known as nocturnal or secondary ozone maximum. Theories about formation of this nocturnal ozone concentration in the studies can be grouped into two major categories which are vertical and horizontal transport processes. In this study, the magnitude, frequency and timing of nocturnal ozone maxima were determined and the reason of nocturnal ozone maxima was examined in May-September 2001-2004 years at Kadikoy and Aksaray stations, in Istanbul. The magnitude and frequency of late and early peaks for peak ozone nights were examined based on stations and years. A total of 40 days which were likely to have secondary ozone maxima due to horizontal transport processes, were selected. HYSPLIT model with back trajectory analysis were conducted for these days in order to determine where air parcel comes from in 24 hours at different ground levels.

**Key Words:** Secondary Ozone Maximum, Horizontal Transport, Vertical Mixing, Back Trajectory Analysis, HYSPLIT.

## 1. INTRODUCTION

The tropospheric ozone is a volatile secondary photochemical pollutant. It is formed in the atmosphere as a result of the photodissociation of nitrogen dioxide ($NO_2$). This reaction occurs only in the presence of ultra-violet night. The typical diurnal cycle of ozone under clear air conditions indicates a maximum during early afternoon, a sharp decrease during the late afternoon, while at night a minimum value is measured. The reason of this minimum value at night is deposition and chemical transformation. Homogeneous and heterogeneous chemical processes in the lower atmosphere at night have long been recognized to have uncertainities stem from several considerations. The reasons of these uncertainties lack detailed kinetic information about reaction of nitrogen compounds and due to the paucity of observations, model description of aerosols and reactive trace gases at night are highly uncertain.

The typical diurnal cycle cannot always be observed, especially at night. Most of the studies about ozone, report an ozone peak in the late night between midnight and

sunrise. Theories about forming of this nocturnal ozone concentration in the studies which are about nocturnal ozone, can be grouped into two major categories. As known, in the absence of any known sources of $O_3$ in the nocturnal boundary layer (NBL), any increase in concentration is likely to result from transport processes; where horizontal transport processes are of importance secondary maxima can occur. As often no significant change in wind direction is correlated with the secondary ozone maxima, horizontal advection of air pollutants near the surface is not likely and vertical mixing of ozone from the reservoir layer to the ground is a proper explanation. But this needs specific conditions like enhanced turbulance. Turbulance typically results from shear associated with changes in wind velocity with height (Salmond, 2002, Lee, 2002).

Ozone, usually has a minimum value at nights, often increases its concentration level, depending on atmospheric movements especially in urban areas. This increased level of ozone at night, known as nocturnal or secondary ozone maximum, has been observed and reported by several authors, around the world. For example; Chung (1977), Samson (1978), Steinberg and Ganor (1980), Zurita and Castro,(1983), Liu et al. (1990), Corsmeier et al. (1997), Eliasson (2003). Most of these studies report an ozone peak in the late night, between midnight and sunrise, and the nocturnal ozone maximum concentrations can be high .

In this study, we examine summer nocturnal ozone maxima and meteorological data from Istanbul, which is located on the both Asia and Europe continents. The city is located at $40^0$ $58^{'}$ N, $29^0$ $05^{'}$ E. Istanbul is an urban district, with its coastal location in combination with industry and heavy traffic, represents one of the most polluted areas in Turkey. Local authorities have monitored ozone ($O_3$) and other pollutants during the last years. The aim of this study is to examine the magnitude, frequency and timing of nocturnal ozone maxima in Istanbul, to determine the reasons of the increase the ozone concentration in the night and to determine horizontal transport processes.

## 2. METHODS

Summer nocturnal ozone pollution episodes have been analysed in Istanbul. Istanbul is the most populated city of Turkey, and it is located on the both Asia and Europe continents. In this city there are two ozone mesurement stations. Ozone measurements were performed with Environmental S.A. O3 41M model ozone mesurement equipment. Meteorological data which were used in this study, had taken from two meteorological stations which were the nearest to the ozone measurement stations.

The study was conducted during 2001-2004 years. During this period, nocturnal ozone formation time were determined as May-September months. It was concluded that total 101 and 74 days have been determinated as a nocturnal ozone periods for Kadikoy and Aksaray sampling stations respectively for this season. In the selection it was determined that; where the reduction of ozone was broken and with an ozone increase of 10 $\mu g/m^3$ or higher, compared to the breaking point, were classified as

nights with nocturnal ozone maximum. The threshold value was chosen based on the accuracy of the instrument in accordance with above (Eliassson, 2003). In these days the concentration of ozone rose on the order of ½ to 2 of the days maximum. In some days or periods, sample collection in ozone measurement stations could not be done because of technical or meteorological problems. In table 1, total number of ozone maxima days and number of late and early peaks, in two stations and different years are given. Late peak is the days which has an ozone increase 3 hours after sunset and early peak is the days which has an ozone increase within the first 3 hours after sunset. It can be seen from table 1, nocturnal ozone maksimum had late peaks of 59% and 32% , respectively in Kadikoy and Aksaray stations.

**2.1 Selection Criteria:**

Nocturnal ozone maxima can be explained by vertical mixing of high ozone concentrations from higher levels or horizontal transportation from other areas, or countries. Previous studies have shown that nocturnal ozone maxima occured during stable atmospheric conditions (Corsmeier, 1997, Eliasson, 2003). In order to select nights, that have such conditions, criteria given in table 2, were conducted during these 175 nights. In order to conclude that the observed nocturnal ozone maximum is caused by horizantal transportation, all of the three criterias shown in Table 2 must be fulfilled with the exception of the basic criterion, the reversed case, i. e. Criteria 2 and 3 are not fulfilled indicates that vertical mixing caused the nocturnal ozone maximum. In this criterisation, Richardson number, which is the one of the best indicators for stability of atmosphere, cannot be used, because in none of the meteorological measurement stations temperature in two stages is measured. Because of the horizontal advection alternative is examined in this study, the selected days are decreased total 40 days depending atmospheric stability of nights, wind speed and changing in wind direction for two stations which are given in Table 2. By this seperation it is determined that the reason of the nocturnal ozone maxima is horizontal advection, the reselected days have been analized in detail, together with meteorological conditions in the measurement period.

Table 1. Frequency and typical nocturnal ozone maksima.

| **Year** | | **$O_1$ (Kadikoy station)** | | | | **$O_2$ (Aksaray Station)** | | | |
|---|---|---|---|---|---|---|---|---|---|
| | | **Late peak** | **Early peak** | **Late+early peak** | **total** | **Late peak** | **Early peak** | **Late+early peak** | **Total** |
| **2001** | **Number** | 5 | - | 2 | 7 | 9 | - | 18 | 27 |
| | **Percent** | 71 | - | 29 | - | 33 | - | 67 | - |
| **2002** | **Number** | 17 | - | 21 | 38 | 2 | 1 | - | 3 |
| | **Percent** | 45 | - | 55 | - | 67 | 33 | - | - |
| **2003** | **Number** | 19 | - | 4 | 23 | 6 | 1 | 3 | 10 |
| | **Percent** | 83 | - | 17 | - | 60 | 10 | 30 | - |
| **2004** | **Number** | 18 | 12 | 3 | 33 | 15 | 14 | 5 | 34 |
| | **Percent** | 55 | 36 | 9 | - | 44 | 41 | 15 | - |
| **Total** | | 59 | 12 | 30 | 101 | 32 | 16 | 26 | 74 |

Table 2. Criteria for analysis of nocturnal ozone transpotation process

| **Criteria** | |
|---|---|
| **1** | Wind speed ≤2 m $s^{-1}$ 3 h before sunset until sunrise and stable stratification |
| **2** | Total cloud cover ≤ 2,5 decas 3 h before sunset until sunrise and stable stratification |
| **3** | Change in wind direction (W-NW to E-SE) at meteorological stations |

## 3. RESULTS

In this study, nocturnal ozone maxima which has been formed in Istanbul were observed in summer and spring days. In these days early peak is an dominant phenomenan for Istanbul. When seen in yearly conjoncture, seeming frequency of night ozone has a decreasing trend from 2001 to 2004. Generally it can be said that, vertical mixing is a dominant reason for night ozone when comparing to horizontal transport process.

### 3.1 Hysplit Projectory analysis

The HYSPLIT (Hybrid Single-Particulate Lanrangian Integrated Trajectory) map shows an aerial view of the path(s) an air parcel(s) took, and a vertical view of its movement at different altitudes (NOAA, 2005).

In this study HYSPLIT back trajectory analysis were conducted to determine where air parcel came from in a 24 hour period at different ground levels for the selected 40 days. From this analysis, when main 16 directions are decreased to 4 directon, it is observed that back trajectory has a northly direction 82 and 64% of the period respectively for Kadikoy and Aksaray measurement station. In table 3, results of hysplit backtrajectory analysis are showed at different heights for Kadikoy and Aksaray stations. In this division, 16 directions are decreased to 8 directions clockwise. It can be easily seen that the NNE-NE direction (Russian-The Crimea-Black Sea) is dominant for 100-500-1000 and 1500 m for both stations. Generally, as height is increased, direction of trajectory goes to North West direction, but as height is decreased direction didn’t change.

In the next sections, hysplit projection analysis are investigated by giving representative examples for 2001, 2002, 2003 and 2004 years.

**Table 3.** Result of HYSPLIT analysis

| Direction | Kadikoy (%) | | | | | | Aksaray (%) | | | | | |
|---|---|---|---|---|---|---|---|---|---|---|---|---|
| | **100** | **500** | **1000** | **1500** | **2000** | **3000** | **100** | **500** | **1000** | **1500** | **2000** | **3000** |
| **I-Scandinavia-Balkans (NNW- N)** | 3,0 | 9,1 | 18,2 | 30,3 | **51,5** | **54,5** | 15,4 | - | 23,1 | 23,1 | 23,1 | **30,8** |
| **II- Russian-The Crimea-Black Sea (NNE-NE)** | **69,7** | **66,7** | **69,7** | **51,5** | 30,3 | 9,1 | **38,5** | **30,8** | **46,2** | **38,5** | 23,1 | 15,4 |
| **III- Russian-The Caucasia-Black sea (ENE-E)** | 21,2 | 18,2 | 6,1 | 9,1 | 3,0 | 3,0 | - | **30,8** | - | 7,7 | - | - |
| **IV- Middle Anatolia (ESE-SE)** | 6,1 | 3,0 | - | - | - | - | 23,1 | 7,7 | - | - | - | - |
| **V- Akdeniz-Taurus Mountains (SSE-S)** | - | 3,0 | 6,1 | - | - | - | 7,7 | 7,7 | - | - | - | - |
| **VI-Africa-Mediterranean Sea (SSW-SW)** | - | - | - | 6,1 | 6,1 | 9,1 | 7,7 | 7,7 | 7,7 | 7,7 | 7,7 | 7,7 |
| **VII Sicily-South Greece-Ageian (WSW-W)** | - | - | - | - | - | 3,0 | - | - | 7,7 | 7,7 | 15,4 | 23,1 |
| **VIII Middle East-North Greece (WNW-NW)** | - | - | - | 3,0 | 9,1 | 21,2 | 7,7 | 15,4 | 15,4 | 15,4 | **30,8** | 23,1 |

***Year 2001:*** In 2001, average numbers are given in Table 4 according to years and stations. In figure 1, ozone concentration and wind velocity graphic related to 19-20-21 July 2001 for Kadikoy station is given as an example. As can be seen from this figure ozone concentration is high and wind velocity is low at ozone peak hours. In the morning of 20 July, there was a peak at 04:00 at 136 $\mu g/m^3$. At this hour wind velocity was about 1,2 m/sec. After this peak, there was a decrease until 10:00 am. And it continued by increasing and decreasing during the day. At 23:00, there was an increase from 51 to 81 $\mu g/m^3$. This increase decreased until 01:00 and at 02:00 there is a second peak until 93 $\mu g/m^3$.

In Figure 2a, HYSPLIT projection of 20 July is given. It can be seen from this figure air parcel came from NNE (Russian-The Crimea-B.Sea) direction in 24 hours (beginning from 05:00 am) for 100, 500 and 1000 m heights for this day.

**Table 4.** Properties of ozone maxima days

| Year | Station | Aver. | Ozone maxima day | Ozone maxima night | Ozone minima day | Ozone minima night |
|---|---|---|---|---|---|---|
| **2001** | **Aksaray** | 65 | 142 (18.05.01, 16:00) | 136 (20.07.01, 04:00) | 2 (18.05.01, 08:00) | 18 (23.07.01, 22:00) |
| | **Kadikoy** | 75 | 125 (20.07.01, 16:00) | 91 (22.07.01, 03:00) | 6 (17.07.01, 01:00) | 36 (17.07.01, 04:00) |
| **2002** | **Aksaray** | 25 | 72 (01.08.02, 13:00) | 54 (01.08.02, 21:00) | 7 (02.08.02, 08:00) | 0 (01.08.02, 03:00) |
| | **Kadikoy** | 49 | 140 (15.07.02, 16:00) | 116 (27.08.02, 06:00) | 3 (15.07.02, 08:00) | 2 (14.05.02, 00:00) |
| **2003** | **Aksaray** | 42 | 128 (04.07.03, 14:00) | 103 (15.08.03, 04:00) | 0 (03.06.03, 06:00) | 4 (09.08.03, 00:00) |
| | **Kadikoy** | 43 | 85 (16.06.03, 14:00) | 83 (27.06.03, 04:00) | 0 (11.09.03, 06:00) | 0 (30.09.03, 23:00) |
| **2004** | **Aksaray** | 27 | 70 (29.07.04, 13:00) | 61 (29.07.04, 04:00) | 2 (23.06.04, 12:00) | 3 (11.06.04, 22:00) |
| | **Kadikoy** | 26 | 87 (29.07.04, 14:00) | 72 (29.07.04, 03:00) | 0 (05.06.04, 09:00) | 0 (05.05.04, 02:00) |

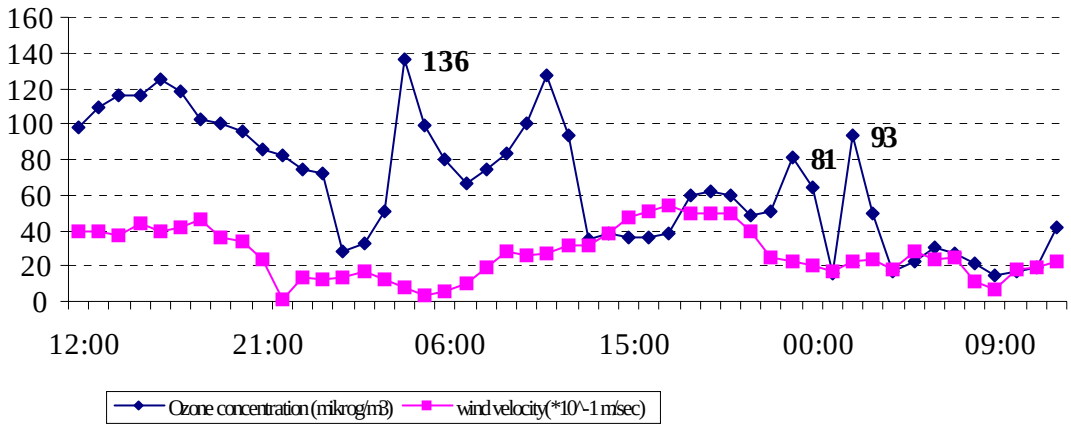


Figure 1. Ozone concentration and wind velocity at 19-20-21 July 2001

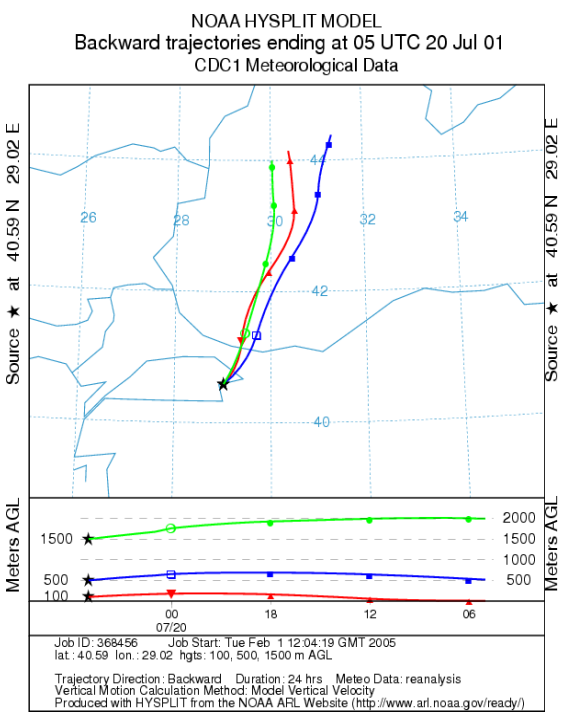


Figure 2.a

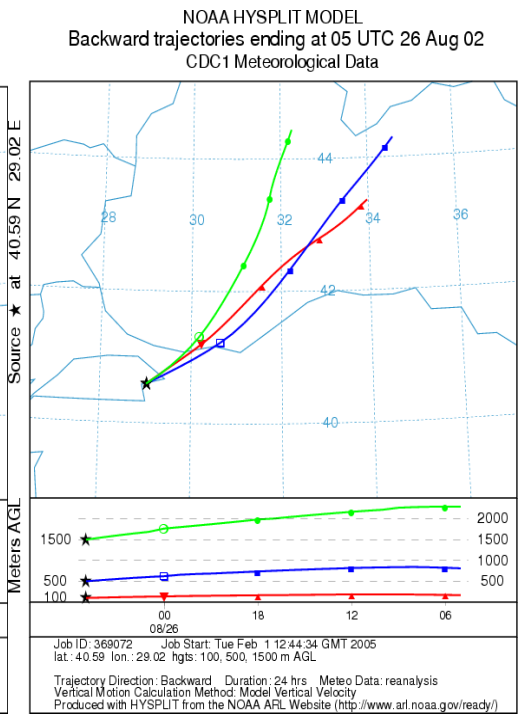


Figure 2.b

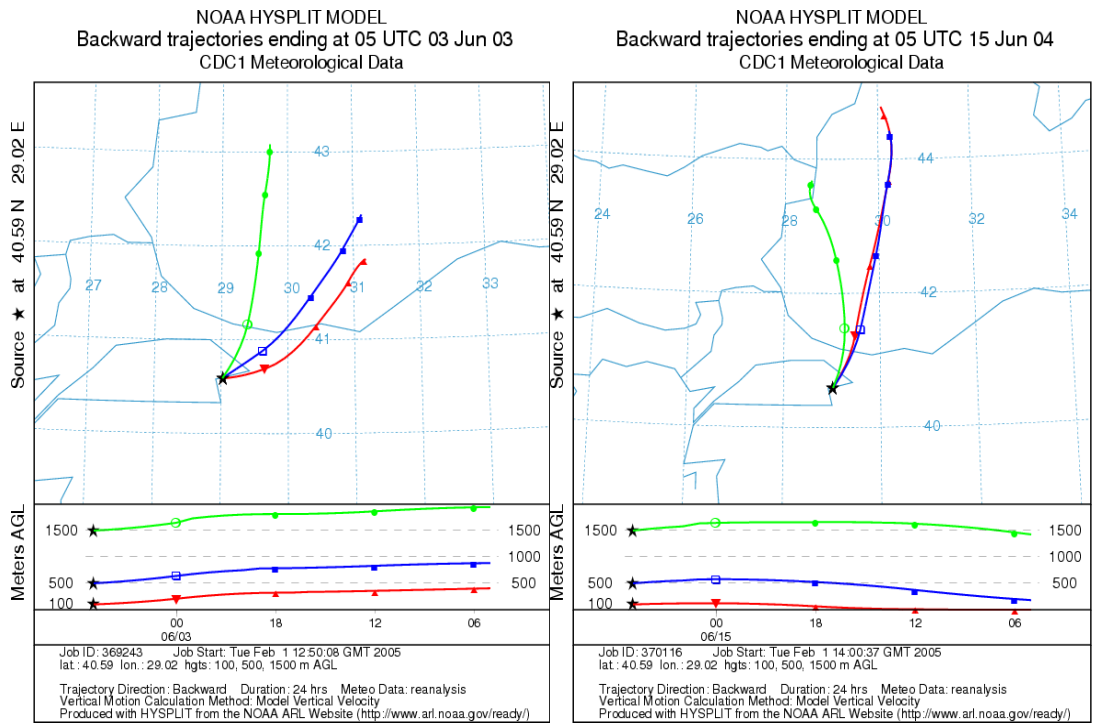


Figure 2.c Figure 2.d

Figure 2. HYSPLIT Projection of example days

***Year 2002:*** For 2002, average numbers are given in Table 4 according to years and stations. In figure 3, ozone concentration and wind velocity graphic related to 25-26-27 August 2002 for Kadikoy station is given as an example. On 25 August 2002, ozone concentration during the day was generally above 60 μg/m$^3$. In night there were two peaks at 01:00 and 04:00. After 05:00 a.m., ozone concentration continued decreasing. On 26 August there were three peaks at 22:00 (73 μg/m$^3$), 23:00 (91 μg/m$^3$) and 05:00 (112 μg/m$^3$) a.m. In figure 2b, HYSPLIT projection for 26 August is given. It can be seen from this figure that the air parcel came from NE (Russian-The Crimea-Black Sea) direction in 24 hours (beginning from 05:00 a.m.) for 100, 500 and 1000 m heights for this day.

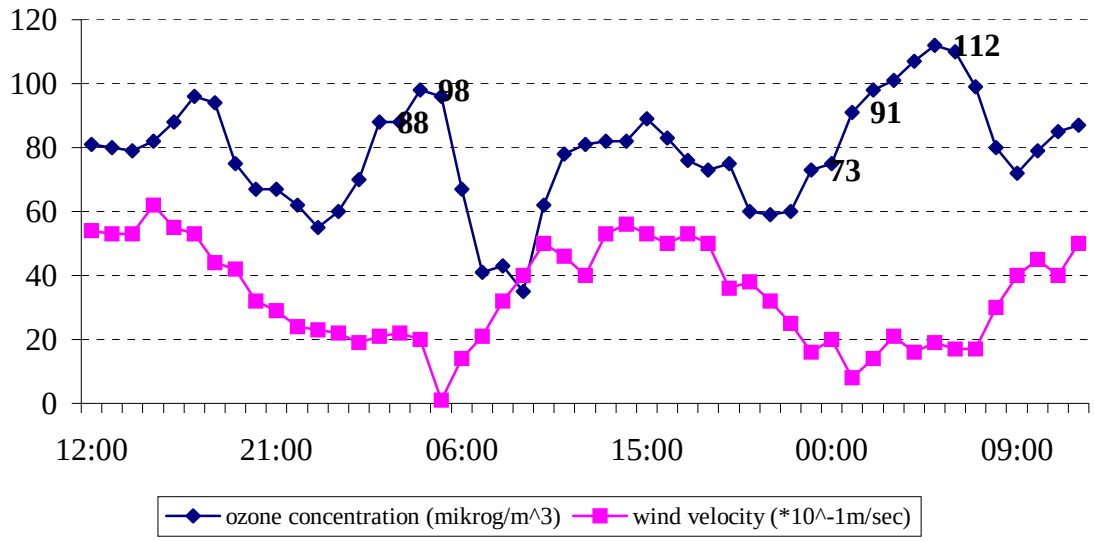


Figure 3. Ozone concentration and wind velocity at 25-26-27 August 2002

***Year 2003:*** Average numbers are given in Table 4 for 2003 according to years and stations. In figure 4, ozone concentration and wind velocity graphic is relating to 02-03-04 June 2003 for Kadikoy station is given as an example. On 02 June 2003, ozone concentration in day generally changed from 42 to 81 $\mu g/m^3$ until 20:00. On 03 June, two peaks formed at 01:00 and 03:00. It continued decreasing during the next day and there were two peaks at 04.00 and 05:00 a.m. subsequently.

In figure 2, HYSPLIT projection of 03 June is given. It can be seen from this figure that the air parcel came from ENE (Russian-The Caucasia-Black sea) direction for 100 m heights and NE and NNE direction (Russian-The Crimea-Black Sea) direction for 500 and 1500 m in 24 hours respectively for this day.

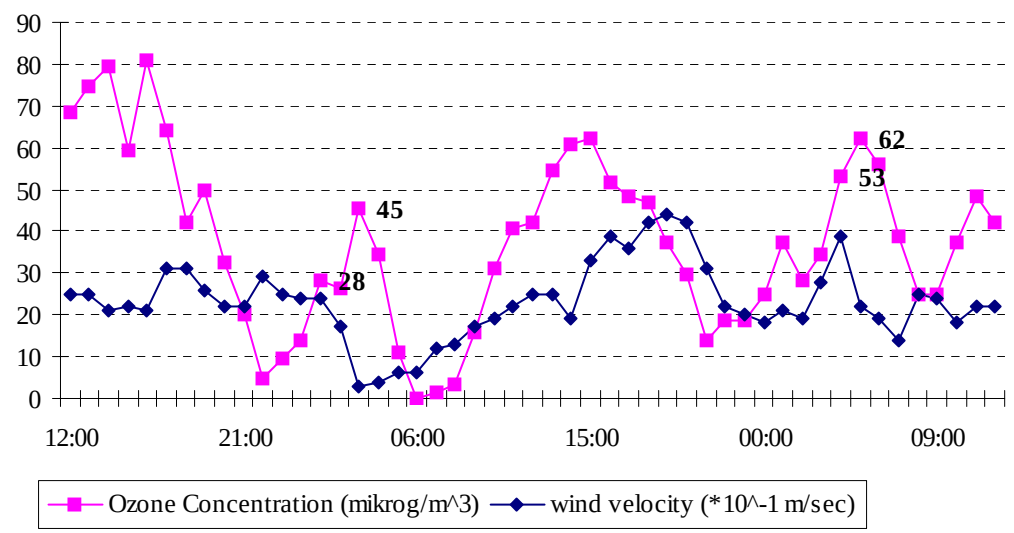


Figure 4. Ozone concentration and wind velocity at 02-03-04 June 2003

***Year 2004:*** Average numbers are given in Table 4 for 2004 according to years and stations. In figure 5, ozone concentration and wind velocity graphic is relating to 13-14-15 June 2004 for Kadikoy station is given as an example. On 13 June 2004, ozone concentration was changing 13-54 μg/m$^3$ and on 14 June there was a peak at 03:00 a.m., daily ozone concentration increased until 60 and on 15 June at 02:00, there was a peak at 44 μg/m$^3$. In figure 2, HYSPLIT projection of 15 June is given. It can be seen from this figure that the air parcel came from NNE (Russian-The Crimea-Black Sea) direction for 100 and 500 m heights and N direction (Scandinavia-Balkans) direction for 1500 m in 24 hours for this day.

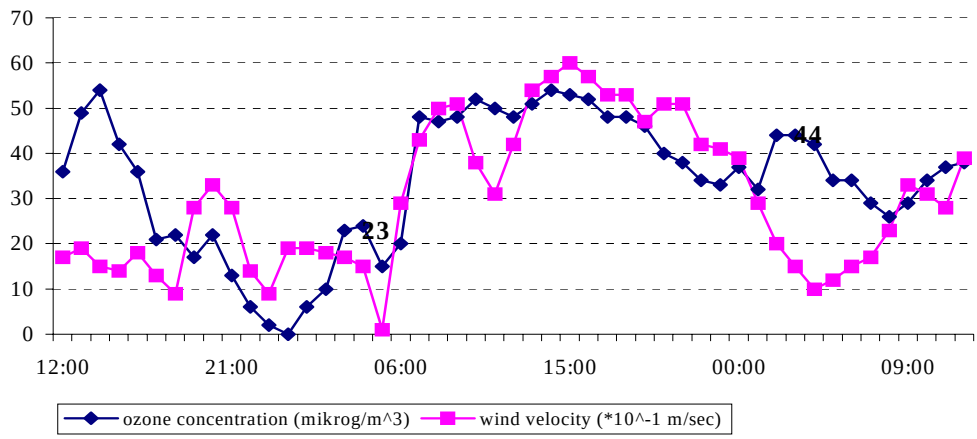


Figure 5. Ozone concentration and wind velocity at 13-14-15 June 2004

As can be seen from this discussion, night ozone concentration could be high in Istanbul at summer months. Sources and contributors of this phenomenan must be investigated by removing meteorological absences (such as Richardson number).

## REFERENCES


Chung, Y.-S., 1977. Ground-level ozone and regional transport of air pollutants. Journal of Applied Meteorology, 16 (11), 1127–1136.

Corsmeier, U., Kalthoff, N., Kolle, O., Kotzian, M., Fiedler, F., 1997. Ozone concentration jump in the stable nocturnal boundary layer during a LLJ event. Atmospheric Environment 31,1977-1989.

Eliasson, I., Thorsson, S., Andersson-Sköld, Y., 2003. Summer nocturnal ozone maxima in Goteborg, Sweden. Atmospheric Environment 37, 2615–2627.

Lee, Y.C., Calori, G., Hills, P., Carmichael, G. R., 2002. Ozone Episodes in Urban Hong Kong 1994-1999. Atmospheric Environment 36, 1957-1968.

Liu, C-M., Liu, S., Shen, S.-H., 1990. A study of Taipei ozone problem. Atmospheric Environment 24A, 1461–1472

NOAA ARL Quality Forecasting internet site, www.arl.noaa.gov

Salmond, J.A., McKendry, I.G., 2002. Secondary ozone maxima in a very stable nocturnal boundary layer:Observations from the Lower Fraser Valley,BC. Atmospheric Environment 36, 5771-5782.

Samson, P.J., 1978. Nocturnal ozone maxima. Atmospheric Environment 12, 951–955.
Steinberger, E.H., Ganor, E., 1980. High ozone concentrations at night in Jerusalem and Tel-Aviv. Atmospheric Environment, 14, 221–225.
Zurita, E., Castro, M., 1983. A statistical analysis of mean hourly concentrations of surface ozone at Madrid (Spain). Atmospheric Environment 17 (11), 2213–2220.

*Proceedings of the Third International Symposium on Air Quality Management at Urban, Regional and Global Scales. 26-30 September 2005, Istanbul – Turkey*

# USE OF CHEMICAL TRANSPORT MODEL FOR OZONE FORECAST IN TAIWAN

**Che-hui Tsai*, Hsu-cherng Chiang* and Ching-wen Hsu****

* Department of Water Resources and Environmental Engineering,
Tamkang University, Tamsui, Taipei-hsien, Taiwan
** Department of Environmental Engineering and Science,
Tajen Institute of Technology. Yanpu, Ping-tung, Taiwan

## ABSTRACT

An operational forecasting system using three-dimensional chemical transport photochemical model for predicting ground-level ozone concentrations in Taiwan has been developed. It consists of an emission model developed by Tamkang University, the mesoscale meteorological model RAMS, and the air quality model CAMx of Environ. In this paper, we introduce the component models, model coupling, and model initialization methods of this system. Then, the performance of this forecasting system during the 2002 ozone season were analyzed and discussed.

**Key Words :** real-time, Photochemical, Validation, RAMS, CAMx

## 1. INTRODUCTION

Ozone concentrations >120 ppbv have been observed relative frequently in Taiwan. Environmental Protection Administration of Taiwan have been forecasting next-day's pollutant standard index (PSI) since the year of 1992 to warn the public of unhealthy air and to encourage people to voluntarily reduce emissions-producing activities. Similar to Taiwan, many local authorities also issue air quality forecast in recent years. A lot of methods exist for forecasting ground-level ozone concentrations (USEPA, 2003). These methods can be classified into two categories, i.e., statistical and deterministic approaches.

The statistical models are based on the relations between a set of environmental predictors and the concentrations measured at different monitoring stations. Statistical approaches have been proposed for ozone forecasting include linear multiple regression, nonlinear regression, neural networks, classification and regression tree (CART). These approaches are easy to develop, however, there are systemic shortcomings that limit their usefulness. They require large training data sets for tuning the model's coefficients; hence they can be applied to regions with length observations only. The statistical models should be updated when emissions conditions change. This is a serious disadvantage in the circumstance of rapidly evolving primary pollutant emissions. In addition, high ozone episodes are rare events that may not be described properly by means of the classical statistical methods.

Deterministic models solve the governing equations that simulate the emission, transport, diffusion, transformation, and removal of air pollution to obtain the concentration distribution of ozone and other photochemical air pollutants. In the past, three-dimensional chemical transport models (CTM) have been widely used in air quality planning at different spatial scales in simulation mode (Russell and Dennis, 2000; Vautard et al., 2001). Currently, there is growing interest in the development of numerical air quality forecast systems by using CTM (McHenry et al., 1999; Chenevez and Jensen, 2001; Vaughan et al., 2004; CHRONOS, 2004). CTM approaches require numerous accurate input data (emissions, meteorology, land cover), which are difficult to collect in real time. This approach is difficult to develop and need large computer time to carried out the computations. In recent years, high performance computing at low cost has become available, so the latter problems should become less and less significant with time.

Although CTM have been widely used in Taiwan, this is the first time a numerical air quality forecasting system has been developed and validated in this island. In this paper, we will introduce this automated ozone forecast system and evaluate its performance.

## 2. BACKGROUND INFORMATION

Taiwan, which is lying between 23-25 N, and 121-123E, is an island located in the eastern side of Taiwan Strait. The topography of Taiwan, as shown in Fig. 1, is characterized by the ridge of Central Mountain. These mountains are steep with an altitude of 3000m and more and half width of few tens of kilometers. About 80% of the populations are live in the western side of Central Mountain. Taipei located in the northern Taiwan is the capital of Taiwan. Kaohsiung is an industrial city in the southern Taiwan.

The airflow in Taiwan is composed of both local and mesoscale wind system along with regional winds. Previous studies suggest that the local meteorology in Taiwan is controlled by several wind systems include the orographic blocking and barrier wind, land-sea breezes, mountain-valley winds, and urban heat island circulations. During summer time, Taiwan is dominated by subtropical high pressure of the Pacific Ocean and SW monsoon and typhoons; the latter two are often accompanied by high wind speed and unstable weather conditions, which are helpful for the dispersion of pollutants. The former, with its lower wind speed and high temperature, easily lead to higher concentrations of pollutants for the whole island. During winter time, Taiwan is dominated by NE wind. The Central Mountain acts as a barrier to the normal flow; a wake region will be developed on the downstream side (SW region of Taiwan). The solar radiations are strong and wind velocities are low at wake region so high ozone concentrations can occur even during early winter season.

As shown in Figure 1, Taiwan is divided into eight air quality forecast regions by Environmental Protection Administration of Taiwan. The geographical characters of each region are shown in Table 1.

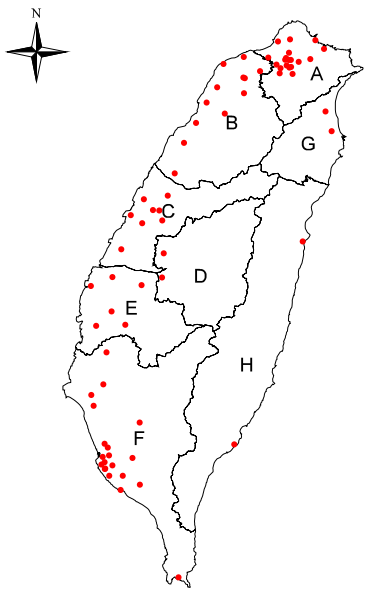


Figure 1. Locations of air quality forecast regions and air quality monitoring stations in Taiwan.

Table 1 Geographic characters of eight air quality forecast regions

| Region | Counties | Characters |
|---|---|---|
| A | Keelung,Taipei | Urban areas with high population density and heavy traffic |
| B | Taoyuan,Hsinchu,Miaoli | Median size cities, industrial areas, rural area |
| C | Taichung,Changhua | Median size cities, rural area |
| D | Nantu | Foothills and Central Mountain |
| E | Yunlin,Chiayi,Tainan | Small cities, agriculture areas |
| F | Kaohsiung,Pingtung | Industrial region |
| G | Ilan | Lower developed agriculture region |
| H | Hualian and Taitung | Lower developed agriculture region |

Figure 2 shows the time series of daily maximum 1h O3 concentrations for eight ozone forecast regions in Taiwan based on the measured data obtained from 71 surface ozone monitor sites in Taiwan. In this figure, the regional daily maximum values are represented by the peak values from all stations if more than one monitor station are site within that area. As shown in this figure, the events of ozone concentrations >120 ppbv occur frequently in all regions except region G and H. The worst months for ozone concentration are May and October. From a regional perspective, the ozone problem in region A and region F are the worst. Region H (Hualien-Taitung) and Region G (Ilan) perennially post the nation's best air quality and poor air quality occurs at the most once a year.

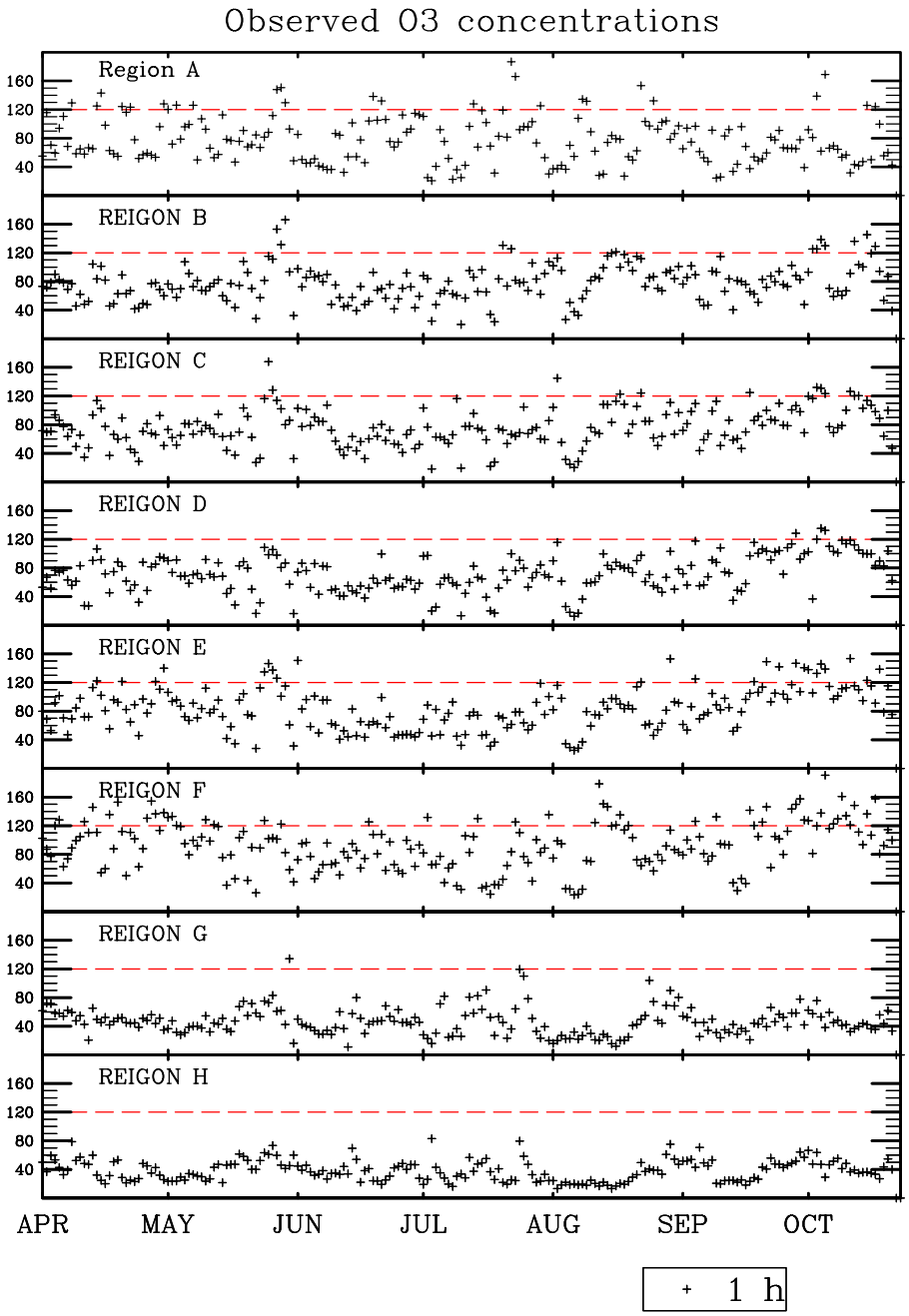


Figure 2. Daily maximum 1h O3 concentrations for eight ozone forecast regions in Taiwan during ozone season of 2002.

## 3. METHODS

This forecast system consists of an emission processing model, a mesoscale meteorological model, and an air quality model. They were integrated to produce forecasts automatically.

The emission model is developed by Tamkang University. The emission data were obtained from three different organizations. The anthropogenic emission data in Taiwan were collected by CTCI and organized into a database called TEDS (Taiwan

Emission Data System). The biogenic emissions are estimated by using AVHRR data. The emission data outside Taiwan were obtained from Center for Global and Regional Environmental Research, University of Iowa (CGRER, 2002). Those data were merged and processed by a emission processing program developed by Tamkang University to generate the required input files for photochemical air quality model.

The meteorological model used in this study is RAMS developed by Colorado State University (Walko and Tremback, 1995). RAMS is running once every day, initialized at 18Z (02LST) and simulate for next 48 hours. Initial and boundary conditions are constructed after downloading AVN forecast file from the National Center for Environmental Prediction (NCEP). RAMS simulations using 3 nested-grids system. As shown in Fig. 3, the coarse (48km) domain covers much of East Asia. The second domain uses a uniform horizontal grid size of 12km. The very high-resolution 4km domain is centered on Taiwan, about 500km long and 300km wide. All RAMS domains use a polar-stereographic projection with 29 sigma-coordinate layers in the vertical.

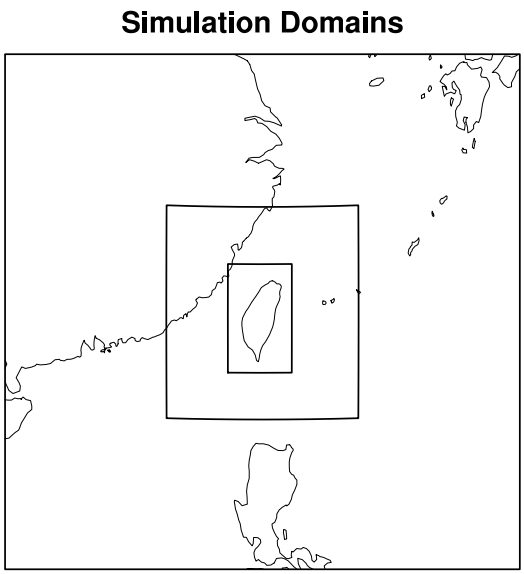


Figure 3. The nested grids used in meteorological simulations.

The photochemical air quality model used in this study is Comprehensive Air quality Model with extensions (CAMx) developed by Environ International (Environ International Co., 2002). CAMx is a 3-D Eulerian photochemical dispersion model. In this study, a modified version of the Carbon Bound IV chemical mechanism was used. The initial value problem is not of importance for the present study since the simulation is continuous. The initial conditions for next-day's simulation were determined from previous day's results. Clean tropospheric background concentrations were set on the boundary of coarse domain.

This system had operated in a real-time mode from April 1 to October 31, 2002. The results of forecast were saved for further analysis.

## 3. RESULTS AND DISCUSSION

(1) Forecasting results for daily maximum 1 h ozone concentrations

The results of day-to-day forecast have been evaluated against data obtained from 71 surface ozone monitor sites in Taiwan. Figure 4 shows the time series plots of observed and predicted daily peak 1-h ozone concentrations.

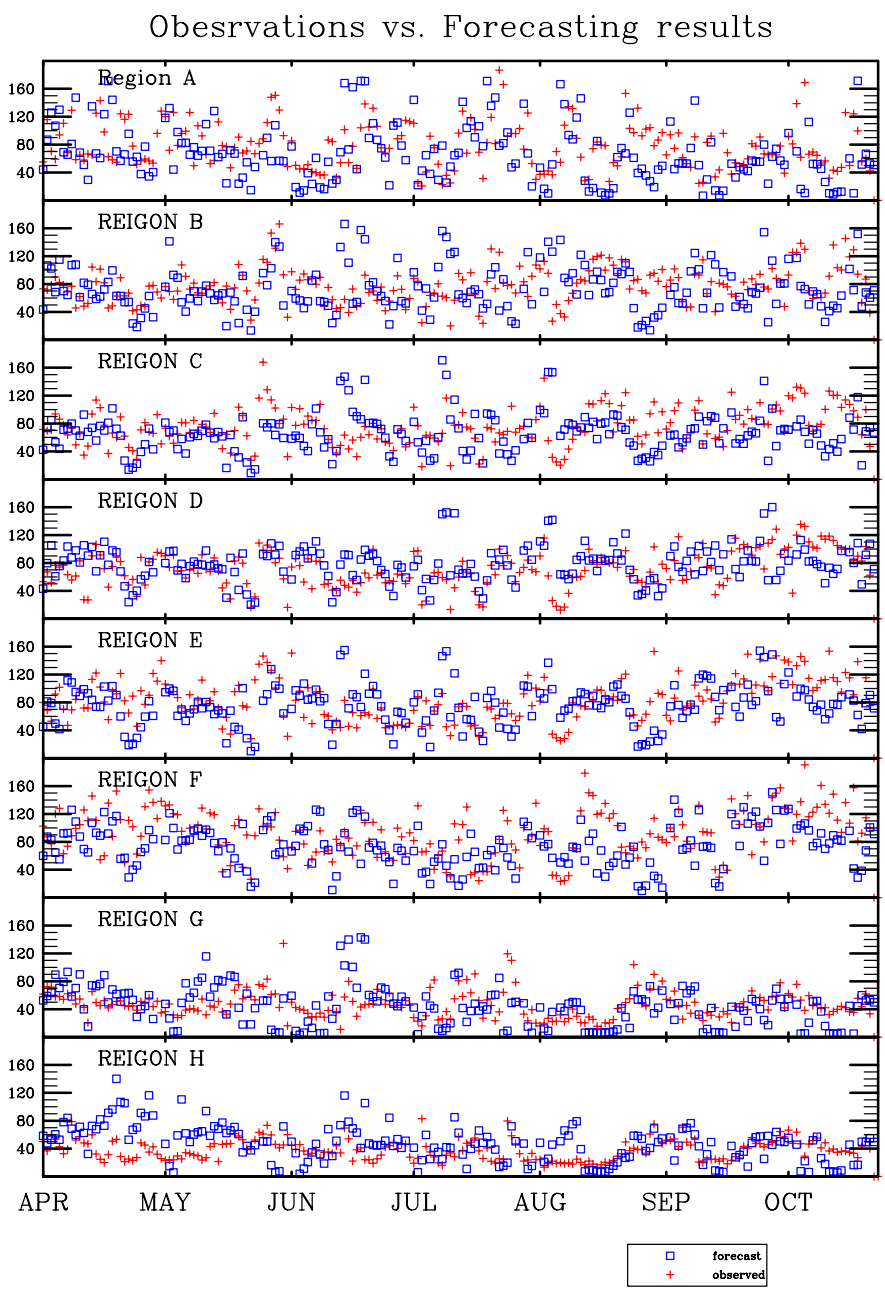


Figure 4. Time series plots of observed and predicted max. 1 h ozone concentrations.

Figure 5 shows the scatter plots of observed and predicted daily peak 1-h ozone concentrations for eight regions. The correlation coefficients ($R^2$) of observed and predicted concentrations are ranged from 0.12 to 0.41. From this prospect, the performance of this forecast system is not very satisfactory.

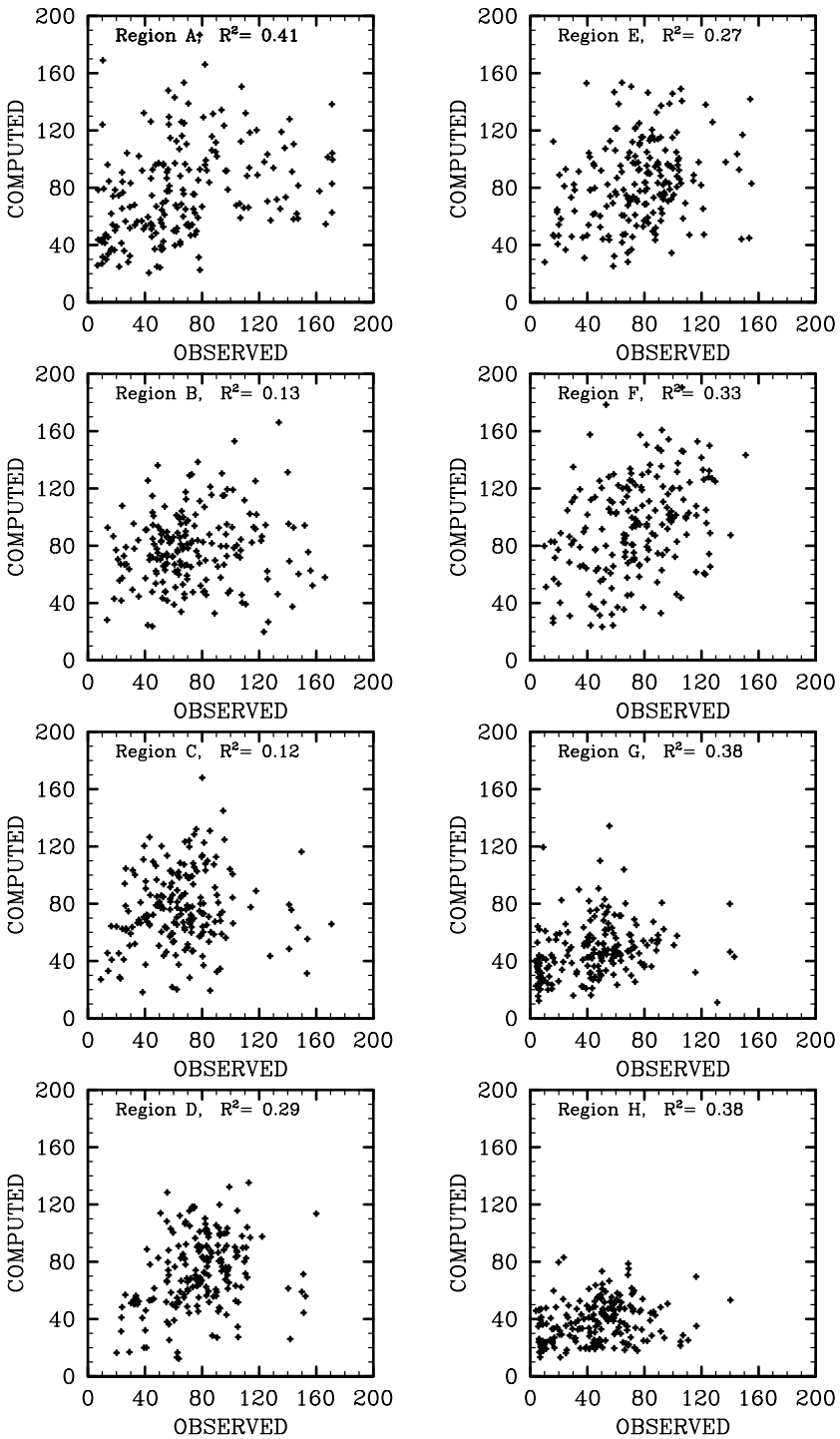


Figure 5. Scatter plots of observed and predicted max. 1 h ozone concentrations for eight regions during ozone season, 2002.

(2) Quantitative performance evaluation

Two different methods were used to evaluate the performance of this forecast system. The first approach is quite standard for model validation. The following measures were calculated for each monitoring station:

$$Bias = \frac{1}{N}\left[\sum_{i=1}^{n}(f_i - o_i)\right]$$

NB is Normalized Bias,

$$NB = \frac{1}{N}\left[\sum_{i=1}^{n}\frac{(f_i - o_i)}{o_i}\right]$$

MAE is mean absolute error,

$$MAE = \frac{1}{N}\left[\sum_{i=1}^{n}|f_i - o_i|\right]$$

In above equations, *f* denotes the daily peak 1-h ozone concentration for a specific stations, *o* is the corresponding ozone observed value. *N* is the number of samples which is equal to the number of stations in an air quality control area times the number of simulation days. This is a paired-in-space validation. The statistical summaries for 2002 simulation are shown in Table 1. The forecast is able to meet some performance criteria for regulatory models. Informal performance standards suggested by USEPA are: normalized bias ±5 to ±15%; normalized gross error ±30 to ±35%; unpaired peak prediction accuracy ±15 to ±20%.

Table 1. Paired-in-space validation for 2002 simulation

| Region | $AVE_s$ (ppb) | BIAS (ppb) | NB (%) | MAE (ppb) |
|---|---|---|---|---|
| A | 60.50 | -4.73 | 2.19 | 28.05 |
| B | 62.19 | -7.03 | -1.90 | 26.11 |
| C | 66.91 | -8.31 | -2.57 | 25.68 |
| D | 66.28 | 3.49 | 15.22 | 24.43 |
| E | 68.66 | -5.99 | 1.33 | 24.96 |
| F | 72.31 | -14.78 | -11.57 | 29.87 |
| G | 49.72 | -0.64 | 6.38 | 21.73 |
| H | 51.76 | -3.33 | -0.74 | 21.38 |

If the modeling targets switch to regional daily peak 1 h ozone concentrations, we will obtain the so called “regional validation”. The regional peak values are calculated as the average of the highest and second highest value in a specific region. The results of regional validation are shown in Table 2. Since the regional peak values were used, the average, bias and normalized bias values are increased.

Table 2. Regional validation for 2002 simulation

| Region | $AVE_p$ (ppb) | BIAS (ppb) | NB (%) | MAE (ppb) |
|---|---|---|---|---|
| A | 76.89 | -7.40 | -3.74 | 33.89 |
| B | 76.43 | -5.27 | 1.86 | 28.54 |
| C | 75.46 | -9.47 | -4.93 | 27.00 |
| D | 72.04 | 3.68 | 12.30 | 22.77 |
| E | 82.21 | -6.91 | -0.23 | 27.07 |
| F | 92.41 | -15.58 | -11.16 | 29.83 |
| G | 52.42 | -2.65 | 1.69 | 20.72 |
| H | 53.31 | -2.70 | -3.15 | 16.67 |

Another method for verification of the ozone forecast utilizes a standard contingency table as shown in Table 3. As shown in this table, perfect forecast program would have values in cells "A" and "D" only. In the real world, imperfect forecasts result in values in cells "B" and "C".

Table 3. Contingency table for a two-category forecast

| | | Forecast | |
|---|---|---|---|
| | | 120ppb | <120ppb |
| observed | 120ppb | A | B |
| observed | <120ppb | C | D |

Table 4 shows a frequency table of the forecasted and observed events. It is constructed by counting the frequency of occurrence of each event and assigning it to the appropriate cell. In this table, the average of the highest and second highest value in a specific region were used for classification. The threshold values in Table 3 were changed to 100 ppb.

According to Table 4 the probabilities of detection (POD), which represents the percentage of ozone events that were correctly forecast, are less than 50%. False alarm rate (FAR) is greater than 50%. In order to maintain public confidence in the ozone forecast, it is desirable that the POD is reasonable high and the FAR should be reasonable low. From this point of view, the performance of this system is not good enough.

It worth to mention that small discrepancies in wind direction can produce significant shifts in the spatial pattern of predicted ozone concentration over a region. Taiwan is an island with steep mountains, a variety of mesoscale meteorological phenomena in the troposphere, including land-water circulation patterns, heat-island effect, and flows in complex topography all exert considerable influence on transport of air pollutants. Thus, many of the challenges associated with air quality forecasting for Taiwan are inherited from the difficulty in weather forecasting for this area. To accurately forecast the ozone concentrations in Taiwan is inherent a difficult task.

## 4. CONCLUSION

The system described here represents a new approach for ozone forecast in Taiwan. Although the performance of this system during the ozone season of 2002 is

reasonable, it is not accuracy enough to be used routinely by air quality managers. Since this system is so complex, there are numerous opportunities for improvements in the future.

Table 4. Frequency table for a two-category forecast

| Region | (A) | (B) | (C) | (D) |
|---|---|---|---|---|
| A | 9 | 30 | 25 | 115 |
| B | 6 | 22 | 24 | 135 |
| C | 1 | 27 | 9 | 145 |
| D | 2 | 12 | 18 | 142 |
| E | 8 | 38 | 17 | 123 |
| F | 27 | 40 | 19 | 89 |
| G | 0 | 2 | 2 | 97 |
| H | 0 | 0 | 2 | 118 |

## REFERENCES


Cardelino, C., Chang, M., St. John, J., Murphey, B., Cordle, J., Ballagas, R., Patterson, L., Powell, K., Stogner, J., and Zimmer-Dauphinee, S., 2001, Ozone predictions in Atlanta, Georgia: Analysis of the 1999 ozone season, Air & Waste Manage. Assoc., **51**, 1227-1236.

Center for Global and Regional Environmental Research, 2002, Emission data, Internet URL http://www.cgrer.uiowa.edu/EMISSION_DATA/

Chenevez, J., and Jensen, C., 2001, Operational ozone forecasts for the region of Copenhagen by the Denish Meteorological Institute, Atmospheric Environment, **35**, 4567-4580.

CHRONOS, 2004, http://gfx.weatheroffice.ec.gc.ca/chronos/index_e.html

ENVIRON International Co., 1997, User's Guide to the Comprehensive Air Quality Model with Extensions (CAMx), Novato, CA.

McHenry, J. N., Ryan, W. F., Seaman, N. L., Coats, C. J., Pudykiewicz, J.A., Arunachalam, Sarav, Vukovich, Jeffery M., 2004, A Real-Time Eulerian Photochemical Model Forecast System: Overview and Initial Ozone Forecast Performance in the Northeast U.S. Corridor, Bull. Amer. Meteor. Soc., 85, 525-548

Russell A. and Dennis, R., 2000, NARSTO critical review of photochemical models and modeling, Atmospheric Environment, **34**, 2283-2324.

USEPA, 2003, Guideline for developing an air quality (ozone and $PM_{2.5}$) forecasting program, EPA-456/R-03-002, Research Triangle Park, NC

Vaughan, J., Lamb, B., Frei, C., Wilson, R., Bowman, C., Figueroa-Kaminsky, C., Otterson, S., Boyer, M., Mass, C., Albright, M., Koenig, J., Collingwood, A., Gilroy, M., and Maykut, N., 2004, A numerical daily air quality forecast system for the Pacific Northwest, Bull. Amer. Meteor. Soc., **85**, 549-560

Vautard, R., Beekmann, M., Roux, J., and Gombert, D., 2001, Validation of a hybrid forecasting system for the ozone concentrations over the Peris area, Atmospheric Environment, **35**, 2449-2461.

Walko,R.L., Tremback,C.J., and Hertenstein,R.F.A., 1995, RAMS (The Regional Atmospheric Modeling System) User's Guide. Fort Collins, CO

*Proceedings of the Third International Symposium on Air Quality Management at Urban, Regional and Global Scales. 26-30 September 2005, Istanbul – Turkey*

# EVOLUTION OF THE TROPOSPHERIC COMPOSITION IN 2030: IMPACT ON EUROPEAN AIR QUALITY

**Szopa Sophie, Didier A. Hauglustaine and Robert Vautard***

Laboratoire des Sciences du Climat et de l'Environnement, CEN Saclay, Orme des Merisiers, Bat. 712, F-91191 Gif-sur-Yvette CEDEX, France, szopa@cea.fr, hauglustaine@cea.fr
*Laboratoire de Météorologie Dynamique, Ecole Polytechnique, F-91128 Palaiseau CEDEX, France, Robert.Vautard@lmd.polytechnique.fr

## ABSTRACT

Over the next decades, the atmospheric composition will be affected by major changes in anthropogenic emissions and in particular by an increasing number of megacities and by climate change. In order to investigate and discriminate the impacts of these changes on the tropospheric composition, several simulations were performed in the framework of the ACCENT network modeling activities. This activity relies on the recent availability of new global emission scenarios developed by the IIASA institute. The LMDz-INCA general circulation model is involved in this activity among 25 global models. Furthermore, additional simulations were performed using the LMDz-INCA results as boundary conditions for the CHIMERE regional model and the IIASA emissions datasets in order to better analyse future air quality trends in Europe. In addition, several model simulations considering separately the emission changes and the global boundary condition changes were carried out. We discuss in particular a possible compensation between European emission reductions and the effects, in Europe, of the global emission increase.

**Keywords :** Air Quality, Global and Regional Modeling, Evolution of Atmospheric Composition

## 1. INTRODUCTION

Ozone is a trace gas species resulting, in the troposphere, from the oxidation of carbonaceous compounds (methane, carbon monoxide, volatile organic compounds) in the presence of nitrogen oxides both emitted by anthropogenic and natural processes. Attention is paid to this molecule for its role as a greenhouse gas impacting global climate as well as for its impact on air quality closed to inhabited areas during smog events causing both human health and vegetation damages. The emissions of ozone precursors (nitrogen oxides and volatile organic compounds) are expected to decline in the European Union (EU-25) until 2020 even under the assumption of accelerated economic growth. However, ozone and its precursors are subject to long-range transport in the atmosphere. Therefore, the future air quality in Europe will not only be a result of local emissions but will also be affected by the global distribution of ozone and its precursors. The future evolution of ozone and associated radiative forcing was recently investigated by 25 state-of-the-art global

atmospheric chemistry models in the framework of the Photocomp experiment (Stevenson et al., 2005; Dentener et al., 2005). In this study, we apply a global climate-chemistry model and a regional chemistry-transport model dedicated to air quality studies to refine these results and investigate the relative impact of anthropogenic emission changes on Western European surface ozone levels in 2030. The relative contribution of the global ozone background modification with respect to the European emission control strategy is subsequently investigated.

## 2. MODELS AND PERFORMED SIMULATIONS

The global simulations were performed using the three-dimensional (3D) LMDz-INCA chemistry-climate model. LMDz (Laboratoire de Meteorologie Dynamique, zoom) is a grid point General Circulation Model (GCM) initially developed for climate studies. LMDz (version 3.3) has a horizontal resolution of 3.75 degrees in longitude and 2.5 degrees in latitude and uses 19 vertical *sigma*-p levels extending from the surface to 3 hPa. The INteractive Chemistry and Aerosols (INCA) model has been integrated into LMDz and simulates tropospheric chemistry, emissions and deposition of primary tropospheric trace species including non-methane hydrocarbons. The INCA chemical scheme used in this study describes the tropospheric photochemistry ($O_3$-$NO_x$-CO-VOC) through 85 chemical species and 303 chemical reactions. A detailed description and evaluation of LMDz-INCA are given in Hauglustaine et al. (2004) and Folberth et al. (2005). For the global scale simulations, the emission scenarios, recently described by Dentener et al. (2004) are used. For each scenario, the simulations were spun up for 3 months and performed over one year, using the nudged meteorology (i.e. meteorological fields are relaxed toward the ECMWF ERA40 reanalysis). Additional simulations were performed using the LMDz-INCA results as boundary conditions for a regional chemistry-transport model: CHIMERE. The CHIMERE model calculates gaseous chemical concentrations over Europe within an horizontal domain, ranging from 10.5°W to 22.5°E in longitude and from 35°N to 57.5°N in latitude. The horizontal resolution ($50x50km^2$) allows to capture the local $O_3$ maxima which is determinant regarding the population exposure to photochemical pollution and thus to determine compliance with the European $O_3$ standard (Schmidt et al., 2001). On the vertical, eight vertical hybrid sigma-p levels represent the atmospheric column from the surface to 500 hPa. The chemical mechanism is adapted from the EMEP chemical mechanism. The dynamical fields are computed using the MM5 model driven by the ECMWF ERA40 reanalysis. For both global and European simulations, the meteorology corresponds to the year 2001.

Three scenarios were tested representing respectively the implementation of current air quality legislation in each individual country around the world (CLE scenario), the maximum reduction of emissions currently technically feasible (MFR scenario) and the scenario SRES-A2 developed for the last Intergovernmental Panel for Climate Change report. For the three 2030 scenarios we applied LMDz-INCA coupled with CHIMERE to investigate the response of European summer pollution episodes relative to present day pollution level to (1) global and European modifications of the anthropogenic ozone precursors emissions; (2) modifications of

global scale chemical composition due to anthropogenic emission changes all around the world except Europe; (3) projected 2030 anthropogenic emissions in Europe considering the current anthropogenic emissions in the rest of the world.

## 3. RESULTS

In this paper we focus on the "current legislation" (CLE) scenario which assumes current perspectives of individual countries on future economic development and anticipated effects of presently decided emission control legislation in the individual countries. Figure 1 shows the ozone change calculated with the global model for the whole world and those obtained with the regional model using the results coming from the global model as boundary conditions. At the global scale, a general increase of ozone concentrations, reaching up to 5-10 ppb over Asia, is observed except for the south of USA and Mexico and southern Europe (also shown by the simulation using the regional model) where an ozone decrease is predicted.

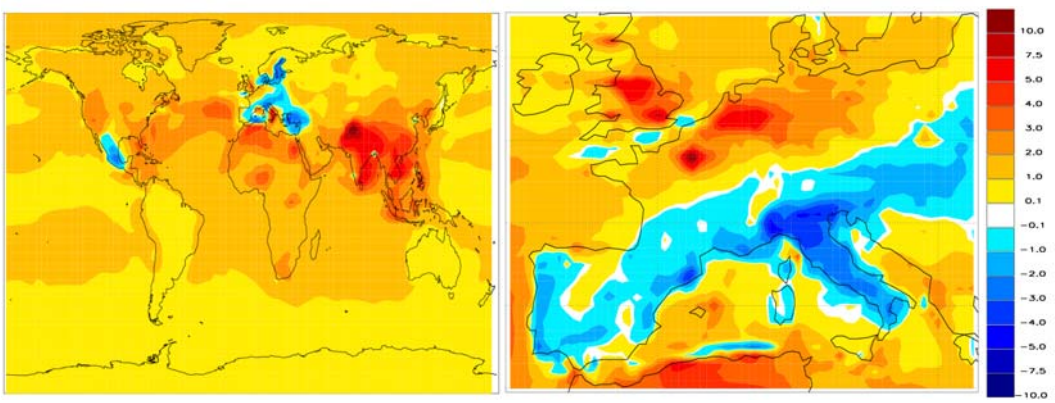


**Figure 1** : Future surface ozone changes, averaged over July (in ppb), considering the "Current Legislation" (CLE) scenario: (right) ozone computed by LMDz-INCA and (right) daily maximum surface ozone computed by CHIMERE (coupled with LMDz-INCA) over Europe.

In order to refine the study over Europe and to discriminate the role of European emission changes and global emission changes, two additional simulations were carried out. The changes of the daily maximum surface ozone mixing ratio are shown in Figure 2 for July conditions. The main conclusions are that the European emission reduction policy would lead to a decrease of maximum ozone daily values for almost all European locations except the main north European towns and suburbs. The global emission modifications have an opposite effect increasing the averaged of the maximum daily ozone values all over Europe from 1 to 3 ppb. This study shows how political decisions could be counterbalanced by the global emission changes and underlines the importance of taking into account the global scale changed to assess the relevance of such policy.

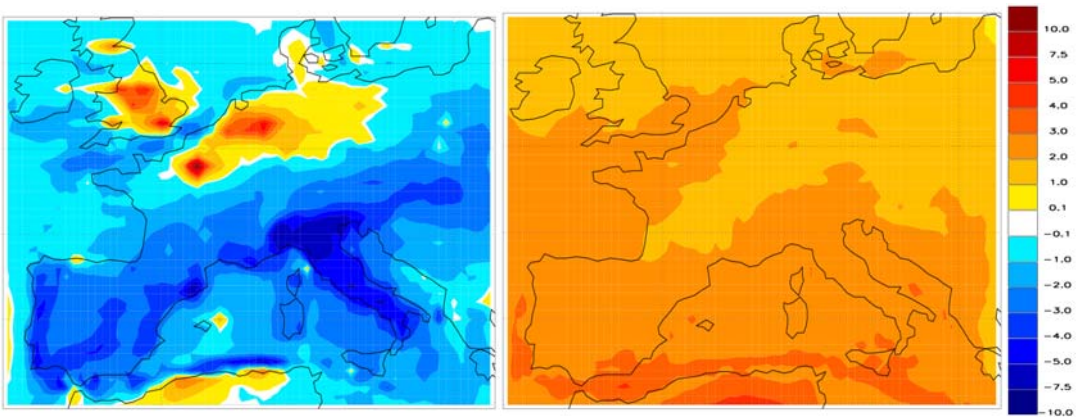


**Figure 2** : Future changes of daily maximum surface ozone averaged over July (in ppb) computed by CHIMERE (left) considering the 2030 changes in emissions such as in the CLE scenario over Europe but without any changes of emissions over the rest of the world and (right) considering no emission modification over Europe but taking into account the 2030 changes of emissions over the rest of the world.

## 4. CONCLUSION

This 3D model analysis coupling a global model with a sub-continental model shows that realistic future emission modifications would lead to heterogeneous repartition of the effects on summertime Western European ozone air quality in 2030. The northern part of Europe, essentially highly inhabited areas, would see an increase of the mean level of surface ozone due to combined effects of both local and global emission changes. On the contrary, the air quality in south part of Western Europe would benefit from the reduction of emission policy managed in Europe despite of the global emission modifications which tend to increase the background ozone level and thus reduce the benefit of European policy. The simulation separating the role of worldwide emission changes and that of European emission control underlines the need of taking into account both global and regional scales to design relevant legislation for air quality management in the next decades.

## 5. ACKNOWLEDGEMENTS

The authors would like to acknowledge EMEP, IER (University of Stuttgart) and UK Dept of Environment for providing present day emissions data for Europe. The global emissions were provided by IIASA and reprocessing by Frank Dentener who made it available for the Photocomp experiment (managed under the umbrella of the European ACCENT network). The study was supported by the RETRO European project under contract EVK2-CT-2002-00170.

## REFERENCES

Dentener, F., D. Stevenson, J. Cofala, R. Mechler, M. Amann, P. Bergamaschi, F. Raes, and R. Derwent, 2004. The impact of air pollutant and methane emission controls on tropospheric ozone and radiative forcing: CTM calculations for the period 1990-2030, Atmos. Chem. Phys., 4, 8471-8538.

Dentener, F., et al., 2005. Global air quality for the next generation, *Geophys. Res. Lett*., submitted for publication.
Folberth, G., D. A. Hauglustaine, J. Lathière, and F. Brocheton, 2005. Impact of biogenic hydrocarbons on tropospheric ozone ; results from a global chemistry-climate model, *Atmos. Chem. Phys*., submitted for publication.
Hauglustaine, D. A., F. Hourdin, S. Walters, L. Jourdain, M.-A. Filiberti, J.-F. Larmarque, and E. A. Holland, 2004. Interactive chemistry in the Laboratoire de Météorologie Dynamique general circulation model : description and background tropospheric chemistry evaluation, *J. Geophys. Res.*, 109, D04314, doi:10.1029/2003JD003957.
Schmidt, H., C. Derognat, R. Vautard, and M. Beekmann, 2001. A comparison of simulated and observed ozone mixing ratios for the summer of 1998 in Western Europe, *Atmos. Environ.*, 35, 6277-6207.
Stevenson, D., et al., 2005. Multi-model ensemble simulations of present-day and near future tropospheric ozone, Atmos. Chem. Phys., submitted for publication.

*Proceedings of the Third International Symposium on Air Quality Management at Urban, Regional and Global Scales. 26-30 September 2005, Istanbul – Turkey*

# AN OPERATIONAL NESTED AIR QUALITY PREDICTION MODELING SYSTEM (NAQPMS) FOR SHANGHAI CITY WITH DATA ASSIMILATION

**Zifa Wang[1], Wenshuai Xu[1], Xiquan Wang[1], Qingyan Fu[2], Jing Wang[2], Dongqin Yang[2] and Yefei Zheng[2]**

[1]LAPC/NZC, Institute of Atmospheric Physics, Chinese Academy of Sciences, Beijing, 100029, China; zifawang@mail.iap.ac.cn;
[2] Shanghai Environmental Monitoring Center (SEMC), Shanghai 200030, China; Qingyanf@semc.com.cn.

## ABSTRACT

An operational nested air quality prediction modeling system (NAQPMS) has been developed to realize the real-time forecast of air quality for Shanghai city, China. The NAQPMS (Wang et al. 2001) investigated the various processes that govern the loading of chemical species and anthropogenic aerosols at various scales of atmospheric motions with emissions from East Asia to urban Shanghai. The model employs flexible horizontal grid resolution with multiple multi-level nested grids from 81, 27, 9, to 3km with options for one-way and two-way nesting procedures in a spherical and terrain-following coordinate. The meteorological driver used here is the NCAR/Penn State Fifth-Generation Mesoscale Model (MM5). Hourly pollutant levels of 25 stations covering Shanghai are used to evaluate the modeling system. Half year's forecasts clearly show that the technique of the model is capable of catching the variations of air pollutants and affording more realistic temporal and spatial structures of concentration fields, processes and precursors, especially for heavy pollution days. Furthermore, several case studies for high PM10 episodes are also discussed in this study to investigate the contributions of various sources. In this study, the spatial objective analysis technique based on the statistical interpolation analysis scheme is used to make data assimilation in NAQPMS. The assimilation of concentration of PM10 for August 2004 shows that that the bias error of assimilation results at independent observational location is smaller than that of model outputs, suggesting that assimilation results are closer to observed values than model outputs

**Keywords:** Operational forecast, air quality, Shanghai, regional and urban scale, numerical model.

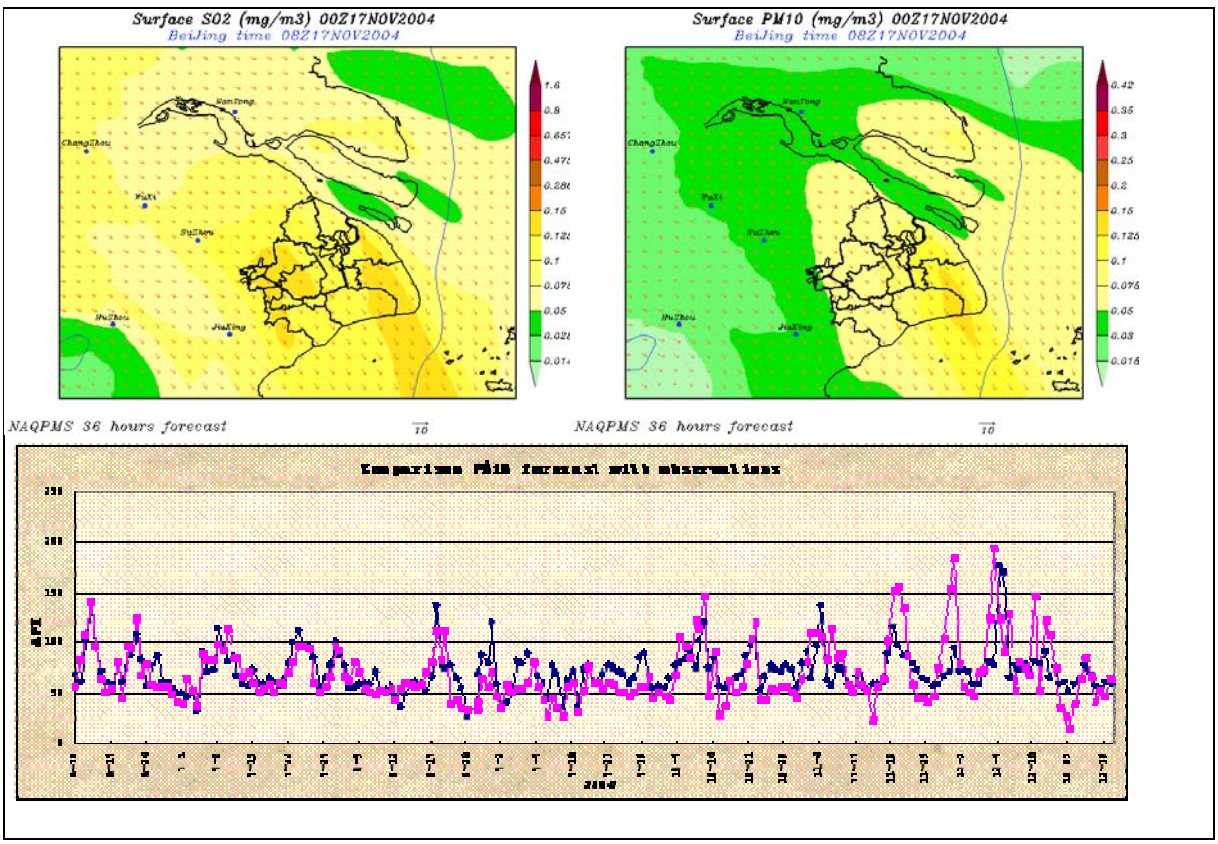


**Figure 1.** Snapshot of 36-hour forecast and comparison models with observed API from June to December 2004

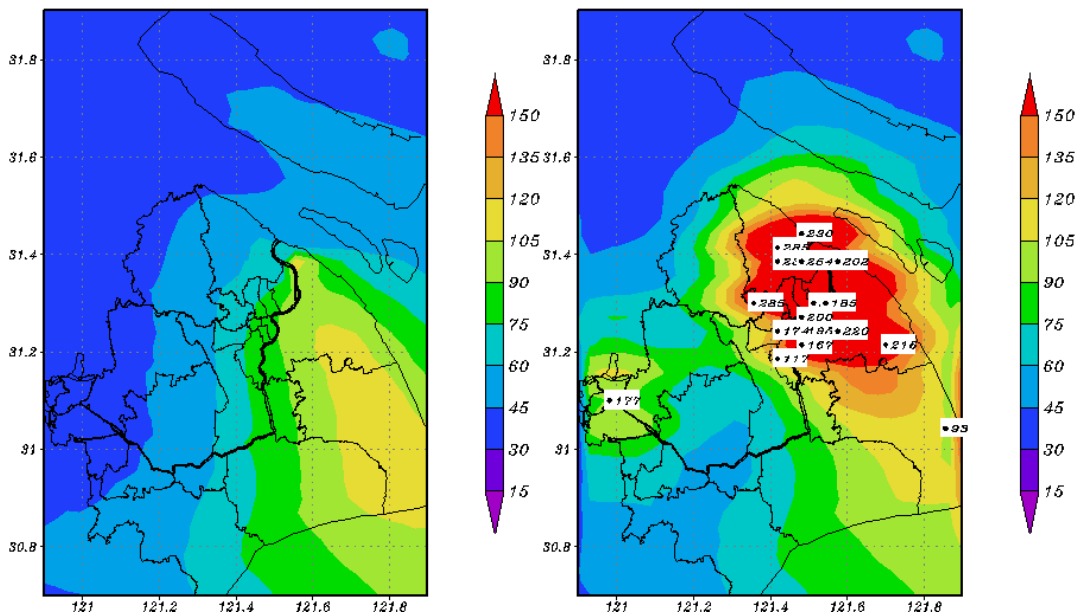


**Figure 2.** Difference between model outputs and assimilation results, indicating that the assimilation results are much larger than model output after assimilation of high observational values.

## REFERENCES

Wang Z., Maeda, T., Hayashi, M., Hsiao, L.-F. ,and Liu, K.-Y. (2001) A nested air quality prediction modeling system for urban and regional scales, application for high-ozone episode in Taiwan, Water, Air and Soil Pollution, 130, 391-396.

*Proceedings of the Third International Symposium on Air Quality Management at Urban, Regional and Global Scales. 26-30 September 2005, Istanbul – Turkey*

# IMPACT AND ASSESSMENT OF MARINE VESSELS EMISSIONS ON THE CORPUS CHRISTI URBAN AIRSHED

**Zuber Farooqui[1] and Kuruvilla John[2]**

1. Department of Environmental and Civil Engineering, Texas A&M University-Kingsville, MSC 213, Kingsville, Texas 78363, zfarooqui@even.tamuk.edu
2. Frank H. Dotterweich College of Engineering, Texas A&M University Kingsville, MSC 188, Kingsville, Texas 78363, k-john@tamuk.edu

## ABSTRACT

The two largest and yet uncertain sub-categories of air emissions from non-road sources include marine vessels and pleasure crafts. Ocean going vessels and pleasure crafts contribute a significant amount of emissions in the Corpus Christi urban airshed (CCUA). CCUA is classified as a near non-attainment area. It is the largest industrialized urban area in South Texas that is currently in compliance with the National Ambient Air Quality Standards (NAAQS) for ozone. Marine vessels represent a significant source with all other sources of emissions of ozone precursors, namely oxides of nitrogen (NOx) and volatile organic compounds in the CCUA. To find out the impact of marine vessels emissions on ozone levels, a comprehensive emission inventory was developed. Methodology adopted by ENVIRON was used to develop an emissions inventory for the Corpus Christi ship channel. It followed the EPA guidance regarding estimation of marine vessel emissions. To accomplish this work vessels-specific activity, engine characteristics, and emission factors information were collected. Vessel-specific information was needed because each ship entering and leaving the ship channel has a unique activity profile (ship cruise, speed, berthing, etc.) and a unique set of emission factors based on the size of the ship, its engines, and its activity profile while operating within the ship channel. It was determined that emissions from large ocean-going vessels contributed approximately 3% to the total NOx in the CCUA and that approximately 66% of the total marine vessels emissions were at docks while hoteling (docking). The NONROAD model was then used to estimate pleasure crafts emissions with local activities, population, temperature and other data collected from surveys. Spatial allocation of the estimated emissions was done using Geographical Information System (GIS) tools. A regional-scale photochemical model (Comprehensive Air Modeling system with extensions - CAMx) was used to evaluate the impact of these two sub-categories of precursor emissions on the urban ozone level of Corpus Christi and surrounding area. A high ozone episode of September 13-20, 1999 was used as the base case for the modeling analysis. The analysis showed that the impact from marine vessels on ozone levels was between 1 and 3 ppb within the urban airshed. Other source categories including on-road mobile sources had larger impact on local ozone levels.

**Keywords:** NONROAD model, marine vessel emissions, pleasure crafts, GIS

*Proceedings of the Third International Symposium on Air Quality Management at Urban, Regional and Global Scales. 26-30 September 2005, Istanbul – Turkey*

# QUANTITATIVE ASSESSMENT OF AIR QUALITY THROUGH MODELING OF POLLUTION CONCENTRATION IN ATMOSPHERE WITH KNOWN SURFACE VALUE IN CIRCULAR REGIONS

**V.P. Saxena and H.S. Jat***

School of Mathematics and Allied Sciences, Jiwaji University, Gwalior – 474011, India saxena_vp@rediffmail.com
*Department of Mathematics, M.P. College of Technology, Gwalior– 474006, India drhsjat@yahoo.co.in

## ABSTRACT

This paper deals with the mathematical model of atmospheric pollution problem when the a near circular ground source emits specific pollutant species vertically upward in still air. The eddy diffusivity is assumed to vary continuously in upward direction and attains very small value at some given height. The values of the concentration distribution are monitored at the ground and at the boundary points of the region under consideration. The Mathematical model, which is expressed in terms of partial differential equation, is solved in exact form yielding Bessel functions and Legendre polynomials. The numerical values of the concentration are computed for certain specific cases.

**Key Words** : Air Pollution, Mathematical Modeling, Numerical Computation, Initial and Boundary Conditions, Concentration Distribution.

## 1. INTRODUCTION

Many of the urban air pollution are related with near circular area source and vertical and radial distribution above the surface. The vertical distribution is influenced by the variation of eddy diffusivity which varies in vertical direction (Seinfeld, 1986) almost parabolically. This paper considers pollution distribution in an atmosphere with circular symmetry incorporating the above situations. Solution of the mathematical model is presented using Laplace transform in terms of modified Bessel functions and Legendre polynomials (Rainville, 1960).

Earlior, attempts have been made to solve mathematical models of pollution by simplified approach (Khan (1992), Kakamari (2001)) and also by advanced method for difficult problems (Saxena, Juneja, Aslan and Durukanoglu (2001)), (Tokgozlu, Saxena, Ocak and Erturk(2001)). Closed form solutions have also been obtained in certain cases (Saxena, Jat, Miri and Juneja (2003A)), (Saxena, Jat, Miri and Juneja (2003 B)), (Saxena and Juneja (2003)).

The mathematical solution of air pollution model obtained in this paper provides a closed from expression which can give air quality and pollution status at

any desired interval and at any location in vertical as well as in horizontal direction. As indicated above the eddy diffusivity of the substances present is assumed to vary in vertical direction in a particular fashion so that it reduces to minimum value at a particular height. The numerical computation is carried out for a particular situation of initial air quality to obtain pollution density in the whole region for different values of time. However, more result can be obtained for other situations also. At the same time model can be utilized for manipulating the air quality for a given pollutant.

## 2. MATHEMATICAL FORMULATION

We consider a near circular ground with known concentration of pollutant all over and a cylindrical region above it which is equally polluted initially but the pollution level falls down gradually. The concentration beyond this resign is supposed to be estimated vertically.

The governing partial differential equation and the allied conditions can be stated as:

$$\frac{1}{r}\frac{\partial}{\partial r}\left(rK_r\frac{\partial C}{\partial r}\right)+\frac{\partial}{\partial z}\left(K_z\frac{\partial C}{\partial z}\right)=\frac{\partial C}{\partial t} \tag{1}$$

where t is time, C is the concentration of pollutants and $K_r$ and $K_z$ are the turbulent diffusion coefficients along radial direction r and z – directions respectively.

We take

C (r, z, o) = L, C ( r, o, t) = L and C (a, z, t) = g(z,t) (given)

Here a = ground radius and L is a fixe value of C.

Now we use the transformation

y ( r, z, t) = L – C ( r, z, t)

Then equation (1) becomes

$$\frac{1}{r}\frac{\partial}{\partial r}\left(rK_r\frac{\partial y}{\partial r}\right)+\frac{\partial}{\partial z}\left(K_z\frac{\partial y}{\partial z}\right)=\frac{\partial y}{\partial t} \tag{2}$$

and condition becomes

y ( r, z, o) = 0, y ( r, o, t) = 0 and y ( a, z, t) = L – g ( z, t)

Further, assuming variable diffusivity in vertical direction reaching lowest value at the top (z=H), we take

$K_z = \lambda ( 1- z^2/H^2)$

Also, we assume

$K_r = K$, and $z/H = u$

Accordingly

$$K\left(\frac{\partial^2 y}{\partial r^2}+\frac{1}{r}\frac{\partial y}{\partial r}\right)+\frac{\lambda}{H^2}\frac{\partial}{\partial u}\left[(1-u^2)\frac{\partial y}{\partial u}\right]=\frac{\partial y}{\partial t}$$

(3)

The initial and boundary conditions are

$y ( r, u, o) = 0$, $y ( r, o, t) = 0$
$y ( a, u, t) = G (u,t)$

(4)

## 3. **SOLUTION**

The Laplace transform is defined as

$$\{y(r,u,t)\}=\bar{y}(r,u)=\int_0^\infty \exp(-pt)y(r,u,t)dt \,\mathrm{Re}(p)>0 \qquad (5)$$

with the inversion formula

$$y(r,u,t) = \frac{1}{2\pi i}\int_{\sigma-i\infty}^{\sigma+i\infty}\exp(pt)\bar{y}(r,u)dp \qquad (6)$$

where $0 < \sigma < 1$. Also we know that

$$\left\{\frac{\partial}{\partial t}y(r,u,t)\right\} = p \quad \{y(r,u,t)\}-y(r,u,0) \qquad (7)$$

Hence with the help of initial condition (4), the equation (3) takes the form

$$\frac{\partial^2 \bar{y}}{\partial r^2}+\frac{1}{r}\frac{\partial \bar{y}}{\partial r}+\frac{\lambda}{KH^2}\frac{\partial}{\partial u}\left[(1-u^2)\frac{\partial \bar{y}}{\partial u}\right]=\frac{p}{k}\bar{y}(r,u) \qquad (8)$$

with the conditions

$$\{y(r,o,t)\} = 0 \qquad (9)$$
$$\{y (a, u,t)\} = G(u)$$

where

$$G(u) = \{G(u,t)\}$$

Using the properties of Legendre's polynomial (Rainville(1962)), we have that if

$$y_n(r) = \int_0^1 \bar{y}(r,u) P_{2n+1}(u) du \quad (10)$$

then

$$\bar{y}(r,u) = \sum_{n=0}^{\infty} (4n+3) y_n(r) P_{2n+1}(u) \quad (11)$$

We also know that the Legendre's polynomial $P_{2n+1}(u)$ is solution of the differential equation

$$\frac{d}{du}\left[(1-u^2)\frac{d}{du}P_{2n+1}(u)\right] + (2n+1)(2n+2)P_{2n+1}(u) = 0 \quad (12)$$

Hence using equation (10) and (11), we get equation (8) in the form

$$\frac{\partial^2 y_n}{\partial r^2} + \frac{1}{r}\frac{\partial y_n}{\partial r} - \xi_n^2 y_n = 0 \quad (13)$$

where

$$\xi_n^2 = \frac{\lambda}{KH^2}(2n+1)(2n+2) + \frac{p}{k}$$

Equation (13) is known as Bessels equation and its solution is given as

$$y_n = AI_0(\xi_n r) + B\,Ko(\xi_n r) \quad (14)$$

But as $r \longrightarrow 0$, $K_0(\xi_n r) \rightarrow \infty$

Therefore B = 0 and from (5)

A = Yn/ $I_0(\xi_n a)$,

$$y_n = \int_0^1 P_{2n+1}(u)\overline{G}(u)du$$

(15)

Substituting in (14), (11) and (6), we get

$$y(r, u, t) = \sum_{n=0}^{\infty}(4n+3)P_{2n+1}(u)\frac{1}{2\pi i}\int_{\sigma-i\infty}^{\sigma+i\infty}Y_n\frac{I_0(\xi_n r)}{I_0(\xi_n a)}\exp(pt)dp$$

(16)

or

$$y(r, z/H, t) = \sum_{n=0}^{\infty}(4n+3)P_{2n+1}(z/H)\frac{1}{2\pi i}\int_{\sigma-i\infty}^{\sigma+i\infty}\frac{Y_n I_0(\xi_n r)}{I_0(\xi_n a)}\exp(pt)dp$$

(17)

But

y ( r, z, t) = L – C ( r, z, t)

Therefore

C (r, z, t) = L – y (r, z, t)

and

$$C(r, z/H, t) = L - \sum_{n=0}^{\infty}(4n+3)P_{2n+1}(z/H)\frac{1}{2\pi i}\int_{\sigma-i\infty}^{a+i\infty}\frac{Y_n I_0(\xi_n r)}{I_0(\xi_n a)}\exp(pt)dp$$

(18)

## 4. SPECIAL CASE

Now as a particular case, we take

$$C(a, z,t) = \left(\frac{L}{H}\right)z$$

So that from equation (9) and (16) and the integrals

$$\int_0^1 x^y P_{2n+1}(x)dx = \frac{1}{4n+3}, y = 2n+1$$
$$= 0, y \neq 2n+1$$

(19)

we get

$$Y_n = \frac{L}{3Hp}$$

Therefore

$$C(r, z/H, t) = \frac{Lz}{H}\frac{1}{2\pi i}\int_{\sigma-i\infty}^{\sigma+i\infty}\frac{I_0(\xi_0 r)}{pI_0(\xi_0 a)}\exp(pt)dp$$

(20)

Here

$$\xi_0 = \left[\frac{2}{H^2} + p/k\right]^{1/2} \qquad \text{at} \quad \lambda = k$$

The zeros of $I_0(\xi_0 a)$ are

$$\frac{2}{H^2} + p/k = -\alpha_n^2$$

(21)

$$\Rightarrow \left(2/H + \alpha_n^2\right) = -p/k$$

or

$$p = -k\left(\frac{2}{H^2} + \alpha_n^2\right)$$

(22)

where $\alpha_n$ are roots of the equation $J_0(a\alpha) = 0$.

Hence evaluating the integral on the right hand side of (20) with the help of residue method, we obtain

$$C(r, z, t) = L - \frac{L\,z}{H}\left[1 - \frac{2}{a}\sum_{n=1}^{\infty}\frac{\alpha_n \exp\left\{-k\left(\frac{2}{H^2}+\alpha^2\right)t\right\}J_0(r\alpha_n)}{\left(2/H^2+\alpha_n^2\right)J_1(a\alpha_n)}\right] \quad (23)$$

## 5. NUMERICAL COMPUTATION

On taking H = 1 km, we get

$$\begin{aligned} C(r, z, t) = L\,[&1 - z + z\,(1.3915)\exp(-25.127\,kt) \times J_0(4.809\,r) \\ &- z\,(1.0440)\exp(-123.881\,kt)\,J_0(11.040\,r) \\ &+ z\,(0.8512)\exp(-301.5322\,kt)\,J_0(17.307\,r) \\ &- z\,(0.7275)\exp(-558.1579\,kt)\,J_0(23.583\,r)\,t \end{aligned} \quad (24)$$

Here

A = .5 km

The numerical values of $C_1$ (r,z,t), where

$$C_1(r,z,t) = C(r,z,t)/L$$

for different r and at the different time values are shown in the Table-1 and Table-2.

Table 1. The concentration distribution at different radius values and different height where t = 60 sec. and k = $3.5 \times 10^{-3}$ km/gm/sec.

| z ↓ \r → | 0.0 | 0.1 | 0.2 | 0.3 | 0.4 | 0.5 |
|---|---|---|---|---|---|---|
| 0.0 | 1.0000 | 1.0000 | 1.0000 | 1.0000 | 1.0000 | 1.0000 |
| 0.1 | .9629 | .9596 | .9650 | .9340 | .9193 | .9001 |
| 0.2 | .9258 | .9192 | .9300 | .8687 | .8386 | .8003 |
| 0.3 | .8888 | .8788 | .8950 | .8031 | .7579 | .7005 |
| 0.4 | .8517 | .8384 | .8600 | .7375 | .6772 | .6007 |
| 0.5 | .8147 | .7980 | .8251 | .6719 | .5966 | .5009 |
| 0.6 | .7776 | .7576 | .7934 | .6062 | .5159 | .4010 |
| 0.7 | .7405 | .7173 | .7551 | .5406 | .4352 | .3012 |
| 0.8 | .7035 | .6769 | .7201 | .4750 | .3545 | .2014 |
| 0.9 | .6664 | .6365 | .6852 | .4094 | .2738 | .1016 |
| 1.0 | .6294 | .5961 | .6502 | .3438 | .1932 | .0018 |

At a = .5 km

H = 1 km;
At t = 60 sec.
k = .001 km/gm/sec.= $1.0 \times 10^{-3} \times$ km/gm/sec.

Table 2. The concentration distribution at different radius values and different height where t = 60 sec. and k = $1.0 \times 10^{-3}$ km/gm/sec.

| z \ r → | 0.0 | 0.1 | 0.2 | 0.3 | 0.4 | 0.5 |
|---|---|---|---|---|---|---|
| 0.0 | 1.0000 | 1.0000 | 1.0000 | 1.0000 | 1.0000 | 1.0000 |
| 0.1 | .9307 | .9288 | .9307 | .9157 | .9087 | .9000 |
| 0.2 | .8614 | .8577 | .8614 | .8315 | .8174 | .8001 |
| 0.3 | .7922 | .7865 | .7921 | .7473 | .7261 | .7002 |
| 0.4 | .7229 | .7154 | .7228 | .6631 | .6348 | .6003 |
| 0.5 | .6537 | .6443 | .6536 | .5789 | .5435 | .5003 |
| 0.6 | .5844 | .5731 | .5843 | .4947 | .4522 | .4004 |
| 0.7 | .5152 | .5020 | .5150 | .4105 | .3609 | .3005 |
| 0.8 | .4459 | .4309 | .4457 | .3263 | .2696 | .2006 |
| 0.9 | .3767 | .3597 | .3765 | .2421 | .1783 | .1006 |
| 1.0 | .3074 | .2886 | .3072 | .1578 | .0870 | .0007 |

**REFERENCES**


Kakamari, Khaleel Ahmed G., 2001. Ph.D. Thesis in Bangalore University.

Khan, Sujit Kumar, 1992. Ph.D. Thesis in Bangalore University.

Rainville, E.D., 1960. Special Functions, McMillan.

Seinfeld, John H., 1986. Atmospheric chemistry and physics of air pollution, John Wiley & Sons.

Saxena, V.P., Juneja, A., Aslan, Z. and Durkanoglu, F., 2001. Modelling of horizontal dispersion of pollutants in the atmosphere with wind: A Core Study in the Proc. of Sec Int. Symp. on Air Quality Management Urban, Regional and Globol Scales, Istanbul – Turkey, 403-409.

Saxena, V.P., Jat, H.S., Miri, Praveen and Juneja, A, 2003-A. Pollution distribution in an urban atmosphere with vertical emittence : A Mathematical Study in the Proc. of Sec. National Conference on Urban air Pollution Issues & Managements, Surat (Gujarat), India, 3.12-3.19.

Saxena, V.P., Jat, H.S., Miri, Preveen and Juneja, A., 2003-B. Mathematical modelling of air pollution in urban atmosphere with surface deposition. Proc of Sec. National Conference on Urban Air Pollution Issues and Management, Surat (Gujarat), India, 3.3-3.11.

Saxena, V.P., and Juneja, A., 2003, Numerical study of air pollution in annular regions with point source. Proc. of Sec. 26th NATO/CCMS Int. Technical Meeting

on Air Pollution Modelling and its Application, Istanbul Technical University, Istanbul – Turkey, 568.

Tokgozlu, A., Saxena, V.P., Ocak, S. and Erturk, F., 2001. Transient concentration distribution of pollutants over Isparta Proc. of Sec. Int. Symp. on Air Quality Management Urban, Regional and Globol scales, Istanbul – Turkey, 396-402.

*Proceedings of the Third International Symposium on Air Quality Management at Urban, Regional and Global Scales. 26-30 September 2005, Istanbul – Turkey*

# LARGE EDDY SIMULATION OF A CONTINUOUS AREA SOURCE IN A CONVECTIVE BOUNDARY LAYER

**Edson P. Marques Filho[(1)], Amauri P. de Oliveira[(1)], Umberto Rizza[(2)] and Robert Bornstein[(3)]**

[(1)] Micrometeorology Group, Department of Atmospheric Sciences, Institute of Astronomy, Geophysics and Atmospheric Sciences - University of São Paulo, Rua do Matao, 1226, 05508-900, Sao Paulo, SP, Brazil.
emarques@model.iag.usp.br, apdolive@usp.br
[(2)] Istituto di Scienze dell'Atmosfera e del Clima - CNR/ISAC, Lecce, Italy
u.rizza@isac.cnr.it
[(3)] Meteorology Department, San José State University, San José, CA, USA
pblmodel@hotmail.com

## ABSTRACT

This work describes the three-dimensional structure of an inert passive atmospheric pollutant continuously emitted by an area source located near to the surface in a highly convective planetary boundary layer (CBL) $\left(-434 \le z_i/L \le -62\right)$. The CBL properties were numerically simulated using a large eddy simulation model development by Moeng. Under quasi-steady equilibrium conditions, the turbulent flow in the CBL is characterized by asymmetric structures composed of updrafts and downdrafts that produce pollutant transport in the layer. The vertical profile of the skewness of pollutant concentration is negative for almost the whole extension of the mixed layer, except in the regions near to the surface and close to the top of CBL. The latter negative fluctuations are related to the penetration of clean air in the top of CBL, which moves towards the surface in horizontally-narrow and vertically-extensive areas, provoking a decrease of pollutant concentration values. This decrease in pollutant concentration in the mixed layer simulated by the LES is $\partial\langle c\rangle/\partial t \approx -0.15\,\mathrm{ppm\,h^{-1}}$, comparable to the time rate of variation of carbon monoxide concentration of $-0.20\,\mathrm{ppm\,h^{-1}}$, as observed on average at the surface in the city of São Paulo.

**Key Words**: LES Model, CBL, Pollutant Dispersion, Source Area, Carbon Monoxide.